Investigation of the functional integration of hESC-derived grafts in models of Huntington's disease

Patricia García Jareño

This thesis is submitted for the degree of Doctor of Philosophy at Cardiff University

December 2023

Supervisors:

Professor Anne Rosser

Dr. Mariah J. Lelos

Summary

Huntington's disease (HD) is an autosomal dominant genetic disorder associated with progressive deterioration of movement, cognition and behaviour. Currently, there are no approved disease-modifying therapies and symptomatic treatments are limited, but cell replacement therapy (CRT), in which striatal medium spiny neurons (MSN) progenitors are transplanted directly into the adult striatum, is in development as a potential therapeutic intervention. Preclinical data and proof-of-concept clinical studies, using foetal-derived donor cells, suggest that striatal grafts containing mature MSNs can alleviate motor and cognitive deficits. It is hypothesized that functional recovery relies largely on reconstruction of the basal ganglia circuitry that is disrupted in the HD brain. The overall aim of this thesis was to investigate if hESC-derived MSNs can reconstruct the damaged basal ganglia circuit principally using the monosynaptic tracing based on the modified rabies virus (ΔG-rabies) technology.

Firstly, a hESC line expressing the TVA receptor and rabies glycoprotein for the ΔG-rabies was made for all host-to-graft experiments in this thesis. In Chapter 3 hESC-derived MSNs were transplanted into the striatal quinolinic acid (QA) lesion model and host-to-graft (Experiment 1) and graft-to-host (Experiment 2) connectivity were investigated. Experiment 1 demonstrated that from 5 weeks post grafting, various efferent striatal areas in the host brain, such as the cortex, thalamus or substantia nigra (SN), made synaptic contacts with the graft, and these contacts were maintained overtime. Interpretation of Experiment 2 exploring graft-to-host connectivity were unfortunately limited because the grafts were very large and ventrally located.

Chapter 4 explored host-to-graft connectivity in the F344tgHD transgenic rat model in young and aged rats. These studies revealed that both wild-type (WT) and F344tgHD rat host brain were able to make synaptic contacts with transplanted hESC-derived MSNs at both ages, although graft volumes were smaller in F344tgHD rats compared to WT rats.

Chapter 5 set out to investigate the expression of immediate early genes (IEG) as possible biomarkers for neural network repair after cell transplantation. Surprisingly, these experiments showed an unexpected cell loss in the globus pallidus (GP) in the QA model. The mechanism underlying this cell loss was explored, with a view to making adjustments to the QA lesion in the striatum so as to make it more suitable for exploring circuit reconstruction.

This work outlines the potential of hESC-derived MSNs for CRT, establishes the proof of concept that this Activin-A-based cell product can form early synaptic contacts with the host brain, and emphasizes the importance of reviewing animal models and selecting the most appropriate to address the research question.

Acknowledgements

“Querido Daniel, cuanto antes usted se dé cuenta de esto, mejor: nada en esta cochina vida vale dos duros si no tienes alguien con quien compartirlo”. (Carlos Ruiz Zafón, from “La Sombra del Viento”)

Dear Daniel, the sooner you realize this, the better: nothing in this filthy life is worthy if you don't have someone to share it with.

I would like to express my deepest gratitude to my PhD supervisors, Professor Anne Rosser and Dr. Mariah Lelos, for their unwavering support and guidance throughout the entirety of my doctoral journey. Their mentorship has been invaluable, and I am profoundly thankful for the opportunity to work under their supervision. Thank you, Anne, for your dedication and the time you consistently made available in your busy schedule to engage in meaningful discussions, provide encouragement, and offer insightful feedback. I would also like to extend my appreciation to Dr. Mariah Lelos, for her expertise and assistance in navigating the technical and experimental aspects of my work.

Thank you to the European Union Horizon 2020 Program for funding this project. Additionally, I wish to acknowledge the ASCTN-Training ITN for their support during this PhD and for providing me the opportunity to share this experience with 13 other fantastic students.

Special thanks to Dr. Sophie Rowlands, whose support has been immensely important. Not only did you support me in the lab and during this thesis writing, but you also consistently cheered me up when I needed it. Additionally, I extend my gratitude to Marija for her invaluable assistance with the *in vitro* aspects of the project.

In addition, I would like to express my gratitude to the past and present BRG members Ana, Feras, Harri, Kübra, Kyle, Mengru, Oly and Rachel Sellick for their assistance and support during this research endeavour. To Heba, for being such an inspirational woman and to Anne-Marie, for her kindness, support, and meticulous help with all the paperwork. I am so grateful to Rach Hills, for her tireless efforts, especially in handling experimental animals, and for her consistent availability whenever I needed assistance.

To my right-hand in this work, Olivia, I could not have imagined a more suitable person to undertake this work together with; thank you for the good times and for always believing in me. I know you will be amazing in your PhD. To my office-mate, Charlie, I am so grateful to have found you to share this adventure. Thank you for the laughs, the tears, the coffees and the discussions. I am so proud of what you have achieved.

Thank you to my parents for their support in my education all these years. To Cris, because her friendship has been a constant source of strength that has help me throughout the whole PhD, especially during tough times. I feel incredibly lucky to have found you.

Finally, thank you to the ones who had always believe in me: my grandma Inés, my number one fan and the most amazing woman in this entire world; I admire you so much. And to Brais, for going through this together, for keeping my sanity and for believing in me more than myself.

To my grandad, who won't read these words, but I know he's so proud.

Table of contents

Abbreviations

3-NP	3-Nitropropionic acid
3V	3rd ventricle
AAD	Anterior amygdaloid area, dorsal part
AAV	Anterior amygdaloid area, ventral part
AcbC	Accumbens nucleus, core
AcbC	Nucleus accumbens, core
Acc	Accessory neurosecretory nuclei
AChE	Acetylcholine esterase
ACo	Anterior cortical amygdaloid nucleus
AM	Anteromedial thalamic nucleus
AOM	Anterior olfactory nucleus, medial part
AOP	Anterior olfactory nucleus, posterior part
AOV	Anterior olfactory nucleus, ventral part
APO	Apomorphine
Astr	Amygdalostriatal transition area
AVDM	Anteroventral thalamic nucleus, dorsomedial part
AVVL	Anteroventral thalamic nucleus, ventrolateral part
BDAs	Biotinylate dextran amines
BDNF	Brain-derived neurotrophic factors
BLA	Basolateral amygdaloid nucleus, anterior part
BLP	Basolateral amygdaloid nucleus, posterior part
BLV	Basolateral amygdaloid nucleus, ventral part
BMA	Basomedial amygdaloid nucleus, anterior part
BMA	Basomedial amygdaloid nucleus, anterior part
BML	Basomedial amygdaloid nucleus, posterior part
BMP	Bone morphogenic protein

BST	Bed nucleus of the stria terminalis
BSTIA	Bed nucleus of the stria terminalis, intraamygdaloid division
BSTL	Bed nucleus of the stria terminalis, lateral division
CAG	Cytosine-Adenine-Guanine
CeL	Central amygdaloid nucleus, lateral division
CeM	Central amygdaloid nucleus, medial division
Cg1	Cingulate cortex, area 1
CGE	Caudal ganglionic eminence
ChAT	Choline acetyltransferase
CL	Centrolateral thalamic nucleus
Cl	Claustrum
CM	Central medial thalamic nucleus
CPu	Caudate putamen
CRT	Cell replacement therapies
CTB	Cholera toxin β-subunit
CTIP2	COUP TF1-interacting protein 2
D1R	Dopamine receptor subtype 1
D2R	Dopamine receptor subtype 2
DA	Dorsal hypothalamic area
DAB	3,3'-diaminobenzidine
DARPP32	cAMP-regulated phosphoprotein 32
DEn	Dorsal endopiriform nucleus
DI	Dysgranular insular cortex
DLO	Dorsolateral orbital cortex
DPBS	Dulbecco's phosphate-buffered saline
E8	Essential 8
ENK	Enkephalin
ESC	Embryonic stem cell

FG	Fluorogold
FGF	Fibroblast growth factor
fmi	Forceps minor of the corpus callosum
FOXP1	Forkhead box protein 1
GDNF	Glial-derived neurotrophic factors
GE	Ganglionic Eminence
GP	Globus pallidus
hESC	Human embryonic stem cell
HD	Huntington's Disease
HRP	Horseradish peroxidase
HTT	Huntingtin
IB	Ibotenic acid
IL	Infralimbic cortex
IMD	Intermediodorsal thalamic nucleus (IMD)
IPACL	Interstitial nucleus of the posterior limb of the anterior commissure, lateral part
IPACM	Interstitial nucleus of the posterior limb of the anterior commissure, medial part
KA	Kainic acid
LaDL	Lateral amygdaloid nucleus, dorsolateral part
LDDM	Laterodorsal thalamic nucleus, dorsomedial part
LGE	Lateral ganglionic eminence (LGE)
LH	Lateral hypothalamic area
LHbL	Lateral habenular nucleus, lateral part
LHbM	Lateral habenular nucleus, medial part
LO	Lateral orbital cortex
LPO	Lateral preoptic area
MCLH	Magnocellular nucleus of the lateral hypothalamus
MCPO	Magnocellular preoptic nucleus

MD	Mediodorsal thalamic nucleus
MDC	Mediodorsal thalamic nucleus, central part
MDL	Mediodorsal thalamic nucleus, lateral part
MDM	Mediodorsal thalamic nucleus, medial part
MeAD	Medial amygdaloid nucleus, anterodorsal part
MeAV	Medial amygdaloid nucleus, anteroventral part
MePD	Medial amygdaloid nucleus, posterodorsal part
MePV	Medial amygdaloid nucleus, posteroventral part
met-ENK	Met-enkephalin
MGE	Medial ganglionic eminence
mHTT	Mutant huntingtin
M1	Primary motor cortex
M2	Secondary motor cortex
MO	Medial orbital cortex
MOI	Multiplicities of infections
MOR	μ-opioid receptor
MSN	Medium Spiny neurons
NMDA	N-methyl-D-aspartate
PBP	Parabrachial pigmented nucleus
PC	Paracentral thalamic nucleus
PD	Parkinson’s disease
PF	Parafascicular thalamic nucleus
PHA-L	Phytohemagglutinin-L
Pir	Piriform cortex
Po	Posterior thalamic nuclear group
PrC	Precommissural nucleus
PrL	Prelimbic cortex
PSC	Pluripotent stem cell

PSTh	Parasubthalamic nucleus
PT	Paratenial thalamic nucleus
PV	Paraventricular thalamic nucleus
QA	Quinolinic acid
RA	Retinoic acid
Re	Reuniens thalamic nucleus
Rt	Reticular thalamic nucleus
SB	SB431542
SEM	Standard error of the mean
SHH	Sonic hedgehog
SI	Substantia innominata
SIB	Substantia innominata, basal part
SID	Substantia innominata, dorsal part
SL	Semilunar nucleus
SM	Nucleus of the stria medullaris
SN	Substantia nigra
SP	Substance P
st	Stria terminalis
STN	Subthalamic nucleus
SubD	Submedius thalamic nucleus, dorsal part
TC	Tuber cinereum area
VA	Ventral anterior thalamic nucleus
Ven	Ventral endopiriform nucleus
VL	Ventrolateral thalamic nucleus
VLH	Ventrolateral hypothalamic nucleus
VM	Ventromedial thalamic nucleus
VMH	Ventromedial hypothalamic nucleus
VO	Ventral orbital cortex

VPL	Ventral posterolateral thalamic nucleus
VPM	Ventral posteromedial thalamic nucleus
VRe	Ventral reuniens thalamic nucleus
VTT	Ventral tenia tecta
WGE	Whole ganglionic eminence
YAC	Yeast artificial chromosome
ZID	Zona incerta, dorsal part
ΔG	Glycoprotein gene (G)-deleted rabies virus

Chapter 1: Introduction

Neurodegenerative conditions are progressive, often clinically complex, and associated with cognitive and mental health decline. These diseases degrade an individual's independence and quality of life and they often have a severe impact on family members and social contact.

Huntington's disease (HD) is the commonest single gene neurodegenerative disorder and represents significant unmet need. Degeneration in the caudate and putamen (striatum) causes progressive deterioration of movement, cognition and behaviour, with individuals being eventually bed-bound and needing full nursing care. Currently, there is no available therapy to halt or slow the disease. However, HD is a particularly suitable condition in which to explore cell replacement therapy as (i) single gene disorders with full penetrance are particularly powerful paradigms for clinical translation and (ii) degeneration is predominantly in the striatum, providing a target for cell replacement.

Cell replacement therapies (CRT) aim, by transplanting new tissue, to restore the functionality of the damaged area. In HD there have already been clinical trials using human foetal tissue as a CRT product, however, foetal tissue involves ethical controversy and technical difficulties and hence the interest in using stem cell-derived cells as a cell therapy product. This project focuses on stem cell transplantation to study and investigate how these cells interact with the damaged brain and, critically, determine if they can restore synaptic connectivity in the damaged basal ganglia circuits.

1.1. The basal ganglia

The basal ganglia is an area of the brain composed of two nuclei, the caudate and putamen (striatum in rodents) and the globus pallidus (GP), and is involved in motor learning and control, executive functions and emotions. The striatum is the main structure of the basal ganglia and the largest subcortical structure of the brain (Schroder et al., 1975). Its main type of neurons are inhibitory GABAergic Medium Spiny Neurons (MSNs), which originate from the lateral ganglionic eminence (LGE) in the developing forebrain. MSNs comprise ~90% of the neurons of the striatum and can be divided into D1-MSNs (dopamine receptor D1, predominantly part of the direct pathway) and D2-MSNs (dopamine receptor D2, predominantly part of the indirect pathway). The

remaining ~10% of the striatal neuronal population are interneurons. The GP is subdivided into the GP internal (GPi) and GP external (GPe) by the medial medullary lamina of white matter (DeLong, 1971).

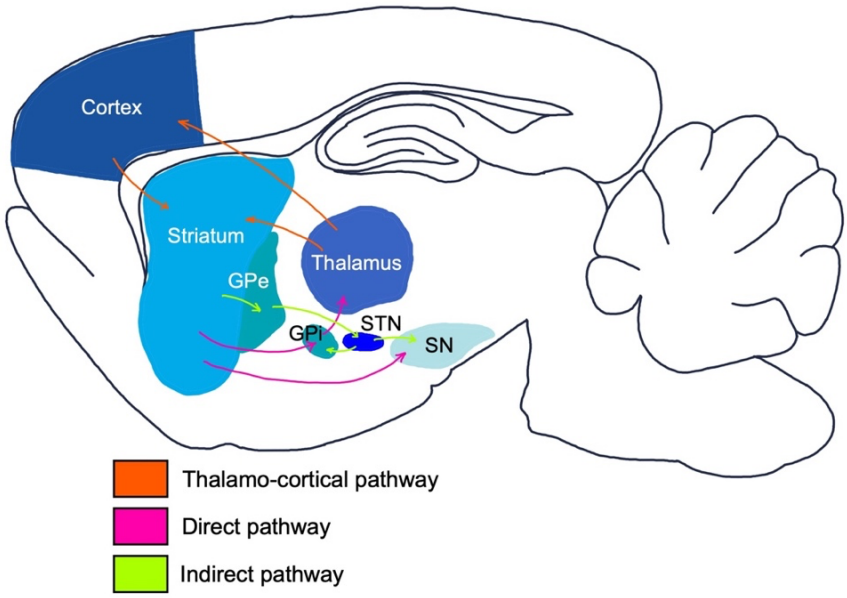

Figure 1 – Diagram of the basal ganglia circuit. The striatum received afferent excitatory connections from the cortex and the thalamus and project efferent connections to the GP and SN. In the direct pathway (in pink), striatal cells project to the GPi and SN. From the GPi projections go to Thalamic areas. In the indirect pathway (in green), striatal cells project to the GPe and from there to the STN. The STN also projects to GPi and SN.

The basal ganglia take part in the cortico-striatal-thalamic network, involved in motor, cognitive and limbic functions (Figure 1). It has other associate nuclei, such as the subthalamic nucleus (STN) and the substantia nigra (SN) (Haber, 2016; Lanciego, Luquin, & Obeso, 2012; McElvain et al., 2021). The SN is further divided into the SN par reticulata (SNr) and SN par compacta (SNc) (Moore & Bloom, 1978). All these nuclei can be categorised as follows: (i) input nuclei (the striatum) that receive inputs from cortical, thalamic and nigral areas; (ii) both GPi and SNr are grouped together as output nuclei, receiving striatal MSN projections as part of the direct pathways, and excitatory glutamatergic projections from the STN (Lanciego et al., 2012). Both afferent systems innervate thalamic targets, such as the ventral anterior motor thalamus (VAdc and VApc) and ventral anterior motor thalamus (VAmc); (iii) intrinsic nuclei, including the GPe, the STN and the SNc, that are between input and output nuclei (Lanciego et al., 2012). The GPe is part of the indirect circuit, receiving D2 striatal projections and transferring information to the STN, as well as to the GPi (Wallace et al., 2017). It has been found that the GPe is a more complex nucleus, as it not only coordinates the indirect pathway, but also has direct connections with the cortex, thalamus or pedunculopontine nucleus

(Eid, Parent, & Parent, 2016; Lavoie & Parent, 1994; Mallet et al., 2012; Milardi et al., 2015; Sato et al., 2000; Saunders et al., 2015; Yasukawa et al., 2004).

1.1.1. The striatum and its origin

The striatum originates from within the developing forebrain. Human brain development involves complex cascades of molecular signaling that start during gastrulation, with the induction of the three germ layers (endoderm, mesoderm and ectoderm) (Leptin, 2005). From the ectoderm layer, the neuroectoderm appears which then forms the neural plate that subsequently folds into the neural tube (Figure 2A) (Darnell & Gilbert, 2017; Pankratz et al., 2007). Once the neural tube is closed, during the third week of gestation, it is subdivided into three different structures, the forebrain (prosencephalon), midbrain (mesencephalon) and hindbrain (rhombencephalon). During the fifth week of gestation, the forebrain will give rise to the telencephalon and diencephalon; and the hindbrain to the metencephalon and myelencephalon (Figure 2B) (Ishikawa et al., 2012). The telencephalon is located at the most rostral end of the neural tube and can be divided in its ventral region, or subpallium and its dorsal region or pallium. Specifically, the ventrolateral telencephalon forms the lateral ganglionic eminence (LGE) that is the origin of the medium spiny neurons of the striatum (Stiles & Jernigan, 2010); the ventromedial telencephalon gives rise to the medial ganglionic eminence (MGE) that is the origin of the interneurons of the striatum, globus pallidus and some cortical areas (S. A. Anderson et al., 2001; Lavdas et al., 1999; Olsson, Bjorklund, & Campbell, 1998); and the caudal ganglionic eminence (CGE) also gives rise to different cortical interneurons (Brazel et al., 2003; Miyoshi et al., 2010; Nery, Fishell, & Corbin, 2002). The dorsal part of the telencephalon forms the neocortex (Rubenstein et al., 1998).

These telencephalic divisions are based on gene expression: *Pax6*, *Neurogenin1/2* and *Emx1/2* are expressed in dorsal regions; and *Gsx2*, *Ascl1*, *Dlx1/2* and *Nkx2.1* are found in ventral regions (Schuurmans & Guillemot, 2002). Telencephalon dorsoventral patterning depends on gradients of different molecular cascades, such as fibroblast growth factor (FGF), sonic hedgehog (SHH), retinoic acid (RA), Wnts and bone morphogenic proteins (BMP) (Chatzi, Brade, & Duester, 2011; Evans et al., 2012; Manuel et al., 2010). High expression of SHH is found ventrally and Wnt and BMP are found dorsally in the telencephalon. The SHH/Wnt expression gradient is critical for the patterning of each particular telencephalic subregion (Figure 3) (Alvarez-Medina et al., 2008; Borycki, Brown, & Emerson, 2000; Gunhaga et al., 2003).

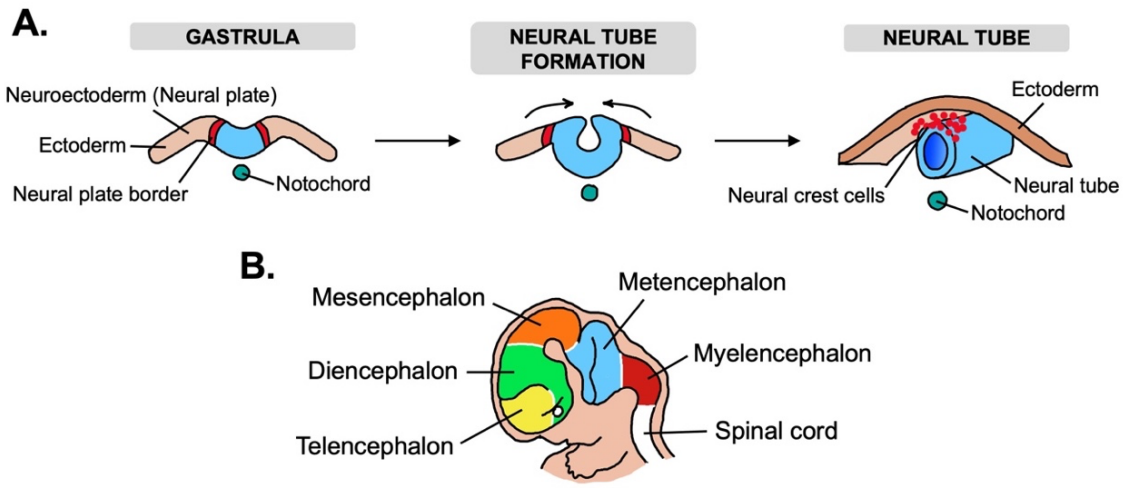

Figure 2 – Schematic representation of human brain development. (A) First stages on human brain development, starting during gastrulation, in which the neural plate starts its folding to give rise to the neural tube, the origin of the central neural system. The neural crest cells are the origin of the peripheric nervous system. (B) A few weeks later the neural tube is divided in the different regions that originate the human brain. The telencephalon is the area that forms the cerebral cortex and the basal ganglia.

One of the earliest recognized telencephalic markers is the transcription factor Foxg1, which has an essential role in forebrain development (Manuel et al., 2010). At E8.5 expression of *Foxg1* starts (Tao & Lai, 1992) and consequently telencephalic subdivisions appear, regulated by the dorsalizing effects of *Gli3* and ventralizing effects of *Shh*. The absence of *Gli3* disrupts dorsal telencephalon development and produces dorsal expression of the ventral genes *Dlx2* and *Gsx2* (Rallu et al., 2002). On the other hand, *Shh* activates transcription factors *Nkx2.1*, *Gsx2* and *Pax6* and SHH expression promotes FGF expression. *Shh* knockout mice produce a reduction in subpallial markers *Dlx2* and *Gsx2*, no expression of FGF and an increase of Pax6 in the ventral telencephalon (Gutin et al., 2006; Rallu et al., 2002). In the double knockout mouse of Gli3 and Shh, ventral patterning is mostly rescued and FGF expression is not attenuated (Gutin et al., 2006; Rallu et al., 2002). Therefore, SHH promotes ventral identity and restricts the dorsalizing function of GLI3 but ventral patterning is independent of SHH expression. FGF expression is promoted by SHH indirectly by repressing GLI3. The absence of *Foxg1* expression produces a loss of ventral markers *Nkx2.1* and *Dlx2* but dorsal markers are expressed through the telencephalon (Martynoga et al., 2005; Xuan et al., 1995) and ventral patterning is not rescued in the double knockout of Foxg1 and Gli3, but there is complete loss of the telencephalon (Hanashima et al., 2007). These results showed the importance of Gli3 and Foxg1 for telencephalic patterning and development.

Although Wnt expression is found dorsally, the Wnt canonical pathway is critical to maintain pallial identity, as the absence of β-catenin results in the expression of ventral markers such as Gsx2, Mash1 and Dlx2 to be expressed in cortical progenitors (Backman et al., 2005). Together with SHH/Wnt morphogens, expression of transcription factors (TF) is also critical for LGE development. For example, Gsx2 is involved in cellular identity of the LGE and its absence produced a loss of ventral markers Ascl1 and Dlx1/2 (Szucsik et al., 1997; Toresson, Potter, & Campbell, 2000), as well as a reduction in cAMP-regulated phosphoprotein (DARPP32) positive neurons, a critical marker for mature MSNs (Toresson & Campbell, 2001).

The LGE can be regionally subdivided depending on its TFs expression, as dorsal LGE is composed by ETV1/Er81 positive cells, lateral LGE is defined by expression of Pax6 and Gsh2 and medial regions with low Pax6 expression and high Gsh2. A recent single cell RNA sequencing study revealed that LGE has a pre-MSN phase, expressing genes related to nervous system development and axon guidance before giving rise to D1 and D2 MSNs (Bocchi et al., 2021). This study also revealed new transcription factors determinants in MSN development such as SP9, ZNF467 and OCT6 (Bocchi et al., 2021).

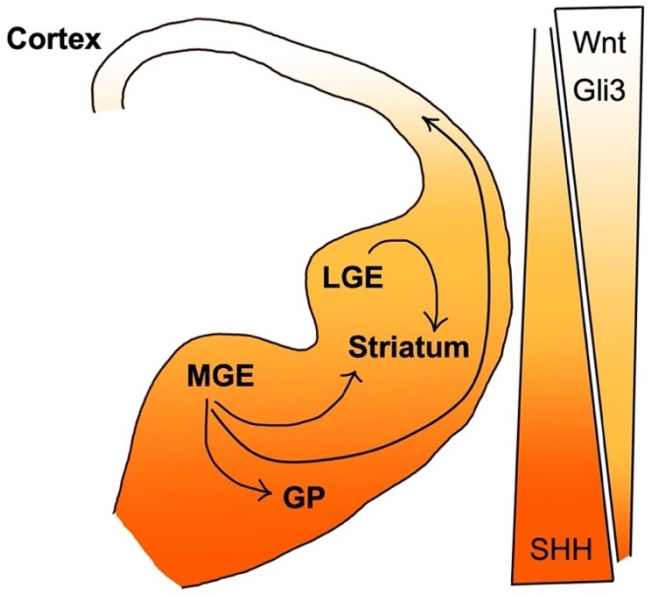

Figure 3 – Schematic representation of a coronal section of the developing telencephalon. Dorsal regions are represented in white and ventral regions are represented in orange, and patterned based on expression of SHH, ventro-dorsal, and Wnt and Gli3, dorso-ventral. Arrows represented cell migration from the LGE to the striatum, as well as interneurons from the MGE to the striatum and cortex and GP cells.

1.1.2. Medium Spiny Neurons

Around E14 in rats and 50 days post fertilization in humans, expression of DLX2 and GSX2 decreases to give rise to BCL11B, DARPP32, FOXP1, FOXP2, ISL1 and EBF1 markers of more mature MSNs (Martin-Ibanez et al., 2012; Onorati et al., 2014). DARPP32 is expressed in around 95% of MSNs and not expressed in any other striatal cell type (K. D. Anderson & Reiner, 1991; Ouimet & Greengard, 1990; Ouimet, Langley-Gullion, & Greengard, 1998; Ouimet et al., 1984). BCL11B, also known as COUP TF1-interacting protein 2 (CTIP2) is a transcription factor expressed by MSNs in the striatum. CTIP2 knockout mice are embryo lethal, as they only survive 24h, and knockout produces abnormalities in the striatal architecture that is striosomes and matrix organization, and affects DARPP32 expression, which is significantly reduced compared to wild type (WT) littermates (Arlotta et al., 2005; Arlotta et al., 2008). Co-localization of CTIP2 with DARPP32 is considered the gold standard MSN markers, as all adult striatal DARPP32 positive cells express CTIP2, and these markers are also individually expressed in the cortex (Onorati et al., 2014). Another relevant MSN marker is FOXP1, a transcription factor relevant for striatal development. Absence of FOXP1 in a mouse knockout model resulted in the absence of DARPP32 expression (Precious et al., 2016). FOXP1 labels progenitors and mature MSNs as well as co-localizing with DARPP32 (Precious et al., 2016).

Striatal MSNs are a heterogenous population that can be subdivided based on various characteristics, such as biochemical composition (expression of dopamine receptors D1 or D2), functional pathway (direct and indirect pathway) or striatal compartments (patch (striosome) and matrix). Depending on biochemical composition and innervation, neurons projecting to the GPe, express the dopamine receptor subtype 2 (D2R) and enkephalin, whereas MSNs projecting to the GPi and SN express dopamine receptor subtype 1 (D1R), substance P and dynorphin (Gerfen et al., 1990; Surmeier et al., 1992). Recent single cell RNA studies report a hybrid group of MSNs that express both D1 and D2 receptors in Rhesus monkeys. Authors also proposed that gene expression in the striatum is based on gradients that define either dorsal or ventral positions (He et al., 2021).

This biochemical composition defines which functional pathway they are involved, such as direct pathway MSNs that express D1 dopamine receptor (D1-MSN), and indirect MSNs that express D2 dopamine receptor (D2-MSN). There is an opposite effect of activation of D1 and D2 receptors (Albin, Young, & Penney, 1989; DeLong, 1990). Therefore, cortical activation produces a glutamate release that activates D1-MSN inhibiting tonic activity of neurons in the GPi and SNr; and that inhibition of the SNr leads

to a disinhibition of glutamatergic thalamic neurons that project to the cortex; activating locomotor activity. On the other hand, activation of D2-MSN inhibits GPe neurons and STN to then excite GPi and SNr neurons, inhibiting motor activity (Kravitz & Kreitzer, 2012).

MSNs can also be classified depending on striatal compartments, for example as striatal patch (striosome) or matrix neurons. These compartments can be defined based on histological characterization, in which striosomes express μ-opioid receptor (MOR), substance P (SP), dopamine D1R, met-enkephalin (met-ENK), calretinin, Nr4a1, pro-dynorphin, GAD2, and EGR1; and matrix express calbindin, somatostatin (SST), enkephalin (ENK), dopamine D2R, and cholinergic markers including acetylcholine esterase (AChE) and choline acetyltransferase (ChAT) (Brimblecombe & Cragg, 2017; Prager & Plotkin, 2019). Striosomes are involved in mood regulation, dopamine release and reward processes (Canales, 2005; Crittenden & Graybiel, 2011) and matrix is related to sensorimotor system (Gerfen, 1984; Kincaid & Wilson, 1996). Matrix and striosomes both contain direct and indirect MSNs, however there is a predominance of direct MSNs in striosomes (Fujiyama et al., 2011; Gerfen, 1984; Jimenez-Castellanos & Graybiel, 1989).

1.1.3. Cortico-striatal-thalamic circuit

In the cortico-striatal-thalamic circuit, the striatum receives glutamatergic inputs from cortical pyramidal cells of layers III and V, and from the thalamus (Doig, Moss, & Bolam, 2010; Martel & Galvan, 2022). Cortical areas (prefrontal, motor, sensory and limbic areas) send glutamatergic projections in a topographic manner to the striatum and, as a consequence, the striatum is regionally divided. The dorsolateral striatum is involved in sensorimotor processing, receiving outputs from the primary motor cortex and premotor cortex; the mediodorsal striatum is related to associative functions, and is connected with the prefrontal cortex; and ventral areas are related to limbic processing, and get connections from the anterior cingulate cortex and medial prefrontal cortex (Balleine & O'Doherty, 2010; Doyon et al., 2009; Hart, Leung, & Balleine, 2014; Perez-Diaz et al., 2017). Recent studies have claimed a fourth domain, in the most caudal part, which integrates different inputs controlled by the amygdala (Hunnicutt et al., 2016). The amygdala is a limbic structure composed of different nuclei involved in emotional processing and it innervates the ventral striatum (Fudge et al., 2002).

The centromedian and parafascicular (CM/Pf) complex in primates or Pf in rodents is the main source of glutamatergic thalamic inputs to the striatum (to the matrix), and

these are sensorimotor, associative and limbic inputs. The Pf receives projections from the SNr, GPi and GPe (Cebrian, Parent, & Prensa, 2005; Smith et al., 2022; Tsumori et al., 2002). There are also other thalamic areas providing inputs to the striatum such as the midline, rostral intralaminar, VA/VL, mediodorsal, and pulvinar (Cover et al., 2023; Day-Brown et al., 2010; Deschenes et al., 1996; McFarland & Haber, 2000; Vertes & Hoover, 2008; Vertes, Linley, & Rojas, 2022), however the topographical organization of these need further studies.

The discussed cortico-striatal-thalamic circuit is considered a classical view of this circuit. The circuit is conceived as a loop in which information from the cortex, modulated to the basal ganglia, travels through the circuit and goes back to the cortex as a signal to produce or inhibit a motor activity. However, new studies are revealing a more complex structure of this circuit, with various loops and domains, dividing the basal ganglia into motor, associative and limbic domains depending on its cortical projections (Buhusi & Meck, 2005; N. N. Foster et al., 2021; Hikosaka et al., 2002; Yin & Knowlton, 2006).

1.2. Huntington's disease (HD)

Huntington's disease (HD) is a neurodegenerative and autosomal dominant genetic disorder caused by an unstable expansion mutation of the cytosine-adenine-guanine (CAG) trinucleotide repeat in exon 1 of the Huntingtin (HTT) gene (IT15) encoding a mutant (mHTT) form of the protein with N-terminal polyglutamine tracts (Caron, Wright, & Hayden, 1993; Colpo, Furr Stimming, & Teixeira, 2019; Connor, 2018; Wijeyekoon & Barker, 2011). The length of CAG repeat influences the age of onset (broadly speaking, the longer the expansion the earlier the manifestation of the disease) (Andrew et al., 1993; Duyao et al., 1993; Langbehn et al., 2004). The polymorphic CAG repeat in a healthy individual is present in the range of 6-35 CAGs; lengths of 36-38 are related to low penetrance of the disease (Kay et al., 2016) and when repeats are expanded ≥40, the individual presents full penetrance of the disease. Patients are diagnosed around 45 years old on average, but there is a group of HD individuals (around 4-10% of total cases) diagnosed prior to 21 years old, and this is referred to as juvenile HD. Juvenile HD patients typically present with ≥60 CAG repeats (Bakels et al., 2022).

The disorder involves motor, cognitive and psychiatric disturbances and diagnosis of disease onset normally occurs when motor symptoms appear ("Unified Huntington's Disease Rating Scale: reliability and consistency. Huntington Study Group," 1996), although cognitive and psychiatric deficits start many years before motor symptoms

(Ross & Tabrizi, 2011; Tabrizi et al., 2013). Motor symptoms include involuntary movements, such as chorea, and impairments in voluntary movements, leading to incoordination, rigidity or bradykinesia (Novak & Tabrizi, 2010). First cognitive impairments that present are difficulty in social relations and emotional communication. These are followed by difficulties in speed of processing, in learning and implicit memory, in perception of the time, attentional deficits, impairment in executive processing, communication deficits and the olfactory system is also impaired (Paulsen, 2011). Psychiatric disturbances have also been reported, such as depression and anxiety and more than 10% of HD patients have attempted suicide at least once (Paulsen et al., 2005).

Patients are classified in five different grades, from 0 to 4 depending on their neuropathology and symptoms (Vonsattel et al., 1985). Grade 0 corresponds to premanifest stages of the disease with patients being asymptomatic, and grade 4 is the highest rate, with 95% loss of the caudate neurons and complete akinesia (Albin et al., 1989). Although recently, a newer staging system has been developed in the field (Tabrizi et al., 2022). The average duration of survival post-disease onset is in the range of 10-20 years (Folstein et al., 1983; Foroud et al., 1999). The most common causes of death are cardiovascular and respiratory problems (Solberg et al., 2018) or infection of ulcer due to immobility (Dubinsky, 2005).

HD is prevalent in all populations but there is a higher frequency between individuals carrying European ancestry, and white and mixed populations have higher rates compared to black populations. The prevalence of the disease is 10.6–13.7 individuals per 100,000 with 4.7–6.9 new cases per million per year in Western populations, but in Asian countries such as Japan, Taiwan or Hong Kong the prevalence is 1-7 individuals per million (G. P. Bates et al., 2015).

1.2.1. Mechanism of the disease and pathology

The *htt* gene is expressed in healthy individuals and it has a crucial role in neurodevelopment. It is involved in tissue maintenance, cell morphology and survival (Saudou & Humbert, 2016) and its knockout is embryo lethal in rodents (Nasir et al., 1995). A recent single cell RNA study revealed upregulation of *htt* in the LGE, compared to surrounding areas, suggesting its important role in striatal development (Bocchi et al., 2021).

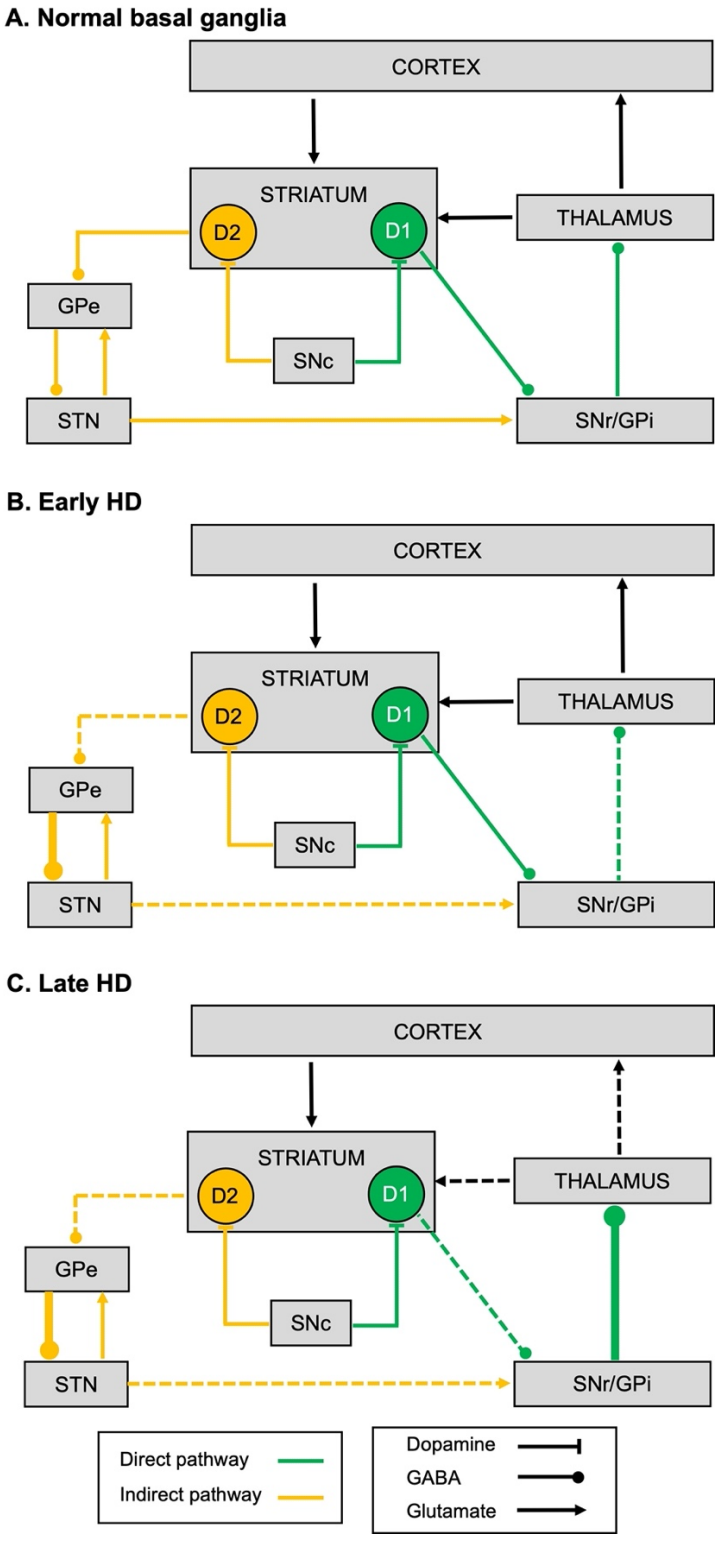

Figure 4 – Basal ganglia circuit in normal stage, early and late stages of HD. Schematic circuit of (A) the basal ganglia on its normal stage. (B) In early stages of HD, in which D2-MSN of the indirect pathway are affected by the disease and producing hyperactivation of the thalamus. (C) In late stages, D1-MSN are also affected and both pathways, direct and indirect are dysregulated, producing hyperinhibition of thalamic nuclei and patients presenting bradykinesia and akinesia.

In HD, mutant HTT (mHTT) nuclear inclusions and cytoplasmic aggregates are the main molecular characteristics of the disease, however, it is still unclear if these inclusions are protective or pathogenic (Walker, 2007). The most vulnerable and affected cell type to the mHTT are the MSNs, located in the striatum (Labbadia & Morimoto, 2013). Further neuropathology of HD is striatal atrophy which appears 15 years earlier than motor symptoms (Aylward et al., 2004), is progressive and correlates with the number of CAG repeats (Ruocco et al., 2006). Furthermore, postmortem studies in brain tissue from HD patients have revealed abnormalities in the shape and size of MSNs spines, and a decrease in their density within the striatum (Ferrante, Kowall, & Richardson, 1991; Graveland, Williams, & DiFiglia, 1985).

Although the main area of the brain affected by HD is the striatum, the GP, thalamus, hypothalamus and cortex are also involved and dysregulated. Imaging and *post-mortem* studies in HD patients revealed atrophy and cell loss in the GP, particularly at later stages of HD (Albin et al., 1989; Deng et al., 2004; Lange et al., 1976; Reiner et al., 1988; Singh-Bains et al., 2016; Vonsattel et al., 1985). The GPe projections are more affected by the disease, with loss of ENK neuropeptide already in early stages, compared to the GPi, that is affected later (Deng et al., 2004; Reiner et al., 1988; Sapp et al., 1995). Cortical atrophy is also present in early stages, with loss of white matter (McColgan et al., 2017), that is also observed in hippocampus, amygdala and thalamus, and this is maintained over all HD grades (de la Monte, Vonsattel, & Richardson, 1988).

Loss and disruptions in all these areas have a critical effect on the cortico-striatal-thalamic circuit (Figure 4A). The early loss of striatal neurons from the indirect pathway (D2-MSN) produces a reduction of the inhibitory impact of these neurons on the GPe and STN. The inhibitory effect of the STN over the GPi is also reduced, as well as the effect from the GPi to the thalamus (Figure 4B) (Albin et al., 1990; Crossman, 1987; Crossman et al., 1988; Deng et al., 2004). In later stages of the disease, loss of striatal D1-MSN projections produces a reduced inhibition of the GPi and SNr, translating into a hyper-inhibition of the thalamus, contributing to bradykinesia and akinesia (Figure 4C) (Albin et al., 1990; Reiner, Dragatsis, & Dietrich, 2011).

1.3. Animal models of HD

Until the discovery of the mutation in the *htt* gene, HD was modelled *in vivo* using neurotoxins that were directly infused into the striatum. Although these models mimic the striatal atrophy and excitotoxicity, they lacked the genetic mutation and did not represent all the pathogenic processes of human disease. Therefore, there are two types of HD *in*

vivo models: neurotoxic and genetically modified animal models. Rodents are the most widely used model (and the one used in this thesis). There are also various other *in vivo* models ranging from invertebrates such as worms or fruit flies, to small mammals or even large animal models, such as sheep, pigs or monkeys, but these are not discussed here.

1.3.1. Neurotoxic models

Neurotoxic models in small or large mammals were some of the first animal models used to investigate HD. In these models, a neurotoxin is used to cause selective medium spiny neuron death and thereby produce striatal atrophy. Excitotoxicity has been described as an excessive neuronal excitation by glutamate, leading to an influx of sodium, calcium and water that produce cell death (Rothman & Olney, 1995) and these models are based on the similarities between neurotoxin and excitotoxic lesions with what is observed in HD patients (Beal et al., 1991). Initially, glutamate receptor agonist kainic acid (KA) and ibotenic acid (IB) were used (Coyle & Schwarcz, 1976; Schwarcz et al., 1984), but KA has a non-selective neuronal effect, damaging different neuronal populations as well as damaging preferentially the cell soma rather than the axons (Schwarcz & Coyle, 1977) and IB unilateral lesions produce a dopamine compensatory mechanism on the contralateral side, increasing expression of D2 receptors mRNA (Narang et al., 1993).

Other toxins replaced these two, namely 3-Nitropropionic acid (3-NP) and quinolinic acid (QA, pyridine-2,3dicarboxylic acid). The effect of 3-NP is that it induces neuronal death through mitochondrial dysfunction producing apoptotic cell death (Rosenstock et al., 2004) and mitochondrial dysfunction has been postulated as one of the early pathological mechanisms in HD (Carmo et al., 2018).

QA is an endogenous N-methyl-D-aspartate (NMDA) agonist (Stone & Perkins, 1981) that, when infused in the striatum, produces an excessive NDMA receptor stimulation and rapid degeneration similar to what has been observed in HD (Beal et al., 1986; A. C. Foster, Collins, & Schwarcz, 1983). NMDA is a glutamate receptor with a high Ca^{2+} permeability that is present at high levels in MSNs (Albin et al., 1992; Standaert et al., 1999), modulating dendritic spine morphology (Vastagh et al., 2012). Its continuous activation, by QA for example, produces an increase of Ca^{2+} that can initiate a cascade of events ultimately leading to cell death, such as apoptosis or necrosis (Dong, Wang, & Qin, 2009; Fan & Raymond, 2007). Striatal lesions by QA produce striatal atrophy, with loss of MSNs and sparing of striatal somatostatin and neuropeptide Y

interneurons (Beal et al., 1986; Beal et al., 1989; Figueredo-Cardenas, Chen, & Reiner, 1997), similar to HD patients.

The striatal QA lesion model can present with deficits in motor (Dobrossy & Dunnett, 2005; Fricker et al., 1997; Kalonia, Kumar, & Kumar, 2011; Lelos et al., 2016; Pundt et al., 1996a; Sanberg et al., 1997), and cognitive behaviors (Dunnett, Nathwani, & Brasted, 1999; Lelos, Harrison, & Dunnett, 2011, 2012; Shear et al., 1998) as well as producing hyperactivity and an increase exploratory and rearing behaviors (Scattoni et al., 2004). Nevertheless, depending on the regional location of the lesion within the striatum, the outcome of the behavioral deficits might be altered. Damage in the dorsolateral striatum impairs habit formation, stimulus-response learning, and Pavlovian stimulus–outcome learning (Lelos et al., 2011). Lesions in medial striatum showed impairments in behavioral flexibility and the formation of attentional sets (Lindgren et al., 2013), serial spatial reversal learning (Castane, Theobald, & Robbins, 2010) and frontal-type executive functions (Dunnett & White, 2006). Finally, lesions in the ventral striatum produce impairments in motivated and rewarded behaviors (Eagle et al., 1999)

The QA lesion model, especially in rats, has been widely used in CRT, as its striatal atrophy is a relevant characteristic to consider in cell transplantation to evaluate striatal repair and circuit reconstruction of grafted cells.

1.3.2. Genetic models of HD

George Huntington first described HD in 1972 but it was not until 1993 that the genetic mutation was identified. From that discovery, a broad range of different HD genetic models have been developed over the last three decades. Models could either incorporate a transgene, expressing the truncated N-terminal fragment of the HTT gene containing the CAG expansions or a full length randomly inserted, or be a knock-in, where the human htt gene is inserted in the mouse htt gene locus (Pouladi, Morton, & Hayden, 2013). Table 1 shows a selective example of some mouse models but not the broader range of different rodent models that exist (Pouladi et al., 2013; Ramaswamy, McBride, & Kordower, 2007).

The first HD genetic models developed, the R6/1 and R6/2 mouse models, contain fragments of the HTT gene. They express exon 1 of the human *HTT*, under the human *HTT* promoter and carry 116 and 144 CAG repeats, respectively. These models display early-onset of symptoms which progress relatively rapidly (Mangiarini et al., 1996). Full length HTT models are normally created using a yeast artificial chromosome (YAC) vector, as the human HTT gene is very large. The YAC128, contains a full-length human

HTT, modified in exon 1 to have 128 CAG repeats (Slow et al., 2003). Other full-length models use a bacterial artificial chromosome (BAC), which contains the HTT gene that is injected into fertilized eggs (Gray et al., 2008). Finally, knock-in models are generated by homologous recombination, in which the endogenous polyQ of the Htt gene is replaced by a pathological one, such as the HdhQ111, carrying a human *HTT* exon 1 with an expanded CAG repeat tract in the endogenous mouse *Htt* gene (Lin et al., 2001). These full-length models have a later onset of the disease, slower disease progression and a milder phenotype compared to the models only expressing a fragment (Gray et al., 2008; Slow et al., 2003; Wheeler et al., 2002).

All these models present with motor and cognitive abnormalities, as well as the presence of mHtt inclusions (Heng, Detloff, & Albin, 2008; Menalled & Chesselet, 2002). However, the high number of CAG repeats (e.g. typically > 100) that they carry make them poorly translational to human HD, since humans with adult-onset HD most commonly have 40-50 CAGs. Even juvenile onset cases most commonly carry fewer than 80 CAGs. In truncated N-terminal models, the higher number of CAG repeats can produce aggressive phenotypes, which may be more similar to juvenile HD rather than the adult-onset of the disease. However, full length models, such as the HdhQ111 mouse line, which also has greater than 100 CAGs, exhibits a later symptom onset. Notably, even though these models present mHtt inclusions and neuronal dysfunction, most of them do not show significant striatal atrophy, as is predominant in the HD human brain (Pouladi et al., 2013).

Another constraint more specific to CRT, is that survival of intrastriatal neural grafts is lower in mouse models of HD compared to rats; although the exact reason is unknown, this could be related to the mouse immune system being more sensitive than that of the rat, or the mouse host response to human cells (Roberton et al., 2013).

Genetic manipulation has been generated earlier in mouse than that in rats and therefore there are only two published HD rat models, the BACHD rat and the F344tgHD (Table 2 summarizes both rat models). The BACHD rat model was generated using a human bacterial artificial chromosome, containing the full-length HTT with 97 CAG repeats. Animals showed motor deficits and anxiety-related symptoms, as well as presented with mhtt aggregates in cortex and striatum (Yu-Taeger et al., 2012).

The F344tgHD rat model is the one used for the experiments presented in this thesis. Previously to the F344tgHD model, the original model was the tgHD rats, on a Sprague-Dawley background. Both tgHD and F344tgHD rats were generated inserting a transgene containing a 1962bp cDNA fragment of the rat htt that contains a human

51CAG repeats fragment, all under an 885bp fragment of the endogenous rat htt promoter (von Horsten et al., 2003). The earliest mHTT aggregates were reported in tgHD rats at 6 months, in the nucleus accumbens, and in lower expression in stria terminals, lateral septal nucleus and geniculate nucleus. At more advanced ages, such as 21 months, aggregates were found in several brain areas: the olfactory bulb and tubercle, the striatum, the hippocampus, the GP, the thalamus, the SN and the cortex (Nguyen et al., 2006). Reduction of striatal volume was reported after 12 months of age (Vlamings et al., 2012). These rats presented reduced anxiety (Bode et al., 2008; Nguyen et al., 2006), increased nocturnal activity (Bode et al., 2008; Urbach et al., 2014), motor deficits from 6 months old in the rotarod and beam walking test (Nguyen et al., 2006) and cognitive impairment from 6-9 months of age in spatial working memory was (Nguyen et al., 2006), deficits in object recognition (Zeef et al., 2012) and in reaction time tasks (Cao et al., 2006; Kantor et al., 2006; Temel et al., 2006). For generation of the F344tgHD model, the tgHD model was optimized into an inbred strain, the F344, in order to avoid increasing genetic diversity. The F344 strain was also smaller therefore animals could be used for MRI scans due to their small size.

Ex vivo MRI assessment of the F344tgHD rats at 15 months showed lower striatal volume and histological characterization at 21 months reported expression of mHTT aggregates in the bed nucleus of the stria terminals, nucleus accumbens, piriform cortex and olfactory tubercle; but also in caudate putamen, neocortex and CA2/CA3 area of the hippocampus in less abundance than previous mentioned areas. These aggregates were detected in the neuropil and in the nucleus of striatal cells (Plank et al., 2018). Behavioral assessments showed that animals presented with reduced anxiety in social interaction tests at 2 months of age; elevated impulsivity traits in operant learning at 3 months of age; and significant increase in nocturnal activity in their home cages at 6 months of age compared to WTs (Plank et al., 2018). Based on the considerations detailed above, in this project, we decided to use a genetic rat model of HD expressing 51 CAG repeats, which should allow for good graft survival and modelling of disease more similar to the clinical situation.

Table 1 – Genetic mouse models of HD

	Truncated N-terminal fragment human HTT		**Full length human HTT**		
	Transgenic models				**Knock in models**
Model	**R6/1**	**R6/2**	**YAC**	**BACHD**	**HdhQ111**
Construct	First 90 a.a. of human htt randomly inserted into mouse genome	First 90 a.a. of human htt randomly inserted into mouse genome	Human htt entire gene	Human htt entire gene	Full length human HTT Exon 1 knock-in
Promoter	1kb human HTT	1kb human HTT	Human HTT	Human HTT	Mouse HTT
CAG repeats	116	144	72 or 128	97	109
mHTT aggregates	Striatum (8 wo)	Cortex and striatum (3-4 wo)	Striatum (3 mo) Cortex and CA1 (12 mo)	Cortex and striatum (1yo)	Striatum (5mo)
Motor symptom onset	13 wo	3 wo	16 mo (YAC72) 6 mo (YAC128)	2 mo	9 mo
Cognitive symptom onset	20 wo	4 wo	8 wo	13 mo	18 mo
Reference	(Mangiarini et al., 1996)	(Mangiarini et al., 1996)	(Slow et al., 2003)	(Gray et al., 2008)	(Wheeler et al., 2000)

Abbreviations: a.a.: amino acids; mo: Months old; wo: Weeks old; yo: years old;

Table 2 – Comparison of BACHD and F344tgHD rats.

	BACHD rats	F344tgHD rats
CAG repeats	97	51
HTT	Full length human mHTT	Truncated N-terminal fragment
mHTT aggregates	▪ Reported aggregates at 12 mo ▪ Aggregates in neocortex, NAc, hippocampus, BnST, and Amyg ▪ Few aggregates in the dorsolateral striatum, GP, and SN (Yu-Taeger et al., 2012)	▪ Reported aggregates at 21 mo ▪ Aggregates in NAc, BnST, Pir and OT. ▪ Few aggregates in striatum, neocortex and CA2/CA3
Home cage nocturnal activity	No differences (Yu-Taeger et al., 2012)	Increased (significant differences only at 6 mo)
Food consumption	Reduction after 3 mo (Yu-Taeger et al., 2012)	Increased during light phase
Motor symptoms	▪ Gait abnormalities at 14 mo ▪ Deficits in rotarod at 1 mo (Yu-Taeger et al., 2012) ▪ No deficits in fine motor behaviours (Manfre et al., 2017)	No differences
Psychiatric symptoms	Reduced anxiety in the EPM (Yu-Taeger et al., 2012)	Reduced anxiety in social interaction test
Cognitive symptoms	▪ Decrease in active social behaviour at 4 and 8 mo (Manfre et al., 2018) ▪ Slowed learning (Clemensson et al., 2017)	Progressive ratio showed elevated impulsivity traits
Breeding	Female rats showed reduced breeding success	No published data

Abbreviations: Amyg: Amygdala; BnST: bed nucleus of the stria terminalis; GP: Globus pallidus; mo: months; NAc: Nucleus accumbens; Pir: Piriform cortex; SN: Substantia nigra; OT: Olfactory tubercle

1.4. Cell replacement therapies (CRT)

CRT aims to replace the damaged tissue affected by injury or disease, by transplanting new cells to restore and recover the functionality of the affected area (Lindvall & Bjorklund, 2004). Over the last few decades, CRT has been in development preclinically in various neurological conditions, such as Parkinson's disease (Cardoso et al., 2018; Kirkeby et al., 2023), stroke (Palma-Tortosa et al., 2020; Tornero et al., 2017), spinal cord injuries (Katoh, Yokota, & Fehlings, 2019; van Gorp et al., 2013) and HD (Kelly et al., 2007; Lelos et al., 2016; Ma et al., 2012).

HD is a good model system for investigating CRTs, firstly, the disease predominantly affects a specific brain location, the striatum, and a specific cell population, the MSNs, providing brain and cell-type targets for homotopic transplantation of cells into the host striatum. This is an advantage, as donor cells are placed directly (homotopically) into the part of the brain from which they are lost, in contrast to PD, where the donor cells are placed ectopically into the area of the host brain where the SN dopamine cells would normally project to (Dunnett et al., 1997). Secondly, because cell loss occurs early, many years before the onset of symptoms, so cell replacement may eventually be an important complementary therapy as and when disease-modifying therapies become available. Finally, HD is a single gene disorder with full penetrance, meaning that affected individuals can be identified with certainly and can also be identified before symptom onset which is helpful in designing powerful clinical trials.

Currently, the strongest evidence of the benefits of CRT in HD has been reported using foetal tissue, either WGE or LGE, as these give rise to striatal tissue (more details in Introduction, Section 1.1.1). The use of mouse and rat embryonic tissue has been extensively studied in HD rodent models, and has been shown not only to integrate into the host brain and express mature markers of MSNs, such as DARPP32 (Deacon, Pakzaban, & Isacson, 1994; Nakao et al., 1996; Wictorin, Ouimet, & Bjorklund, 1989), but also to induce functional benefits in motor (Klein, Lane, & Dunnett, 2013; Lelos et al., 2016; Nakao et al., 1996; Watts, Brasted, & Dunnett, 2000) and cognitive tasks (Deckel et al., 1986; Dunnett et al., 2006; Isacson, Dunnett, & Bjorklund, 1986). Rat WGE transplanted cells induced improvements in motor tests, such as the paw reaching task and correlation has been shown with positron emission tomography (PET) signals, reporting significant increase of D1 and D2 receptors in animals which showed behavioural recovery in transplanted IB lesion rats (Fricker et al., 1997). Also rat WGE grafted cells were capable of creating new functional connections with the host striatum, from 5-6 weeks post transplantation, as shown by electron microscopy in KA lesion rats (DiFiglia, Schiff, & Deckel, 1988). Mouse WGE was transplanted into QA lesion mice and

not only restored synaptic transmission with the host striatum, but also the graft mediated synaptic plasticity processes demonstrated by electrophysiological recordings from 4 weeks post grafting (Mazzocchi-Jones, Dobrossy, & Dunnett, 2009). Rodent foetal tissue grafts have also been shown to extend connections to other brain regions of the basal ganglia circuit, such as the GP (Hurelbrink & Barker, 2005; Kelly et al., 2007; Klein et al., 2013; Pritzel et al., 1986; Watts et al., 2000; Wictorin, Ouimet, et al., 1989), SN (Hurelbrink et al., 2005; Kelly et al., 2007; Pritzel et al., 1986), cortex (Hurelbrink et al., 2005; Kelly et al., 2007) and thalamus (Kelly et al., 2007). Host-to-graft connectivity has been observed from the thalamus and SN using wheat germ agglutinin- horseradish peroxidase (WGA-HRP) retrograde tracer (Pritzel et al., 1986).

Unfortunately, fewer studies have explored functional recovery using human-foetal derived GE grafts into rodent models (xenografts). All published human (primary foetal striatal cells)-to-rodent data is summarized in Table 3. These transplant studies reported evidence of DARPP32 expression (Armstrong et al., 2000; Grasbon-Frodl et al., 1996, 1997; Hurelbrink et al., 2000; Hurelbrink et al., 2003; Lelos et al., 2016; Naimi et al., 1996), behavioural improvements in the vibrissae and adjusting stepping motor tasks (Lelos et al., 2016) and improvements in drug-induced rotations (apomorphine (APO) rotations) (Lelos et al., 2016; Pundt et al., 1996b; Sanberg et al., 1997). Human grafted GE cells were able to create new synaptic contacts with the host brain (Belkadi et al., 1997), innervate the host striatum and extend projections to the GP, SN, cortex (Hurelbrink et al., 2005; Kelly et al., 2007) and thalamus (Kelly et al., 2007).

So, foetal tissue transplantation had established the preclinical potential of this therapy and all this evidence led to Phase II clinical studies with HD patients. Clinical trials reported firstly that this therapy is safe with no indication of tissue overgrowth (A. Bachoud-Levi et al., 2000; Rosser et al., 2002). Secondly, post-mortem studies showed evidence of long term graft survival in the putamen after 6 (Keene et al., 2007) and 10 years post transplantation (Cicchetti et al., 2009), without presence of mHTT aggregates, differentiated into striatal phenotypes (Capetian et al., 2009; Freeman et al., 2000) and suggesting transplanted cells extended new synaptic contacts within host striatum (Cicchetti et al., 2009). Finally, although some trials had shown limited functional improvement, there were also patients who benefit from this therapy and improved their symptoms (A. C. Bachoud-Levi et al., 2000; Reuter et al., 2008; Rosser et al., 2002). In the french trial from Bachoud-Levi et al. (2000), five patients were grafted and three of them improved/stabilized their motor symptoms and attention/executive cognitive functions. Four patients were grafted in the UK study from Rosser et al. (2002) and although no significant cognitive improvements were observed, motor symptoms trend

to improvements. Finally, two more patients in the UK were grafted and results from Reuter et al. (2008) reported significant improvements in patients' motor score and significant improvements in some cognitive tests.

Preclinical and clinical evidence of CRT potential has been demonstrated with foetal tissue, however, there are many serious constraints associated with using foetal-derived donor cells; starting with ethical controversy, the difficulty accessing it, the impossibility so far of successful cryopreservation, and the challenge of performing quality control on tissue that must be transplanted within a short window after collection (Hurelbrink et al., 2003). Human pluripotent stem cells (hPSC) have emerged as a potential CRT donor product alternative, having the potential to circumvent these constraints, thus making them a much more readily applicable donor source due to its ability of self-renew, proliferation and differentiation into any mature cell-type.

1.4.1. The use of hPSC for CRT in HD

hPSCs have emerged as an alternative to foetal tissue as a cell source from which a CRT can be generated, with the aim of obtaining a cell product with similar characteristics to striatal foetal tissue (LGE). To achieve this, there are several differentiation protocols that have been generated, which are based on subpallial development signals, and which attempt to generate a CRT product with a striatal progenitor phenotype. A summary of the key studies that are mentioned in this section is shown in Table 4.

The first published protocol was reported by Aubry et al., in which SHH and DKK1 were used to promote an LGE phenotype (Aubry et al., 2008). During differentiation, cells expressed telencephalic markers as CALB1, FOXG1, SOX1, PAX6, SIX3, GAD67 and DARPP32. In later *in vitro* stages, in which cells achieved a more mature stage (DIV62-72), only 22% were MAP2 positive, meaning that only 22% of the population showed a neuronal phenotype. Of that population, 53% were DARPP32 positive and 36% GABAergic. Cells were transplanted into the QA lesion model and after 3-5 months post grafting and expression of DARPP32 was observed, around 21% of total grafted population. However, in this study, the size of the grafts was very large, and no functional assessment was performed. This was the first evidence of the possibility of obtaining striatal progenitors for transplantation using hPSC and, since this study, changes had been made to the protocol to improve the CRT product.

Table 3 – Summary of all published human foetal tissue into rodent HD models transplantation studies.

STUDY	DISSECTED TISSUE	TISSUE AGE (post conception weeks)	MODEL/ SPECIES	TRANSPLANT	FUNCTIONAL ASSESSMENT
Grasbon-Frodl et al. (1996)	MGE and LGE	6-8 weeks	IB lesion/rat	**Cells TX:** 65,000-330,000 **Graft:** 9-25 wk. D32+, low TH+; CALB+, NADPH+	N/A
Naimi et al. (1996)	LGE	5-10 weeks	KA lesion/rat	**Cells TX:** 1,000,000 - 1,500,000 **Graft:** 2, 4 and 8wk. D32+	N/A
Pundt et al. (1996b)	WGE	7, 8 and 10 weeks	QA lesion/rat	**Cells TX:** 400,000 **Graft:** 9-17 wk. AChE+, TH+, NADPH+. GFAP+ surrounding graft edges	**IHC Graft-to-host:** TH fibers within transplant neuropil
Pundt et al. (1996a)	WGE	14 weeks	QA lesion/rat	**Cells TX:** 400,000 **Graft:** 28 wk. AChE+, NADPH+	**APO:** Improvements after 11 weeks PT, being significant at 23-26wk
Sanberg et al. (1997)	LGE	7-9 weeks	QA lesion/rat	**Cells TX:** Not mentioned **Graft:** 10 wk. AChE+	**APO:** Improvements after 1mo
Belkadi et al. (1997)	Brain stem tissue	8 weeks	KA lesion/rat	**Cells TX:** 800,000-1,600,000 **Graft:** 2 wk, 1, 2 or 3 mo	**Electron microscopy:** Synaptic contacts at 3 months

Grasbon-Frodl et al. (1997)	LGE and mixed MGE+LGE	6-8 weeks	IB lesion/rat	**Cells TX:** Not mentioned **Graft:** 15-17 wk, low D32+, OX42+, Vimentin+, PCNA+	**IHC Graft-to-host:** HNF fibers within graft and graft-to-host. From the cc to the other hemisphere and along the internal capsule to the GP. GAP43 within graft and graft edges
Armstrong et al. (2000)	WGE	9 weeks	QA lesion/rat	**Cells TX:** 800,000-1,000,000 **Graft:** 12 weeks. Low D32+ and AChE+	**IHC Graft-to-host:** graft fibers extending to the internal capsule and striatal areas
Hurelbrink et al. (2000)	WGE	9-12 weeks	QA lesion/rat	**Cells TX:** 500,000 **Graft:** 6-7 wk. D32+, AChE+	**IHC Graft-to-host:** Human specific tau showed innervation of the graft edges but no projections outside of the striatum
Hurelbrink et al. (2002)	WGE	7-8 weeks	QA lesion/rat	**Cells TX:** 500,000 **Graft:** 6 wk and 6 mo. 6wk: ki67+. 6mo: D32+, AChE+, TH+. Less ki67+ than at 6wk.	**IHC Graft-to-host:** Increased of tau positive cells from 6wk to 6mo
Hurelbrink et al. (2003)	WGE	8-11 weeks	QA lesion/rat	**Cells TX:** 500,000 **Graft:** 6wk. D32+ around graft edges	N/A
Hurelbrink et al. (2005)	WGE (human, mouse and rat)	8 weeks	QA lesion/rat	**Cells TX:** 500,000 **Graft:** 4 and 12 wk.	**IHC Graft-to-host:** GFP and tau fibers found in olfactory bulb, frontal cortex, GP, SN and cerebral peduncle
Kelly et al. (2007)	WGE (human and mouse)	7-11 weeks	QA lesion/rat and mouse	**Cells TX:** 500,000 **Graft:** 12 wk	**Graft-to-host:** Used of anterograde tracers BDA, Neurobiotin and PHA-L. Graft projections found rostrally to the graft in the olfactory bulb, and caudally in the GP, SN, basal nucleus, internal capsule, corpus callosum, ventrolateral thalamic nucleus and entopeduncular nucleus.

Lelos et al. (2016)	WGE (human and rat)	~8 weeks	QA lesion/rat	**Cells TX:** 500,000 **Graft:** 21 wk. D32+, TH+	**APO:** Reduction in rotations from 15wk PT **Staircase:** No improvements **Vibrissae:** Improvements in both rWGE and hWGE **Adjusting steps:** Improvements in both rWGE and hWGE

Abbreviations: CALB: Calbindin, D32: DARPP32, N/A: Not applicable, HNF: Human Neurofilament, cc: corpus callosum, GAP43: Growth associated protein, wk: week, mo: month, PT: post-transplant

The next published evidence of the hPSC-derived striatal progenitor cells was performed by Ma et al., in 2012 (Ma et al., 2012), who optimized SHH exposure and to date, is the protocol with the highest proportion of DARPP32 positive population, obtaining a 75% from the total neuronal population. Indeed, *in vitro*, the neuronal population accounted for 93% of the total culture. Then *in vivo*, grafted neuronal population was 86% of the total and 8.43% of the population was reported as astrocytes. From the total neuronal population 62.8% were GABA positive cells and grafts contained 59% DARPP32 positive cells from the transplanted population after 4 months post transplantation in QA lesion rats. In this study, functional assessments were performed for motor symptoms and improvements in the rotarod, open field and treadscan were found after 16 weeks post graft, showing cells were able to alleviate some motor symptoms.

Subsequent studies using PA6 stromal cell co-cultured with BDNF to obtained hESC- or hiPSC-derived GABA neuronal progenitors also showed evidence of motor improvements in the QA model in the adjusting stepping test, staircase and APO rotations after 6-12 weeks post grafting (Jeon et al., 2012). As well motor improvements in genetic models of HD as the YAC128 after 3 weeks post transplantation in the rotarod (Jeon et al., 2014). In 2013, Delli Carri et al., introduced the dual SMAD inhibition (Chambers et al., 2009) in their differentiation protocol, obtaining at DIV80 51% of MAP2, 10.2% DARPP32, 30.6% CTIP2 and 40% of GABA from total population. When these cells were grafted into QA lesion rats, DARPP32 expression was observed *in vivo* after 9 weeks post grafting and improvements in APO rotations at 3-6 weeks (Delli Carri, Onorati, Lelos, et al., 2013). In 2015, Arber et al., published a new version of the differentiated protocol using the dual SMAD inhibition for the initial neural induction stages, but instead of using SHH to differentiate cells to an LGE phenotype, Activin A, a TGFβ family protein, was used instead. *In vitro,* cells displayed a rapid expression of CTIP2, NOLZ1 and FOZP1 already after 9 days and by DIV43, DARPP32 expression was around 40% and 80% for CTIP2. At 16 weeks post-transplantation of the cells in QA lesion rats, expression of GABA cells was ~85% and DARPP32 expression was ~49% of the grafted population. Unfortunately, no improvements in APO rotations were observed (Arber et al., 2015).

Transplantation in mouse models has also yielded improvements in motor tasks in QA lesion mice (Wu et al., 2018) and in the R6/2 genetically modified mouse strain (Adil et al., 2018). Interestingly, graft volumes seemed to be smaller in mutant animals compared to wild-type (WT), but no quantification was performed in the manuscript (Adil et al., 2018). Nevertheless, grafted R6/2 showed synaptic connectivity from the graft to

the SN after 10 weeks post transplantation, as assessed by Fluorogold (FG) infusion (Adil et al., 2018). More evidence of synaptic connections with the host brain was reported by Comella-Bolla et al., using transmission electron microscopy to identify efferent connections from grafted cells to GP neurons (Comella-Bolla et al., 2020).

Lastly, Besusso et al. (Besusso et al., 2020) and Schellino et al. (Schellino et al., 2023) used the monosynaptic tracer based on the modified rabies virus to assess host-to-graft connectivity in transplanted QA lesion rats. In Besusso et al., authors showed host-to-graft connectivity only within the graft and striatal areas after one and two months post grafting. However, Schellino et al. showed evidence of host-to-graft connectivity from frontal cortex, thalamus, hypothalamus, SN and amygdala after 6 months post transplantation. In both studies the same cell product was used, based on a modified version of Delli Carri et al., 2013 differentiation protocol (Delli Carri, Onorati, Castiglioni, et al., 2013). Cells at DIV50 expressed 30% CTIP2 and 18% DARPP32/CTIP2 of total *in vitro* population (Besusso et al., 2020). After the precursors were transplanted, 45.3% of the cells in the graft expressed CTIP2 and 2.8% co-expressed DARPP32/CTIP2 at 2 months post-transplant (Besusso et al., 2020). Schellino et al., reported an increase to 55% CTIP2 and 11% DARPP32/CTIP2 expression of total population after 6 months. These studies also observed improvements in motor tasks, such as the vibrissae-evoked hand placing and adjusting stepping test in Besusso et al., and in the rotarod in Schellino et al. In Besusso et al., grafted cells generated action potentials and showed spontaneous excitatory potentials. The impact of environmental enrichment was also assessed in Schelino et al., as there is evidence that an enriched environment and training could increase graft functional outcome through enhancing the degree of innervation and synaptic contacts (Dobrossy & Dunnett, 2001, 2003, 2004). Sham lesion and transplanted rats were housed in standard environment (SE) or in enrich environment (EE) and an EE not only enhanced spine density in grafted cells, but also increased the number of traced cells found in the host brain, which translated into a higher number of new synaptic contacts compared to SE grafted animals. However, when these animals were assessed in the rotarod, sham and grafted EE animals both showed improvements when compared to SE sham and the associated grafted group. This data could lead us to misinterpret that lesion rats would not need to be grafted but exposed to an EE to improve their motor symptoms, therefore is critical to unravel the mechanism behind CRT to improve our understanding behind functional recovery.

Table 4 – Summary of key manuscripts reporting human PSC derived MSN cell therapy products. Table adapted from Garcia Jareño et al., 2022 (Garcia Jareno et al., 2022)

STUDY	MODEL	CELLS	TRANSPLANT	FUNCTIONAL ASSESSMENTS
Ma et al. (2012)	Unilateral QA SCID mouse Unilateral transplant	**Source:** hESC **Target:** LGE progenitors ***In vitro:*** DIV 47 (ICC) **β-TUB** 93%; **D32** 75%; **GABA** 83.7%	**Cells TX:** 100,000 **Graft:** 4 mo, 58.6% of grafted cells were D32+/GABA+	**Rotarod**: Improved at *16 wk.* **Open field**: Improved centre ratio and crossing at *8-16 wk.* Improved total distance at *16 wk.* **Treadscan**: Improved at *16 wk.*
Jeon et al. (2012)	Unilateral QA rat Unilateral transplant	**Source:** hESC, hiPSC & HD-hiPSC (72CAG) **Target:** forebrain GABAergic NPCs ***In vitro:*** DIV 30 (ICC) **MAP2** 89%; **D32** 27%; **GABA** 75%	**Cells TX:** 200,000 **Graft:** 12 wk some D32+ cells; % not reported.	**Adjusting stepping test**: hiPSC improved at *4-12 wk.* hESC and HD-hiPSC improved at *6-12 wk.* **Staircase:** hESC and hiPSC improved at *2-12 wk*, HD-hiPSC, improved at *4-12 wk.* **APO:** hESC and HD-hiPSC improved at *6-12 wk,* compared to the sham group. hiPSC improved at *2-8 wk* only.
Delli Carri, Onorati, Lelos, et al. (2013)	Unilateral QA rat Unilateral transplant	**Source:** hiPSC/hESC **Target:** Ventral telencephalic prec ***In vitro:*** DIV 80 (ICC) **MAP2** 51%; **D32** 10.2%; **CTIP2** 30.6%; **GABA** 40%	**Cells TX:** 500,000 **Graft:** 9 wk, HuNu+/D32+ & other neuronal/MSN markers identified in graft; % not reported.	**APO**: Improved at *3-6 wk.*
Jeon et al. (2014)	YAC128 Bilateral transplant *TX at 12 mo*	**Source:** HD-hiPSC (72CAG) **Target:** forebrain GABAergic NPCs **In vitro:** reference Jeon 2012 (see above)	**Cells TX:** 100,000 **Graft:** 12 wk some D32+ cells; % not reported.	**Rotarod**: Improved at 3 *wk.*

Arber et al. (2015)	Unilateral QA rat Unilateral transplant	**Source:** hESC **Target:** LGE progenitors ***In vitro:*** DIV 43 (ICC) **D32** 40%; **CTIP2** 60%; ARPP21^{+}; CALB1^{+}; PENK^{+}; TAC1^{+}; GAD1^{+}	**Cells TX:** 400,000 **Graft:** 16wk, 86% & 49% HuNu+ cells were GABA+ & D32+ (respectively). Further MSN markers identified.	**APO:** No improvements observed.
Adil et al. (2018)	R6/2 mouse Bilateral transplant *TX at 5 wk*	**Source:** hESC **Target:** MSN precursor ***In vitro:*** DIV 60 **MAP2** 78%; **D32** 43%; **CTIP2** 54.6%; **GABA** 48%	**Cells TX:** 100,000 per hemisphere **Graft:** 12-15 wk HNA+/D32+ cells in graft; % not reported.	**Rotarod**: Improved at *5 wk.* **Clasping:** Improved at *2-20 wk.* --- **Fluorogold** injection in the substantia nigra (SN) 10 weeks after transplant showed retrograde labelling
Wu et al. (2018)	Unilateral QA SCID mouse Unilateral transplant	**Source:** hESC **Target:** LGE progenitors ***In vitro***: DIV 21 **D32** 87% of MAP2; **D32** 85% of GABA; **D32** 90% of TUJ1; **GABA** 89% of TUJ1; **CALBINDIN** - 90% of TUJ1; PSD95^{+}, SYNAPSIN1^{+}	**Cells TX:** 100,000 **Graft:** 16wk hN+ cells express 48.7% D32, 90% GABA, 90% TUJ1, 80% CTIP2, 30% SP and 10% ENK	**Rotarod**: Improved at 8-16 *wk.* **Open field**: Improved total distance at *16 wk.*
Comella-Bolla et al. (2020)	B6CBA mouse *TX at P2*	**Source:** hiPSC/hESC **Target:** Ventral telencephalic ***In vitro*:** DIV 37 **MAP2** 95-99%; **D32/CTIP2** 6%; **CTIP2** 60%; **GABA** 40% of MAP2; GSX1, GSX2, ASCL1, DLX1, DLX2, DLX5, DLX6, EBF1	**Cells TX:** 15,000 cells **Graft:** 82% Ctip2, 5% D32	**Transmission electron microscopy (TEM)** showed synaptic connections from grafted cells with GP neurons. Inhibitory and excitatory connections were identified

Besusso et al. (2020)	Unilateral QA rat Unilateral transplant	**Source:** hESC **Target:** MSN precursor ***In vitro:*** DIV 50 **CTIP2** – 30% **EBF1** – 20% **ISL1** – 15% **D32/CTIP2** – 18%	**Cells TX:** 300,000 **Graft:** 2 mo 45.3% Ctip2+ of total graft; 2.8% D32+/Ctip2+	**Rotarod:** No improvements observed. **Vibrissae-Evoked hand placing:** Improved at *1 mo,* not at 2 mo. **Adjusting step test:** Improved at *1-2 mo.* **Monosynaptic tracing using modified rabies virus**: Traced cells were only observed in the striatum. Starter and traced cell numbers were increased from 1 to 2 mo. **Electrophysiology:** at 2 mo post graft in acute brain slices. Grafted cells have a complex dendritic arborization, generate action potentials and show spontaneous excitatory potentials. **PET:** Raclopride showed no changes in expression of D2/D3 receptors compared with sham controls
Schellino et al. (2023)	Unilateral QA rat Unilateral transplant	**Source:** hESC **Target:** MSN precursor	**Cells TX:** 300,000 **Graft:** 2 mo and 6mo. 2mo: ~70% NESTIN+, ~2% GFAP+, ~40% Ctip2+ and 5% D32+/Ctip2+of total graft. 6mo: ~15% NESTIN+, ~8% GFAP+, ~55% Ctip2+ and 11% D32+/Ctip2+	**Rotarod:** Improvements from 2wk but only significant at 6mo. Sham EE animals also showed improvements compared to sham SE. **Monosynaptic tracing using modified rabies virus**: Traced cells were found in frontal cortex, thalamus, hypothalamus, Sn and amygdala after 6 mo post graft.

Abbreviations: QA, quinolinic acid lesion; TX, transplanted; mo, months; wk, weeks; HNA, human nuclear antigen; NSC, neural stem cell; NPC, neural progenitor cell; APO, apomorphine-induced rotations; D32, DARPP-32; GFAP: Glial fibrillary acidic protein; DIV, days in vitro; ICC, immunocytochemistry; P, postnatal day; EE: Enrich environment; SE: Standard environment.

1.4.2. Mechanism of CRT

To date, the mechanism(s) behind the efficacy of CRT have not been definitively established. Two broad mechanisms are hypothesized; (i) the trophic support that transplanted cells provide to host cells, protecting and supporting them and/or (ii) that transplanted cells are able to integrate and reconstruct the damage neuronal circuit.

Data from preclinical work using foetal tissue and clinical trials suggests that functional recovery is a slow process that required time, as the earliest patient who showed improvements was after 6 months post transplantation (Bachoud-Levi & Perrier, 2014), but there are preclinical studies that observed behavioural improvements in less than a month (Adil et al., 2018; Jeon et al., 2012). These fast improvements raised the possibility that the mechanism behind short-term improvements in animal models might be different to the mechanism of long-term effects. Short-term effects appear to be ligated to a first stage of trophic support, followed by, or even happening at the same time as, a long-term effect in which cells are maturing and extend new connections to the host brain (Freeman et al., 2000).

Trophic support could be through the release of neurotrophic factors, such as glial derived- and brain-derived neurotrophic factors (GDNF and BDNF) (Allen et al., 2013), or support could also be provide in other way, such as releasing neurotransmitters (Campbell et al., 1993), excretion of cell matrix factors or by modifying the environment - e.g. adjusting pH, mopping up neurochemicals, excretion of exovesicles, facilitating access to nutrients (Obara, Szeliga, & Albrecht, 2008; Sattler & Rothstein, 2006; Seifert, Schilling, & Steinhauser, 2006). An example of the benefits of trophic support is the use of mesenchymal stem cells (MSCs) as vectors to deliver trophic factors. Transgenic mouse models, such as YAC128 or R6/2, have been grafted with MSCs that were genetically modified to overexpress BDNF and showed some functional benefit, such as improvements in motor tasks, increased neurogenesis or reduction of striatal atrophy (Dey et al., 2010; Pollock et al., 2016). A different example is the use of glial cells as CRT product. Glial cells are a heterogenous population with very important supporting roles. There are studies transplanting human glial progenitor cells (Benraiss et al., 2016) that showed that transplanted R6/2 survived longer and performed better in some behavioral tasks, such as the rotarod and T-maze, compared to the sham transplanted R6/2 group. Glial cells, such as astrocytes, are a significant source of neurotrophic factors (Poyhonen et al., 2019) and could have an important role either supporting host cells or transplanted along with neuronal progenitors as a combined CRT product (White & Barry, 2015). However, when the atrophy and cells loss is extensive, supporting host cells might not be sufficient and hence the best option may be to reconstruct the damaged area.

The proposed long-term mechanism is that transplanted cells survive long-term, integrate into the host brain expressing the desire phenotype and create new synaptic connections to form new neuronal networks. The newly grafted MSNs will not recreate exactly the anatomy previous to the damage, but create new networks based on neuronal plasticity to restore the lost function (Fantie, 2015).

However, just transplanting cells to reconstruct the neuronal circuit might not be enough to recover the functionality of the area, as environment and experience could have an important effect in recovery. Transplanted animals that are maintained in environmentally enriched environments performed significantly better than standard cage animals in different behavioural tasks, as well as showing larger projection neurons and increased levels of BDNF (Dobrossy et al., 2004). Training could also have a significant impact in recovery, as rats trained in a behavioural task, striatal lesioned and subsequent grafted, need to be re-train in the trained task in order to perform it again (Brasted et al., 1999; Coffey, Lund, & Rawlins, 1989; Dobrossy et al., 2003). This fact has been termed as “learn to use the transplant” (Mayer et al., 1992).

Assessing circuit reconstruction is fundamental to gain a better understanding of CRT mechanism and, to do that, neuronal tracers are available as a tool to assess anatomical integration and neuronal connectivity.

1.4.3. Neuronal tracers

Neuronal tracers can be classified based on (i) their direction of travelling within neurons (anterograde or retrograde) and (ii) in their composition (conventional or viral tracers) (Saleeba et al., 2019). Anterograde tracers travel from the cell body to the axon, and retrograde tracers travel from the axon terminals to the cell body. Viral tracers can be categorized as static tracers, that remain within the first neuron they enter, and transsynaptic tracers that can be monosynaptic, travelling only one synapse, or polysynaptic, travelling across multiple synapses.

Conventional anterograde and retrograde tracers include enzymes, toxins or fluorescent molecules. Horseradish peroxidase (HRP), cholera toxin β-subunit (CTB) and fluorogold (FG) are examples of conventional retrograde tracers and biotinylate dextran amines (BDAs) and phytohemagglutinin-L (PHA-L) are conventional anterograde tracers (X. Xu et al., 2020). Although conventional tracers are very popular, there are limitations as their intense, diffuse and non-specific labeling (Saleeba et al., 2019), or that they can be taken up by fibers and lead to an incorrect projection’s identification (Conte, Kamishina, & Reep, 2009b; Dado et al., 1990). For example, CTB is known to be a very sensitive tracer, however, fiber uptake is a

known problem and has been reported in different studies (S. Chen & Aston-Jones, 1995; Conte, Kamishina, & Reep, 2009a), but it is still unknown if this is due to damage or undamaged fibers. On the other hand, with FG, it has been shown that damaged fibers can uptake it, where intact fibers do not (Schmued & Fallon, 1986).

Viral tracers have been used for decades, not only for their characteristics of propagation and transmission, but also to overcome conventional tracers' limitations, as they can be genetically modified to be cell or circuit type-specific. Viruses are composed of a nucleid acid (RNA or DNA) and are surrounded by a protein capsid, some viral families have an extra covering, a lipoprotein envelope (FENNER F, 1987). The capsid and the envelope are involved in interactions with the receptors of the host cell and can be changed (this is called pseudotyping) to modified vector characteristics (Payne, 2023).

1.4.4. Monosynaptic tracing based in the modified rabies virus

There are many examples of viral tracers but, since a few years ago, the glycoprotein gene (G)-deleted rabies virus (ΔG) has been used in different CRT preclinical studies (Besusso et al., 2020; Cardoso et al., 2018; Grealish et al., 2015; Palma-Tortosa et al., 2020; Tornero et al., 2017) and is the main technique used in this thesis. The rabies was the virus chosen due to its lower cytopathicity (changes in cell morphology caused by viral infection) and its greater infection efficiency than other viruses, like herpesviruses (Card, Enquist, & Moore, 1999; Ito et al., 2001; Lafay et al., 1991; Norgren & Lehman, 1998; Ugolini, 1992)

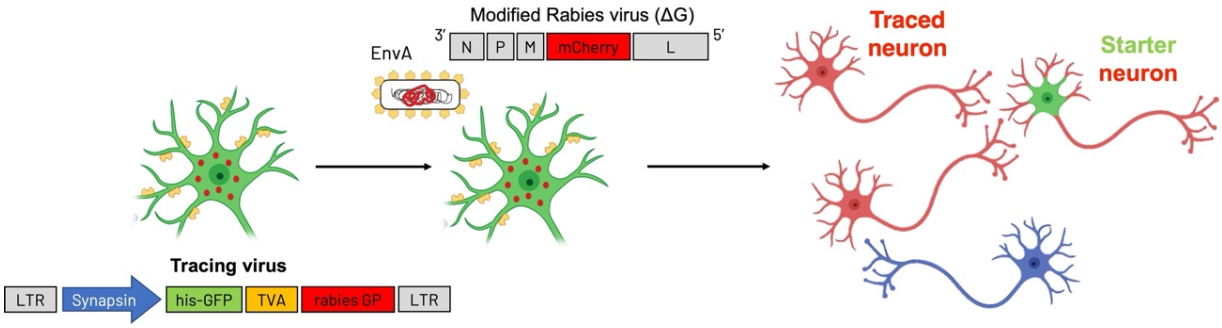

Figure 5 – Monosynaptic tracing based in the modified rabies virus. Differentiated hESC-derived MSNs expressed the tracing virus, containing the TVA receptor (in yellow), GFP (in green), rabies glycoprotein (GP in red) under the synapsin promoter (in blue) and these are the starter cells. When the modified rabies virus (ΔG-rabies) is infused, the EnvA protein recognizes the TVA receptor and attach to it infecting the cell. Therefore, the starting neuron express GFP and mCherry, and any other neuron that is making synaptic contact with it express mCherry, being a traced neuron.

The ΔG is a retrograde viral tracer that lacks its glycoprotein envelope, that is pseudotyped with the avian sarcoma leucosis virus glycoprotein EnvA. The glycoprotein gene has been exchanged for a fluorescent protein (mCherry) and, as the glycoprotein is required for transsynaptic spread, this modification limits the spread to only be monosynaptic and also, limitied to only infect cells expressing the TVA receptor, a receptor only expressed in birds but not in mammals (Barnard, Elleder, & Young, 2006; P. Bates, Young, & Varmus, 1993; Federspiel et al., 1994; Young, Bates, & Varmus, 1993). For mammalian cells to express the TVA receptor, a second virus is required, called the 'Tracing virus'. The Tracing virus is a lentivirus containing the TVA receptor, the rabies glycoprotein and the fluorescent protein GFP, all under the synapsin promoter. As represented in Figure 5, a neuron will be transfected by the Tracing virus and secondly, once the ΔG is infused, will recognize the TVA receptor and infect that cell. This cell expressing the TVA receptor and infected by the ΔG is called the starter cell and can be identified by co-labelling of GFP and mCherry. If that starter cell is making any synaptic contact with any other cell, that cell will be called the 'traced cell' and will express the mCherry protein.

1.5. Thesis aims

The aim of this thesis was to investigate if hESC-derived MSNs can reconstruct the damaged basal ganglia circuit affected by HD. To assess neuronal connectivity the main technique used was the monosynaptic tracing based on the modified rabies virus (ΔG-rabies) technology. Circuit reconstruction was investigated in two different rat model of HD.

Specifically for each chapter the aims were:

Chapter 3 aimed to investigate if hESC-derived MSNs could extend host-to-graft and graft-to-host connectivity in the QA lesion model.

In Chapter 4 there were two scientific questions to consider. First, if hESC-derived MSNs were capable of extended host-to graft connectivity in the F344tgHD transgenic model, and second, if there were any differences between host-to-graft connectivity in young or aged F344tgHD rats.

Finally, Chapter 5 aimed in the first instance to evaluate IEG as possible biomarkers to assess connectivity between the graft and the host brain. However, an unexpected finding shaped two new scientific question in this chapter: (i) why there is a significant cell loss in the GP after QA striatal infusion and (ii) how surgical parameters changes affected the behavioural output and the GP cell loss in the QA lesion model.

Chapter 2: Materials and methods

2.1. Experimental acknowledgments

In vitro procedures such as plasmid purification and viral packaging were performed by myself under supervision by Dr Marija Fjodorova. Cell sorting was performed by Jolene Twomey and CNV array was performed by Cardiff University Genomics Hub Group. ΔG-rabies was purchased from viral vector core, Kavli Institute, NTNU (Norway). Dr Kimberley Jones carried out the high throughput qPCR.

2.1.1. Chapter 3

Striatal QA lesions were performed by Dr Oliver Bartley, Olivia Edwards, Dr Mariah Lelos and myself. Transplantation and viral infusions were performed by Olivia Edwards and myself. Olivia Edwards also assisted in intracardiac perfusions. Brain sectioning, histological characterization, imaging and analysis was carried out by myself, except IF of HuNu/ki67 that was performed by Dr Charlotte Bridge and myself.

2.1.2. Chapter 4

Transplantation and ΔG-rabies infusions were performed by Olivia Edwards and myself. Olivia Edwards also assisted in intracardiac perfusions. Brain sectioning, histological characterization, imaging and analysis was carried out by myself.

2.1.3. Chapter 5

Experimental in vivo procedures and brain sectioning from Experiment 4 was performed by Dr Mariah Lelos and from Experiment 5 by Dr Harri Harrison. Procedures from Experiment 6 and 7, as well as brain sectioning, histological characterization, imaging and analysis was carried out by myself.

2.2. Lentiviral production of psPAX2 and pMD2.G

2.2.1. Transformation of DNA plasmids

The plasmids required for the lentivirus expression of TVA receptor and histone-GFP, under the synapsin promoter, were stored in L-glycerol aliquots at -80°C. These plasmids are psPAX2 (p756) (#12260, Addgene) and pMD2.G (p757) (#12259, Addgene).

Bacterial cultures were prepared by scratching, with 20-200µl pipette with a tip, the frozen culture of each of the plasmids separately. The tip was dropped into 3ml LB medium with ampicillin (100µg/mL) in 15ml centrifuge tubes and incubated for ~6hr at 37°C on the shaker. After this time, cultures were cloudy and 1ml was transfered to 150ml LB medium with ampicillin (100µg/mL) and incubated overnight at 37°C on the shaker.

2.2.2. DNA purification

Purification of plasmid DNA was performed using MAXIprep kit (QIAGEN, #12163), following the manufacturer protocol. DNA was resuspended in 1xTE buffer for long term storage at -20°C.

2.2.3. DNA digestion

A restriction enzyme digestion was performed for each of the obtained plasmids to confirm DNA obtained corresponded to the appropriate plasmid. For the reaction, 1 µg of DNA was mixed with 2 µl of the corresponding NEB 10x buffer, 1 µl of each restriction enzyme(s) and appropriate amount of PCR-grade water to bring a total volume of 20 µl. Samples were incubated at 37°C for 2-3h. Details of restriction enzymes are in Table 5. Once the reaction is complete, samples were mixed with 6x loading dye and run on 1% agarose gel at 90V for 2h. The gel was checked under ultraviolet (UV)-light.

Table 5 – Plasmids and corresponding restriction enzymes

Plasmid and catalog number	**Total plasmid size (bp)**	**Restriction enzymes (single cutters)**	**Digestion products (bp)**	**Catalog number NEB**
psPAX2 (p756) #12260	10,668	Afl II Nhe I HF	8683bp 1985bp	R0520S R3131S
pMD2.G (p757) #12259	5822	Age I HF Not I HF	4352bp 1470bp	R3552L R3189L

2.2.4. Viral packaging

HEK cells were used to generate the lentivirus (LV) carrying pMD2.G and psPAX2 plasmids. Cells were cultured and maintained in T25 flasks with DMEM, FBS (Thermo Fisher), NEAA (100X, Thermo Fisher), L-Glu (200mM, Thermo Fisher) and MycoZap™ (Lonza) until

the desired confluency was reached (~95-99%). Cells were transfected using lipofectamine 3000 (P3000) (Thermo Fisher) following the manufacturer instructions. Two solutions need to be prepared for this procedure, solution A (OptiMEM media (Thermo Fisher) with lipofectamine) and solution B (OptiMEM media with 14µg pBOB-HTB, 5µg pMD2.G and 9µg psPAX2). Solutions A and B were mixed (1:1) and incubated for 15 min at room temperature. Then 50% volume of media was removed from the cells, 'A and B' mix was added, and cells were incubated for 6h at 37°C. Afterwards, media was removed and replaced by LV packaging media (OptiMEM, 5% FBS and sodium pyruvate (1mM, Thermo Fisher)). After 24h, first viral supernatant was collected, cell media was replaced with fresh LV packaging media, cells were incubated further at 37°C and 52h post transfection, the second viral supernatant was collected.

Each supernatant was frozen down and stored at -80°C, or directly concentrated through ultracentrifugation (Optima XPN 80 Ultracentrifuge, Thermofisher, with SW 32 Ti rotor, at 90,000g, 2hrs and 30mins, 4˚C). Following centrifugation, the viral pellet was resuspended in 200µl of distilled water, aliquoted and stored at -80°C.

2.2.5. Viral titering in hESC-derived MSNs

Both lentivirus batches were tested in DIV27 hESC-derived MSNs. Cells were transfected using serial dilutions of the vector (Figure 6) and incubated for 24h. A control with viral-free media was included and cells were fixed after 5 days with 4%PFA for 10minutes. Afterwards fixed cells were washed 3 times with PBS, incubated for 5minutes with DAPI and washed 3 times again with PBS. Wells were covered with coverslips using fluorescence mounting media (Dako) for subsequent imaging and quantification.

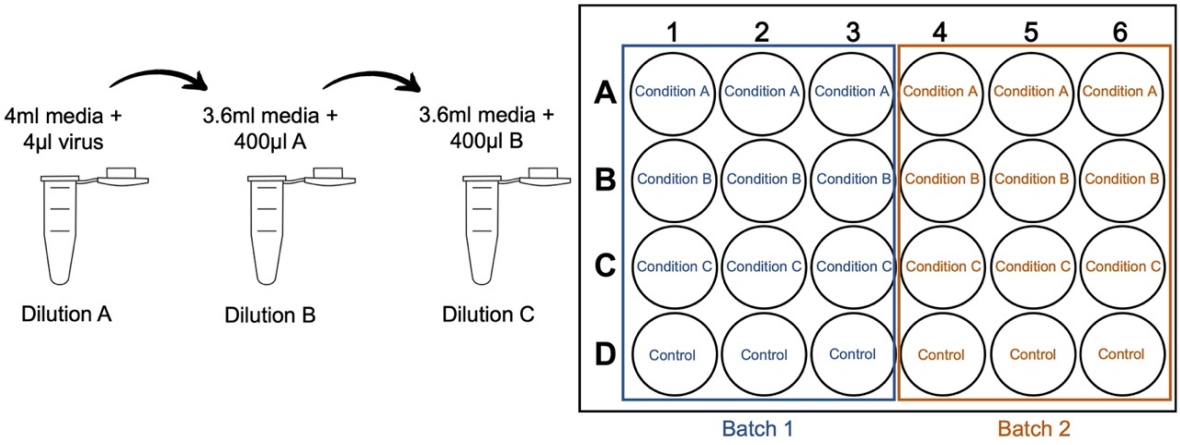

Figure 6 – Representation of viral tittering dilution and well-plate conditions. Two viral batches, batch 1 and batch 2 were tested in a 24 well plate. Dilution A is for Condition A, Dilution B for Condition B and Dilution C for Condition C.

For quantifications, five fields of each well were randomly acquired and the number of DAPI and GFP positive cells were counted on each field. The titer was calculated using the following formula:

$$Titer\left(\frac{particles}{ml}\right) = \frac{number\ of\ target\ cells\ (at\ day1)\ x\ proportion\ of\ GFP\ cells}{Volume\ of\ vector\ in\ (ml)}$$

2.3. Stem cell culture

2.3.1. Culturing and expansion of human ESCs

Cell culture experiments were conducted in a Class II Safety Cabinet under sterile conditions. Cells were grown on treated cell culture plastic Nunc™ multi-well plates (Thermo Scientific) and maintained in an incubator at 37°C and 5% CO_2. hESCs were cultured in 6 well plates and differentiation of hESCs was performed in 12 well plates. Subsequent characterization of differentiated cells was performed in 96 well plates (Details of plate diameters and volumes is on Table 6).

The hESC RC9 line from Roslin Cells was the line used for all experiments in this thesis. Cells were used between passage 35 and 50 (p35-p50). Expansion and maintenance of hESC cultures was performed using Matrigel™ Matrix (Corning) coated plates and Essential 8 (E8) Flex™ medium (Thermo Fisher). Media changes were performed every other day and cell passaging was performed at around 80% of confluency. Passaging was performed approximately every 4-5 days at a 1:3-1:6 ratio depending on experimental requirements. There was no cell quantification for plating after every passage.

Table 6 – Cell culture plate types, diameter and volume per well

Well type	Plate diameter	Volume of media per well
6 well plate	9.6 cm^2	2-4ml
12 well plate	3.5 cm^2	2ml
24 well plate	1.9 cm^2	1ml

For cell passaging, media was removed, and cells were washed once with Dulbecco's phosphate-buffered saline (DPBS) (Thermo Fisher). Afterwards, Gentle Cell Dissociation Reagent (GCDR) (STEMCELL Technologies) was added to the well (1ml/well in a 6 well plate) and the plate was placed back in the incubator for 2mins until cells showed signs of detachment. Then, GCDR was removed, and fresh E8 Flex was added. Cells were scraped

from the well using a 5ml stripette and collected into a 15/50ml tube for centrifugation at 1500 RPM for 3minutes. Supernatant was aspirated and the pellet was carefully resuspended in fresh E8 Flex media, avoiding single cell suspension. Cells were then plated into a new plate at the desired passage ratio.

2.3.2. Directed differentiation of hESC towards a striatal Medium Spiny Neuron fate

Human ESCs were differentiated using a modified version of a published protocol (Arber et al., 2015) (Figure 7). Cells were plated in 12-well plates coated with Reduced Growth Factor (RGF) Matrigel™ (Corning) and maintained with Essential 8 (E8) Flex™ medium. The protocol starts when cells reached 70-80% confluency (Days *in vitro* (DIV) 0) and media was changed to N2B27 media, consisting of 1:1 DMEM/F12 and Neurobasal medium (Gibco), 1% L-glutamine (Gibco), 1% N2 supplement 100x (N2; Gibco), 2% B27 without retinoic acid supplement 50x, (B27-RA; Gibco), 0.2% MycoZapTM plus CL (Lonza), 0.1% β-mercaptoethanol (Gibco). N2B27 media was supplemented with 0.1 μM LDN-193189 (LDN; Tocris), 20 μM SB-431542 (SB; Tocris) and 1μM XAV939 (XAV; Tocris) until DIV 5, when SB was removed. Fresh media was replaced every other day.

On DIV10, cells were passaged (P1). Cells were incubated for 1h at 37°C with N2B27 with 50ng/ml Activin A (R&D), 1μM XAV and 10μM Y-27632 (ROCK inhibitor; Millipore). Media was collected into a 50 ml tube and cells were washed with DPBS and incubated in EDTA for 1-2mins at 37°C. EDTA was removed, and the previous collected media was added back to the cells. Using a 5ml pipette and a cell scraper, cells were gently scraped and collected into a new 50ml tube. The suspension was pipetted up and down 2 to 3 times to dissociate larger clumps and cells were split at a 2:3 ratio and plated into a new 12-well plate coated with PDL/Fibronectin (15μg/ml, Millipore). Media was replaced the following day with N2B27, Activin A and XAV. Media was again replaced for fresh media every other day.

On DIV20, cells were passaged a second time (P2) and of note at this step, the cells can be cryopreserved. Media was removed and cells were washed once with DPBS and incubated with Accutase (Sigma) for 10min at 37°C. After the first 5 minutes, the plate was removed from the incubator and cells were detached by gently pipetting up and down the Accutase. After 5 more minutes, Accutase was gently pipette over the surface of the well to complete the detachment and the suspension was collected in a 50ml tube. The same volume of N2B27 media was added to the 50ml tube to stop the dissociation process and a sample of cells were taken to be counted while the suspension was centrifuged for 12 mins at 1200RPM.

After centrifugation, cells were either frozen at 5,000,000 cells per vial (Section 2.3.3) or re-plated at a density of 100,000 cells/cm^2 into N2B27 media with RA with 20ng/ml BDNF (Peprotech), 0.1 mM dbcAMP (Sigma), 0.5 mM valpromide (Sigma) and 25 ng/ml Activin A on PDL/Laminin (10µg/ml, Sigma). Media was replaced every 5 days.

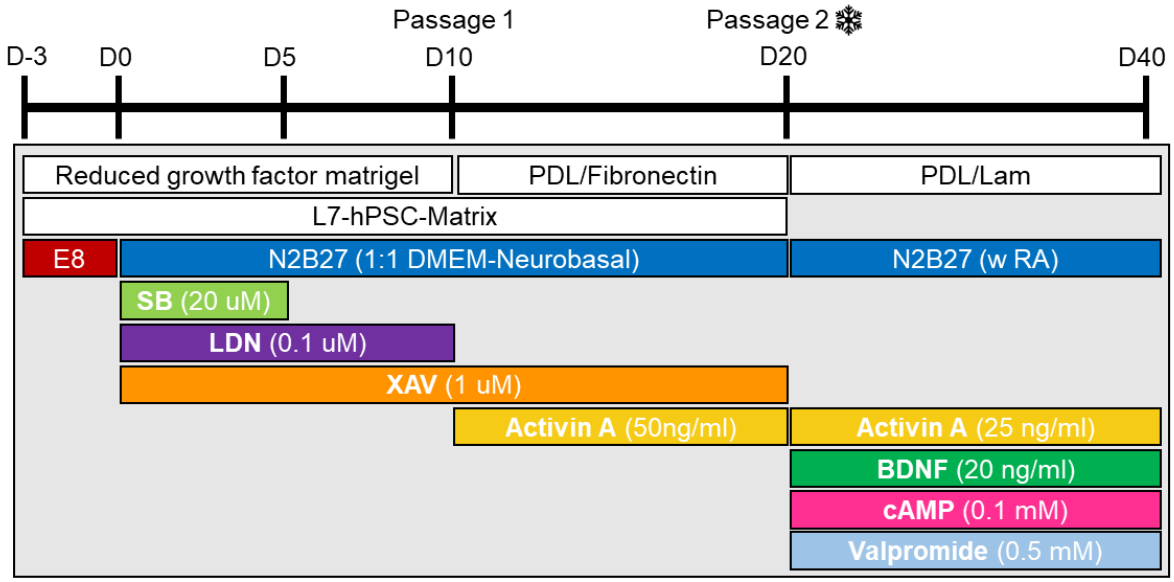

Figure 7 - Timeline of differentiation protocol for MSNs – Protocol started with hESC cells plated either on reduced growth factor Matrigel or L7-hPSC matrix on D-3 in E8 media. Cells were passaged on DIV10 and DIV20 and also on DIV20 cells were cryopreserved. Cells were maintained until DIV40 and fixed for immunocytochemistry.

2.3.3. Freezing and thawing of hESC and hESC-derived MSNs

After detachment from the well plate and subsequent centrifugation, the cell pellet was resuspended in the required amount of Cryostor CS10 freezing media (StemCell Technologies) and transferred into a cryovial. Vials were stored for 24h (or the weekend) in a Cool Cell Freezing Container (BioCision) at -80°C and then transferred to liquid nitrogen for long term storage. For hESC cryopreservation, cells were not quantified, so 1 well of a confluent 6-well plate (70-80% confluency) was frozen into three vials. For hESC-derived MSN progenitors, cells were counted, and 5,000,000 cells/vial were frozen.

For thawing cells, a vial was placed into an automated cell thawing platform (ThawSTAR, Biocision) and suspension was gently added dropwise into a 15ml tube containing 9ml of the relevant basal maintenance media (E8 for hESC and N2B27 for hESC-derived MSN progenitors). Cells were centrifuged at 1000RPM for 3 min and the cell pellet was resuspended in the required volume of fresh media supplemented with RevitaCell™ 100X (Gibco) under the appropriated cell culture conditions (For hESC details in section 2.3.1 and for hESC-derived MSN progenitors details in section 2.3.2).

2.3.4. Cell suspension preparation for transplantation

On the day of transplantation cells were thawed from liquid nitrogen following adapted thawing protocol from section 2.3.3. Thawing media was N2B27 (25ml DMEM, 12.5ml Neurobasal, 0.25ml N2, 0.25ml B27 and 0.375ml L-Glutamine). Once cells were thawed, cell suspension was gently added to the 15ml tube and the cryovial was washed with 500µl fresh N2B27 media and again added gently to the 15ml tube. If more than one vial was thawed, this procedure was repeated. Once all vials were thawed, cells were centrifuged for 5minutes at 300g, supernatant was discarded, and the cell pellet was resuspended in 1ml N2B27 media. For cell quantification, 5µl cell suspension was diluted in 45µl N2B27 media and from that dilution, 10µl was mixed with 10µl Trypan blue (0.4% Trypan blue solution, Thermo Fisher) (1:20 dilution). From that dilution 10µl was added into the hemocytometer chamber (Marienfeld) for counts. Four squares from the chamber were counted and the number of cells was calculated using this formula:

$$\frac{Number\ of\ cells}{ml} = \frac{Total\ cell\ counts}{Number\ of\ squares} \times 20 \times 10 \times 1000$$

In the meantime, cell suspension was transferred to a 1.5ml Eppendorf tube and centrifuged again at 1000RPM for 3 min. Supernatant was discarded and the cell pellet was resuspended in N2B27 with Dornase alpha (20U/ml, Pulmozyme, Roche) (1ml of N2B27 with 20 µl of dornase alpha) to obtain 250,000 cells/µl.

2.3.5. Generating a hESC line expressing the TVA receptor required for the rabies tracing

The RC9 hESC line was transfected with the LV containing the TVA-GFP-G construct (Details in Section 2.3.5.1) and cell sorted for GFP (Details in Section 2.3.5.2). Cells were re-plated after sorting, maintained and banked.

Cells generated the standard colonies expected of a pluripotency culture (Figure 8A) and were also differentiated to an MSNs phenotype (Differentiation protocol in detail in Section 2.3.2, Figure 8B). Genomic DNA from the hESC-TVA-GFP-G line and from a hESC-RC9 control line were sent to Cardiff University Genomic Hub for CNV array. The results revealed that both samples had a similar deletion at 8q24.23 (Chromosome 8) and a duplication at 20q11.21-q11.22 (Chromosome 20).

GFP expression was confirmed by qPCR (Section 2.3.8, Figure Figure 8C), showing a band of 490 bp in both samples; at a pluripotent stage (hESC-RC9) as well as during differentiation (DIV 10).

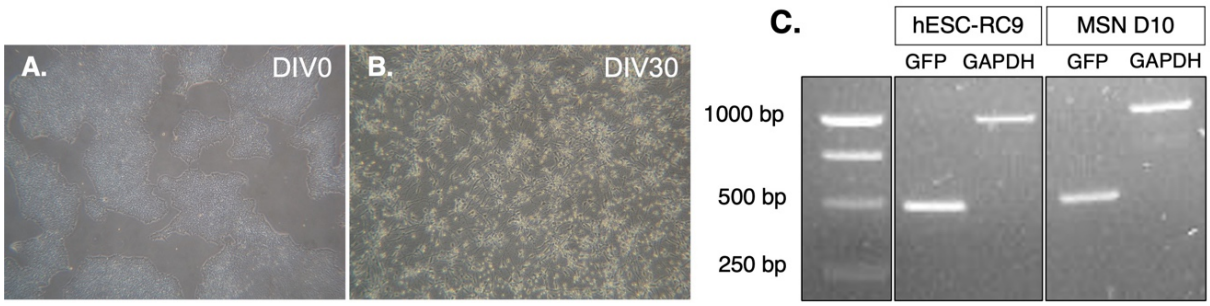

Figure 8 – Generation of a new hESC line expressing the TVA-GFP-G construct. Brighfield images of hESC-TVA-GFP-G derived MSNs on (A) DIV0 and (B) DIV30 of differentiation. (C) Agarose gel image from qPCR run. Two samples were run, one for the hESC-TVA-GFP-G line and a second sample from DIV10 of the MSN differentiation of this line. Both samples yielded a band of 490bp corresponding to GFP and a band for the housekeeping gene GAPDH, at 1000bp.

2.3.5.1. Transfection of hESC with LV-TVA-GFP-G

RC9 cells were plated in a 6-well plate and transfected at p39 with three different viral concentrations and with a GFP plasmid as a positive control, using lipofectamine 3000 (P3000) (Thermo Fisher) and following commercially available protocol (Check for L3000001). After 24h, media was changed, and cells were maintained and split once before undergoing cell sorting.

2.3.5.2. Cell sorting

On the day of sorting, cells were incubated 1h with 1X RevitaCell™, washed, harvested with TryplE (Life Technologies Inc) and centrifuged at 250g for 3 mins. Cells were resuspended in E8 and kept on ice for transport them to the cell sorter.

The sorting was performed in a FACS sorter (FACS Aria Fusion, BD Biosciences) by the technician of the facility, Jolene Twomey. Sorting parameters were established based on the GFP positive control. After sorting, an average of 700 cells were plated in a 6-well plate and approximately 50 cells per well of a 96-well plate. Cells were kept in E8 media supplemented with 1X RevitaCell™ and FGF2 (10ng/ml, Sigma) for 24h. After this time, cells were maintained, passaged and cryopreserved as a standard hESC culture, detailed in section 2.3.1.

2.3.5.3. Transfection of hESC(GFP-TVA)-derived MSNs with the EnvA pseudotyped ΔG mCherry rabies tracer

Differentiated hESC-GFP-TVA RC9 cells at DIV20 were platted on 24-well plate at a density of 100,000 cells/cm^2. On DIV36 media was changed for a media containing the ΔG-rabies virus at two different multiplicities of infection (MOI), MOI 0.5 and MOI 1 (Figure 9). Media was changed after 24h and cells were imaged after 3 days.

Cells expressed GFP in culture and were successfully infected by ΔG-rabies as show in Figure 10 by positive mCherry expression in both groups MOI 1 and MOI 0.5.

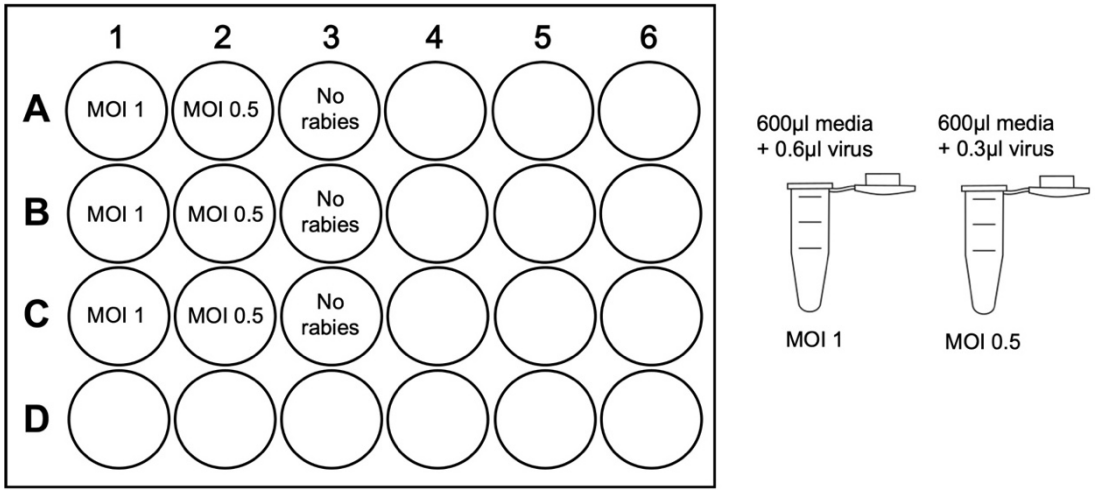

Figure 9 - Well plate representation of transfected hESC-derived MSNs expressing TVA-GFP-G using ΔG-rabies virus. Nine wells of a 24-well plate were plated with DIV20 hESC-derived MSNs expressing the TVA receptor, GFP and rabies glycoprotein. On DIV36 three wells were transfected with ΔG-rabies MOI 1, three wells with ΔG-rabies MOI 0.5 and three wells without transfection as control. MOI 1 contains 600µl of media with 0.6 µl of ΔG-rabies and MOI 0.5 contains 600µl of media with 0.3 µl of ΔG-rabies. MOI: Multiplicities of infections; DIV: Days *in vitro*.

2.3.6. RNA extraction

RNA extraction in this thesis was performed on *in vitro* cultured cells. Cells were detached as detailed in section 2.3.1 or 2.3.2 and processed for RNA extraction using the Qiagen RNAeasy mini kit and QiaShredder (Quiagen, UK) following manufactures's protocol. RNA concentration was measured using a NanoDrop™ (NanoDrop™ one, ThermoFisher Scientific) and samples were stored at -80°C until processed for cDNA synthesis.

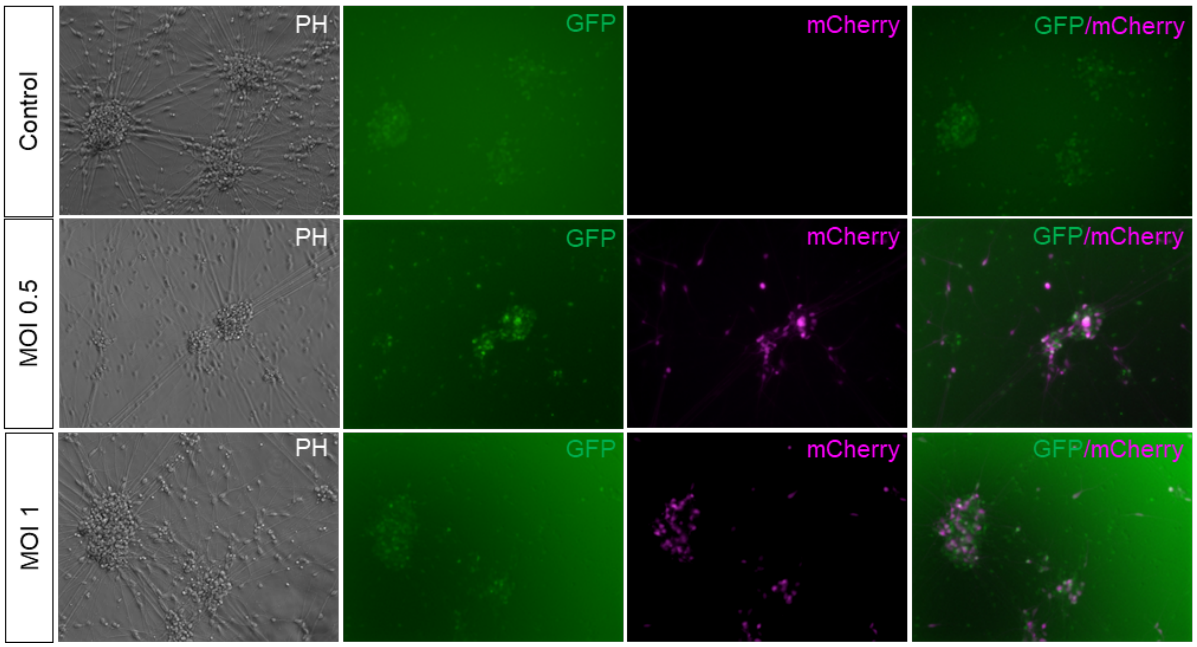

Figure 10 – Differentiated hESC-TVA-GFP-derived MSNs were infected with rabies virus on DIV38. Three groups were tested, control group with no virus, and two different ΔG-rabies concentrations, MOI 0.5 and MOI 1. Figure shows PH images in the first column, GFP fluorescence images in the second column, mCherry fluorescence in the third column and co-labelling of GFP and mCherry in the last column. MOI: multiplicities of infections; PH: Phase contrast.

2.3.7. cDNA synthesis

Synthesis of cDNA was performed with up to 1µg RNA. To remove genomic DNA ezDNase kit (Invitrogen) was used, following manufacturer's instructions, before synthesis of cDNA. Following this, RNA was incubated with 50µM random primers (Eurofins Genomics) and 10mM dNTP buffer (Invitrogen) for 5 mins at 65°C and afterwards kept on ice for 1min. RNA was then mixed with SuperScript™ IV First Strand buffer (Invitrogen), 100 mM DTT, RNaseOUT™ Recombinant RNase Inhibitor (Invitrogen), and SuperScript™ IV Reverse Transcriptase (Invitrogen) and incubated for 10 mins at 23°C, 10 mins at 55°C and 10 mins at 80°C. cDNA was stored at -20°C.

2.3.8. Reverse Transcription Polymerase Chain Reaction (RT-PCR)

RT-PCR was performed following PCR Biosystems HS Taq Mix Red protocol. Final total volume reaction was 50µl consisting of 25µl 2x PCRBIO HS Taq Mix Red, 2µl of 10µM forward primer (Table 7), 2µl of 10µM reverse primer (Table 7), 1µl template DNA (70ng) and the remaining volume was 20µl of PCR grade dH_2O. The qPCR reaction consisted of an initial denaturation at 95°C for 1 minute, and then underwent 32 cycles of denaturing at 95°C for 15

seconds, annealing at 57°C for 15 seconds and extension at 72°C for 90 seconds. PCR products were visualized by electrophoresis using 1.5% agarose gel. Samples were run at 92V for 50 mins and visualized using SafeView™ (ABM) under a UV light.

Table 7 - PCR primer details

Gene	Forward Primer (5'-3')	Reverse primer (5'-3')
GAPDH	GTCGGAGTCAACGGATTTGG	ATGGAATTTGCCATGGGTGG
GFP	ACGTAAACGGCCACAAGTTC	GGTGTTCTGCTGGTAGTGGT

2.3.9. High throughput qPCR

High throughput qPCR was performed by Dr Kimberly Jones. The cDNA samples from both cell products were provided to her. Samples were preamplified using Preamplification master mix following a thermal cycler program of 2 minutes of 95ºC hold and 14 cycles of 15 seconds at 95ºC and 4 minutes at 60ºC; finally, there was a 4ºC hold. Reactions preamplifed products were cleaned using Exonuclease I, digested at 37ºC for 30 minutes and inactivated at 80ºC for 15 minutes. Gene expression on diluted preamplified samples (1:5 diluted in DNA suspension buffer) was performed using SsoFast EvaGreen Supermix and binding dye. Primers used for each of the selected genes are on Table 8. For reference guides refer to Fluidigm: PN 1000-7070 and PN 100-9792.

Table 8 – Primers used for high throughput qPCR

Gene	Forward Primer (5'-3')	Reverse primer (5'-3')
UBC	GGGATTTGGGTCGCAGTTCT	GTCAAGTGACGATCACAGCG
ATP5F1B	TCTGCTAGCTCCCTATGCCA	CTCCAGCACCACCAAAAAGC
DARPP32	CTG AGG ACC AAG TGG AAG AC	GAT GTC CCC TCC ACT TCC TC
GAPDH	CAATGACCCCTTCATTGACC	GAC AAG CTT CCC GTT CTC AG
FOXP1	TGC AAG AAT CTG GGA CTG AG	AGA CCG CCG CAC TCT AGT
FOXP2	GGGGCCTCTCACACTCTCTA	CACCACCTGCATTTGCACTC
EBF1	GTG GAG ATC GAG AGG ACA GC	AAG CTG AAG CCG GTA GTG AA

DRD1	TGCCATAGAGACGGTGAGTA	CAGCATGTGGGATCAGGTAAA
DRD2	CTCTTCGGACTCAATAACGCA G	GACGATGGAGGAGTAGACCAC
FOXG1	AGA AGA ACG GCA AGT ACG AGA	TGT TGA GGG ACA GAT TGT GGC
DLX2	GCC TCA ACA ACG TCC CTT ACT	TCA CTA TCC GAA TTT CAG GCT CA
SHH	CTC GCT GCT GGT ATG CTC G	ATC GCT CGG AGT TTC TGG AGA
Nkx2.1	AGG ACA CCA TGA GGA ACA GC	CCC ATG AAG CGG GAG ATG
GSX1	AGTTCCACTGCATCTCTGTG	GGCGGGACAGGTACATATTAG
ETV1	TGCATATGACTCAGGCTGTAT GTT	GTGATCCTCGCCGTTGGTAT

Control tissue was LGE coming from products of conception that were donated through medical terminations of pregnancy using South Wales Initiative for Foetal Tissue (SWIFT). Tissue was dissected by tissue bank staff at Brain Repair Group, Cardiff University and stored in physiological medium (Hibernate-E) at 4 degrees until collection and processing. All used samples with correspondent age and crown-to-rump length are summarized on Table 9. All procedures were approved by ethics committee (project # SWIFT-RTB45).

Table 9 – SWIFT foetal samples information

Name	**Age (post conception day)**	**Crown-to-rump-length (CRL)**
SWIFT #2449	71	~70
SWIFT #2452	63	~59.6
SWIFT #2457	76	~71.5
SWIFT #2458	82	~87
SWIFT #2459	62	~46
SWIFT #2462	73	~52
SWIFT #2544		116

SWIFT #2513	92	113
SWIFT #2535	86	95

2.3.10. Immunocytochemistry (ICC)

Cells were washed once with DPBS and fixed with 4% PFA for 10min. Afterwards wells were washed three times with DPBS. Cells were incubated for 10 minutes with PBST (5ml PBS with 10µl Triton X-100 0.2% pH 7.4) and washed again three times for 5 minutes with PBS. Subsequently cells were blocked for 1h in blocking solution (3% BSA with 3% of appropriate serum) and incubated overnight at 4ºC with primary antibody (Table 10) in 3% BSA. The following day cells were washed in PBS three times and incubated for 1h in secondary antibody (Table 10) in 3% BSA with 1% serum, at room temperature. Then cells were washed again three times in PBS, incubated in Hoechst (1:10,000 in 3%BSA) for 5 minutes and finally washed three times in PBS. Cells were kept in PBS and plates were stored at 4°C.

Table 10 - Primary and secondary antibodies used for immunocytochemistry.

Primary antibody	**Species**	**Concentration**	**Supplier**	**Cat no.**
CTIP2	Rat	1:500	Abcam	Ab18465
FOXP1	Rabbit	1:250	Abcam	Ab16645
hDARPP32	Rabbit	1:500	Abcam	Ab40802
β-tubulin	Mouse, monoclonal	1:400	Merck	T8660
Secondary antibody	**Species**	**Concentration**	**Supplier**	**Cat no.**
Alexa 594 goat anti rabbit	Rabbit	1:200	Invitrogen	A21207
Alexa 594 goat anti mouse	Mouse	1:200	Invitrogen	A11032
Alexa 594 goat anti rat	Rat	1:200	Invitrogen	A11007

2.4. Animal health care and surgical procedures

2.4.1. Animal models and health care

All the animal experiments were performed in compliance with local ethical guidelines and approved animal care in accordance with the United Kingdom Animals (Scientific Procedures) Act 1986 and its subsequent amendments.

All rats were housed in cages with up to 3 (males) or 4 (females) animals, under standard conditions in a 14:10 light/dark cycle with lights on between 6am and 8pm. Animals had access to food and water *ad libitum*, unless further experimental requirement. Temperature and humidity were maintained at 21±2°C and 60±1% respectively.

Grafted animals received daily immunosuppression with intra-peritoneal injections of 10mg/kg Cyclosporine A (Novartis). Animal weights were checked weekly and Cyclosporine A dose was adjusted accordingly.

Lister Hooded rats

Adult female Lister Hooded rats (Charles River, UK) weighing 200-250g were used for QA lesion and subsequent transplantation in Chapter 3 and QA lesions from Chapter 5. Animals were delivered to the facility and left for 1 week to acclimatize to the new environment before starting any procedure.

F344tgHD rats

Transgenic F344tgHD male and female rats were bred in the animal facility. Heterozygous male and female were mated, and litters were weaned 21 days after birth. Males and females were housed in separate cages but in the same holding room. Animals at 4- and 14-months old were used for transplantation studies (Chapter 4).

2.4.2. General surgical procedures

On surgery day animals were weighed before the procedure and placed in an induction chamber to be anaesthetized using 5% isoflurane gas (Abbott, UK) in oxygen. Once the animal was anesthetized, the head was shaved, and the rat was positioned in the stereotactic frame. The animal was maintained under anaesthesia during the whole procedure, using 2-3% of isoflurane with oxygen through a nose mask. A subcutaneous (s.c.) injection of the painkiller meloxicam 2.5mg/kg (Metacam, Boehringer Ingelheim, Germany) was administered before the surgery. Before creating the incision, swabbing of the surgical area was performed using a dilute povidone-iodine solution (Videne) and 70% Ethanol solution. Skull was exposed and

bregma was located. Holes were drilled as required, at the anterior-posterior (AP) and medio-lateral (ML) stereotaxic coordinates described in each of the following procedures.

When the stereotactic procedure was finished, a s.c. injection of 5 ml 0.9% glucose saline was administered to prevent dehydration and the incision was closed with Vicryl™ sutures (5-0 for females and 4-0 for males, Ethicon, UK). Animals were placed into a warm recovery chamber before being returned to their cages.

2.4.3. Unilateral striatal lesion using Quinolinic Acid

Lesion surgery was performed unilaterally, using stereotactic coordinates in Lister-Hooded female adult rats using the neuroexcitotoxin quinolinic acid (QA, Sigma-Aldrich, UK, P6320-4). The toxin solution was prepared on the surgery day, diluting the stock concentration to 0.09M using 0.1 M phosphate-buffer solution (PBS, Thermo Fisher) and kept it on ice.

General surgical procedures were described in Section 2.4.2. QA toxin was delivered using a Hamilton syringe to deliver the toxin. Infusion volume was 0.5µl per site (total volume of 1µl per hemisphere) at 0.25µl/minute at each depth (1 minute per infusion site). Diffusion time was 3 minutes per dorsal site. When the surgery was finished a s.c. of diazepam (Hameln Pharmaceuticals Ltd, UK) was administered to prevent seizures.

Lesion coordinates for Chapter 3 were Site 1: AP +0.4, ML -3.0, DV -4, -5 and Site 2: AP +1.2, ML -2.9, DV -4, -5. Lesion coordinates used in Chapter 5 are presented in Table 11. Tooth bar was set at -2.3mm in all cases.

2.4.4. Striatal transplantation

Cell suspension was prepared as described in section 2.3.4 and was kept on ice during the whole procedure. Surgical procedure was as described in Section 2.4.2, using a 5µl Hamilton syringe to deliver the cell product. The stereotactic coordinates were AP +0.8, ML ±2.9 and DV -4, -5. Infused volume was 1µl per depth and a total of 2µl per hemisphere at 1µl per minute at each depth. Diffusion was 3 minutes per dorsal site. Tooth bar was -2.3mm.

Table 11 – Surgical coordinates for QA lesion groups

Group name	**Original**	**Coord 1**	**Coord 2** (high dose)	**Coord 2_LD** (low dose)	**Single**	**GP**
Coordinates	**Site 1:** AP -0.4 ML -3.7 DV -4,-5 **Site 2:** AP +1.2 ML -2.9 DV -4,-5	**Site 1:** AP +0.2 ML -3.6 DV -4,-5 **Site 2:** AP +1.2 ML -2.9 DV -4,-5	**Site 1:** AP +0.4 ML -3.0 DV -4,-5 **Site 2:** AP +1.2 ML -2.9 DV -4,-5	**Site 1:** AP +0.4 ML -3.0 DV -4,-5 **Site 2:** AP +1.2 ML -2.9 DV -4,-5	AP -0.4 ML -3.7 DV -4,-5	AP -1.2 ML -3.2 DV -6
QA volume	1µl	1µl	1µl	0.5µl	1µl	1µl

Coord 1: Coordinates 1; Coord 2: Coordinates 2; Coord 2_LD: Coordinates 2 Low Dose; GP: Globus pallidus; AP: Anteroposterior; ML: Mediolateral; DV: Dorsoventral; QA: Quinolinic acid.

2.4.5. Viral infusion (TVA-GFP-G and ΔG-rabies)

Dilution of TVA-GFP-G and ΔG-rabies viruses was performed in DPBS in a Class II Safety Cabinet under sterile conditions and virus was kept on ice during the whole surgical procedure. Infusion of LV-TVA-GFP-G virus was performed using a cannula. Coordinates for the infusion in the GP were AP -1.2, ML -3.2 and DV -6, -6.5, -7. Infusion volume was 0.5µl per depth (total of 1.5µl per site) at a rate of 0.2µl/minute at each depth. Diffusion was 2 minutes per dorsal site. Tooth bar was -2.3mm.

Coordinates for the infusion in the SN were Site 1: AP -5.3, ML -1.6 and DV -7.2 and Site 2: AP -5.3, ML -2.6 and DV -6.7. Infusion volume was 1µl per site (total of 2µl per site) at a rate of 0.2µl/minute at each depth. Diffusion was 2 minutes per dorsal site. Tooth bar was -3.5mm.

Infusion of ΔG-rabies was performed using a Hamilton syringe. For host-to-graft connectivity, stereotactic coordinates were Site 1: AP +0.4, ML ±3 and DV -4 and -5; Site 2:

AP +0.8, ML ±2.9 and DV -4 and -5 and Site 3: AP +1.2, ML ±2.9 and DV -4 and -5. For graft-to-host connectivity stereotactic coordinates are the same as those used for TVA-GFP-G infusion. Infusion volume was 1µl per depth at a rate of 0.5µl/minute at each depth and 3 minutes diffusion.

2.4.6. Fluoro-gold infusion

Fluorogold (Fluorochrome) was dissolved in 0.9% saline to make a 1% concentration solution. Bilateral infusions were performed using a 1µl Hamilton syringe to deliver the tracer, delivering 0.1µl/site (total volume of 0.2µl/hemisphere) at 0.02µl/minute with a total infusion of 5mins and a diffusion time of 5 minutes. The stereotactic coordinates were AP -1.2, ML ±3.2 and DV -6.

2.5. Behavioral testing

2.5.1. Adjusting stepping test

At 28 days post lesions animals were assessed on the adjusting steps test (Olsson et al., 1995). One forelimb is restrained by the researcher, and the researcher counts the number of adjusting steps of the unrestrained forelimb along a flat surface moving forwards 100cm and then backwards the same distance. The test was performed twice, and the data are presented as the number of adjusting steps made with the contralateral and ipsilateral paw in forward and backward trajectories.

2.5.2. Apomorphine-induced rotations task

Animals were treated with 2mg/kg apomorphine hydrochloride hemi-hydrate (Sigma-Aldrich) administered s.c., an elastic band connected to a wire was put around their abdomen and they were placed in an automated rotometer bowls (Rotorat; Med Associates, St. Albans City, VT, USA) for 60mins to record the frequency of clockwise and anticlockwise rotations. Rotation scores were expressed as net rotations over the test session (ipsilateral minus contralateral).

2.6. Histological procedures, characterization and quantification

2.6.1. Perfusion and tissue sectioning

Rats were terminally anesthetized with sodium pentobarbital (Euthatal; Merial, Woking, UK) and transcardially perfused with 0.01 M phosphate buffer followed by 4% paraformaldehyde (pH 7.4; Sigma-Aldrich). Brains were postfixed for 4h in 4% PFA before being transferred to 25% sucrose solution. Tissue was sectioned on a freezing sledge microtome at 30µm thickness in a 1:12 series. Sections were stored in antifreeze solution (di-sodium hydrogen orthophosphate anhydrous, sodium dihydrogen phosphate, ethylene glycol and glycerol in distilled water) at -20°C.

2.6.2. Immunohistochemistry on free-floating tissue sections with DAB

One series of brain sections from the 12 cut per rat was placed in an individual pot and washed with tris-buffered solution (TBS, Tris-base and sodium chloride in distilled water, pH 7.4) and were placed on an orbital shaker. Antigen retrieval was performed treating sections with citric buffer (pH6.0) at 70°C for 30minutes. Tissue was cooled down at room temperature and washed three times in TBS. Afterwards, to reduce endogenous peroxidase activity sections were treated for 5 minutes with quenching solution (10% methanol, 3% hydrogen peroxide (H_2O_2) (10% w/v) in distilled water) and washed again in TBS three times for 10 minutes each. Free-floating sections were blocked in 3% normal serum in TXTBS (0.2% Triton-X-100 in TBS) for 1h, then incubated in primary antibody (Table 12) with 1% serum in TBS for 3h at room temperature. The next day tissue was washed three times in TBS for 10minutes each and incubated in secondary antibody (1:200) (Table 12) with 1% serum in TBS for 3h at room temperature. Avidin-biotin complex (Vectastain ABC HRP kit, PK-4000) kit was prepared 30minutes before use (1:200 concentration) and premixed with TBS and 1% normal serum to allow binding of the complex. Sections were washed again in TBS 3 times for 10minutes and incubate them in ABC solution for 2h at room temperature. Subsequently, tissue was washed 3 times for 10minutes each in TNS (Tris-base in distilled water without NaOH, pH 7.40). DAB solution (3,3'-diaminobenzidine, DAB, Sigma) is prepared with 2ml DAB (0.66mg/ml) in 40ml TNS with 12µl of 30% H_2O_2. DAB solution was added onto to the sections and depending on the intensity of the staining, sections were incubated for 5-30minutes and washed with TNS, then TBS to stop the reaction.

If staining for a second marker using Vector SG, previous steps were repeated from the blocking step until washing in TNS. Instead of using DAB colour solution, tissue was incubated

in Vector® SG Substrate kit (Vector Laboratories), which contains 3 drops of Vector SG solution and 3 drops of H_2O_2 in 10ml of TNS.

Finally, sections were mounted on double-subbed gelatinized slides and air-dried before starting dehydration in 70%, 95% and 100% ethanol for 5minutes each before being cleared in xylene. Tissue is cover-slipped with glass coverslips and DPX (a mixture of distyrene, a plasticizer and xylene; Merck) under a fume-hood and dried for 2-3 days.

2.6.3. Immunofluorescence on free-floating tissue sections

Immunofluorescence protocol was adapted from immunohistochemistry protocol (Section 2.6.2). Differences from Section 2.6.2 were the absence of antigen retrieval treatment. Incubation time in secondary antibody (1:200, Table 12) in TBS for 3h at room temperature but in the dark, due to using fluorescent secondary antibodies. Sections were washed three times in TBS for 10 minutes each, incubated for 5 minutes in Hoechst (1:10,000 in TBA) and washed again three times in TBS for 10 minutes. Sections were mounted on double-subbed gelatinized slides and coverslipped using Vectashield Vibrance® Antifade mounting media (Vector Laboratories) for mCherry and GFP stainings and Fluoromount-G™ mounting media for the rest of the markers.

For FG infused brains, sections were incubated in DRAQ5™ fluorescence probe solution (1:1,000) in TBS for 30 minutes at room temperature in the dark.

2.7. Imaging acquisition, analysis and statistical analysis

2.7.1. Imaging acquisition

Brightfield images of coronal sections were acquired using the Axioscan Z1 Slide Scanner (Zeiss) and images were visualized using Zeiss ZEN lite software. Brightfield higher magnification images were taken with Leica DM6 B Upright microscope with Leica CTR6 LED camera, using Visiopharm acquisition software (v2017.2). Fluorescence images of coronal sections were obtained using the Upright Leica DM6000 B and higher magnification images were taken using the Leica DM6000 B Inverted microscope and the Zeiss LSM 710 Confocal Laser Scanning Microscope, using Zeiss ZEN lite software to visualize images.

Table 12 - Primary and secondary antibodies for immunohistochemistry and immunofluorescence

Primary antibody	Species	Concentration	Supplier	Cat no.
c-fos	Rabbit, polyclonal	1:10,000	Synaptic systems	226003
CTIP2	Rat, monoclonal	1:500	Abcam	Ab18465
CTIP2	Rabbit, polyclonal	1:500	Abcam	Ab70453
EGR-1	Rabbit, polyclonal	1:1,000	Santa Cruz	sc-189
FOXP1	Mouse, monoclonal	1:500	Abcam	Ab32010
GFP	Mouse, monoclonal	1:500	Merck	MAB3580
DARPP32 (Human)	Rabbit	1:500	Abcam	AB40802
DARPP32 (Human) conjugated with Alexa 594	Rabbit	1:200	Abcam	Ab
HuNu	Mouse, monoclonal	1:1,000	Merck	MAB1281
Iba-1	Rabbit, monoclonal	1:8,000	WAKO	019-19741
Ki67	Rabbit, polyclonal	1:500	Abcam	Ab15580

mCherry	Rabbit, polyclonal	1:500	Abcam	Ab167453
NeuN	Mouse, monoclonal	1:2,000	Millipore	MAB377
OX42	Rat monoclonal	1:1,000	Bio-rad	MCA275G
S830	Sheep	1:20,000	Gillian Bates	Not applicable
STEM121	Mouse, monoclonal	1:3,000	Takara	Y40410
Secondary antibody	**Species**	**Concentration**	**Supplier**	**Cat no.**
Anti-Mouse (Rat adsorbed) IgG Biotinylated	Mouse	1:200	Vector Laboratories	BA2001
Anti-Rabbit IgG Biotinylated	Rabbit	1:200	Vector Laboratories	BA1000
Anti-Sheep IgG Biotinylated	Sheep	1:200	Vector Laboratories	BA6000
Alexa 488 goat anti rabbit	Rabbit	1:200	Invitrogen	A11034
Alexa 594 goat anti rabbit	Rabbit	1:200	Invitrogen	A21207
Alexa 488 goat anti mouse	Mouse	1:200	Invitrogen	A11029
Alexa 594 goat anti mouse	Mouse	1:200	Invitrogen	A11032

2.7.2. Imaging analysis

2.7.2.1. Cell quantification from ICC

Cells were plated on 96wp and 5 images from five randomly selected fields were taken with a x20 objective (200x magnification). Two wells were used per marker. Immuno-positive cells were counted in each field, an average of all counts was taken, and the percentage of expression was calculated based on total number of Hoechst cells.

2.7.2.2. Graft volume

Graft volume was evaluated using STEM121 staining in Chapters 3 and 4. Images from coronal sections were opened in Zeiss ZEN lite software and a region of interest (ROI) was delineated around the graft core to determine the area of the graft covered per section. Graft volume was calculated using the following formula and mean volume was calculated for each group.

$$Graft\ volume\ (mm^3) = \frac{\left(\Sigma\ all\ areas\ (\mu m^2)\right) \times section\ thickness\ (\mu m) \times series\ frequency}{1{,}000{,}000{,}000}$$

2.7.2.3. Area fractioning

Area fractioning was used to calculated hDARPP32 (Chapter 3 and 4) and mCherry (Chapter 3) expression. Images were processed in ImageJ/FIJI software, transformed into 8bit and draw a ROI around the grafted area to analysed. Threshold was adjusted to match as close as possible the original image and software measured threshold area. The percentage of area was provided by the software. All sections containing grafted tissue were analysed and average of all measurements was calculated for each animal. Average of expression percentage was calculated within all animals of the same group.

2.7.2.4. Optical density

Optical density was calculated using OX42/Iba1 staining in Chapter 4. The grafted area was divided in two groups, inside the graft and outside the graft, and a control area was used which was the cortex. Between 4-5 sections per animal were used and a minimum of 5 areas per group and section. All animals' IHC processing was performed together, and images were taken at 20x (200x magnification) all under the same exposure time. Calibration was performed before analysis following online manual (Link to manual). Data is presented as Optical density OX42/Iba1.

2.7.2.5. Unbiased stereological analysis

In Chapter 5, quantifications of IEG (EGR-1 and c-Fos) and NeuN was performed using Visiopharm Software. Images of sections were initially acquired using a 1.25x objective under a Leica CTR6 LED camera and ROI for each section was drawn and selected to establish the area of counting. Cells were manually counted, under a 40x objective and a 1000 μm^2 frame that was moved through the ROI by the software. To calculate cells per area the following formula was used:

$$Cells\ per\ area = \left(\frac{\sum ROI\ area}{Frame\ size\ \times\ \sum samples}\right) \times \sum cells\ counted \times 12$$

2.7.3. Statistical analysis

All statistical analyses were conducted using SPSS (v27; IBM). In **Chapter 3**, all data from hDARPP32 and STEM121 quantifications was analysed using one-way analysis of variance (ANOVA) with Group (5-, 9-, 12- and 17-weeks post graft) as a between groups factor with Tukey's *post hoc* test to perform multiple comparisons. In **Chapter 4**, graft volume and hDARPP32 and OX42/Iba1 expression was analysed using the independent samples t-test comparing the mean of rats' graft volume, hDARPP32 percentage or OX42/Iba1 optical density from F344tgHD rats and WT littermates. Statistical analysis for **Chapter 5** was explained in the chapter. Results were considered to be statistically significant with a value of $p < 0.05$.

Chapter 3: Monosynaptic tracing of hESC-derived MSNs in the QA lesion model

3.1. Introduction

The striatal atrophy in HD is progressive and results in degeneration of the efferent projections to the GP and SN, but also of cortical afferent connections. Cortical projections are vulnerable to the disease, with loss of white matter tracts observed in early stages of the disease (McColgan et al., 2017). This loss is not only observed in cortex, but also in hippocampus, amygdala and thalamus, and this is maintained over all pathological grades of HD, meaning that this loss occurred in early stages of the disease (de la Monte et al., 1988). Supporting and preserving host neurons may preserve cortical integrity of cortical afferent connections. Thus, CRT not only aims to replace those damage neurons to reconstruct the damaged neuronal circuit, but also to provide neurotrophic support to the remaining host cells. The mechanisms behind the efficacy of CRT have not been fully established yet, but there has been proof of concept, using foetal cells as the donor cells, that striatal transplants can receive host innervation from major afferents, as in a healthy striatum (Clarke & Dunnett, 1993; Clarke et al., 1988; Wictorin & Bjorklund, 1989; Z. C. Xu, Wilson, & Emson, 1991) and also that transplanted cells extend synaptic contacts to basal ganglia areas (Wictorin & Bjorklund, 1989; Wictorin et al., 1991) and that those connections are functional (Mazzocchi-Jones et al., 2009). This evidence supports the hypothesis that circuit reconstruction is a mechanism for long-term functional recovery seen after grafting a neuronal progenitor product into the striatum. There is also evidence from transplant studies in Parkinson's disease (PD), that long term behavioural recovery is directly correlated with the extent of neurite outgrowth of the grafted cells (Hills et al., 2023).

To date, there is still a limited literature relating to circuit reconstruction using hPSC-derived cells as the donor cells but published studies have indicated their potential in this respect. Following transplantation of hPSC-derived cells, there are reports of improvements in motor tasks, such as the rotarod (Adil et al., 2018; Jeon et al., 2014; Ma et al., 2012; Schellino et al., 2023; Wu et al., 2018), open field (Ma et al., 2012; Wu et al., 2018) or the adjusting stepping test (Besusso et al., 2020; Jeon et al., 2012), as well as evidence of electrophysiological activity (Besusso et al., 2020). There is also evidence of synaptic connectivity of the graft with the SN at 10 weeks post graft using the neuronal tracing Fluorogold (Adil et al., 2018), and host-to-graft connectivity after 6 months post-transplant from

cortical areas, thalamus, hypothalamus, amygdala and SN using the monosynaptic tracing based in the modified rabies virus (ΔG-rabies) (Schellino et al., 2023)(for more details check Chapter 1 Section 1.4.1). The studies from Besusso et al. and Schellino et al., were the only ones to use the ΔG-rabies tracing in the QA lesion model after transplanting hESC-derived striatal progenitors. However, although the same model is used in this chapter, their CRT product is different to the one used in this thesis. Specifically, our CRT product was originated from the hESC RC9 line, a good manufacture practice (GMP) line suitable for clinical translation, and the differentiation protocol applied was different, as ours was based on Arber et al., using Activin A as the main neuronal drivers to an MSN phenotype (Arber et al., 2015). Besusso et al. and Schellino et al used a SHH exposure and Wnt inhibitor DKK1 to obtain striatal progenitors.

Therefore, the aim of this chapter is to assess the ability of our hESC-derived MSN product to assess whether (1) normal host afferent projections to the striatum, such as those from the cortex and thalamus, are able to innervate and make synaptic contacts with grafted cells; and (2) transplanted cells are able to extend efferent projections to normal striatal projection regions such as the GP and SN (See Chapter 1 Section 1.1, Figure 1 for more details of the cortico-striatal thalamic circuit).

To assess circuit reconstruction, the viral monosynaptic tracing technique based on the ΔG-rabies was used. The ΔG-rabies is a retrograde tracer that has been modified to delete its rabies glycoprotein required for transsynaptic spread, and introduce a fluorescence protein, mCherry. The ΔG-rabies also contains an envelope that expresses the EnvA protein, providing the virus the specificity of only infecting cells that express the TVA receptor. These modifications, in combination with a lentivirus containing the TVA receptor and the rabies glycoprotein (LV-TVA-GFP-G), allow the virus to only spread monosynaptically. The starter cells will be infected by the LV-TVA-GFP-P, expressing the TVA receptor required for the ΔG-rabies to recognize the cell to infect; GFP to localize the infected cell and the rabies glycoprotein, that will travel synaptically if the starter cells are making any contact with any other cell in the brain. Once starter cells are infected by the ΔG-rabies, these cells will co-express GFP and mCherry and the traced cells that make synaptic contact with the starter cells will express only mCherry (See Figure 5 in Chapter 1).

To investigate host-to-graft connectivity (Experiment 1) a new hESC cell line was created to express the TVA receptor, GFP and rabies glycoprotein (See Chapter 1 section 2.3.5), so that grafted cells expressed the LV-TVA-GFP-G and the ΔG-rabies was infused within, and around the edges of the graft (Figure 11). To measure graft-to-host connectivity (Experiment 2) the LV-TVA-GFP-G was infused in two different brain regions of the cortico-

striatal-thalamic circuit; the GP and the SN. The ΔG-rabies was subsequently infused into these same regions (Figure 11).

The hESC RC9 and hESC-RC9-TVA-GFP-G line has been directly differentiated based in the modified protocol of Arber et al., but on different cell batches. Cells were transplanted into QA lesioned rats to model striatal atrophy. **Experiment 1** comprised two different experiments: Experiment 1A was designed to establish the ΔG-rabies technique and to determine the best viral concentration, but also allowed assessment of host-to-graft projections at a relatively short survival time. In Experiment 1B, the ability of the host to innervate the grafts at longer survival times was assessed. The aim of **Experiment 2** was to investigate whether the graft was able to project to, and make synaptic contacts with, two relevant areas of the basal ganglia circuit, the GP and the SN.

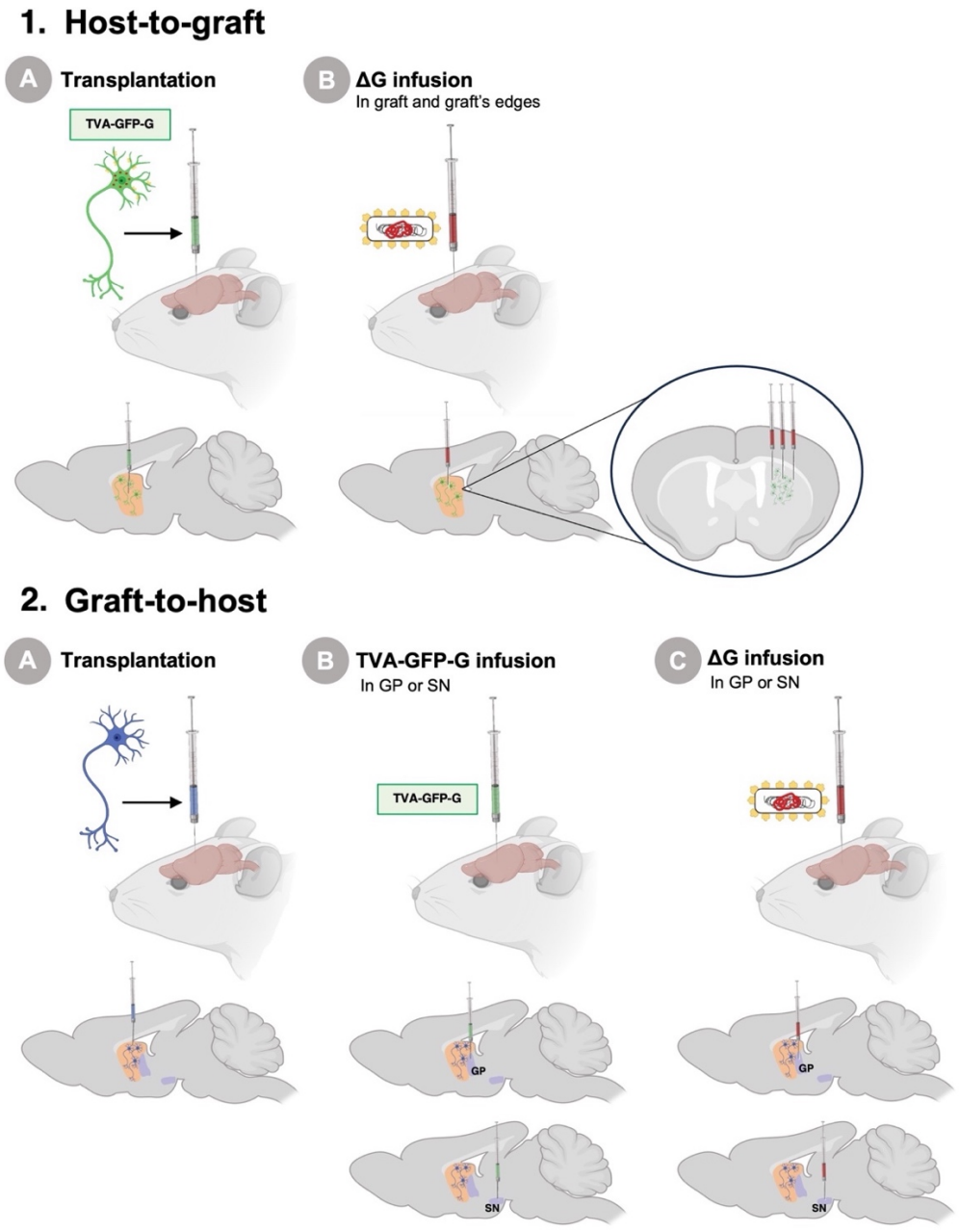

Figure 11 - Use of the ΔG-rabies in host-to graft and graft-to-host connectivity experiments. Top diagram showed transplanted hESC-derived MSN in green as cells expressed the TVA-GFP-G construct and bottom diagram showed hESC-derived MSN in blue. Infusion of TVA-GFP-G virus or TVA-GFP-G hESC-derived MSN is represented in a green syringe and infusion of ΔG-rabies is represented with a red syringe. (1) Host-to-graft connectivity involves (A) the transplantation of hESC-derived MSN expressing TVA-GFP-G in the striatum (B) and posterior infusion of ΔG-rabies in the graft and graft edges one week prior to infusion. (2) In graft-to-host connectivity, (A) non-transformed hESC-derived MSN are grafted into the striatum (blue); (B), 16 weeks later, infusion of LV-TVA-GFP-P is performed in the SN or in the GP; (C) One week before infusion, ΔG-rabies is infused in the SN or GP. Sagital view of the brain at the bottom of each figure represents infusion sites of each experimental timepoint. GP: Globus palludus; SN: Substantia nigra; ΔG: Modified rabies virus.

3.2. Differentiation of hESC to MSNs progenitors for cell transplantation

The hESC RC9 and hESC-RC9-TVA-GFP-G lines were directly differentiated based on the modified protocol of Arber et al. (See Chapter 2 Section 2.3.2). The hESC-RC9 line was differentiated using a GMP grade coating (L7™ hPSC Matrix (Lonza)) and the hESC-RC9-TVA-GFP-G was differentiated using Reduced Growth Factor (RGF) Matrigel™ and PDL/Fibronectin. Cells were cryopreserved on DIV 20 for subsequent transplantation (In this chapter and chapter 4) and characterized by high throughput qPCR on DIV 20 and ICC on DIV 40.

High throughput qPCR was performed by Dr. Kimberley Jones but, unfortunately, there was only one biological replicate of each of the samples and only space for two technical replicates, therefore statistical analysis was not performed. The panel of markers were all neuronal markers based on telencephalic development as well as markers for mature MSNs phenotypes. Samples from DIV20 of differentiation for both hESC-RC9 and hESC-RC9-TVA-GFP-G were compared to a LGE foetal tissue control (More details in Chapter 2 Section 2.3.9). All assessed markers were upregulated compared to LGE control as fold changes levels were higher than 1-fold changes (below 1-fold changes markers were downregulated compared to control sample and above 1-fold changes were upregulated). Markers from a mature MSN phenotype were evaluated and relative expression levels between both batches were similar, although hESC-RC9 batch showed higher expression in all markers compared to hESC-RC9-TVA-GFP-G (Figure 13). The highest level was from DARPP32 (Figure 13A), followed by DRD1 (Figure 13E) and DRD2 (Figure 13F). Levels of FOXP1 (Figure 13B) and FOXP2 (Figure 13C) were 10 times lower than DARPP32, and EBF1 showed the lowest value (Figure 13D) being most similar to LGE expression. When looking at telencephalic markers, ETV1 (Figure 13L), a transcription factor of dorsal LGE, showed the highest level of all telencephalon markers, but was only expressed in hESC-RC9 batch and not in hESC-RC9-TVA-GFP-G.

SHH was highly upregulated in both lines (Figure 13I), but levels were higher in hESC-RC9 batch. Showing 10 times lower expression than SHH or ETV1, were Nkx2.1 (Figure 13J) and Gsx1 (Figure 13K), this was only expressed in hESC-RC9-TVA-GFP-G. Finally, DLX2 (Figure 13H) and FOXG1 (Figure 13G) were the two markers with more similar expression to the LGE.

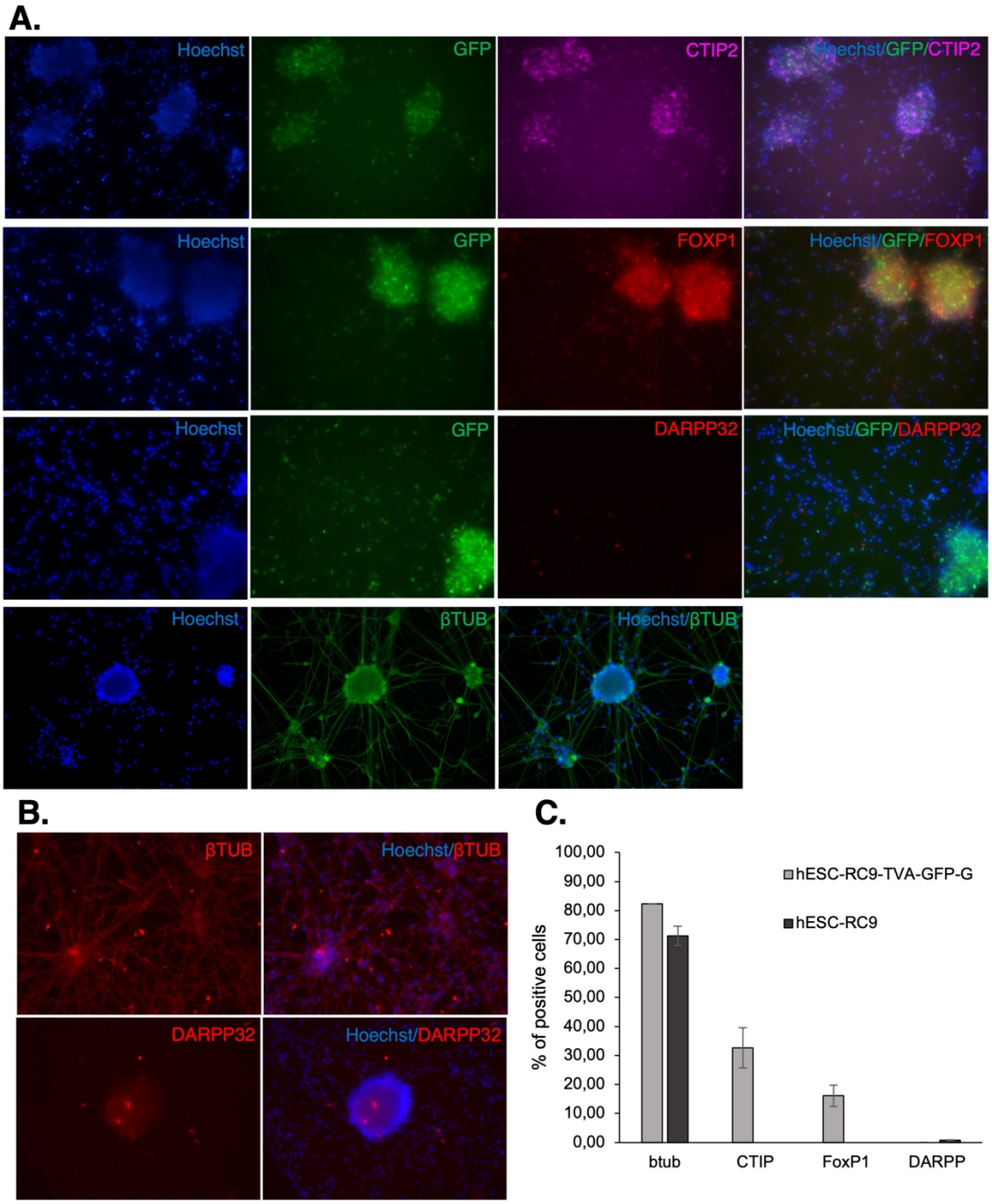

Figure 12 – Characterization of hESC-derived MSN at DIV 40. (A) Immunofluorescence images of hESC-RC9-TVA-GFP-G derived MSN for CTIP2, FOXP1, DARPP32 and βtub. (B) Immunofluorescence images of hESC-RC9 derived MSN for DARPP32 and βtub. (C) Quantification of ICC markers by percentage of positive cells calculated based in total Hoechst population. Each bar represents the mean of each group and error bars represent ±SEM.

On DIV40, ICC was performed for DARPP32, CTIP2, FOXP1 and β-Tubulin (βTUB). Differentiated cells from hESC-RC9-TVA-GFP-G showed no DARPP32, but 32.62±6.90% CTIP2, 16.11±3.65% FOXP1 and 82.33±0.07% of βTUB (Figure 12A and C). For differentiated hESC-RC9 cells, DARPP32 expression was 0.77±0.12% and 71.27±3.30% for βTUB, but no signal of CTIP2 or FOXP1(Figure 12B and C).

3.3. Host-to-graft connectivity

3.3.1. Experimental design

Experiment 1A and 1B animals were from an initial cohort of 30 female adult Lister Hooded rats that were unilaterally lesioned in the right striatum with QA prior to transplantation. This initial group of rats was allocated to three cohorts (Experiment 1A, 1B and Experiment 2). In all animals, grafts were placed into the lesion site with DIV20 hESC-RC9-TVA-GFP-G and underwent daily cyclosporine injections for the duration of the experiment, starting from two days before transplant surgery. All animals received a viral injection of the ΔG-rabies one week prior to perfusion.

In **Experiment 1A**, 10 out of the 30 lesioned rats were grafted at 4 weeks post lesion, to determine the best ΔG-rabies concentration. Concentrations used are shown in Table 13, and were calculated based on ΔG-rabies stock concentration (10^{10}-10^{11} TU/ml). The first four rats were injected with 5% and 20% ΔG-rabies concentration and taken after 5 weeks post grafting, the next two rats were injected with 10% concentration and taken after 9 weeks and four more rats were infused with 10% and 30% ΔG-rabies and perfused after 12 weeks (Figure 14). The rationale behind concentrations and times post-graft is described in detail in Section 3.3.2.1.

Table 13 – **Different ΔG-rabies viral concentrations used in Experiment 1A.**

ΔG-rabies stock	5% of ΔG-rabies	10% of ΔG-rabies	20% of ΔG-rabies	30% of ΔG-rabies
10^{10}-10^{11} TU/ml	5x10^{8} TU/ml	1x10^{9} TU/ml	2x10^{9} TU/ml	3x10^{9} TU/ml

Abbreviations: TU: Transducing Units

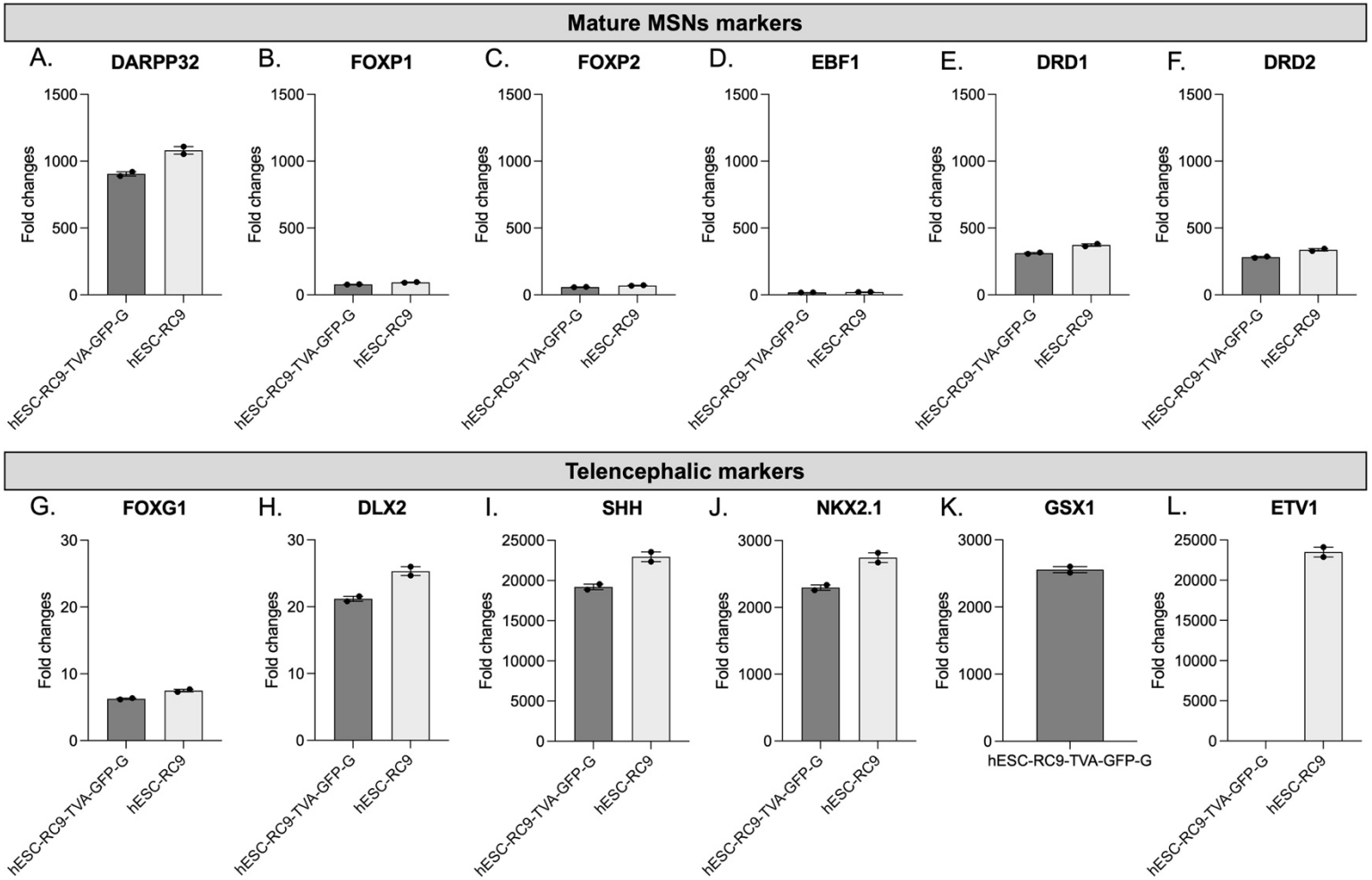

Figure 13 – **Mature MSN and telencephalic markers were highly upregulated compared to the LGE.** Bar charts represented fold changes from high throughput qPCR of markers of a mature MSN phenotype as (A) DARPP32, (B) FOXP1, (C) FOXP2, (D) EBF1, (E) DRD1 and (F) DRD2; and also markers of telencephalic development as (G) FOXG1, (H) DLX2, (I) SHH, (J) Nkx2.1, (K) GSX1 and (L) ETV1. Each bar represents the mean of each group and error bars represent ±SEM.

In **Experiment 1B** a second cohort of 7 out of the 30 lesioned rats were grafted at 15 weeks post lesion to assess connectivity at longer survival times. Animals were perfused after 12-, 17- and 21-weeks post transplantation, using the selected ΔG-rabies concentration (Figure 14). Results from animals in Experiment 1A and 1B were analysed all together as a single cohort; as this was designed as a proof-of-concept study, all animals were grafted with the same batch of cells and numbers of animals per group were low. The rest of the lesioned rats (N=13) were used in **Experiment 2** (Section 3.4).

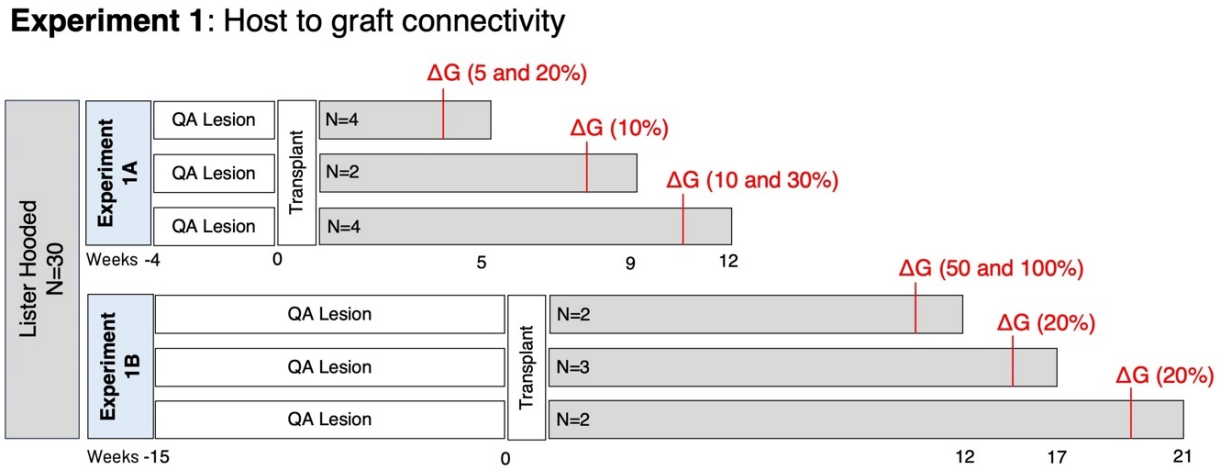

Figure 14 – Experimental design for host-to-graft connectivity. In Experiment 1A animals were grafted 4 weeks post lesion and were perfused at 5-, 9- and 12-weeks post transplantation. In Experiment 1B rats were transplanted 15 weeks post lesion and were culled after 12-, 17- and 21-weeks post grafting. All animals in every group received an infusion of the ΔG-rabies one week before perfusion. ΔG-rabies concentration is written in brackets for every timepoint. N=Number of animals in each group.

3.3.2. Results

3.3.2.1. Selection of surgical parameters of ΔG-rabies infusion

Experiment 1A aimed to verify surgical coordinates and optimise viral concentration. There were three infusion sites, one site directly within the transplant, and the two others were surrounding the edges of the graft (Figure 11 Host-to-graft). These sets of coordinates (See Chapter 2 Section 2.4.5 for details of the coordinates) were considered successful after perfusing the first group of animals at 5 weeks and observing the graft placement after histological characterization. These surgical coordinates were maintained for all groups in Experiment 1A and 1B. Infusion volumes of 1µl per depth was used, with two depths per site and an injection rate of 0.5µl. These volumes were based on published literature (Grealish et al., 2015).

For optimizing ΔG-rabies concentration, different viral concentrations were tested (Table 13, Figure 16), starting with 5% concentration which was used successfully by Grealish et al. (2015). Our ΔG-rabies virus was produced by a different group to the one in Grealish et al. (2015) therefore a starting point was to test the 5% concentration and a higher concentration, 20%, to guaranteed infection was successful. The initial plan for Experiment 1A was to infuse ΔG-rabies concentrations to tested at 4 weeks post graft and to maintain the rest of the animals until 12 weeks post graft (with ΔG-rabies at 11 weeks). However, 5% and 20% infusions did not provide the answers required so an intermediate timepoint (9 weeks post graft) was added to try to establish the optimal ΔG-rabies concentration.

As ΔG-rabies in higher concentrations could be cytotoxic, a 10% concentration was tried at 9 weeks post graft and again at 12-weeks post graft along with a higher concentration (30%). By the time Experiment 1B started, no mCherry signal had been seen in the grafts and as there was no sign of cytotoxicity using 20% concentration, further increases of 50% and 100% ΔG-rabies concentration were used. By the time the first group of animals in Experiment 1B were perfused, I realized that the lack of staining was due to an error in the antibody used for histological characterization. Use of the correct antibody showed that all concentrations had resulted in graft infection, with the area fractioning of mCherry positive staining being around 30% in all groups (Figure 15), except in the 100% ΔG-rabies concentration, which had the lowest mCherry expression (9.60%). As all concentrations resulted in positive mCherry staining were efficient, I decided to use 20% concentration for ΔG-rabies as this is at the lower end (to reduce risk of toxicity) but high enough to avoid pipetting errors when using small volumes, as required for 5 and 10% concentrations.

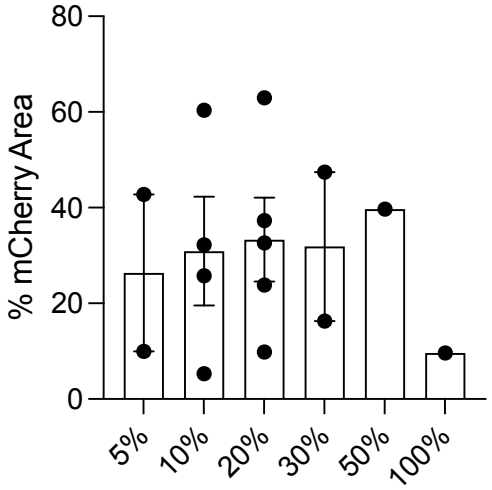

Figure 15 – Expression of mCherry was observed in every condition. Percentage of mCherry expression per graft. Each bar represents the mean of each group and error bars represent ±SEM.

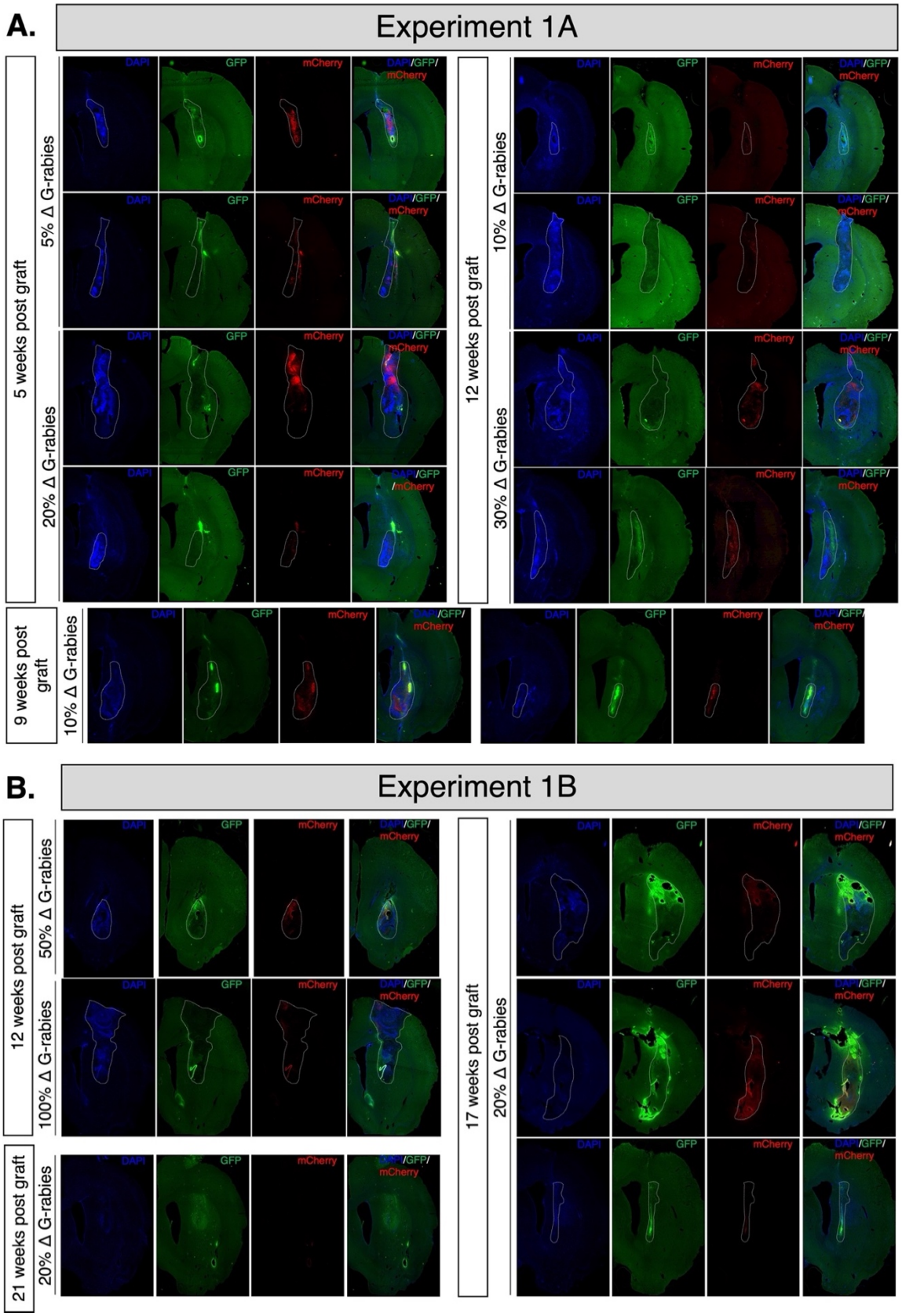

Figure 16 - Different ΔG-rabies concentrations showed similar percentage of mCherry at all concentrations except at 100% dilution. Coronal sections showed immunofluorescence images from DAPI, GFP, mCherry and all three markers together in (A)

Experiment 1A and (B) Experiment 1B grafted animals showing different timepoints and different ΔG-rabies dilutions.

3.3.2.2. hESC-derived MSNs express CTIP2 and DARPP32 markers

To validate that the transplanted progenitors matured into MSN-rich grafts, IHC was conducted for DARPP32 and CTIP2. Grafted cells already expressed the MSN marker DARPP32 (human DARPP32 (hDARPP32) by 5 weeks after transplantation (Figure 17A-B), showing dense hDARPP32 positive fiber bundles around the edges of the graft (Figure 17C). This extensive fiber outgrowth was also evident at 9- (Figure 17D-F), 12- (Figure 17G-I) and 17-weeks post-transplantation (Figure 17J-L). The percentage of hDARPP32 (both fiber bundles and cell bodies) was calculated and no significant differences were found in percentage of hDARPP32 between groups ($F_{3,8}$=0.937, n.s.) (Figure 17M).

Transplanted cells also express CTIP2. Figure 17N-Q shows double staining of hDARPP32 and CTIP2. CTIP2 positive cells, in blue, are found in the host striatum and inside the graft. In brown are hDARPP32 positive cells and white arrows point to cells co-expressing both markers (Figure 17P and Q).

3.3.2.3. Human cytoplasm staining demonstrates that hESC-derived MSNs survive and project to relevant areas of the basal ganglia circuit.

Brain tissue from all groups was stained for human cytoplasm marker (STEM121) to determine graft survival size and to visualise graft projections. From 17 transplanted rats, only four had no surviving graft, resulting in a 76.5% graft survival for this experiment. Unfortunately, in both animals carrying 21 weeks post transplantation, the graft did not survive and, therefore, there were no results for this last time point. Graft volume was calculated for every timepoint (Figure 18D) and there was no significant difference in graft volume between all timepoints ($F_{(3, 9)}$ = 2.394, n.s.) (Figure 18D).

Figure 18A shows a coronal section of a representative graft from an animal in each group at all timepoints. In Figure 18B, the same graft is shown in higher magnification and the white square denotes the area that is depicted at higher magnification (Figure 18C), showing fibers extending into the neuropil, strongly suggesting graft innervation within the host. Transplanted cells already innervated the host brain at 5 weeks post grafting, and that was maintained at every timepoint. Transplanted cells not only innervated within the host striatum, but they also extended projections to different brain regions of the basal ganglia circuit (Figure 19). At all timepoints, transplanted hESC-derived MSN projections are seen in prefrontal

cortical areas (Figure 19A, G, M and S), GP (Figure 19D, J, P and V), thalamic areas (Figure 19E, K, Q and W) and the SN (Figure 19F, L, R and X).

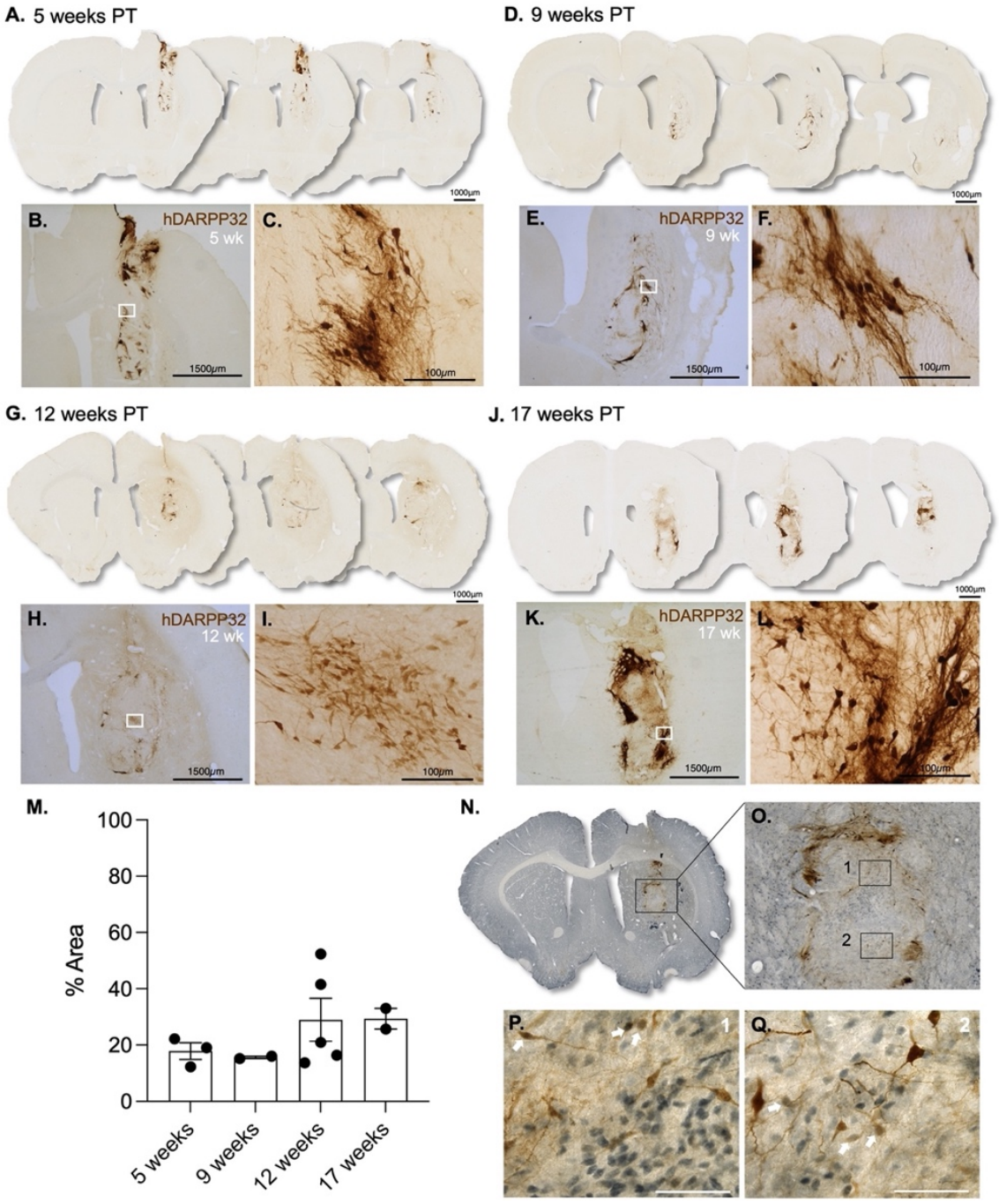

Figure 17 - Grafted hESC-derived MSNs express DARPP32 and CTIP2. Representative images of brain sections stained for hDARPP32 after 5- (A), 9- (D), 12- (G) and 17-weeks post graft (J). Images under coronal brain sections represented a graft overview (B, E, H, K) and the white square indicates the area zoomed to a higher magnification image (C, F, I, L) for every timepoint. (M) Percentage of hDARPP32 area. Immunohistochemistry images of hDARPP32 in brown (DAB) and CTIP2 in blue (Vector SG) from a coronal section (N) that showed an overview of the graft and black square zoom the graft (O). Images 1(P) and 2(Q) are two different graft areas in higher magnification. White arrows point to co-labelling of both markers. Scale bars are 1000 µm, 1500 µm and 100 µm. Scale bar for images P and Q is 50µm. PT=Post transplantation.

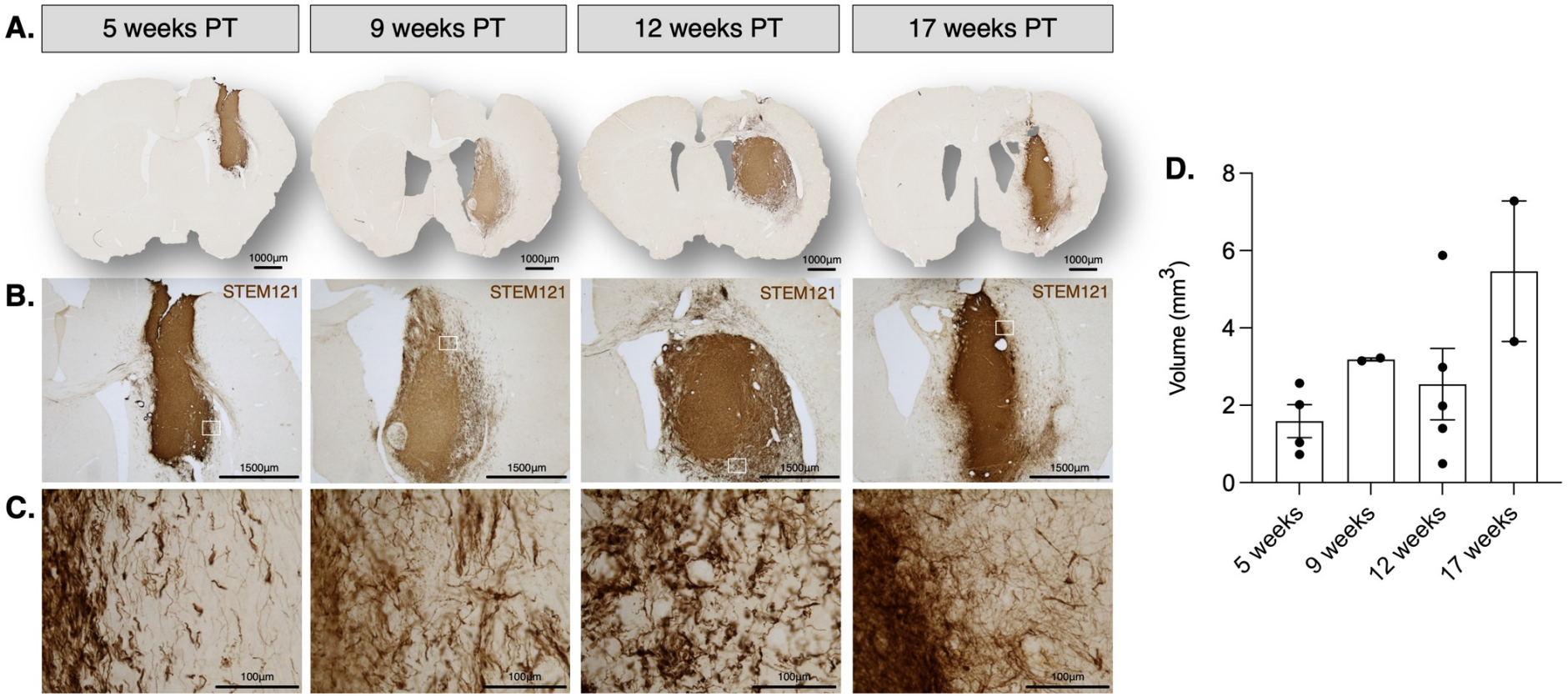

Figure 18 – Transplanted cells innervate the host brain. (A) Representative brain sections through the graft region, showing human cytoplasm staining (STEM121) showed projections from graft cells extending into into the host brain at all timepoints and have started to innervate by 5 weeks post grafting. (B) Higher magnification of the graft, (C) a higher power view of the white square located in the graft border in B to show graft innervation. (D) Graft volume was calculated at every timepoint. Each bar represents the mean of each group and error bars represent SEM. 5 weeks: N=4, 9 weeks: N=2, 12 weeks: N=5 and 17 weeks: N=2. PT: Post-transplant

As represented in Figure 19C, transplanted cells extended projections around graft borders already after 5 weeks post grafting. From 9 weeks (Figure 19H), 12 weeks (Figure 19M) and up to 17 weeks (Figure 19R), graft innervation was denser. Another interesting feature was the fiber bundles around graft edges that were present at every time point (Figure 19B, H, N and T) and also, became denser within time. Similar fiber bundles, but in smaller size were also present in thalamic areas (Figure 19E, K, Q and W).

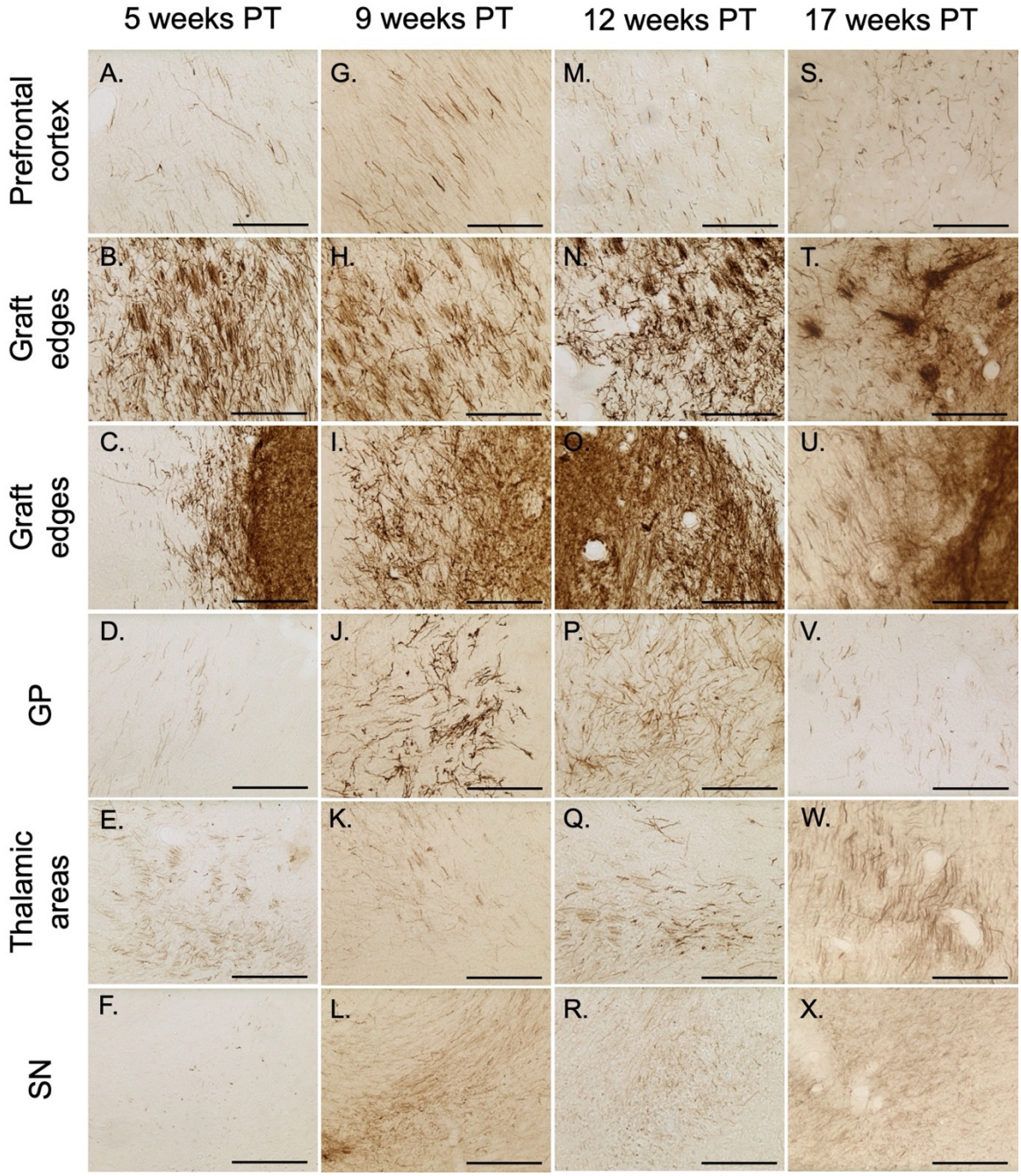

Figure 19 – Transplanted hESC-derived MSN innervate the host brain and extend projections to other brain regions. Immunohistochemical images of STEM121 across all timepoints and different brain areas. At 5 weeks (A-F), 9 weeks (G-L), 12 weeks (M-R) and 17 weeks (S-X) post grafting, transplanted cells extend projections to cortical areas, GP, thalamic areas and SN as well as withing graft edges. Scale bar is 200µm. PT: Post transplant.

3.3.2.4. *Monosynaptic tracing using ΔG-rabies showed traced cells in relevant areas of the basal ganglia circuit demonstrating host-to-graft connectivity by 5 weeks post transplantation*

Transplanted hESC-derived MSNs expressed GFP *in vivo* as shown by immunofluorescence (Figure 20A and D) and immunohistochemistry (Figure 20H and I). Infection with the ΔG-rabies was confirm by mCherry positive staining (Figure 20B, E, J and K) and starter cells were located within the graft, co-expressing GFP and mCherry (Figure *20*C and G).

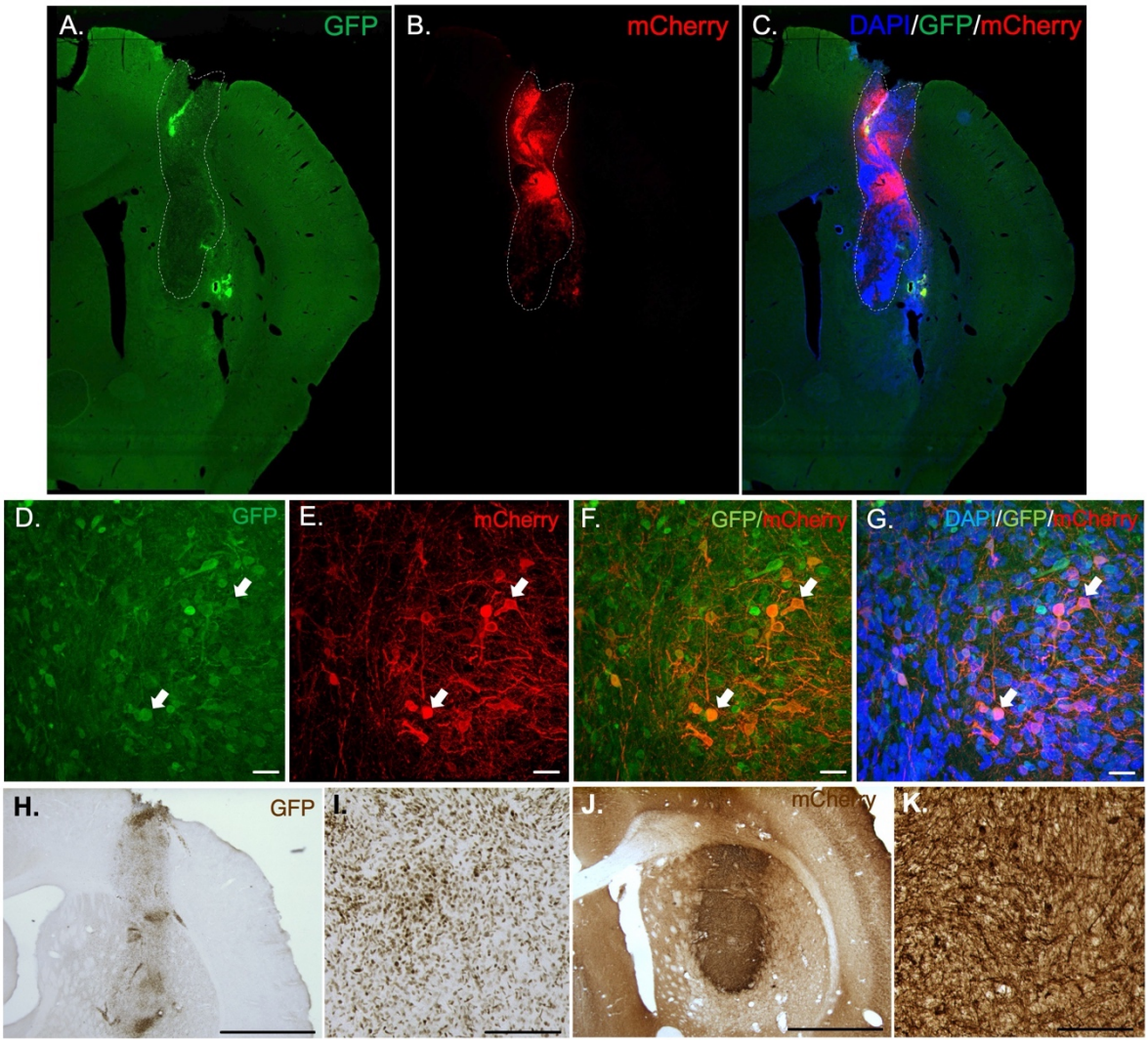

Figure 20 – Transplanted hESC-derived MSN express GFP in vivo and were successfully infected by the ΔG-rabies. Coronal sections showing immunofluorescence images of (A) GFP grafted cells and (B) mCherry and (C) DAPI, GFP and mCherry positive cells. Higher magnification images of (D) GFP; (E) mCherry; (F) co-labelling of GFP and mCherry and (G) DAPI, GFP and mCherry. White arrows point to starter cells co-expressing GFP and mCherry. (H) Left image shows histological representation of the graft expressing GFP and the right image is a high magnification image. (B) Left image show mCherry positive cells within the graft and right image is a high magnification image of the graft. Scale bar H and J: 1500μm; scale bar L and K: 200μm. Scale bar D-G: 20μm

Traced cells were found in representative areas of the basal ganglia (Figure 21), from cortical and thalamic areas, as well as the SN. In cortical areas, host cells were extending projections from primary motor cortex (M1) (Figure 21A and G), secondary motor cortex (M2) (Figure 21D) and ventral orbital cortex (VO) (Figure 21J). In thalamic areas, connections were coming from ventromedial thalamic nucleus (VM) (Figure 21B, E and H), anteroventral thalamic nucleus ventrolateral (AVVL) (Figure 21K), ventrolateral thalamic nucleus (VL) (Figure 21C), mediodorsal thalamic nucleus (MDL) (Figure 21F) and anteromedial thalamic nucleus (AM) (Figure 21I and L).

Specifically, at 5 weeks traced cells were found in cortical regions (M1) and thalamus (AM, Po, VL, VM, LPMR). Not only traced cells but there were also projections found in cortical areas (M1, M2, S1, S1FL), forceps minor of the corpus callosum (fmi), GP, stria terminalis (st), thalamic areas (RT, VA, CL, VPL, PF), parabrachial pigmented nucleus (PBP) and SN (Appendix Figure 1). By 9 weeks traced cells were found in cortical areas (M2, Lo, VO), stria terminals (BSTL) and thalamic areas (PC, MDC, MDL, VM). At this timepoint, projections were found in cortical areas (M2), claustrum (Cl), striatal areas (AcbC, CPu) and thalamic regions (IPACL, MDM, VA, PF, MD) (Appendix Figure 2). At 12 weeks traced cell bodies are found in different thalamic regions (AVDM, AM, CL and VM). Projections were found in cortical areas (M1), CPu, GP, thalamic areas (VA, MDC, LPMR, PF, VPPC) and SN (Appendix Figure 3). Finally at 17 weeks, mCherry positive cell bodies were found in cortical regions (Pir, VO, LO) and thalamus (AVVL). Projections are shown in cortical regions (M1, M2, LO, PrL, DLO, VO, Cg1, IL), olfactory nucleus (AOV, AOP), CPu, GP, lateral preoptic area (LPO), thalamic areas (PT, Rt, AM, VRe, CM), amygdala (AAD), anterior commissure (IPACL, IPACM) (Appendix Figure 4 and Appendix Figure 5) and SN (Figure 21O).

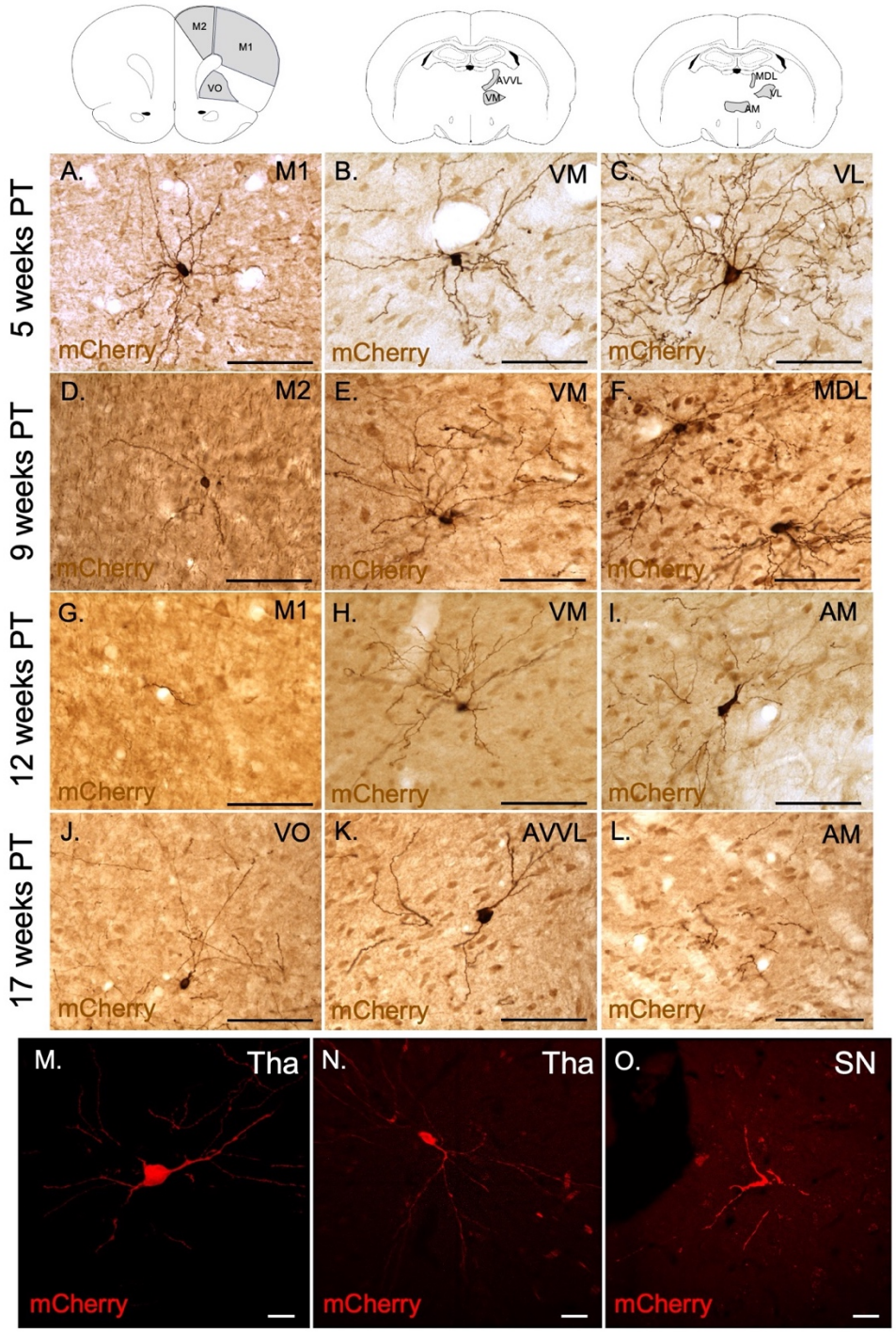

Figure 21 – Traced cell bodies are found in cortical and thalamic regions. Immunohistochemistry and immunofluorescence images for mCherry. Coronal sections on the top of the figure represents the areas where traced cells are found. Traced cells are shown in (A) M1, (B) VM and (C) VL at 5 weeks post graft; in M2 (D), VM (E) and MDL (F) at 9 weeks post-transplant; in M1 (G), VM (H) and AM (I) at 12 weeks post grafting and in VO (J), AVVL (K) and AM (L) after 17 weeks post transplantation. Traced cells are also found in thalamic areas (M-N) and SN (O). Scale bar for A-L is 100µm and for M-O is 20µm. PT: post-transplant; M1: primary motor cortex; M2: secondary motor cortex; VO: ventral orbital cortex; VM: ventromedial thalamic nucleus; AVVL: anteroventral thalamic nucleus, ventrolateral part; VL: ventrolateral thalamic nucleus; MDL: mediodorsal thalamic nucleus, lateral part; AM: anteromedial thalamic nucleus; SN: substantia nigra; CM: central medial thalamic nucleus; Tha: Thalamus.

3.4. Graft-to-host connectivity

3.4.1. Experimental design

As outlined in section 3.3.1, thirteen of the original QA lesioned rats were allocated to **Experiment 2**. Three rats die due to illness before transplant so 10 were grafted with hESC-derived MSN DIV20 (by this time they were 21-weeks post lesion) and underwent daily cyclosporine injections from two days before transplant surgery. A further rat died 9 weeks post graft due to intestinal blockage and a second rat died 24h after viral infusion of LV TVA-GFP-G. Brains from these two animals were also harvested for posterior analysis. At 21 weeks post graft the remaining 8 rats were perfused. At 16 weeks post graft, four rats received an infusion of the LV TVA-GFP-G into the SN and five rats into the GP (Figure 22). Four weeks afterwards, all received a ΔG-rabies infusion (20%) in the same area as the previous viral infusion, and a week later they underwent transcardial perfusion and the brain tissues were harvested for immunohistochemical analysis.

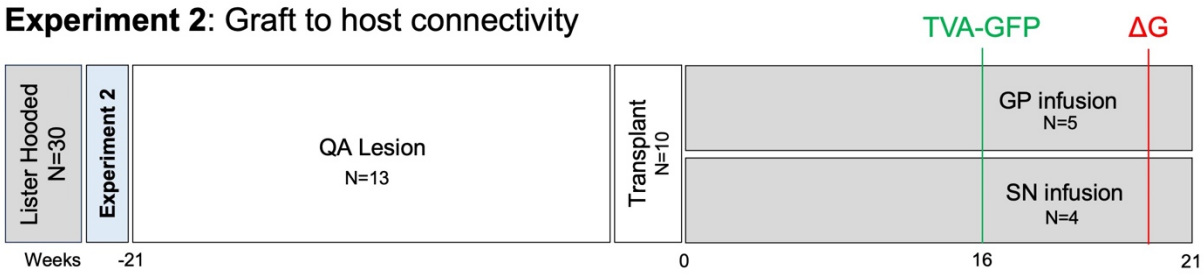

Figure 22 - Experimental design. Animals were grafted 21-weeks post lesion and received an infusion of the TVA-GFP-G virus 16 weeks post grafting either in the SN or the GP. All animals received an infusion of the ΔG-rabies one week before perfusion.

3.4.2. Results

3.4.2.1. Grafts overgrew and had limited projections

From 10 transplanted rats, three rats had no graft survival (70% graft survival), and the rest (7) showed a large graft volume (36,56±14,52 mm^3). Two of the rats with surviving grafts were the ones that died prematurely and so did not undergo ΔG-rabies infusion.

STEM121 staining showed fibers innervating around the graft's borders, but not in brain areas outside of the striatum (Figure 24). Different graft placements were identified, Rats #1 (Figure 24A) and #4 (Figure 24G) had very ventral grafts, with graft #4 extending into ventral areas of the intact hemisphere. Rat #2 also had a ventral placed graft in which extended into the medio-dorsal areas of the striatum (Figure 24C). Rat #3 and #5 (#5 is not included in the

figure as most of the tissue was damaged after sectioning), had giant grafts filling the whole striatal area and extending into cortical areas (Figure 24E).

Large graft volumes suggest graft overgrowth/tumorigenesis, therefore, fluorescent immunostaining for Human Nuclei (HuNu) and the proliferative marker Ki67 were performed in Experiment 2 (Figure 23A-F), and compared to Experiment 1 animals (Figure 23G-L). No quantifications were performed but ki67 expression (Figure 23A) in Experiment 2 grafts was more distributed, with small, clustered areas of staining than Experiment 1 (Figure 23H), in which ki67 expression was more sparse.

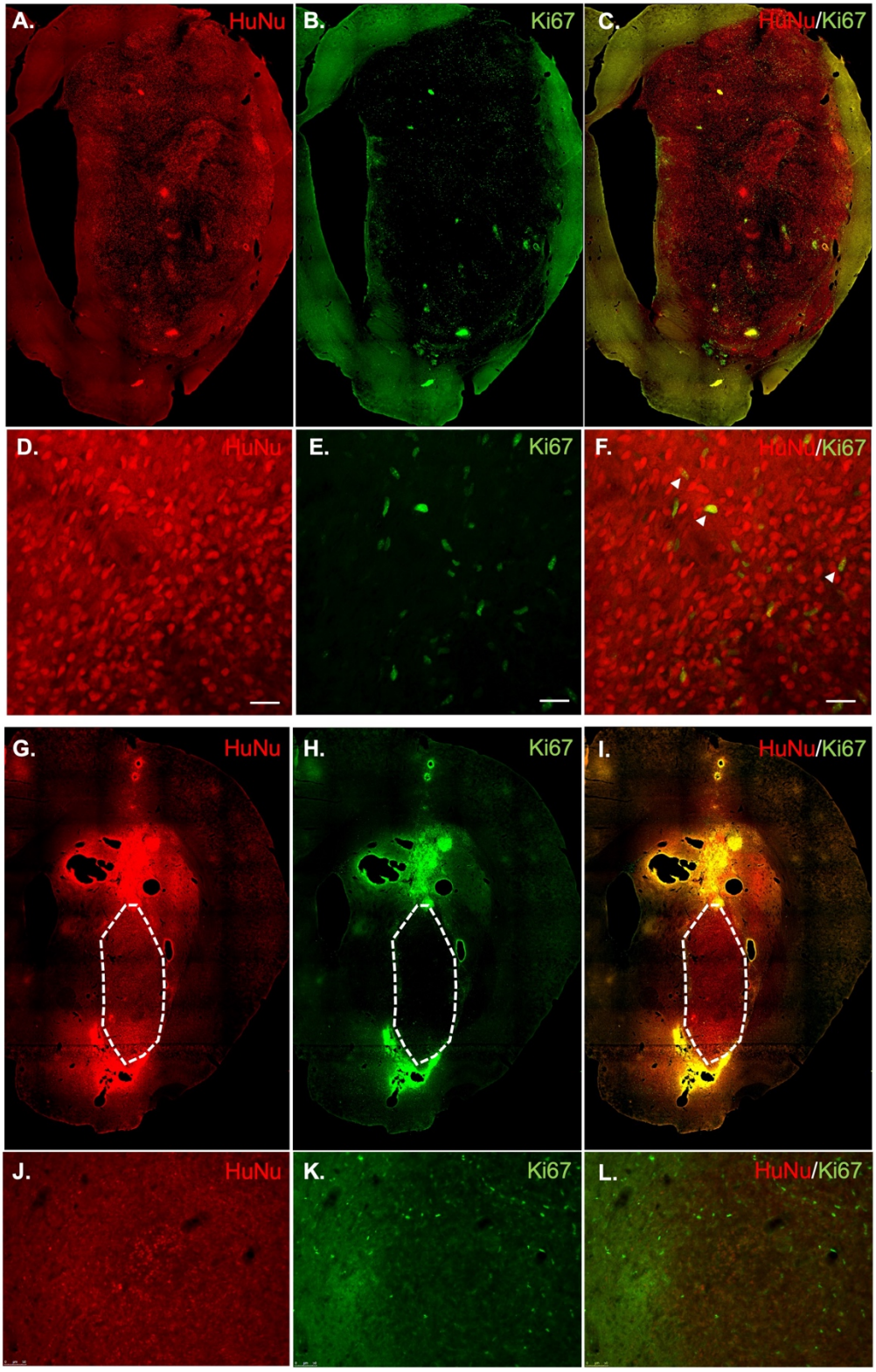

Figure 23 - Grafted cells from Experiment 2 co-express HuNu and Ki67. Experiment 2 animals immunofluorescence staining for (A) HuNu, (B) Ki67 and (C) co-localization of both markers. Higher magnification of (D) HuNu, (E) Ki67 and (F) co-labelling of both. White arrows show cells co-labelling HuNu and Ki67. Experiment 1 immunofluorescence staining for (G) HuNu, (H) Ki67 and (I) co-localization of both markers and higher magnification of (J) HuNu, (K) Ki67 and (L) co-labelling of both. Scale bar = 20 μm

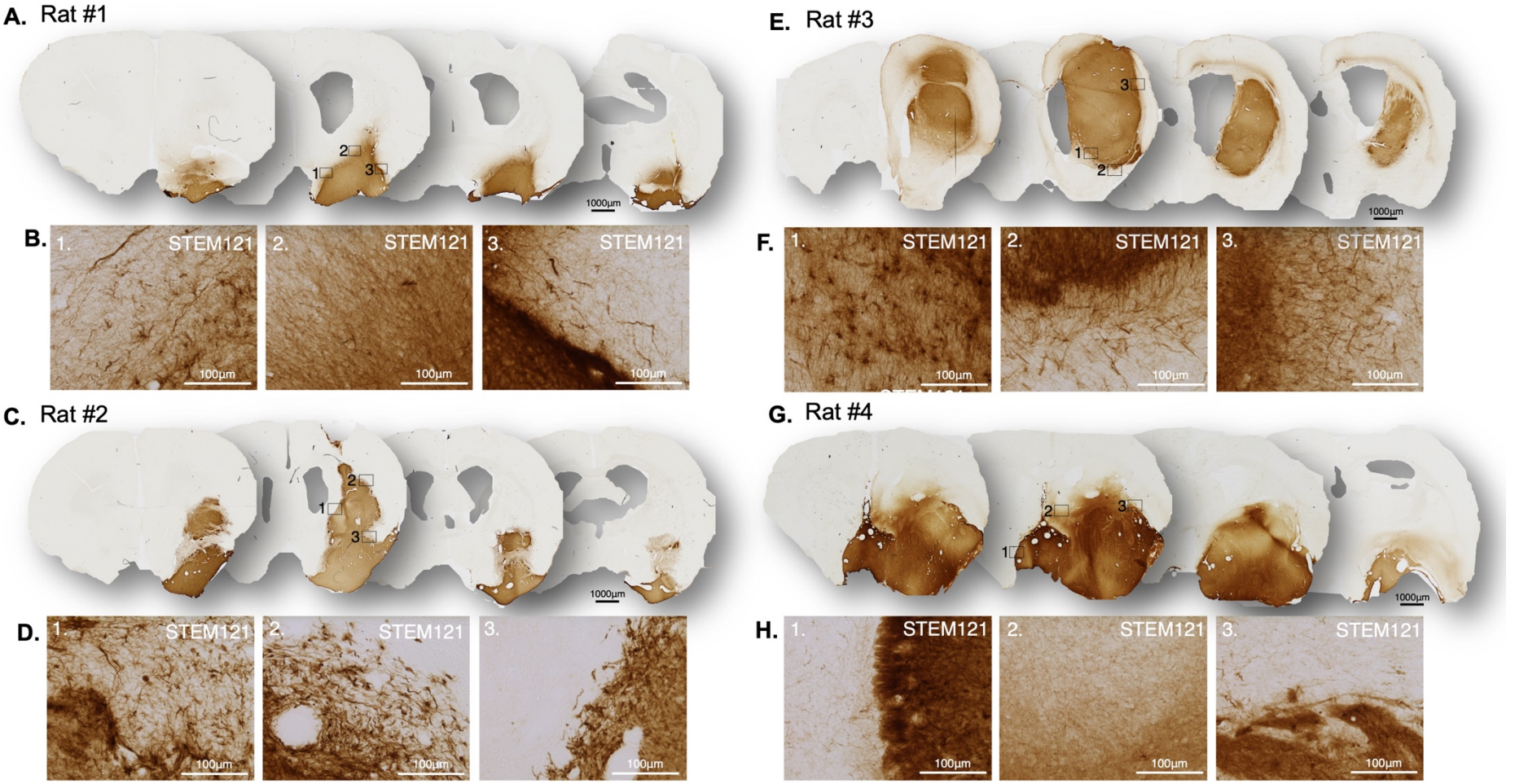

Figure 24 – Human cytoplasm immunohistochemistry (STEM121) revealed large grafts in transplanted animals. Four different rats are shown in this image (A, C, E, G) and three different areas of the grafts, marked with a black square, are zoomed to observe cell innervation (B, D, F, H). Scale bars are 1000µm and 100µm

3.4.2.2. Grafted cells express MSN-like markers, such as DARPP32 and CTIP2

Although the grafts were considerably bigger than those in Experiment 1, they all showed positive expression of hDARPP32, as shown in Figure 25. Within these grafts, hDARPP32 positive cells covered all grafted area, with a less patchy appearance than the grafts reported in Experiment 1 (seen in high magnification in Figure 25B, D, F, H). Grafted cells were also positive for the MSN markers CTIP2 (Figure 25A-C).

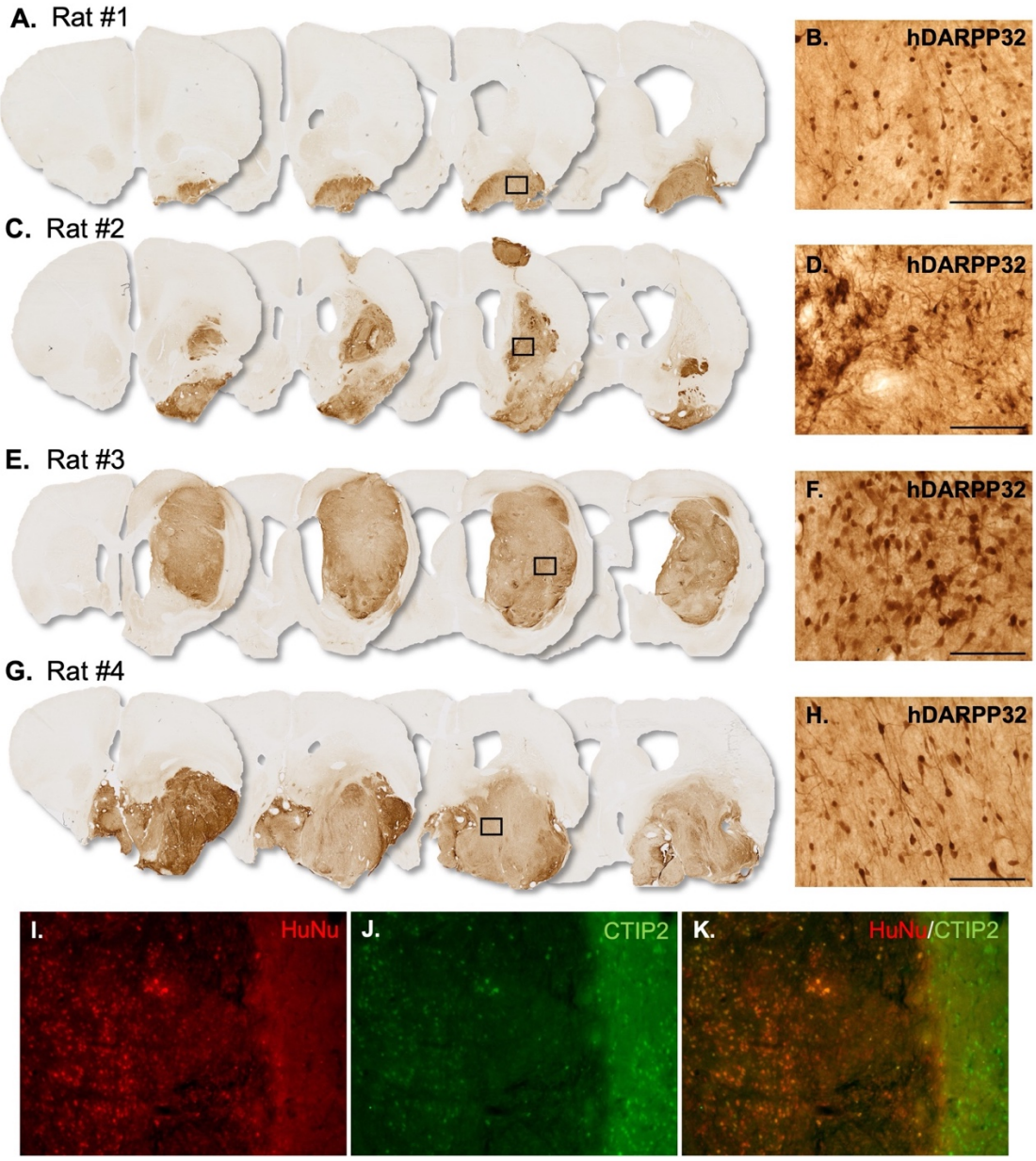

Figure 25 – hESC-derived MSN grafts express hDARPP32 and CTIP2. Coronal sections overview of (A) Rat #1, (C) Rat #2, (E) Rat #3 and (G) Rat #4 hDARPP32 IHC. Black square represents the zooming area of hDARPP32 (B, D, F and H). Immunofluorescence of (I) Human Nuclei, (J) CTIP2 and co-localization of both (K). Scale bars are 1000µm and 100µm.

3.4.2.3. No traced cells found within the graft

In this experiment, animals received a viral infusion of the TVA-GFP-G virus either in the GP or in the SN. Figure 26A and D shows infusion in the SN and Figure 26C and F starter cells in that area. Figure 26G and J represents the infusion in the GP and Figure 26I and L showed starter cells.

Positive mCherry staining was only seen in one graft in which mCherry projections were found around the edges of the graft (Figure 26N and O). Human cells are shown in brown by DAB staining of human nuclei (HuNu) and mCherry in blue by Vector SG (Figure 26M).

3.5. Discussion

The main aim of the experiment was to investigate whether hESC-derived MSN grafts were able to integrate and reconstruct the damaged circuit in a model of HD. Specifically, **Experiment 1** explored host-to-graft connectivity, to measure the ability of host cells to make synaptic contact with transplanted cells and **Experiment 2** investigated graft-to-host connectivity, assessing if transplanted cells could synapse with host cells.

In **Experiment 1**, STEM121 staining showed that hESC-derived MSN were able to integrate and innervate the host brain, as well as express characteristic MSN markers such as CTIP2 and DARPP32. Host cells from a range of brain regions, such as the prefrontal cortex or the thalamus, made synaptic contacts with the transplanted cells. In **Experiment 2**, hESC-derived MSN progenitor transplants resulted in very large grafts that were mostly mis-placed ventrally. These grafts also expressed the MSN markers CTIP2 and DARPP32 but demonstrated very limited innervation, and only one rat showed evidence of synaptic contacts with host cells.

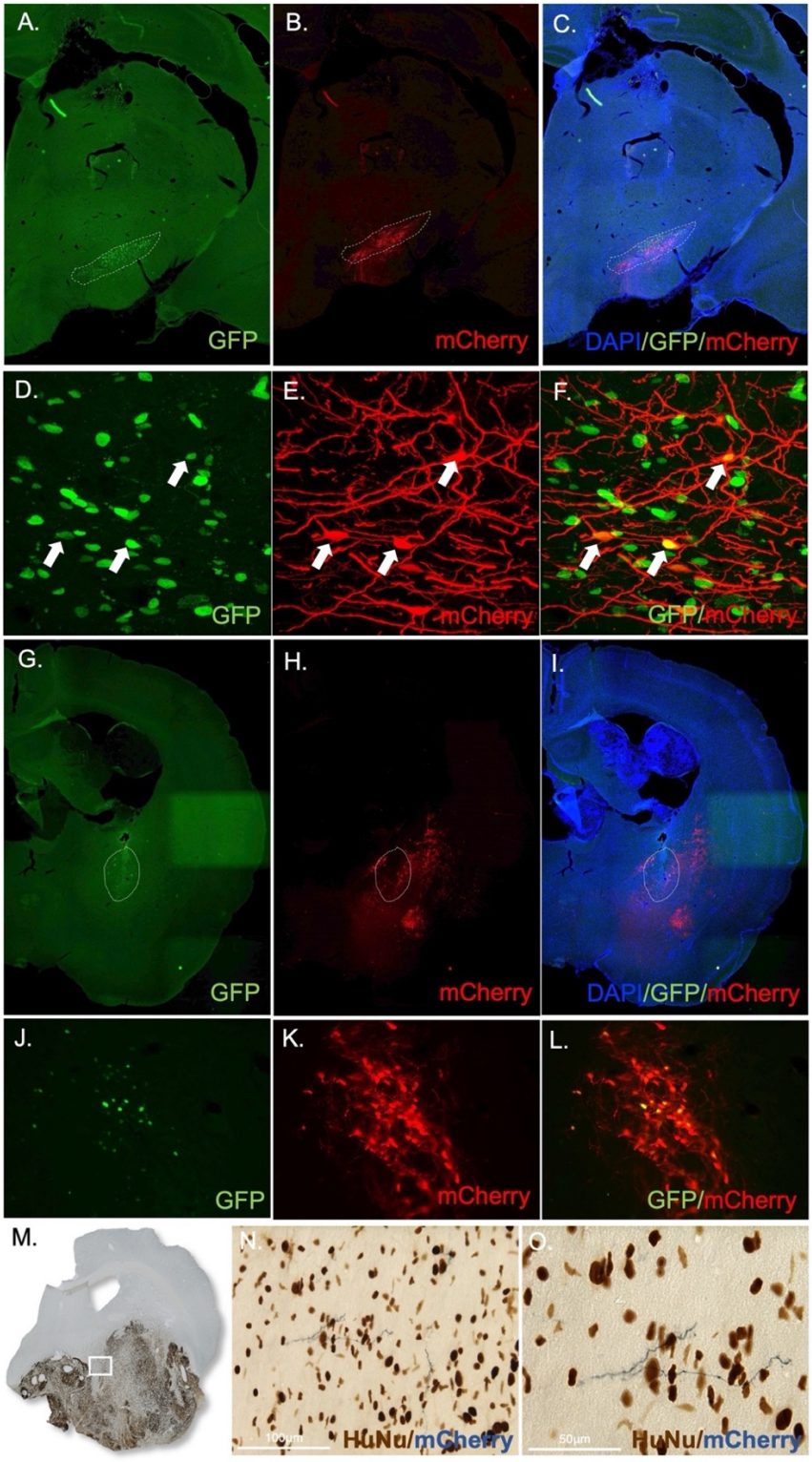

Figure 26 – Starter cells in the GP and SN and traced projections at the graft edge. Immunofluorescence images showed injections of TVA-GFP-G into the SN (A)(D) and the GP (G)(J). Images of mCherry positive staining after ΔG-rabies infusion in SN (B)(E) and GP (H)(K). Starter cells co-express GFP and mCherry in the SN (C)(F) and in the GP (I)(L). Immunohistochemistry for HuNu (DAB) and mCherry (Vector SG) is shown in coronal section (M) and white square represents the zoomed in area in (N) and (O). Scale bar 100μm and 50μm.

***In vitro* characterization of MSN progenitors**

The two batches of cells used in this chapter (hESC-RC9 and hESC-RC9-TVA-GFP-G) were characterized at DIV20 by high throughput qPCR (Fluidigm) and DIV40 by ICC. Data from Fluidigm was compared to a human LGE of between 62- and 92-days post conception (between 9 and 13 weeks) (all LGE samples are shown in Table 9 from Chapter 2). As mentioned in the results section, it was unfortunate that there was only one biological replicate of each of the samples and only space for two technical replicates, therefore statistical analysis was not performed. All tested markers were upregulated compared to human LGE control tissue, and hESC-RC9 batch showed higher fold changes in all markers, compared to hESC-RC9-TVA-GFP-G, except for *Gsx1* for which no signal was found. The *Gsx1* gene is known to be involved in subpallial development (Toresson et al., 2001) so its absence in hESC-RC9 cells could be that at this developmental timepoint in which differentiated cells were, this marker was already downregulated to lead out to a more MSN mature phenotype. On the other hand, hESC-RC9-TVA-GFP-G line presented lower fold changes compared to hESC-RC9 batch and no expression of *Etv1*. Expression of *Etv1* in hESC-RC9 batch, which was upregulated compared to LGE control, more than 20,000 folds, is likely to mean a possible interneuron population within those cells, as *Etv1* transcription factor is expressed in striatal interneurons (Mi et al., 2018). A relevant MGE gene is *Nkx2.1*, which was 2,000 folds upregulated in both lines compared to the LGE. Another marker upregulated more than 20,000 folds in both lines was *Shh*, a morphogen significantly important in telencephalic development (Gutin et al., 2006; Rallu et al., 2002). Highest expression of *Shh* in the telencephalon was found ventrally, in the subpallial area where the MGE originates, translating in an MGE-like possible population in our cells. *Foxg1* with around 7 fold changes and *Dlx2* with 20-25 folds, were the only two markers with more similar expression to the LGE. When looking at mature MSN markers assessed on Fluidigm, DARPP32 showed the highest expression with 1,000 folds increased when compared to the LGE. Supporting DARPP32 expression, with around 300 fold changes DRD1 and DRD2 were expressed, *FoxP1* and *FoxP2* were in between 60 and 90 fold changes and *Ebf1* with 20 fold changes. The LGE is still an immature population compared to the striatum so these data could mean that within both populations of MSN lines there were already some mature cells. Although is difficult to draw firm conclusions with low sample numbers and no other characterization, results from these telencephalic markers showed a possible MGE- and LGE-like population, a more MSN differentiated population of cells and evidence of interneuron phenotypes within the whole population on both cell batches.

There was no ICC data available for DIV20, but for DIV40 the results showed that more than 70% of the population were neurons, as shown by βTUB, in both cell batches. DARPP32 was very low in the hESC-RC9 cells, with less than 1% and no expression of CTIP2 and FOXP1, although I believed this is due to a technical issue of the staining, as *FoxP1*, for example was already detected on DIV20 in the Fluidigm data and, according to the literature, all adult striatal DARPP32 positive cells express CTIP2 (Onorati et al., 2014), but unfortunately did not have the time to repeat to confirm it. For MSN-TVA, no DARPP32 expression was found, CTIP2 was 32.62% and FOXP1 was 16.11%. Expression of DARPP32 was relatively low compared to as Ma et al., who showed 75% at DIV47 (Ma et al., 2012); Jeon at al., 27% at DIV30 (Jeon et al., 2012) or Arber et al., with 40% at DIV43 (Arber et al., 2015). Expression of CTIP2 is similar to Besusso et al., with 30% expression at DIV50 (Besusso et al., 2020), but lower compared to Arber et al. or Comella Bolla et al. with 60% (DIV 43 and DIV37, respectively) (Arber et al., 2015; Comella-Bolla et al., 2020).

For future cell products, it would be interesting to have a characterization over a more extensive period of differentiation, for example DIV0, 10, 15, 20, 30 and 40, with ICC, qPCR or FACS to have a better understanding of our cell product, as with this data is challenging to draw conclusions about the exact phenotype of the population.

Graft characterization

Graft volume

In both experiments, graft survival of more than 70% was observed, however, the main difference between the grafts in Experiment 1 and 2 was that the grafts in Experiment 2 were very large and were also misplaced, most being more ventral than was intended. Grafts volumes from Experiment 1 were 1.59±0.43 mm^3 at 5 weeks, 3.18±0.04 mm^3 at 9 weeks, 2.55±0.92 mm^3 at 12 weeks and 5.46±1.82 mm^3 at 17 weeks. These values are similar to published data using hPSC-derived progenitors, as in Arber et al. (2015), in which grafts volumes were 1.47 mm^3 at 4 weeks, 0.78 mm^3 at 8 weeks and 10.66 mm^3 at 10weeks, or in Besusso et al. (2020) who reported 6.53±0.6 mm^3. However, the average graft volume for Experiment 2 was 36.56±14.52 mm^3, with the largest graft volume of 109.02 mm^3.

It is not clear why grafts appeared over-large in Experiment 2 but not in Experiment 1. This could relate to differences in the parent hPSC line or to differences in the cell differentiation processes. The transplanted cells in Experiment 1 and 2 were both derived

from the RC9 hESC line but were differentiated in two different batches and cells in Experiment 1 were engineered to express the TVA-GFP-G construct to make it suitable to use with the ΔG-rabies (See Chapter 2 Section 2.3.5 for more details). The same basic differentiation protocol (See Chapter 2 section 2.3.2 for more details) was used to derived MSNs for both experiments, but for the first stage of differentiation, cells in Experiment 1 were plated on Reduced Growth Factor (RGF) Matrigel™ and cells from Experiment 2 were plated in L7™ hPSC Matrix (Lonza), a GMP grade coating. It is possible that plating on L7™ hPSC Matrix or some other, as yet unidentified element of the differentiation process, led to cells with a greater proliferation potential.

The precise nature of the "overgrowth" in Experiment 2 is also unclear. First, it is important to distinguished between tumorigenesis, in which cells grow out of control, forming a space-occupying lesion and eventually causing raised intracerebral pressure, and an over-large graft which contain differentiated cells of either the required phenotype or an undesired phenotype. Large graft volumes, between 200-800 mm^3, were reported in Aubry et al. (2008), and animals were unwell (lethargy, weight loss, hemiparesis). When brains were harvested, grafts showed expression of the cell proliferation marker ki-67 and although there are no quantifications of this marker, ki-67 positive cells also express pax-6, a marker for neuronal cortical progenitors (Duan et al., 2013; Manuel et al., 2022); but not mature MSNs markers as DARPP32, indicating that ki-67 population might still be immature and therefore proliferating. Like Aubry et al. (2008), grafts with large volumes and cells expressing ki-67 were seen in Experiment 2, but a very large proportion of grafted cells expressed MSN markers, such as DARPP32, suggesting that a great proportion of the transplanted population had matured. Neither did rats in Experiment 2 show signs of illness, in contrast to Aubry et al. (2008) Together, these finding might suggest that growth was not uncontrolled, but this does not exclude the possibility of having islands of tumor cells. Therefore, other assessments would be needed to confirm this, as assess pluripotent (e.g. Nanog, Sox2, SSEA1/4) or other proliferative markers (e.g. MCM-2).

One mechanism underlying non-tumerogenic overgrowth could be due to off-target cell types proliferating within the graft. In Experiment 2, large numbers of DARPP32 cells were found which may have been of a neocortical, rather than MSN, phenotype. Given the huge disparity between the eventual size of the human and mouse cortex, one might predict that human cortical cells would have a very high proliferative capacity and that a larger than anticipated proportion of cortical progenitors in the transplanted cell suspension could have led to much larger grafts than expected. Another possible off-

target cells type are astrocytes, a proliferative brain population (Colodner et al., 2005) that could be present in the transplanted population and contribute to increase graft size. Unfortunately, striatal transplantation studies using hPSC have not reported astrocytes quantification and neither this study, but single cell transcriptomic in dopaminergic grafts reported not only neuronal population within transplanted cells, but also oligodendrocytes, astrocytes and vascular leptomeningeal cells (Tiklova et al., 2020).

Although the exact mechanism behind this excessive cell overgrowth is still unknow, the different cell batches, the expression of proliferative cell markers, or the presence of other cell types, could be possible factors for an overgrowth graft. This is a significantly important challenge to address specially when the field is moving to clinical translation. Future striatal transplant studies should characterise not only neuronal population, but also other possible cell types in the graft to unravel graft volume increased and have a better understanding of graft composition.

Graft expression of MSN markers

Key markers of MSN differentiation, including DARPP32 and CTIP2, were seen in grafts in all groups using IHC. Grafted cells from Experiment 1 expressed DARPP32 already by 5 weeks after transplantation, showing dense DARPP32 positive fiber bundles around the edges of the graft. This extensive fiber outgrowth was also evident at 9-, 12- and 17-weeks post-transplantation. The percentage of DARPP32 expression per area in Experiment 1 was 17.84%±2.93 at 5 weeks, 15.68±7.63 at 9 weeks, 28.98±1.34 at 12 weeks and 29.40±1.59 at 17 weeks. Transplanted cells from Experiment 2 expressed also DARPP32 but no quantification was performed for two reasons; firstly, because the staining background inside the graft did not allow to calculate area fractioning, as this measured is based in staining intensity. Secondly, because of time restrictions, no quantification of HuNu cells was performed to know the total population of the graft and quantified using stereology the number of positive DARPP32 cells based in total grafted population. Interestingly, no fiber bundles around graft edges of DARPP32 expression were observed in Experiment 2, only single cell bodies were DARPP32 positive. Although the reason for this difference in graft shape is unknown, not having enough space or other host MSNs to extend its axons and innervate the striatum, that had been completely undertaken by other grafted cells, could be a possible explanation.

When comparing DARPP32 percentage of Experiment 1 with the literature, it showed that it felt within what has been published on the last few years, although the percentage of DARPP32 expressing transplanted cells in the literature is variable. The highest expression was reported by Ma et al. (2012) with 58.6% expression of DARPP32 from GABA positive cells; to 21% of DARPP32 from NeuN population in Aubry et al. (2008) and 49% of HuNu positive grafted cells after 16 weeks post transplantation in Arber et al. (2015). Other authors quantified DARPP32 expression based on co-expression of DARPP32 with CTIP2, as in Besusso et al. (2020) with 3% of co-labeling of CTIP2 with DARPP32 in and in Schellino et al. (2023), with 11% in non-environmentally enriched animals and 17% in environmentally enriched animals. Co-expression of DARPP32 and CTIP2 was also showed in Experiment 1 although no quantification was performed. It would be recommendable to quantify, specially to know if all DARPP32 positive cells express CTIP2, as all adult striatal DARPP32 positive cells express CTIP2 (Arlotta et al., 2008). Another relevant marker for mature MSN is FOXP1, which has not been assessed in neither Experiment 1 and 2, but is also known it is co-express with DARPP32 in mature MSNs (Precious et al., 2016). These three markers would be critical to assess in future studies to have a better understanding of the phenotype of our cell transplantation product.

Of note, DARPP32 quantification is challenging, as observed in the images of this chapter; because DARPP32 positive staining is not only expressed individually in cell bodies within the graft, but it is also expressed along the fibers. In Schellino et al. (2023) authors not only quantified percentage of CTIP2/DARPP32 positive cells from HuNu population, but also analysed DARPP32 compartmentalization and calculate the percentage of patch-like zones per animal based on total transplant area. These results showed around 7% in non-environmentally enriched animals and 15% in environmentally enriched animals of patch-like zones area. Each publication quantified DARPP32 expression differently, making direct comparison challenging and we need to be cautious in interpreting marker counts due to the variability.

Host-to-graft connectivity

In this thesis in Experiment 1, traced cells were found in areas that are known to be part of the basal ganglia (sensorimotor cortical areas and thalamus) as well some projections in the SN, already 5 weeks post transplantation. After 17 weeks post-transplant, these connections were maintained. Afferent connections outside of the host striatum in Experiment 1 were found at earlier timepoints that what has been showed in

the literature, as compared to what had been published, Besusso et al. only observed traced cells within the graft and surrounded striatal areas at 1- and 2-months post grafting but not in afferent regions (Besusso et al., 2020) and Schellino et al. found afferent traced cells outside of the striatum at 6 months post transplantation (Schellino et al., 2023). Nevertheless, it is worth mentioning the cell product from these studies differ from the one in this thesis, being the main difference the use of SHH to drive a striatal phenotype (Delli Carri, Onorati, Castiglioni, et al., 2013) instead of Activin A. The exposure of SHH in combination with DKK1 inhibit the WNT pathway, ventralizing dorsal progenitors from the telencephalon (Li et al., 2009). On the other hand, Activin is a TGFβ family protein, that regulate phosphorylation and stimulation of SMAD proteins in the developing subpallium (Maira et al., 2010), and there is evidence of the presence of activin receptors during development in the subpallium as well (Feijen, Goumans, & van den Eijnden-van Raaij, 1994; Maira et al., 2010). This difference in the differentiation protocol could possibly affect maturation time of the product, accelerating it in our protocol, as cells showed DARPP32 expression (a marker for mature MSNs) already at 5 weeks post grafting, as well as host-to-graft connectivity, and both were maintained over time. On the other hand, expression of DARPP32 in Schellino et al. increased from two to six months post transplantation and host-to-graft connectivity was only observed after 6 months post graft. A similar timing pattern to Experiment 1 had previously been observed in PD models, where host-to-graft innervation has been also shown already at 6 weeks post-grafting, not only locally around graft areas, but also in prefrontal and sensorimotor cortex, thalamus, dorsal raphe nucleus and SN, and after 6 months post-transplant, these connections were maintained (Grealish et al., 2015).

When observing in detail which specific brain regions were extending synaptic contacts with the graft, starting from cortical regions, Schellino et al. (2023) found traced cells in infralimbic, agranular insula and orbital area as well as motor cortex. Experiment 1 showed cortical traced cells also in orbital (VO) and motor cortex (M1 and M2), as well as found projections in the insular cortex. Traced cells were also found in thalamus and hypothalamus in Schellino et al. (2023), although no specific areas are named. Experiment 1 also showed traced cells in the thalamus, in ventromedial (VM), ventrolateral (VL), mediodorsal (MDL) and anteroventral (AVVL) thalamic nucleus, but no traced cells in hypothalamic areas. Schellino et al. (2023) also found traced cells in the SN and amygdala, and in our study only projections were found in these two areas. In general, connectivity from both studies is very similar and matches the known afferents striatal areas. In Experiment 1, only one exception to this was found: the anteromedial thalamic nucleus (AM), in which neurons are reported to project to the cortex but not the

striatum, (Nelson, 2021). This finding could be an indication of a cortical population within transplanted cells.

In this chapter a traced cell was considered to be a cell in which we could observed the cell body and axons when looking under the microscope. However, not only cell bodies, but also fibres, from traced cells were found in various brain areas. Sometimes fibres were found in brain regions in which no traced cell was observed, and these might be axons from a cell body in that same brain area or could just be travelling through the brain region and have their cell body located remote to that region. As an example, only fibres but no mCherry positive cell bodies were found in the SN. Thus, these fibres could have originated in the SN but, as only 1:12 brains sections were used for each stain, the cell body may have been missed or those fibers could have come from a traced cell in another region such as thalamic region. Unfortunately, it is not possible to distinguished between those two options with the current data. For future studies, combining coronal sections with also sectioning some brains in sagittal sections or even brain clearing for imaging (Doerr et al., 2017) could be ways to distinguish from where these projections are coming and where they end.

Graft-to-host innervation

Human cytoplasm staining (STEM121) revealed that grafted cells from Experiment 1 also extended efferent projections to various areas of the basal ganglia circuit from as early as 5 weeks post-transplant, with increasing innervation density over time. STEM121 positive projections were seen in cortical areas, globus pallidus, thalamus and SN. One interesting featured that was noticed were the fiber bundles around graft edges that were present at every timpoint, and similar but in smaller size were found in thalamic nucleus. Published data of fetal tissue grafts in HD model showed striatal grafts project along and inside myelinated bundles of the internal capsule (Wictorin, Clarke, Bolam, & Bjorklund, 1990) and, interestingly, all timepoints showed a similar anatomical feature, the fiber bundles, close to graft edges and also in the thalamus. These bundles were becoming denser with time and could be myelinated bundles that are approaching striatal efferent areas as the GP. These fiber bundles had also been observed in dopaminergic grafts from other lab members, but data has not been published.

In the normal brain, striatal efferent connections projected to GP and SN (Lanciego et al., 2012), but there was no evidence of MSNs extending direct efferent connections to the cortex. There are several possibilities that could explain these off-target

projections. First, due to reflux of the cell suspension along the needle tract during surgery, in some animals cells refluxed into the cortex, and these may account for some of the projections to prefrontal cortical areas. However, projections to cortical areas, were also seen in animals with no evidence of cortical reflux. Another possibility relates to the heterogenous nature of the cell product. Specifically, as both cortical neurons and MSNs arise from the whole ganglionic eminence (WGE) (Stiles et al., 2010) and, although all transplanted neuronal progenitors had undergone the same differentiation protocol, a certain population could be more susceptible to mature to a more cortical phenotype, which could be expected to project to cortical regions. A similar explanation could apply to the finding of the traced cells in thalamic areas that normally only extend afferents to cortical areas, as mentioned in previous paragraphs. Thus, understanding this better will benefit from a more comprehensive characterization of graft composition. It is also possible that neither of these explanations are correct or complete, and that other mechanisms underlie the presence graft projections to areas of the brain not normally part of basal ganglia circuitry.

Graft-to-host connectivity

To date, there are no published reports of ΔG-rabies tracing of graft-to-host connectivity in HD models after transplanting hPSC-derived MSNs; only in PD, in which infusions were performed in the striatum to assess local connectivity and in the prefrontal cortex to test long distance connectivity. Dopaminergic grafts showed, after 6 months post-transplantation, graft -to-host connectivity with both areas (Grealish et al., 2015).

For our graft-to-host connectivity experiment, two efferent striatal regions were chosen, the GP and SN, to assess if the grafted cells could make synaptic contact with them. Unfortunately, as discussed above, transplants from Experiment 2 were larger and mis-placed ventrally. In some animals (e.g. Rat#3 or #4) the grafts were so large that they occupied efferent areas, as the GP. Although transplanted cells showed innervation around the borders of the graft, there were no projections found in the GP and SN with STEM121 staining.

Not finding STEM121 projections in efferent areas is aligned with the ΔG-rabies results, as no traced cells were found in the graft in any of the grafted animals, except for two projections in the graft edge of one of the animals. Even though graft overgrowth seemed like the most relevant limitation of this study, it would be important to consider another limitation to future experiments which is the injection site of both TVA-GFP-G

and ΔG-rabies viruses. As even if the injection was successfully delivered and starter cells were found in both GP and SN, might be that the number of starter cells is not enough or that infected cells are not innervating the graft location, but other region of the striatum. However, given the encouraging finding of STEM121 positive projections to expected efferent regions in Experiment 1 the same experiment is currently being repeated.

In summary, STEM121 and rabies tracing together demonstrated that human ESC-derived cells driven towards an MSN phenotype were able to form grafts that supported connectivity with the host brain, and that these largely involve normal elements of the cortico-striatal thalamic circuit, such as the cortex and the thalamus. Assessing graft to host synaptic connectivity was severely limited by the over-large grafts in Experiment 2, but the finding of extensive STEM121 projections in Experiment 1 have encouraged us to repeat this study, to hopefully obtain clearer data.

Chapter 4: Assessing host-to-graft connectivity in the F344tgHD rat model

4.1. Introduction

The previous chapter examined connectivity in a QA lesion model as this is a standard model and most research over the last few decades has used this or similar lesion models. The QA lesion recapitulates the excitotoxicity and MSN loss seen in HD however, it lacks other aspect of the disease as the neuronal pathology. The presence of the mutant gene is known to have a toxic gain of function effect, and leads to downstream changes such as abnormalities of cell metabolism, changes to the immune system etc. The question is whether transplanted cells can integrate in this environment and whether they can also differentiate appropriately, put out processes and make synaptic connections. It is also possible that the graft could have local effects on host striatum that could be beneficial or detrimental. Another important challenge is to know which is the best time window for transplantation. It is still unknown if transplanting outcome is better when grafting at early onset, into a younger brain, or if grafting at later stages into a more aged brain. To unravel all these questions, would be important to use a genetic model in which at least one copy of the mutant allele is present.

To date, there is a wide variety of HD rodent models available, especially in mice. Although mouse models are commercially available and manageable to handle, maintain and breed; the high number of CAG repeats results in animals with very aggressive phenotypes, more similar to juvenile stages of the disease rather than to adult onset. Therefore, in this chapter, the F344tgHD rats were used. This is a recent rat model carrying only 51 CAGs repeats, more translational to human HD adult onset. These animals have been behaviourally characterized previously and showed mHTT aggregates on different brain regions (Plank et al., 2018).

The aim of this chapter is to (1) assess host to graft connectivity in mutant F344tgHD rats compare to their WT littermates and (2) to investigate differences in graft integration and connectivity between a young and an aged brain. To achieve that, a group of young and a group of aged mutant F344tgHD rats and their WT littermates are bilaterally transplanted, and neural connectivity host-to-graft is assessed 10 weeks post grafting using the monosynaptic tracing based in the modified rabies virus. There is not a stablished timepoint during the disease that the transplant will be more successful,

therefore the comparison between ages to unravel any differences in graft integration and connectivity.

4.2. Experimental design

Four groups of rats; young F344tgHD, young WT, aged F344tgHD and aged WT rats were transplanted with hESC-derived MSNs expressing the TVA receptor and rabies glycoprotein required for the ΔG-rabies. The aged group of rats were part of a behavioural cohort that underwent the open field and cylinder tasks every two months, as well as circadian activity assessment using locomotor boxes; starting at four months of age. As part of a separate study (being analyzed by another member of the lab) all four experimental groups of rats were trained and tested on the 5CSRTT and elevated plus maze (EPM) tasks, that were performed 1 week pre- and 7 weeks post transplantation. This data does not form part of this thesis.

In the F344tgHD rat line, mutant animals can be divided into animals with high (F344tgHD^{high}) or low (F344tgHD^{low}) expression of the mutant transgene. However, in this chapter, I grouped high- and low-expressing animals for statistical analysis in order to increase the power. Animals were then stratified into high- and low- expressing groups if the combined analysis yielded significant differences.

Two groups of young rats were transplanted bilaterally at 4 months of age, a F344tgHD group of rats (N=4; all females) and a WT (N=2; all males) group. There were also two groups of aged rats transplanted bilaterally at 14 months of age; a F344tgHD group (N=6; 2 male and 4 female) and their WT littermates (N=4; 1 male and 3 females), of both genders. Transplanted cells expressed the TVA receptor, GFP and Glycoprotein required for the ΔG-rabies. One week prior to perfusion, animals received an infusion of ΔG-rabies into the graft and the graft edges. Starter cells express GFP and mCherry and traced cells only express mCherry. All animals were perfused at 10 weeks post transplantation and brains were harvested and processed for histological characterization. Experimental timeline is represented in Figure 27.

Of note, the original intention was that ΔG-rabies was infused in both hemispheres. The first two animals (14-month-old rats) did not survive bilateral viral infusion surgery, so I decided to infused ΔG-rabies in the right hemisphere only. In this aged group, 4 out of 10 animals died during rabies surgery (2 WT and 2 F344tgHD), with post-mortem analysis showing tissue damage in the grafted area possibly due to a bleeding. In the younger group, 1 of 6 grafted animals (F344tgHD) rat died during ΔG-rabies infusion.

These surgical deaths had an impact in groups size, reducing the number of experimental animals.

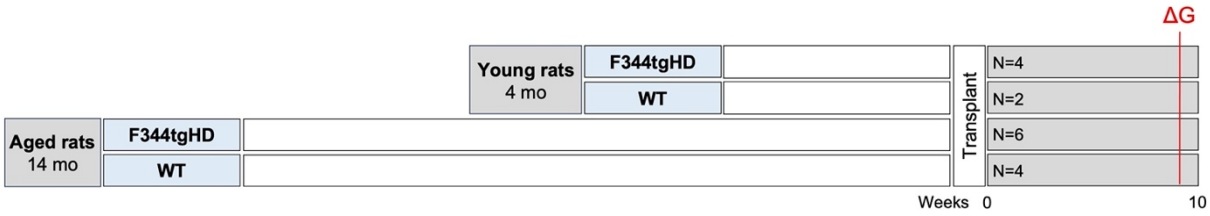

Figure 27 – Experimental timeline of transplanted experiment in F344tgHD rats. Four groups of animals were grafted, young F344tgHD, young WT, aged F344tgHD and aged WT rats. All groups were grafted for 10 weeks and a week before perfusion received an infusion the ΔG-rabies.

4.3. Results

4.3.1. Transplanted cells express MSNs markers FOXP1 and DARPP32

Transplanted hESC-derived MSNs at 10 weeks post grafting express hDARPP32 in young and aged animals, in both WT and F344tgHD animals (Figure 28A-H). Expression of hDARPP32 was mostly found around the edges of the graft, as shown in coronal sections (Figure 28A, C, E, G), with areas of grouped fibers and cells (Figure 28B, D, F, H). Calculation of hDARPP32 area was performed using area fractioning (See Chapter 2 section 2.7.2.3), and percentage of DARPP32 expression was based on total graft area across all sections, revealed no differences between WT and F344tgHD in both young (Figure *28*I) ($t(3)=0.041$, p=n.s., two tailed) and aged (Figure 28J) animals ($t(5)=0.533$, p=n.s., two tailed).

Cells in the grafts also expressed FOXP1, another important cellular marker of MSNs, and confocal images from Figure 29 show co-labelling of FOXP1 marker with hDARPP32 in WT and F344tgHD animals at both ages transplanted (examples shown by white arrows, one animal per group was stained to confirm FOXP1 expression) (Figure 29A, D, G, J).

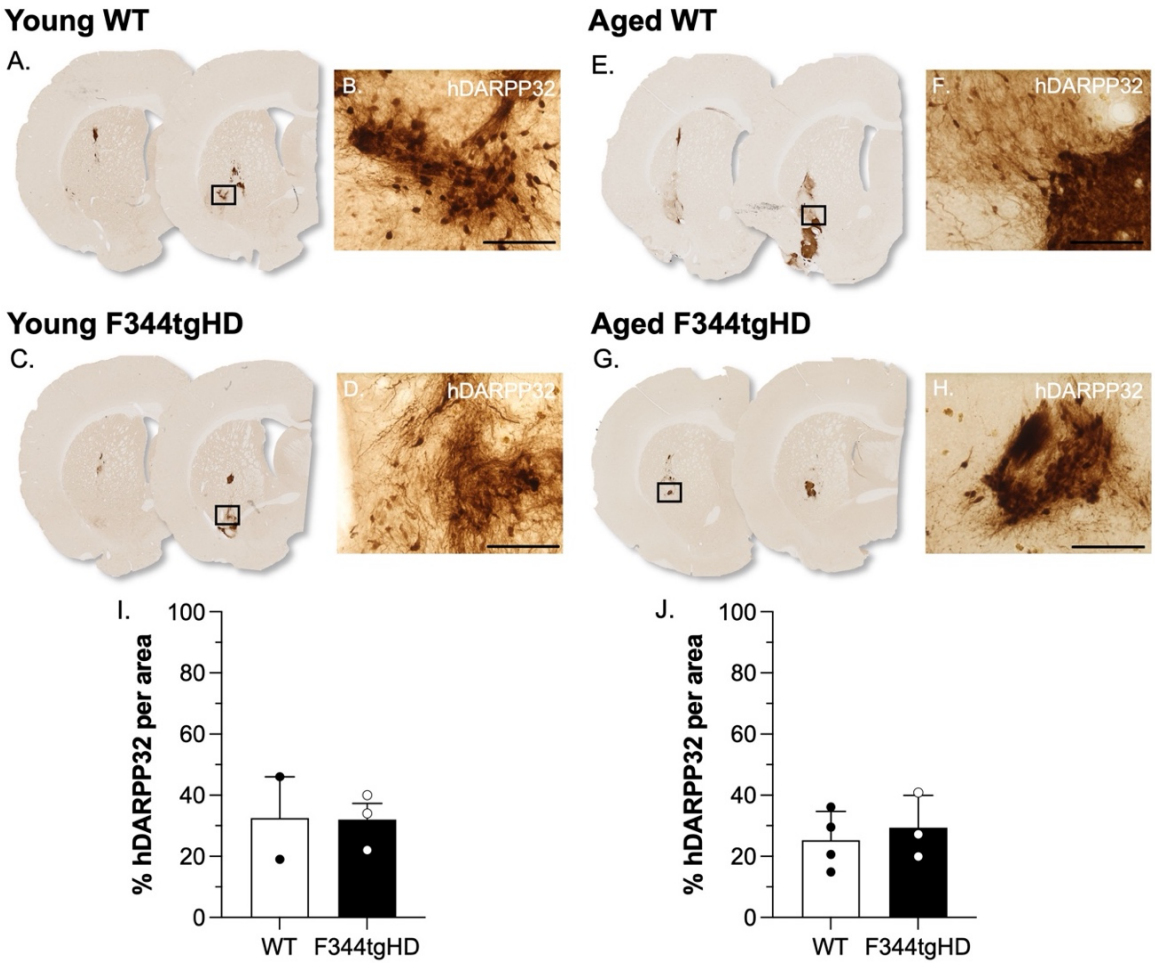

Figure 28 – Transplanted cells express hDARPP32 in WT and F344tgHD animals in both transplanted ages. Staining of hDARPP32 in coronal sections of young WT (A), young F344tgHD (C), aged WT (E) and aged F344tgHD (G). A black square in coronal sections represents the area of a higher magnification images of young WT (B), young F344tgHD (D), aged WT (F) and aged F344tgHD (H). Bar chart represents percentage of hDARPP32 per area in young (I) and aged (J) rats. Each bar represents the mean of each group and error bars represent SEM. Scale bar is 100µm.

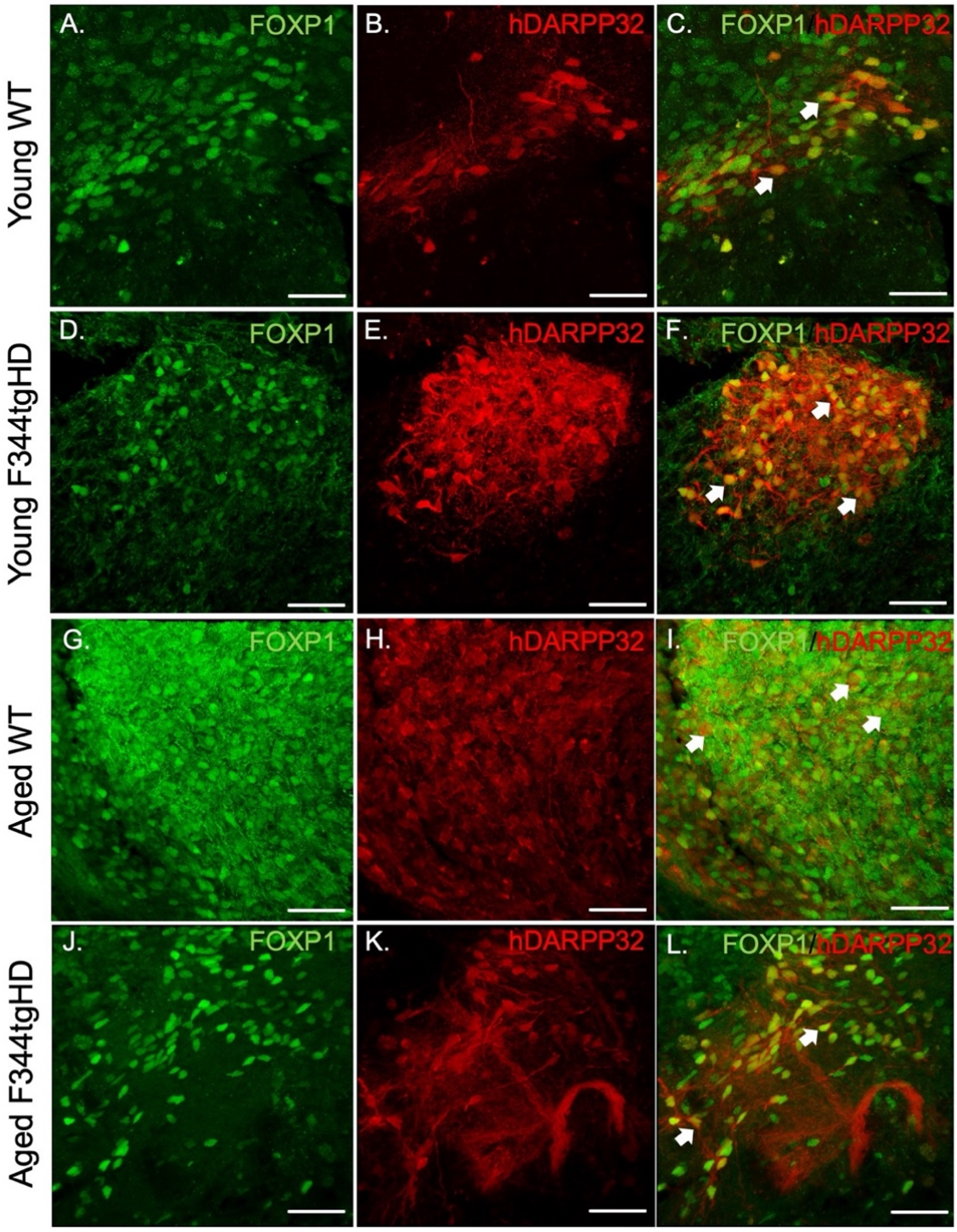

Figure 29 – Transplanted cells co-expressed FOXP1 and hDARPP32 in F344tgHD and WT animals at both young and aged animals. Immunofluorescence images of FOXP1 (green) and hDARPP32 (red) in young WT (A-C), young F344tgHD (D-F), aged WT (G-I) and aged F344tgHD (J-L). White arrows point to co-localization of FOXP1 and hDARPP32 markers. Scale bar is 20μm.

4.3.2. Human cytoplasm stained showed hESC-derived MSNs survive and integrate into the host brain of the F344tgHD rat, projecting to relevant areas of the basal ganglia circuit

At 10 weeks post grafting, grafted cells survived in both F344tgHD and WT littermates at both ages (Figure 30A, D, I, L). Graft volume was calculated on the basis of human cytoplasm staining (STEM121). Transplanting into either young F344tgHD or young WT animals, resulted in graft volumes that were not significantly different ($t(4)=1.685$, p=n.s., two tailed). When young F344tgHD animals were split into low and high transgene expressors (Figure 30H) there were no significant differences in graft volume between any of the groups ($F_{2,3}=2.342$, p=n.s.). However, in aged hosts graft volumes were significantly smaller in F344tgHD compared to their WT litter mates ($t(8)=4.887$, p=0.0012, two tailed, Figure 30O). Both aged F344tgHD^{low} and F344tgHD^{high} had significant smaller volumes when compared to WT (Figure 30P) ($F_{2,7}=5.093$; WT vs. F344tgHD^{low} p=0.02 and WT vs. F344tgHD^{high} p=0.01).

STEM121 positive staining revealed transplanted cells are able to extend neurites within the striatum (Figure 30A, B, D, E, I, J, L and M) and project to other brain areas of the thalamocortical circuit as the motor cortex (Appendix Figure 6), GP (Figure 30C, F, K and N), thalamic areas (Figure 30C, F, K and N), amygdala (Appendix Figure 6) and the SN (Figure 30C, F, K and N).

4.3.3. Rabies tracing demonstrated host to graft connectivity in both WT and F344tgHD rats

Figure 31 shows representative immunofluorescence images of the graft in a young WT and F344tgHD rat. Coronal sections showed an overview of the grafts expressing DAPI, GFP and mCherry in WT (Figure 31A-C) and F344tgHD (Figure 31H-J) rat. Starter cells are shown in higher magnification images of the graft showing the co-labelling between GFP and mCherry in WT (Figure 31D-G) and F344tgHD (Figure 31K-N) animals. Aged WT (Figure 32A-C) and F344tgHD (Figure 32H-J) rats graft, also show starter cells within the graft in WT (Figure 32D-G) and F344tgHD (Figure 32K-N).

Traced cells were found at both ages in WT and F344tgHD animals, in prefrontal cortical areas, GP, thalamic areas and SN. A summary of all areas in which traced cells /projections were found is in Table 14.

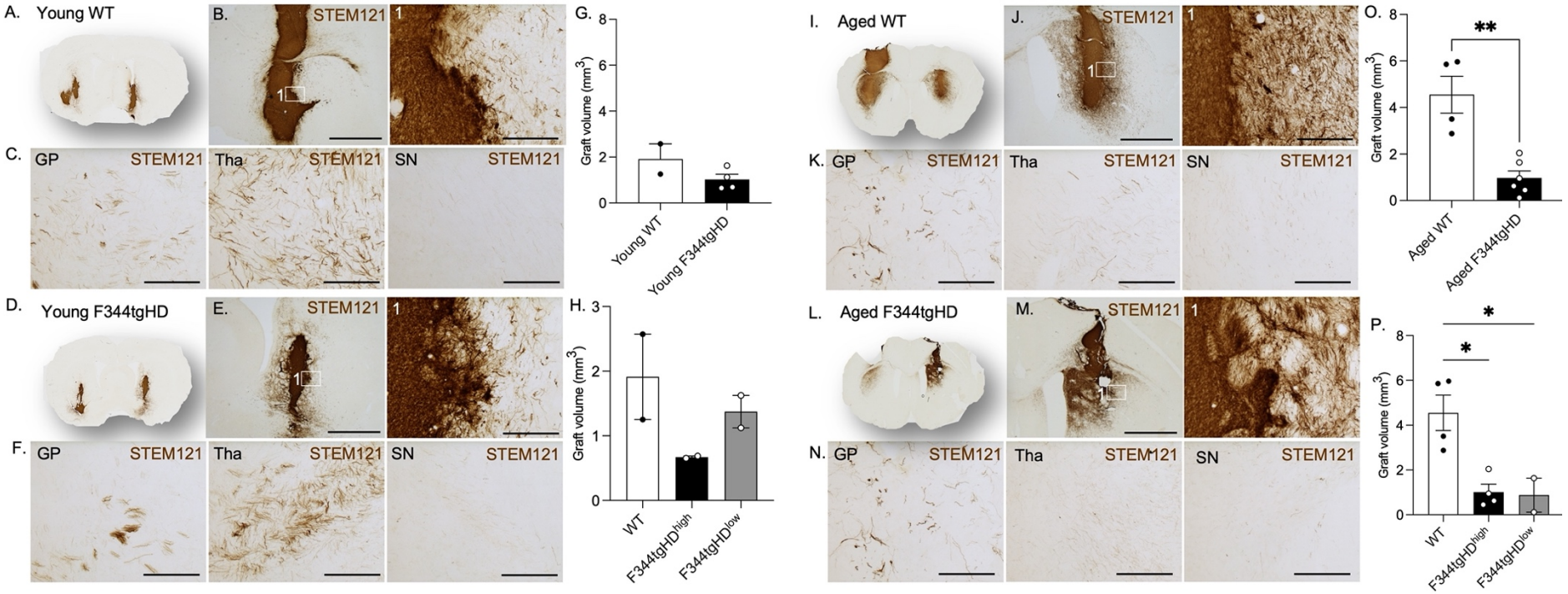

Figure 30 – Grafted cells integrate into the host brain and project to relevant areas of the thalamo-cortical circuit and graft volumes in F344tgHD animals were significantly smaller in aged rats. Histological representation of STEM121 in bilateral transplant (A, D,I, L). One of the grafts was shown in higher magnification and a zooming into the graft edges represented by the white square, to show graft projections in young WT (B), young F344tgHD (E), aged WT (J) and aged F344tgHD mutant (M) rats. Projections in GP, Tha and SN are represented in young WT (C), young F344tgHD (F), aged WT (K) and aged F344tgHD mutant (N) rats. STEM121 volumes expressed in mm^3 in young (G) and aged F344tgHD and WT rats (O), and in young (H) and aged (P), $F344tgHD^{high}$ and $F344tgHD^{low}$ and WT rats. Each bar represents the mean of each group and error bars represent SEM (*p<0.05), (**p<0.01). Each dot represents an animal. Scale bar for B, E, J and M=1500µm and rest of the images=200µm

In young WT rats, traced cells were found in infralimbic cortex (IL) (Figure 33A) and precommissural nucelus (PrC) (Figure 33C). There were also projections from prefrontal cortical areas, GP (Figure 33B), thalamic areas, amygdala, substantia innominata, preoptic nucleus, stria medullaris, anterior commissure, accessory neurosecretory nuclei, tuber cinerum area, zona incerta and SN (Figure 33D, Appendix Figure 7, Appendix Figure 8, Appendix Figure 9).

In young F344tgHD rats, traced cells were found in primary motor cortex (M1) (Figure 33E), GP (Figure 33F), paracentral thalamic nucleus (PC) (Figure 33G), central medial thalamic nucleus (CM) (Figure 33H), but also projections were found from various prefrontal cortical areas, CPu, thalamic areas, amygdala, habenula nucleus, endopiriform nucleus, dysgranular insular cortex, zona incerta, stria terminalis (Appendix Figure 10, Appendix Figure 11) and SN (Figure 33R, Appendix Figure 10 and Appendix Figure 11).

In aged WT rats, traced cells were found in M1 (Figure 33I) and mediodorsal thalamic nucleus, lateral part (MDL) (Figure 33K) and projections from GP (Figure 33J) and SN (Figure 33L). Projections were also found from cortical areas, CPu, thalamic areas and amygdala (Appendix Figure 13, Appendix Figure 14).

In aged F344tgHD rats showed traced cells in substantia innominate, basal part (SIB) (Figure 33O) and thalamus (Figure 33S), with projections from ventral orbital cortex (VO) (Figure 33M), GP (Figure 33N) and SN (Figure 33P). There were also projections in CPu, thalamic areas, amygdala, endopiriform nucleus, substantia innominata (), preoptic area, stria terminals and zona incerta (Appendix Figure 15, Appendix Figure 16).

Table 14 – Summary traced cells and projections for each group

	Young				Aged			
	WT		F344tgHD		WT		F344tgHD	
	Traced cells	Projections	Traced cells	Projections	Traced cells	Projections	Traced cells	Projections
Cortex	IL	Cg1, **IL**, PrL, VO	M1	M2, MO, PrL	M1	**M1** and M2		VO
Thalamus	PrC	CM, DA, LH, MCLH, Re, Rt, VL, VLH, VM, VMH, VPL, VPM	PC, CM	CL, **CM**, IMD, LDDM, LH, MCLH, MDC, MDM, **PC**, PF, Po, PSTh, PV, Rt, SubD, VL, VM		AVVL, CL, CM, MDC, PC, Rt, VL, VM	Thalamus	LH, MD, Rt, PSTh
Amygdala		AAD, AAV, ACo, BLV, BMA, BMP, CeL, CeM, LaDL, MeAV, MePV		BMA, BLA, BLP, MDL, MeAD, MePD	MDL	MDL		Astr, BSTIA, CeM, MeAD, MePV
GP		GP	GP			GP		GP
SN		SN		SN		SN		SN
Other regions		SI, SID MCPO SM IPACL Acc TC ZID		CPu LHbL, LHbM DEn DI ZI St		CPu		CPu Den, VEn SIB, SID LPO BST ZI

Abbreviations: AAD: anterior amygdaloid area, dorsal part; AAV: anterior amygdaloid area, ventral part; Acc: accessory neurosecretory nuclei; Aco: anterior cortical amygdaloid nucleus; Astr: amygdalostriatal transition area; AVVL: anteroventral thalamic nucleus, ventrolateral part; BLA: basolateral amygdaloid nucleus, anterior part; BLP: basolateral amygdaloid nucleus, posterior part; BLV: basolateral amygdaloid nucleus, ventral part; BMA: basomedial amygdaloid nucleus, anterior part; BMP: basomedial amygdaloid nucleus, posterior part; BST: bed nucleus of the stria terminalis; BSTIA: bed nucleus of the stria terminalis, intraamygdaloid division; CeL: central amygdaloid nucleus, lateral division; CeM: central amygdaloid nucleus, medial division; Cg1: cingulate cortex, area 1; CL: centrolateral thalamic nucleus; CM: Central medial thalamic nucleus; CPu: caudate putamen; DA: dorsal hypothalamic area; Den: dorsal endopiriform nucleus; DI: dysgranular insular cortex; GP: Globus pallidus; IL: infralimbic cortex; IMD: intermediodorsal thalamic nucleus; IPACL: interstitial nucleus of the posterior limb of the anterior commissure, lateral part; LaDL: lateral amygdaloid nucleus, dorsolateral part; LDDM: laterodorsal thalamic nucleus, dorsomedial part; LH: lateral hypothalamic area; LHbL: lateral habenular nucleus, lateral part; LHbM: lateral habenular nucleus, medial part; LPO: lateral preoptic area, M1: primary motor cortex; M2: secondary motor cortex; MCLH: magnocellular nucleus of the lateral hypothalamus; MCPO: magnocellular preoptic nucleus; MDC: mediodorsal thalamic nucleus, central part; MDL: mediodorsal thalamic nucleus, lateral part; MDM: mediodorsal thalamic nucleus, medial part; MeAD: medial amygdaloid nucleus, anterodorsal part, MeAV: medial amygdaloid nucleus, anteroventral part; MePD: medial amygdaloid nucleus, posterodorsal part; MePV: medial amygdaloid nucleus, posteroventral part; PC: paracentral thalamic nucleus; PF: parafascicular thalamic nucleus; Po: posterior thalamic nuclear group; PrC: precommissural nucleus; PrL: prelimbic cortex; PSTh: parasubthalamic nucleus; PV: paraventricular thalamic nucleus; Re: reuniens thalamic nucleus; Rt: reticular thalamic nucleus; SI: substantia innominata; SIB: substantia innominata, basal part; SID: substantia innominata, dorsal part; SM: Nucleus of the stria medullaris; SN: Substantia nigra; St: stria terminalis; SubD: submedius thalamic nucleus, dorsal part; TC: tuber cinereum area; VEn: ventral endopiriform nucleus; VL: Ventrolateral thalamic nucleus; VLH: ventrolateral hypothalamic nucleus; VM: Ventromedial thalamic nucleus; VMH: Ventromedial hypothalamic nucleus; VO: ventral orbital cortex; VPL: ventral posterolateral thalamic nucleus; VPM: ventral posteromedial thalamic nucleus; ZI: zona incerta; ZID: zona incerta, dorsal part.

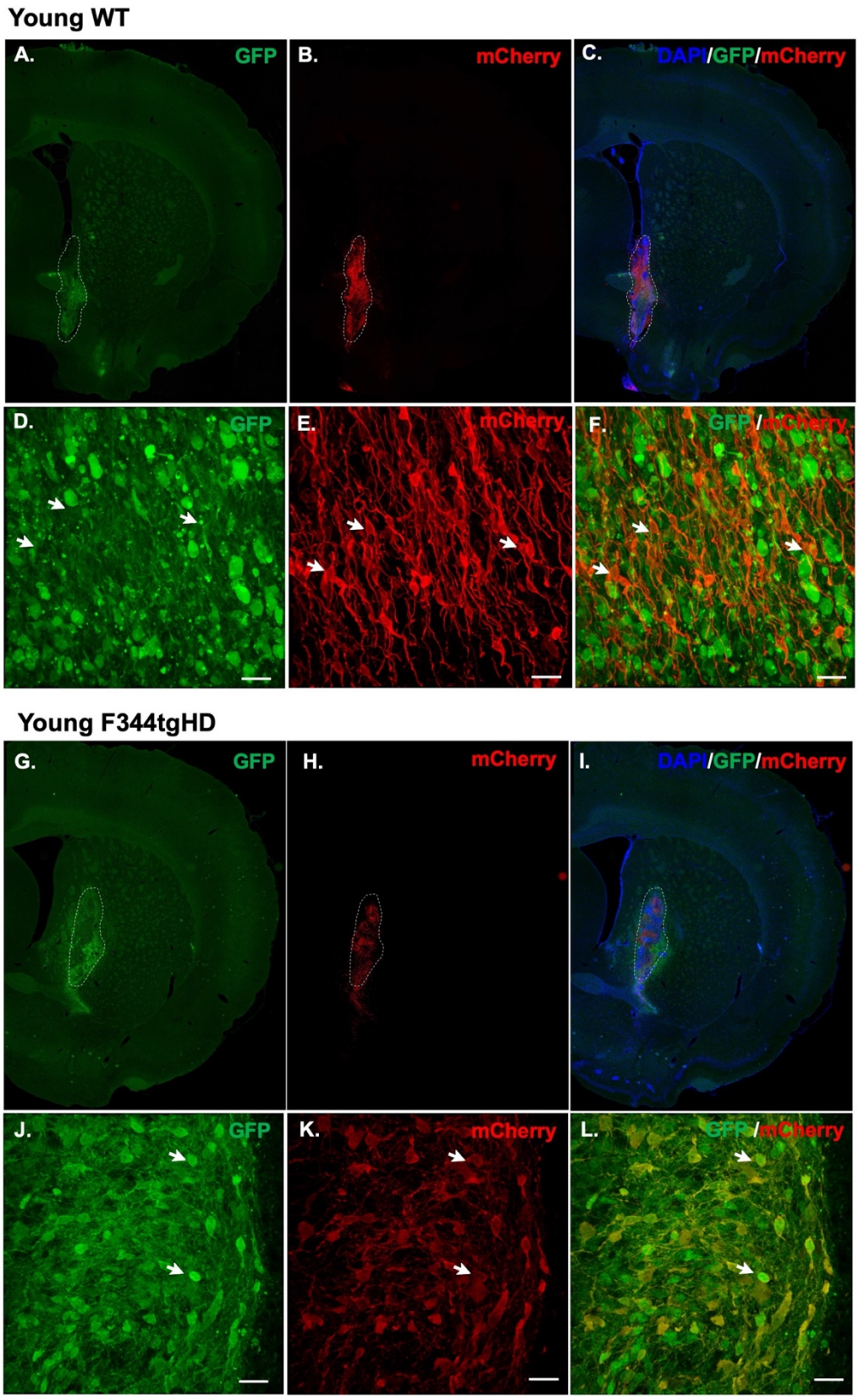

Figure 31 – Transplanted cells integrated into the host brain and starter cells were found within the graft in young F344tgHD and WT rats. Representative fluorescence images of the graft expressing GFP and mCherry are shown in WT (A-C) and F344tgHD

animals (G-I). Starter cells within the graft co-expressed GFP and mCherry in WT (D-F) and F344tgHD rats (J-L) and are marked with a white arrow. Scale bar= 20µm

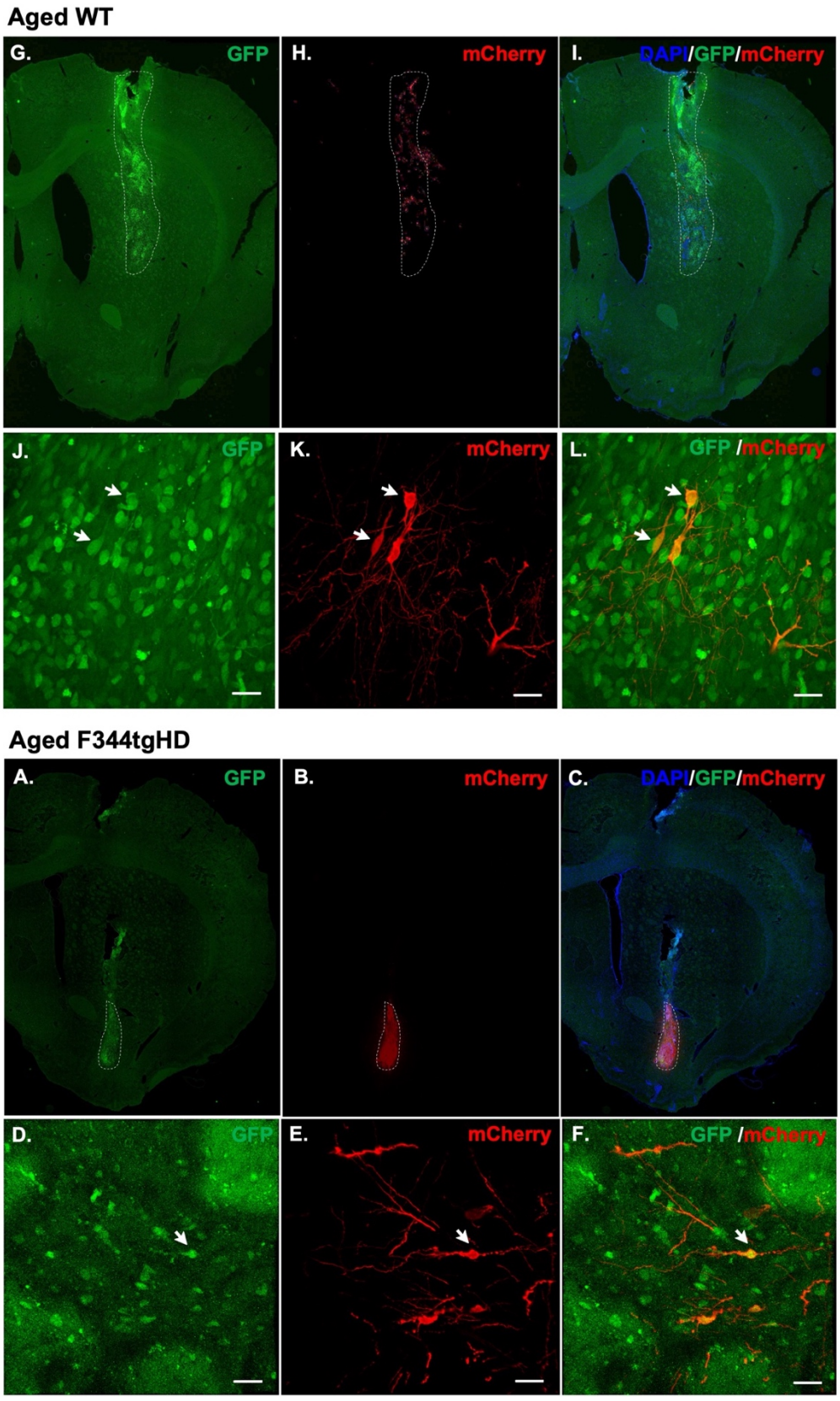

Figure 32 – Starter cells within the graft in F344tgHD and WT rats. Representative images of the graft expressing GFP and mCherry are shown in WT (A-C) and F344tgHD

animals (G-I). Starter cells co-expressed GFP and mCherry in WT (D-F) and F344tgHD rats (J-L). Co-labelling is shown with white arrows. Scale bar=20µm

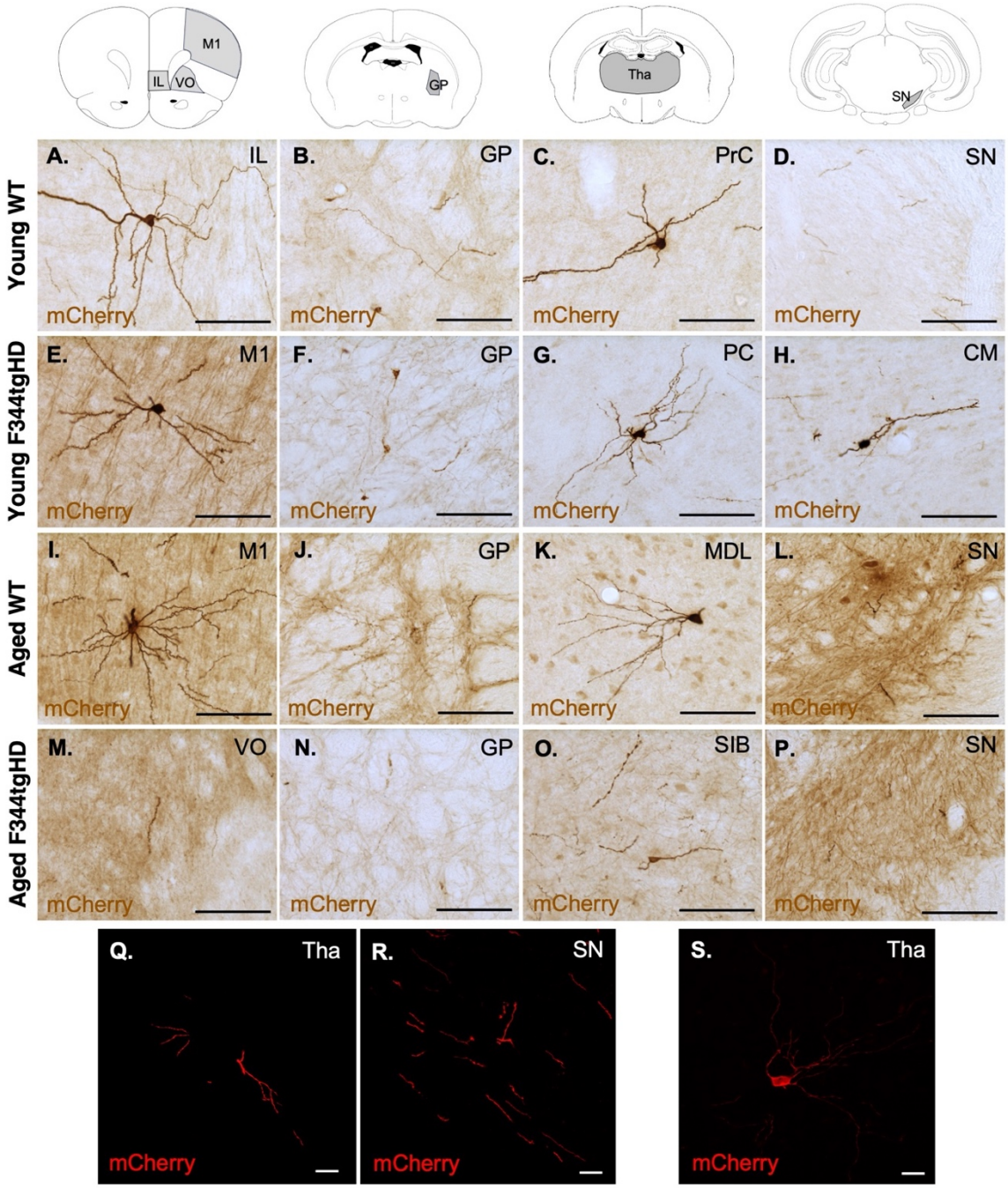

Figure 33 – Host brain made synaptic contacts with grafted cells in young and aged WT and F344tgHD rats. Coronal sections at the top of the figure represent the the key brain regions, in grey, where traced cells were found. Traced cells are shown by immunohistochemistry (A-P) and immunofluorescence (Q-S) images of mCherry protein. Young transplanted WT rats received synaptic contacts from IL (A), GP (B), PrC (C) and SN (D). Young mutant rats traced cells were found in M1 (E), GP (F), PC (G) and SN (H). In aged WT rats traced cells were located in M1 (I), GP (J), MDL (K) and SN (L) and in aged F344tgHD rats host cells from VO (M), GP (N), SIB (O) and SN (P) connected with grafted cells. Immunofluorescence images of traced cells in a F344tgHD young rat were found in thalamic areas (Q) and SN (R) and in an aged F344tgHD rat in thalamic areas (S). Scale bar A-P = 100µm. Scale bar Q-S=20 µm. IL: infralimbic cortex; M1:

primary motor cortex; VO: ventral orbital cortex; GP: globus pallidus; PrC: precommissural nucelus; PC: paracentral thalamic nucleus; MDL: mediodorsal thalamic nucleus, lateral part; SIB: substantia innominate, basal part; SN: substantia nigra; CM: central medial thalamic nucleus; Tha: Thalamus.

4.3.4. No differences in microglial expression at 10 weeks post grafting

Differences in graft volumes between WT and F344tgHD rats cold be due to host environment. The HD brain is known to be an environment with an increased inflammatory response, with activation of microglia prior to disease onset (Tai et al., 2007), as well as an increased number of microglia cells and morphology changes (Sapp et al., 2001). In CRT studies, it has been reported the effect of grafts to induce an inflammatory response, with the presence of microglia and astrocytes within the graft and surrounding graft areas (Cicchetti et al., 2009; Schellino et al., 2023).

In this study, the inflammatory response was investigated using OX42 (to detect activated microglia) and Iba1 (to detect all microglia stages and macrophages) immunohistochemistry in three brain areas: inside the graft, outside the graft and in the cortex (Figure 34A). All groups were stained at the same time and microglial marker expression was assessed through optical density quantification. There were no significant differences in optical density of OX42/Iba1 between F344tgHD and WT young rats in any of the areas (outside: $F_{1,2}$=0.941, n.s.; inside: $F_{1,2}$=1.000, n.s.; cortex: $F_{1,2}$=1.280, n.s) (Figure 34B). Neither were significant differences found between F344tgHD and WT aged animals in any of the areas evaluated (outside: $F_{1,2}$=0.245, n.s.; inside: $F_{1,2}$=6.853, n.s.; cortex: $F_{1,2}$=0.108, n.s) (Figure 34C).

However, although there was no cell quantification, images revealed an increased number and stronger staining of OX42 positive cells inside the graft and surrounding graft edges in younger animals compared with the aged group. Microglia morphology, showed by Iba1 expression, suggested more ramifications in microglia in young F344tgHD rats compared to their WT littermates.

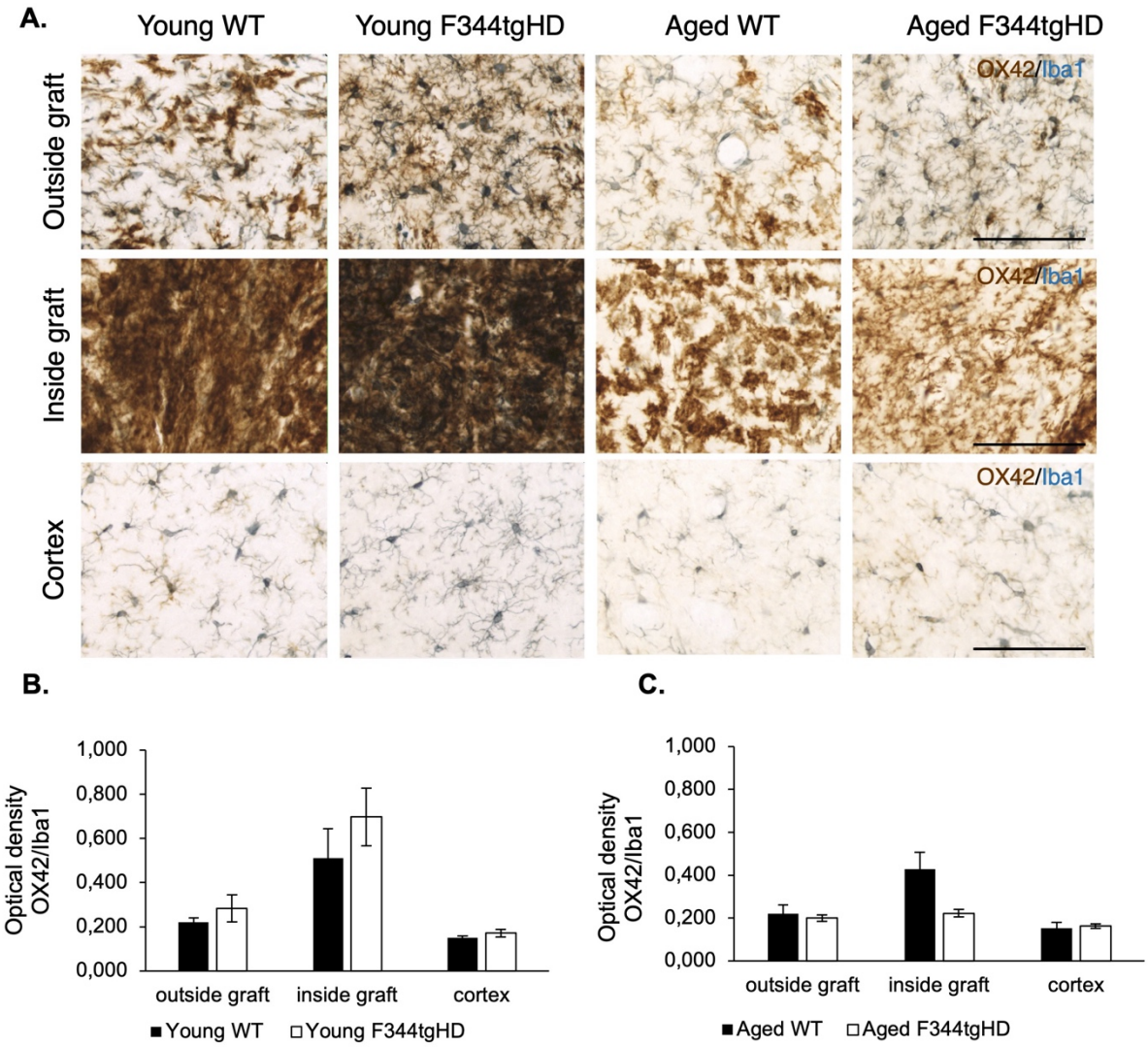

Figure 34 - Inflammatory response in grafted F344tgHD rats. (A) Histological images of OX42 (in brown) and Iba1 (in blue) in young and aged WT and F344tgHD rats inside and outside the graft as well as in the cortex. (B) Optical density quantifications in young and in (C) aged WT and F344tgHD rats. Each bar represents the mean of each group and error bars represent SEM. N=2 for all groups. Scale bar=100µm

4.3.5. Expression of mHTT in aged F344tgHD but not in young mutant animals

A key pathological feature of HD is the presence of mHTT aggregates within the brain. The presence of aggregates has been reported in the F344tgHD rat in the caudate putamen, but also in the bed nucleus of the stria terminalis, the nucleus accumbens, the piriform cortex and olfactory tubercle at 21 months of age. Expression of mutant HTT was assessed using S830 antibody in combination with human nuclei (HuNu) staining, in order to investigate if healthy human transplanted cells are affected by the disease.

Host striatum of young WT and F344tgHD did not show any mHTT expression (Figure 35C and F). No mHTT expression was found in host striatum of aged WT (Figure 35I) but aggregates were found in the striatum of aged F344tgHD rats (Figure 35L). Graft core and graft edges of young WT (Figure 35A and B) and F344tgHD (Figure 35D and E) rats did not present mHTT expression. No presence of aggregates was neither observed in graft core of aged WT (Figure 35G) and F344tgHD animals (Figure 35J). Neither were aggregates in graft edges in aged WT animals (Figure 35H), however, in graft borders of aged F344tgHD rats, aggregates were seen in the area in close proximity to or apparently co-incident with HuNu positive cells (Figure 35K, mark with white arrows), although it was not confirmed whether mHTT aggregates were within human cells or in a different layer of tissue.

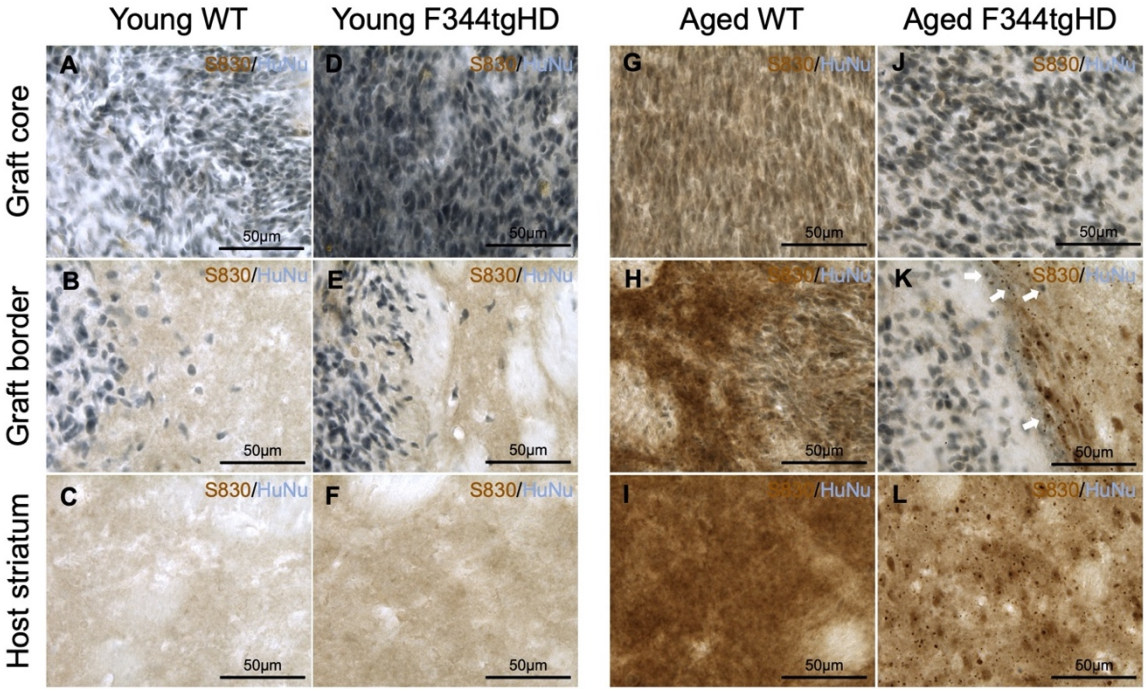

Figure 35 – Mutant huntingtin aggregates were shown in aged F344tgHD animals host striatum but not within the graft. Mutant huntingtin was shown using S830 antibody and human grafted cells were identified using human nuclei (HuNu). Graft core is represented in young WT (A), young F344tgHD (D), aged WT (G) and aged F344tgHD (J). Graft border with host striatum is shown in young WT (B), young F344tgHD (E), aged WT (H) and aged F344tgHD (K). Host striatum is shown in young WT (C), young F344tgHD (F), aged WT (I) and aged F344tgHD (L). Scale bar is 50µm. White arrows show possible human cells carrying mhtt aggregates.

4.4. Discussion

In this chapter the aim was to (1) assess host to graft connectivity in mutant F344tgHD rats compare to their WT littermates and (2) to investigate differences in graft integration and connectivity between a young and an aged brain. Findings showed that the mutant host brain is capable of making synaptic contact with transplanted human cells, comparable to a WT brain. Also, transplanted cells successfully integrated and extended projections within the host brain at both ages.

Graft characterization

There was 100% graft survival in rats that reached the experimental endpoint of 10 weeks post-grafting. Several rats died before this time point, during ΔG-rabies infusion surgery (1 young F344tgHD, 2 aged WT and 2 aged F344tgHD). After processing the tissue, grafts from these rats could be seen to be damaged, possibly due to intracranial bleeding, leaving one hemisphere of the grafted tissue unviable for histological characterization. Nevertheless, the other hemisphere was included in the analysis. It is known that the adverse effects of anaesthesia and surgery in aged individuals have a more significant impact compared to young individuals (Strom, Rasmussen, & Sieber, 2014) and specifically in this F344 strain, aged rats take longer to recover from anaesthesia as well as having a brain more sensitive to anaesthetic compared to young rats (Chemali et al., 2015). Therefore, the higher number of deaths in aged rats could be due to age and the higher risk of adverse effects with anaesthetic or surgical recovery.

This was the first time this strain was used for stereotactic surgery in the lab and there is no previous evidence in the literature of transplantation studied in this strain. Striatal location of the grafts in the young group, was more ventral than desirable. Stereotactic coordinates were established in Lister-Hooded strain (See Chapter 2 Section 2.4.4); thus, coordinates will need to be revised for future transplant experiments, particularly in younger (smaller) rats.

Although graft location in young rats was not as planned, immunohistochemistry and immunofluorescence revealed transplanted cells in both young and aged WT and F344tgHD host brain expressed the key MSN markers DARPP32 and FOXP1. DARPP32 quantification revealed no differences between grafts implanted into WT or F344tgHD animals or between ages. There was no quantification of co-labelling of these two markers due to time shortage, but will be interesting to quantify in future experiments,

to know if there are any differences between grafts implanted into F344tgHD versus WT brain.

Previous transplant studies using hPSC-derived striatal progenitors in mouse genetic HD models also showed DARPP32 expression in mature grafts; this was seen in R6/2 after 12-15 weeks post grafting (Adil et al., 2018) and in YAC128 after 12 weeks post transplantation (Jeon et al., 2014), although DARPP32 was not quantified in either study. In transplanted animals from this chapter, DARPP32 expression was mostly found around graft edges, grouped in fibers surrounded by single cells bodies. This appearance made it challenging to quantify its expression precisely. In this chapter, DARPP32 expression was measured based on percentage of DARPP32 positive area compared to total graft area using ImageJ, with no distinction between cell bodies and fibers. As mentioned in Chapter 3 discussion (Section 3.5), each publication quantified DARPP32 expression differently, making direct comparison challenging.

Nevertheless, the expression of DARPP32 in these grafted F344tgHD rats was around 30% higher than in other published studies of hPSC-derived grafts at similar post-graft survival times, with 5% expression after 3 months post grafting in B6CBA mice (Comella-Bolla et al., 2020) and 18% of DARPP32/CTIP2 co-expression in QA lesion rats after 2 months post transplantation (Besusso et al., 2020). There are also other studies with higher DARPP32 expression, such as in QA lesion mice 4 months post grafting with 58.6% DARPP32/GABA (Ma et al., 2012) and 48.7% expression (Wu et al., 2018). Longer time post graft does not necessarily result in higher expression of MSN markers over the time, as has been shown in Chapter 3 (QA transplanted rats at different timepoints post graft) and is also mentioned in Aubry et al. (2008), in which striatal grafts increased size over time but not DARPP32 expression. Unfortunately, there is not yet an established expression threshold of DARPP-32 expression to indicate a functional graft. It will be interesting to know in future experiments if longer times post grafting leads to higher expression of MSN markers.

The influence of the HD environment on the graft

Although no differences in MSNs markers expression were found between WT and F344tgHD animals at either age, there was a difference in graft volume. Grafts in F344tgHD animals were significantly smaller in aged F344tgHD compared to WT rats and showed a similar (non-significant) trend in younger animals. Both F344tgHD^{high} and F344tgHD^{low} aged rats had significantly smaller grafts than their WT littermates. Differences in graft volumes between WT and F344tgHD animals were also reported in

Adil et al. (2018), in which the authors noted that graft volumes were smaller in R6/2 compared to WT animals. Although no quantification was shown, these authors hypothesized the smaller size could be due to the pathology of the disease, as they found mHTT aggregates not only in host mouse tissue but also in transplanted human cells. In this chapter, aggregates were found in host striatum of aged F344tgHD rats, but not within the graft core. Some aggregates were seen in human cells in the graft border, but with the current images it was challenging to draw conclusions. An IF staining of S830 with HuNu could be helpful to elucidate if there is co-localization.

The presence of huntingtin aggregates in the striatum could have an impact on graft volume and survival in aged rats, but no aggregates were found in younger rats. Young F344tgHD rats showed smaller (non-significant) graft size compared to WT but the presence of aggregates is not necessarily related to disease presence, as there are other mechanisms related to the pathogenesis of the disease as transcriptional dysregulation, altered protein homeostasis, mitochondrial and glial dysfunction, altered synaptic plasticity or axonal transport defect (Jimenez-Sanchez et al., 2017), that could be happening in younger brains.

Graft volume could be also affected by inflammatory processes. Results from this chapter reported microglial activation in the graft and surrounding graft edges by OX42 positive staining, but no significant differences were found in optical density quantification of OX42/Iba1 in any of the groups or ages in all areas assessed. Expression of OX42/Iba1 markers was measured based on the marker's intensity, which is a first approach to unravel any differences in this model after transplantation. However, this was not the most precise evaluation, as Iba1 is normally evaluated based on its morphology (Green, Murphy, & Rowe, 2022). No significant differences could be due to the low number of animals per group. Although differences were not significant, young F344tgHD rats had higher optical density values inside the graft and images also showed a more intense expression of OX42 compare with WT animals. As OX42 is a marker for activated microglia, it could indicate that an inflammatory process was occurring that might have affected graft survival.

Also, in young F344tgHD rats Iba1 expression, although there was no quantification, histological images revealed young F344tgHD microglia is more arborized than WT rats. In aged animals, arborization looked very similar in both genotypes. Arborization or ramification of microglia has been investigated in the R6/2 model, using Iba1 marker. At 3 and 10 weeks of age, arborization area of microglia is higher in R6/2 compared to their WT littermates but, at 13 weeks of age, microglia area arborization is similar in R6/2 and WT mice (Savage et al., 2020). The reduction of ramification with age

is a natural process, decreasing with age (Davies et al., 2017) but hyper-ramification has been described before as an unusual microglial state that is present in situations of higher stress and excitotoxicity (Hinwood et al., 2012). The activated, plus the hyper-ramified, microglia conditions could contribute negatively to cell survival producing smaller grafts that in WT animals. There are no previous studies about the brain immune system in the F344tgHD rats, but there is evidence of the impact of microglia activation on human grafted tissue in a human post-mortem study (Cicchetti et al., 2009) and in hESC-derived striatal progenitors in QA lesion model (Schellino et al., 2023). There is also evidence of inflammatory changes in the brain of HD patients even before symptom onset (Tai et al., 2007), which could correlate with these younger rat phenotypes.

Graft connectivity

Graft innervation was seen with human cytoplasm staining, STEM121 in both ages and both genotypes. Grafts innervated within the striatum and extended projections to other areas of the basal ganglia circuit as the cortex, GP, thalamic areas and SN. Again, due to the low number of animals per group there was no quantification of innervation density within the graft edges, although images did not reveal any significant differences between any of the groups or ages.

MSNs in the striatum are known to extend efferent projections to the GP and the SN, but not to cortical or thalamic areas. However, projections in thalamic areas have been observed before in VM thalamic regions (Besusso et al., 2020) when transplanted hESC-derived striatal progenitors in a rat QA model. On the other hand, innervation to prefrontal cortical areas has not been reported before in any transplantation study using hPSC-MSNs. A possible explanation might be due to the *in vitro* differentiation process transplanted neuronal progenitors undergo before being transplanted. Direct differentiation protocols aim to mimic neuronal development, through signal modulations of a variety of molecular pathways (Fowler, Ang, & Loh, 2020). Cortical and striatal cells have their common origin in the ganglionic eminences (Boitor-Borza et al., 2021), an area that is divided into three main regions (LGE, MGE and CGE) and to date it has been challenging to develop *in vitro* protocols that regionalized precisely these profiles (Hunt et al., 2023). This challenge, combined with the difficulties in the stem cell field to obtain a homogenous population of the desire cell type after differentiation (Fowler et al., 2020; Watt & Hogan, 2000) could be an explanation for these results. For future studies will be interesting to characterize the graft with cortical markers as TBR1, FOXP2 and CTIP2

(Arlotta et al., 2005; Bulfone et al., 1998; Ferland et al., 2003) to have a more comprehensive understanding of the grafted population.

Not only was the graft able to extend projections to the host, but various regions of the host brain appeared to be making synaptic connections with the graft. Monosynaptic tracing based on the modified rabies virus revealed host-to-graft connectivity in both WT and F344tgHD animals at both ages. All grafts, irrespective of the host, received neuronal inputs from host cortical, thalamic, amygdala and nigral areas. However, there are more areas found with traced cells and projections in young animals, both WT and F344tgHD, compared to aged rats. Appendix figures (from 7 to 16) shows one rat from each group with all traced cells and projections found within that brain. When looking at young rats, there were traced cells/projections in 45 different areas in WT and 47 in young mutant compared to 16 in aged WT and 30 in aged mutant rats. Although there was no quantification of starter cells, fluorescence images revealed that mCherry expression within the graft in aged animals was lower than in young ones and might be a possible reason why there were fewer traced cells. It is also important to mentioned that IF was performed in 1:12 brain sections, and this could limit the presence of traced cells, underpowering the result.

It is known that neuronal plasticity declines with age, as for aged individuals the acquisition of new knowledge is more challenging compared to young ones (Ghasemian-Shirvan et al., 2020), and this could be likely associated with less synaptic connections in aged animals. For future studies it would be interesting to combine neuronal tracing with certain behavioral tasks to have a better understanding of the mechanism behind these connections and maybe unravel possible differences between young and aged individuals. To date the best age window for transplantation is unknown and requires more studies.

The striatum afferent connections come from cortex, thalamus, amygdala, SN and raphe (Lanciego et al., 2012), matching the areas where traced cells were found in this experiment in all groups. The only evidence of hPSC-MSN graft connectivity in a genetic model of HD is from the SN, where Fluorogold injections were infused (Adil et al., 2018). Host-to-graft connectivity has been also reported in neurotoxic models such as ibotenic acid lesion rats transplanted with rat fetal tissue, using the retrograde tracer Fluorogold in the graft, observing connectivity from cortex, thalamus, amygdala, SN and dorsal raphe (Wictorin & Bjorklund, 1989) and the most recent evidence is from 2023 using the ΔG-rabies in QA lesion rats transplanted with hESC-derived striatal progenitors and reporting traced cells in frontal cortex, thalamus, hypothalamus, SN and amygdala (Schellino et al., 2023).

Of note, graft placement was different between young and aged rats and not consistent in all animals. As mentioned at the beginning of this discussion, stereotactic coordinates were not evaluated in this strain and neither in young (and smaller) brains. Placement of transplanted cells could have a significant impact in graft connectivity, as different striatal regions might have received different afferent connections. For example, the amygdala extends inputs to ventral areas of the striatum (Choi, Ding, & Haber, 2017). Young rats graft location was in the ventral striatum and these groups also showed traced cells and projections in more areas of the amygdala than the aged rats, with grafts located more rostromedial. The relevance of graft location has been studied in PD models, as L-DOPA induced dyskinesias are effectively reduced when cells are grafted in caudal but not rostral areas of the striatum (Carlsson et al., 2006). It will be important for future studies with this strain to improve surgical coordinates but also will be interesting to know if graft placement has a significant impact in functional recovery.

In summary, traced cells are located in areas related to the basal ganglia circuit, confirming functional synaptic connectivity of the host with the graft in young and aged F344tgHD rats and WT littermates.

Chapter 5: IEG expression as an assessment of functional recovery and reviewing the excitotoxic model QA

5.1. Introduction

The aim of this chapter was to investigate the use of immediate early genes (IEG) as a biomarker to assess neural network activity after transplantation in the QA lesion model. The project explored how the QA striatal lesion affected the expression of IEG in relevant areas of the basal ganglia circuit, to determine whether this could be modulated by the presence of a graft.

IEGs are a group of genes rapidly and transiently activated in response to cellular stimuli. They are involved in neuronal plasticity and cognitive functions (such as memory) and have the potential to be used as a tool for mapping neuronal activity (Okuno, 2011; Sagar, Sharp, & Curran, 1988), social behaviour (Miura et al., 2020), memory (Meenakshi, Kumar, & Balaji, 2021), or the neuroendocrine system (Kovacs, 2008) providing information about where and when certain neurons have been activated. *c-fos* and *egr-1* have been the most commonly used markers to measure neuronal activity (Thomas A. Terleph, 2006) and their time-course of expression is well studied (Bisler et al., 2002; Zangenehpour & Chaudhuri, 2002), although in this chapter basal levels were assessed to identified hypo- or hyper-activity as a result of a neural damage. Therefore, the activity of these genes was selected for use as biomarkers of neural network activity in the QA model.

Egr1, which belongs to the Egr family of proteins, is sensitive to environmental stimuli (Brennan, Schellinck, & Keverne, 1999), learning and memory (Grimm & Tischmeyer, 1997; Nikolaev et al., 1992; Okuno & Miyashita, 1996), and is also induced by drugs of abuse (Bhat, Cole, & Baraban, 1992; Moratalla, Robertson, & Graybiel, 1992; Valjent et al., 2001). The *c-fos* gene belongs to the FOS family and c-Fos has been described as a transient protein (Sagar et al., 1988), whose expression is induced by Ca^{2+} and cAMP signaling (Sheng & Greenberg, 1990). It has a relevant role in development, as illustrated by *c-fos* knock-out mice which show developmental abnormalities (Johnson, Spiegelman, & Papaioannou, 1992) as well as learning deficits (Paylor et al., 1994). C-Fos expression is used as a marker for neural activity associated

with learning (Bertaina-Anglade, Tramu, & Destrade, 2000), memory (Vann et al., 2000), synaptic plasticity (Calais et al., 2015), fear processing (Nikolaev et al., 2002) or stress (Machida, Lonart, & Sanford, 2018).

The original intention of this chapter was to use IEG expression as biomarkers of neural network repair after cell transplantation into a QA model of HD. To achieve this, I first aimed to determine whether intra-striatal QA lesion affected the expression of IEG in efferent or afferent regions of the basal ganglia circuit, with the subsequent goal of assessing whether transplanted cells could rescue those neural network changes. Although the first part of the chapter explored this IEG expression, an unexpected significant reduction of globus pallidus cell number was found and raised the possibility that the striatal lesion had resulted in direct damage also to the globus pallidus. Thus, the rest of the chapter focussed on the analysis of this finding.

This work illustrates the importance of reviewing neurotoxic models, to ensure their suitability for addressing specific scientific questions. In particular, how surgical parameters might impact on the lesion site, area and behavioral deficits, and how relevant this could be for establishing the appropriate model depending on the experimental question.

5.2. Materials and methods

In this chapter there are four different experiments (Experiment 4-7). All experiments were performed in adult Lister-Hooded female rats. Striatal QA lesions and brain tissue from Experiment 4 was performed and provided by Dr. Mariah Lelos and from Experiment 5 by Dr. David Harrison. Striatal coordinates for Experiments 4 and 5 are Site 1: AP -0.4; ML -3.7; DV -4,-5 and Site 2: AP +1.2; ML -2.9; DV -4,-5. Concentration of QA in Experiment 4 is 0.12M and for Experiment 5 is 0.09M. Surgical and IHC methods are explained in detail in Chapter 2 and the experimental designs for each experiment are presented below aligned with the associated results.

5.2.1. Unbiased stereological analysis

Quantifications of IEG (EGR-1 and c-Fos) and NeuN was performed using Visiopharm Software. Sections were initially acquired using a 1.25x objective under a Leica CTR6 LED camera and ROI for each section was drawing and selected to establish the area of counting. Cells were manually counted, under a 40x objective and a 1000 μm^2 frame that was randomly moved through the ROI by the software. To calculate cells per area the following formula was used:

$$Cells\ per\ area = \left(\frac{\sum ROI\ area}{Frame\ size\ \times\ \sum samples}\right) \times \sum cells\ counted \times 12$$

5.2.2. Statistical analysis

Statistical analyses were conducted using SPSS (v27; IBM). All data from **Experiment 4** was analysed using the independent samples t-test comparing the mean of cell number from control and lesion group for EGR-1, c-Fos and NeuN data on each of the brain regions. In **Experiment 5 and 7**, data was analysed using the independent samples t-test comparing the mean of number of cells per area in the GP from intact and lesion hemisphere; or as a one sample t-test comparing the mean to a 100%. In **Experiment 7**, APO rotations and adjusting stepping test data was analysed as one-way analysis of variance (ANOVA) with Group (Original, Coord1, Coord2, Coord2_LD, Single and GP) as a between groups factor using (Dunnett's) correction to compare each group to control only.

5.3. Results

5.3.1. Expression of Egr1 and c-Fos, is downregulated in M1, Cg1/Cg2 and GP following a unilateral striatal QA lesion.

In the first experiment, **Experiment 4**, expression of IEG after QA lesion was investigated. The aim was to assess IEG expression in afferent and efferent striatal regions to determine its basal expression and how the neural network could be affected after QA striatal lesion. In this experiment, three nuclei of the cortico-striatal-thalamic circuit were chosen, the motor cortex (M1), the cingulate cortex (Cg1/Cg2) and the globus pallidus (GP) (Figure 36A and B), because all take part in the cortico-striatal-thalamic neural network.

Rats received unilateral QA lesion (n=9) and were perfused 21 weeks post lesion (Figure 36). There was a second group remaining as control (n=9) without undergoing any surgery. Expression of the IEGs, Egr-1 and c-Fos, in these 3 regions was assessed in the side ipsilateral to the lesion using immunohistochemistry, following unilateral striatal QA lesion.

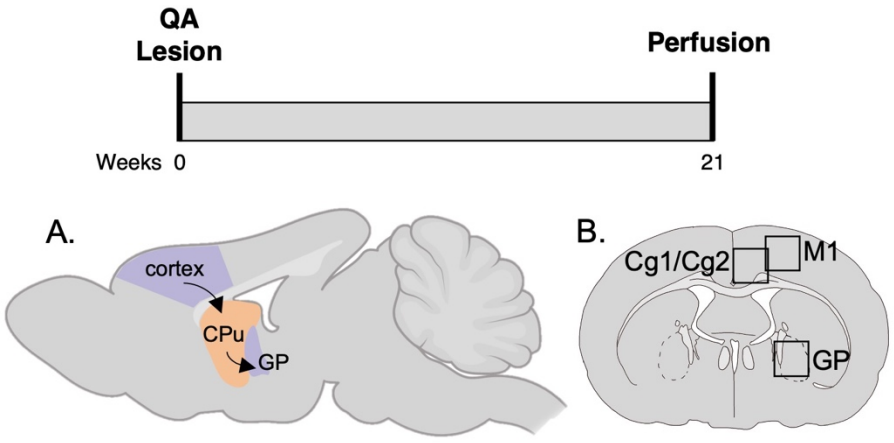

Figure 36 - Experimental design Experiment 4. Animals received a striatal infusion of QA and were perfused 21 weeks post lesion. (A) Sagittal view of striatal circuit showed the two selected areas assess in Experiment 4, the cortex as a striatal afferent and the GP as a striatal efferent. (B) Coronal view of analysed areas, two cortical regions (Cg1/Cg2 and M1) and GP.

There was no expression of Egr-1 in the GP in either lesion or control animals. In both the cortical regions, significant differences in expression of Egr-1 were seen, with lower expression in lesion rats than control rats (M1: $t(16)=3.965$, $p=.001$, two tailed; Cg1/Cg2: $t(16)=3.314$, $p=.004$, two tailed) (Figure 37B). In contrast, c-Fos was expressed in all three brain regions, but there was no significant difference in c-Fos expression between lesion and non-lesioned animals in any of the measured areas (M1: $t(16)=0.184$, p = n.s., two tailed; Cg1/Cg2: $t(16)= -0.461$, p = n.s., two tailed; GP: $t(16)= 1.441$, p = n.s., two tailed) (Figure 37C).

To confirm that any reduction in IEG expression was not the result of cell loss in the area, the tissue was stained for NeuN. No differences in NeuN expression was observed in either of the cortical areas (M1: $t(16)= -0.507$, p = n.s., two tailed; Cg1/Cg2: $t(16)= -0.292$, p = n.s., two tailed) (Figure 37D and E), suggesting a downregulation of IEG activity. There were significantly fewer NeuN positive cells in the GP in the QA lesion group compared with the control group ($t(16)= 3.691$, $p=.002$, two tailed) (Figure 37D and E).

In summary, there was a downregulation of Egr-1 expression in cortical areas which was not accompanied by neuronal loss, suggestive of reduced neural activity after a striatal QA lesion. However, a key finding was the unexpected significant neuronal cell loss in the GP. It is unknown if this loss is due to a long-term degeneration, as these animals were perfused 21 weeks post lesion, or if could be due to direct diffusion of the QA from its infusion site in the striatum to the adjacent globus pallidus, or due to an indirect effect, perhaps due to excessive activation of striato-pallidal projections following

QA infusion resulting in excessive glutamate release and cell death or any other unknown mechanism that could be related to degeneration or inflammation.

To assess if GP cell loss is due to a long-term degeneration, the next experiment investigated the timeline of the QA lesion model, quantifying number of cells in the GP at every timepoint.

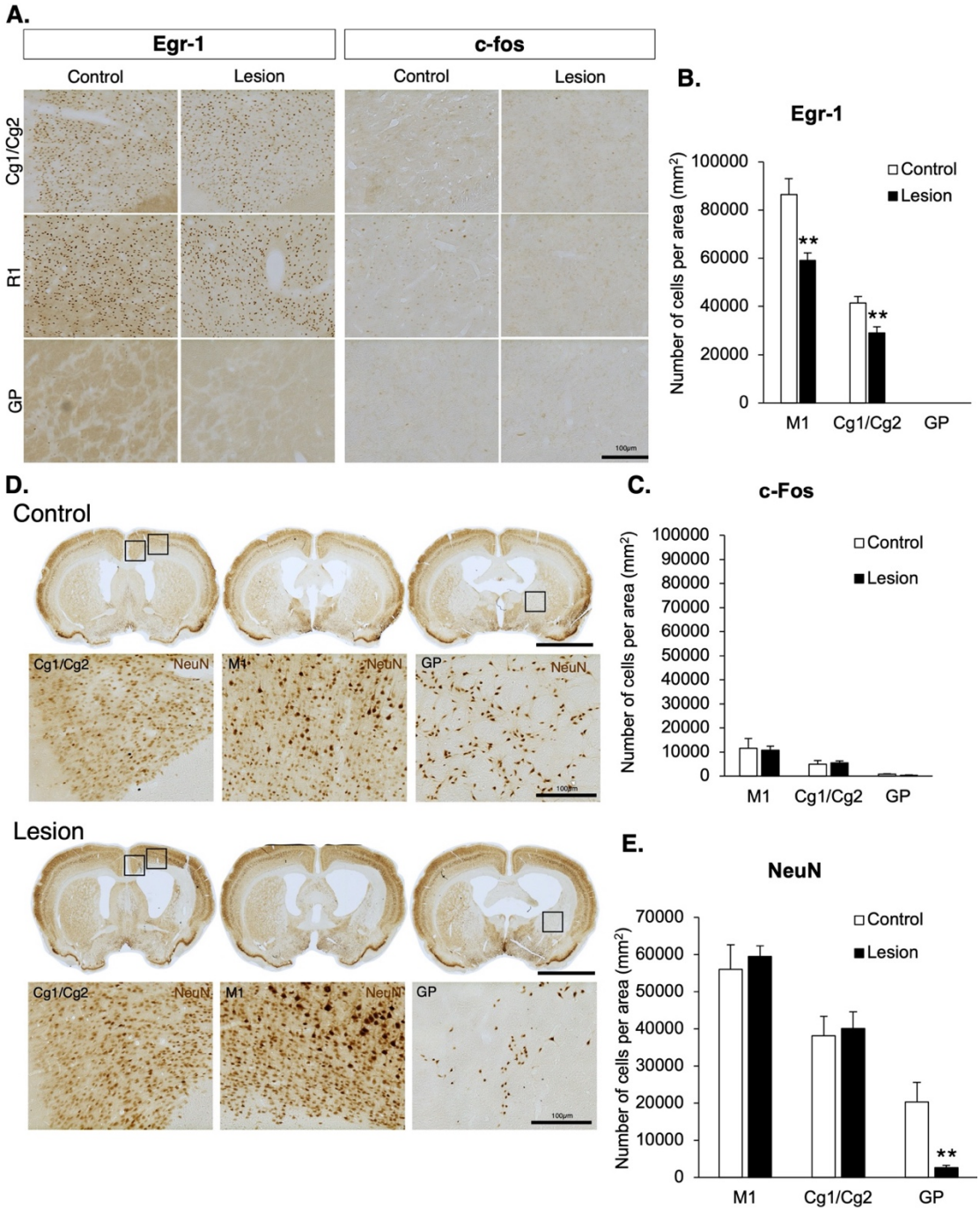

Figure 37 – QA lesioned animals showed reduced cortical Egr1 expression without neuronal loss and unexpected loss of neurons in the GP. (A) Representative photomicrographs of Egr-1 and c-Fos staining in control and lesion animals in Cg1/Cg2, M1 and GP. (B) Number of Egr-1 positive cells per area (mm^2) and (C) c-Fos-positive

cells in both cortical areas and GP. There is no GP quantification of Egr-1 because there was no expression of this marker in that area. (D) Representative photomicrographs of NeuN staining in control and lesioned animals. (E) Number of NeuN -positive cells per area. Scale bar for whole section=1500μm; Scale bar for higher magnification image=100μm. Each bar represents the mean of each group and error bars represent SEM (**p<0.01).

5.3.2. Neurons in the GP are significantly decreased already 4 days post QA lesion

Based on the cell loss observed in QA lesion animals in the GP after NeuN quantification in the previous section, **Experiment 5** aimed to elucidate the time course of this loss after QA infusion in the striatum, if GP cell loss is due to an acute effect of the toxin or due to a long-term degeneration.

Adult female Lister-Hooded rats were unilaterally lesioned and perfused at different timepoints post lesion, 4-, 16-, 28- and 90-days (N=6 for each group) (**Figure 38**). Striatal lesion coordinates are the same as Experiment 4 and QA concentration is 0.09M (Check section 2.4.3 in Chapter 2 for more details).

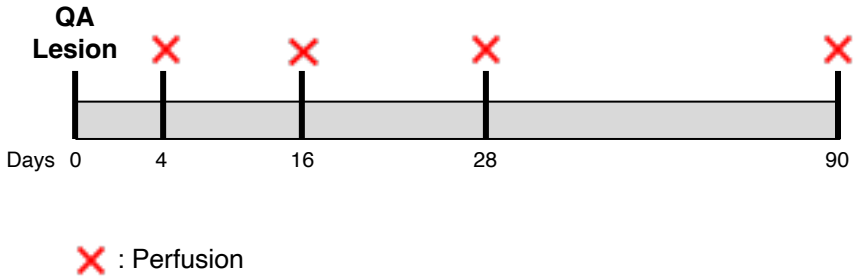

Figure 38 - Time course of experiment 5. All animals were lesioned with QA and perfused at different timepoints after 4-, 16-, 28- and 90-days post lesion.

Histological quantifications of NeuN demonstrated differences in GP cell survival across time (Figure 39A). Comparing the number of cells per area in the intact versus QA lesioned hemisphere, no differences were found 4- and 16-days post lesion (4-days: t(10)= 2.113, p=n.s., two tailed; 16-days: t(10)= 1.534, p=n.s., two tailed); but there were significant differences after 28- (t(10)= 2.371, p=0.039, two tailed) and 90-days (t(10)= 3.222, p=0.009) post lesion (Figure 39B), with significantly fewer NeuN positive cells present in the GP of the lesioned hemisphere compared with the intact hemisphere. The percentage of surviving NeuN positive cells in the GP of the lesioned hemisphere based on the intact hemisphere was significantly lower in all timepoints when compared to a 100% (4 days: t(5)= -6.229, p=0.002, two tailed; 16 days: t(5)= -3.879, p=0.012, two

tailed; 28 days: t(5)= -3.233, p=0.023, two tailed; 90 days: t(5)= -6.644, p=0.001, two tailed) (Figure 39C).

There was a significant loss of GP neurons already at 4 days post striatal QA infusion, when normalizing the data to percentage of cell survival, however when comparing to the intact hemisphere there is a significant cell loss of GP neurons at 28 days post lesion. Therefore, 28 days is the chosen timepoint to further characterise this cell loss.

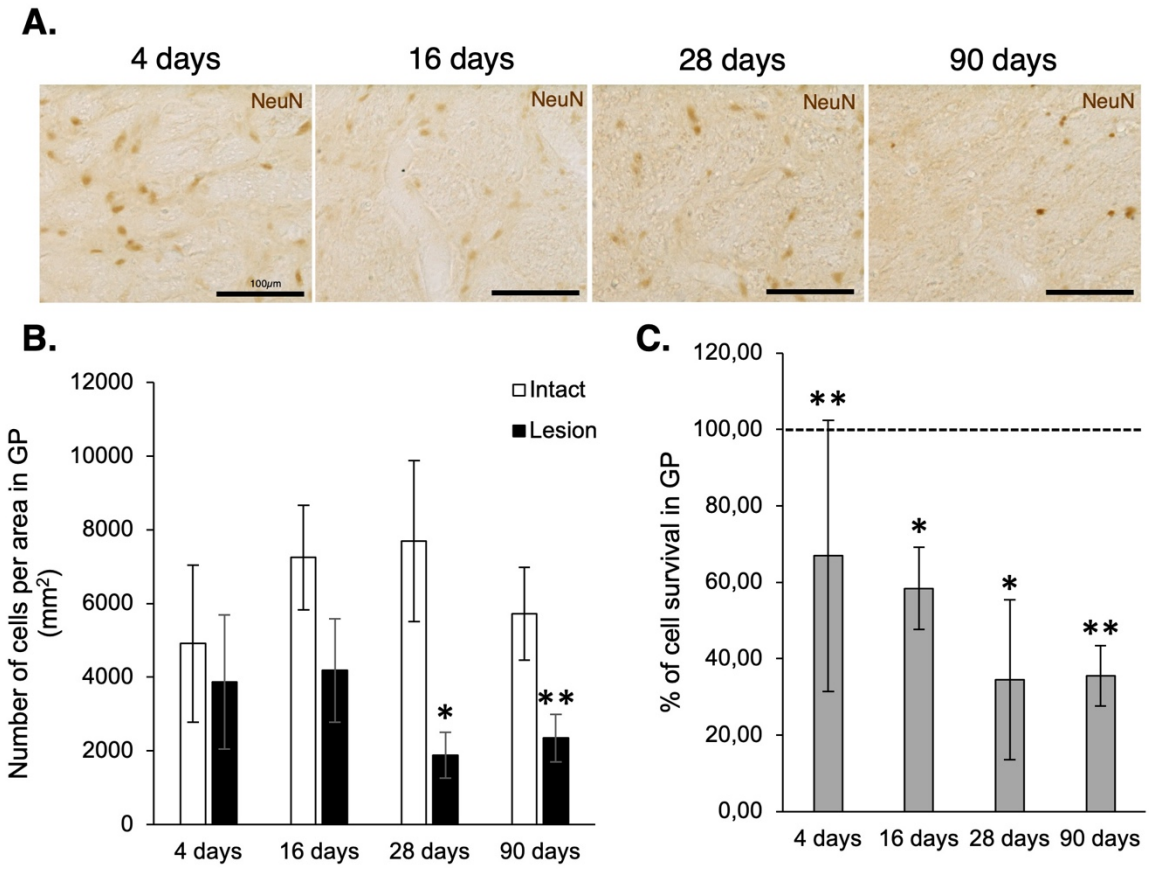

Figure 39 – NeuN expression in the GP in QA lesioned animals at different timepoints post lesion. (A) Representative images of NeuN in the GP at different timepoints post lesion. (B) Percentage NeuN positive cell survival in the GP in the lesioned hemisphere as compared to the GP in the intact hemisphere. (C) Graph represents number of positive NeuN cells per area in the intact and lesion hemisphere. Each bar represents the mean of each group and error bars represent SEM (*p<0.05), N=6. Scale bar=100µm.

Knowing this timepoint, and in order to have a better understanding of the mechanism behind this cell loss, the next experiments aimed to investigate if the infusion of the toxin in the striatum had a direct or indirect effect on the GP. Before modifying the toxin injection sites, in the next section, an infusion of Fluorogold (FG) tracer was

performed to determine wheter there was relatively even innervation from across rostro-caudal, medio-lateral and dorso-ventral or a particular striatal subregion(s) preferentially projected to the GP. This would provide us with the boundaries within which to target a striatal lesion to observe an indirect impact on GP integrity, as well as to identify the correct stereotactic coordinates to hit the GP.

5.3.3. Retrograde tracer revealed lateral neostriatal regions project to the GP

Using the retrograde tracer FG, an infusion in the GP of a healthy rat was performed to determine the area of the striatum that is directly projecting to the GP. Figure 40 shows infusion of FG into the GP and that projections are coming predominantly from the dorso-lateral striatum. Sections were also stained with DRAQ5™, a far-red DNA stain, used instead of DAPI as FG fluorescence is in the UV-blue region of the spectrum.

The infusion confirmed the stereotactic coordinates reached the correct target and that area is receiving projections from the dorso-lateral area of the striatum. With this set of coordinates, in the next section, the GP was targeted with QA toxin in order to assess the direct effect of it, as well as investigated the indirect effect of QA in the GP.

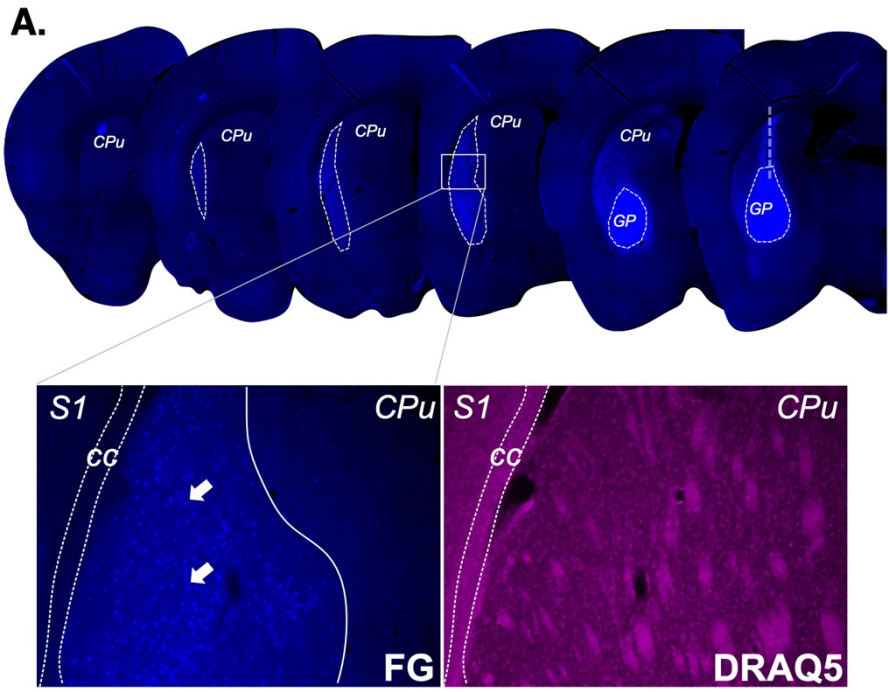

Figure 40 - FG injection into the GP reveals projections from predominately lateral neostriatal regions to the GP. Coronal sections showed FG infusion and expression across the striatum. Below, images of the striatum (CPu) at x100 magnification, showing DRAQ5 staining (pink) on the left image, allowing visualization of all cells of the section,

and fluorogold (FG) (blue) on the right. In the FG image, a white line delineates the area where FG positive cells are expressed and the injection track. Examples of FG positive cells are indicated by white arrows.

5.3.4. Altering lesion site affects GP integrity and behavioural outputs

The observed cell loss in the GP could have a significant impact in CRT as it aims to reconstruct the basal ganglia circuit affected in HD, transplanting new cells into the striatum. If an efferent area is also significantly damage it could have an impact in the therapy output. Therefore, an optimised lesion model is essential for CRT in HD. In this section, the aim is not only to determine if the loss of GP neurons was due to the direct toxic activity of QA or due to an indirect effect, but also to optimised lesion coordinates to maintain GP integrity, preserving enough striatal damage to allow for testing functional deficits, and therefore behavioural analysis of motor function was undertaken.

To investigate all these, a direct infusion of QA into the GP was performed to assessed if GP neurons are affected by QA and surgical coordinates were modified in order to move the site of the lesion away from the GP and thus avoid direct exposure to the toxin. Thus, to assess behavioural deficits, all animals were tested on the apomorphine (APO) rotation task and the adjusting stepping test a day prior to perfusion. As has been shown in the previous experiment, a significant cell loss in the GP was seen at 28 days post QA infusion, and therefore all animals were perfused at that time point (Figure 41).

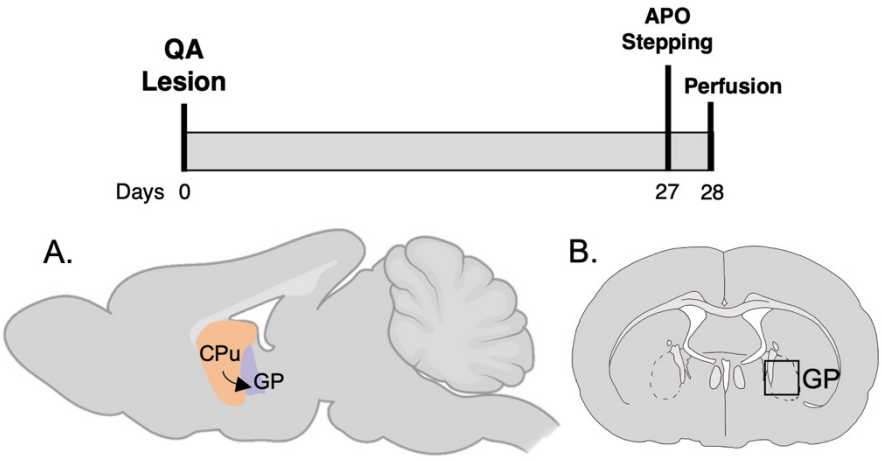

Figure 41 – Time course of Experiment 7. Animals received a striatal infusion of QA, after 27 days animals underwent APO rotations and adjusting stepping test and were perfused 28 days post lesion. (A) Sagittal view of striatal circuit showed the striatal efferent GP. (B) Coronal view of GP.

Seven groups of adults Lister-Hooded rats underwent unilateral QA lesion with different surgical coordinates and volumes of QA toxin (Table 15). Original coordinates were published coordinates (Lelos et al., 2016) that were also used in Experiment 4 and 5. The groups Coord 1 and Coord 2 were a new set of coordinates based in Original group but site 1 was moved to more rostral areas to move away of the GP. Same coordinates as Coord 2 but using half of the infusion volume of toxin was Coord2_LD, a single injection site was Single group and finally GP group is an infusion in the GP. A non-lesioned control group was also included. Brains were harvested, sectioned, and analysed through IHC for NeuN and DARPP32 markers (for more details see Chapter 2).

Table 15 - Summary of surgical parameters for each lesion group. Table shows the coordinates, concentration and volume of QA and the number of animals per group of the seven different lesioned groups. Last comment column explains more in detail the origin of each group.

Group name	Coordinates	QA concentration	QA total volume	Number of animals	Comments
Original	**Site 1:** AP -0.4 ML -3.7 DV -4,-5 **Site 2:** AP +1.2 ML -2.9 DV -4,-5	0.09M	1µl	6	Set of coordinates already published and commonly used in the lab (Lelos et al., 2016)
Coord 1	**Site 1:** AP +0.2 ML -3.6 DV -4,-5 **Site 2:** AP +1.2 ML -2.9 DV -4,-5	0.09M	1µl	6	New set of coordinates based on Original group. Site 2 was moved more rostral
Coord 2 (high dose)	**Site 1:** AP +0.4 ML -3.0 DV -4,-5 **Site 2:** AP +1.2 ML -2.9 DV -4,-5	0.09M	1µl	3	New set of coordinates based on Coord 1 group. Site 2 was moved more rostral

Coord 2_LD (low dose)	**Site 1:** AP +0.4 ML -3.0 DV -4,-5 **Site 2:** AP +1.2 ML -2.9 DV -4,-5	0.09M	0.5µl	3	New set of coordinates based in Coord 2 but infusing half of the volume of toxin (0.5µl of QA)
Single	AP -0.4 ML -3.7 DV -4,-5	0.09M	1µl	3	Single injection of QA, using the more rostral set of coordinates of Original group
GP	AP -1.2 ML -3.2 DV -6	0.09M	1µl	3	Lesion located in the GP

Images of NeuN IHC are shown in Figure 42 for each group. Quantifications of NeuN positive cells in the GP showed significant cell loss in the ipsilateral GP in Original ($t(10)=2.729$, $p=0.021$) and Coord 1 ($t(8)=4.122$, $p=0.003$) groups compare to the intact hemisphere at 28 days post-lesion (Figure 42H). The percentage of cell survival in the lesion side, obtained based on the intact side, is significantly lower in Original ($t(5)= -3,332$, $p=0,021$) and Coord 1 ($t(5)= -6,959$, $p=0.002$) groups (Figure 42I) compared to a 100% survival.

Figure 43 shows a sequence of DARPP32 staining for each of the groups and a representation of the size of the lesion within the group. The green area marks the animal with the biggest lesion in the group and the yellow area the animal with the smallest lesion. The red dots represent the surgical coordinates. Although there is no quantification of DARPP32, visual inspection of the images revealed some degree of cell loss in the striatum in all striatal lesion groups. Denervation in the GP was only observed in Original and Coord 1 group, but less in Coord 2, Coord 2_LD, and single groups (Figure 43).

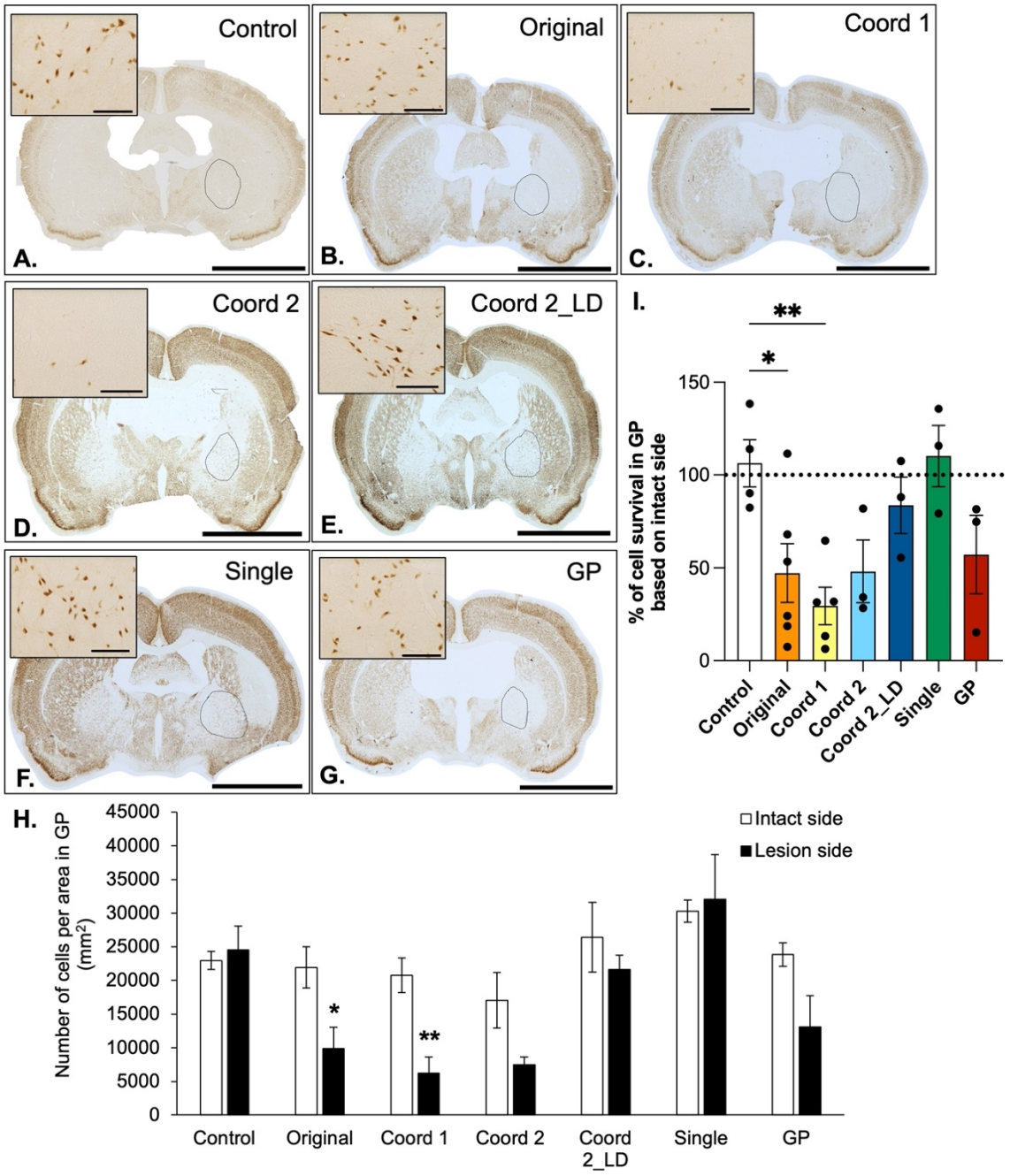

Figure 42 - NeuN quantifications of the different surgical groups. Representative photomicrographs of NeuN staining of whole brain sections and higher magnification inserts (top left) of the GP from the lesion hemisphere in (A) Control, (B) Original, (C) Coord 1, (D) Coord 2, (E) Coord 2_LD, (F) Single and (G) GP group. GP is delineated by a dotted black line in the lesion hemisphere. (H) Number of NeuN cells per area (mm^2) in the GP in the intact and lesion hemisphere of each of the experimental groups. (I) Percentage of NeuN positive cells based on the intact side for every group. Each bar represents the mean of each group and error bars represent SEM. (* indicates significant different from Sham Lesion, # indicates significant difference from intact group hemisphere) (#p<0,05, * p<0,05, ** p<0,01, ***p<0,001). Scale bar for whole section = 1500µm; Scale bar for the higher magnification image = 100µm.

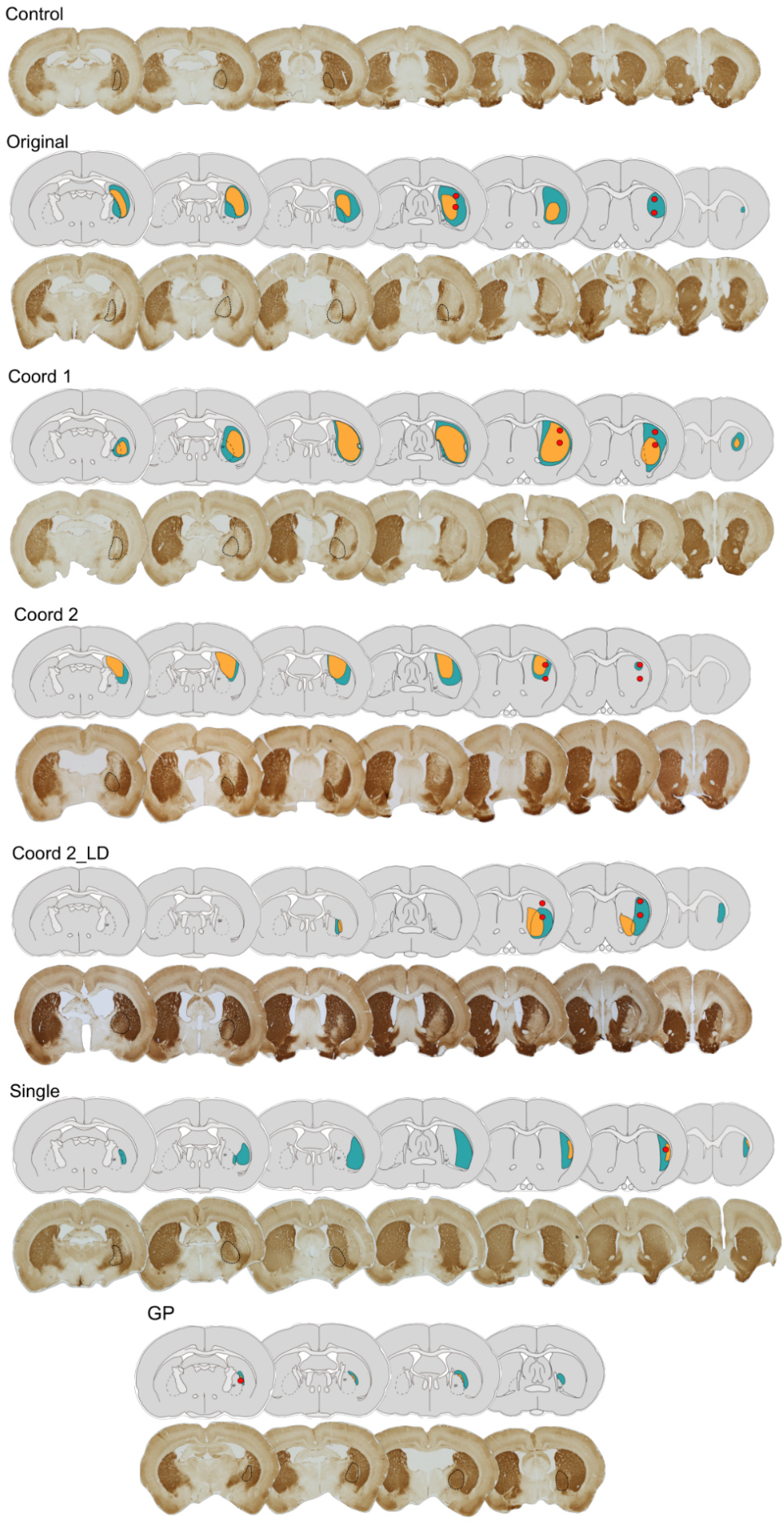
Control
Original
Coord 1
Coord 2
Coord 2_LD
Single
GP

Figure 43 - IHC for DARPP32 revealed the extension of the lesion on the striatum and how the GP is also denervated depending on the size of the lesion. Images have the GP delineated. Each group has a representation of the biggest lesion within the group (in green) and the smallest (in yellow). The infusion sites are represented by the red dots. GP is delineated on the lesion hemisphere.

Behavioral tasks showed that Original, Coord1 and Coord2 groups rotated significantly more in response to apomorphine than non-lesioned rats [$F_{7,24}$=8,701, p<0,001] (Figure 44A). There is a significant increase in net rotations in Original (p=0,024), Coord 1 (p=0,001) and Coord 2 (p=0,022) groups compare to the control group. Groups Coord 2_LD, Single and GP showed no difference in number of net rotations compared to non-lesioned animals. Adjusting stepping test revealed significant differences between groups in the number of steps in the ipsilateral side forwards [$F_{7,24}$=13,204, p<0,001] and backwards [$F_{7,24}$=8,042, p<0,001] and contralateral side forward [$F_{7,24}$=5,255, p<0,001] and backwards [$F_{7,24}$=3,551, p=0,009] (Figure 44B, C, D and E). In the ipsilateral side forward, there were a significant reduction in the number of steps between non-lesioned and Coord 2 (p<0,001), Coord 2_LD (p<0,001) and single groups (p=0,002). In the ipsilateral side backwards, there were fewer steps in Coord 2 (p<0,001), Coord 2_LD (p<0,001) and single (p=0,037) groups compare to control group. In the contralateral side forward, there was significant less steps in Coord 1 (p=0,002), Coord 2 (p=0,007), Coord 2_LD (p=0,031) and single (p<0,001) groups and in the contralateral side backwards there were significant less steps in Original (p=0,023) group compare all to non-lesioned control.

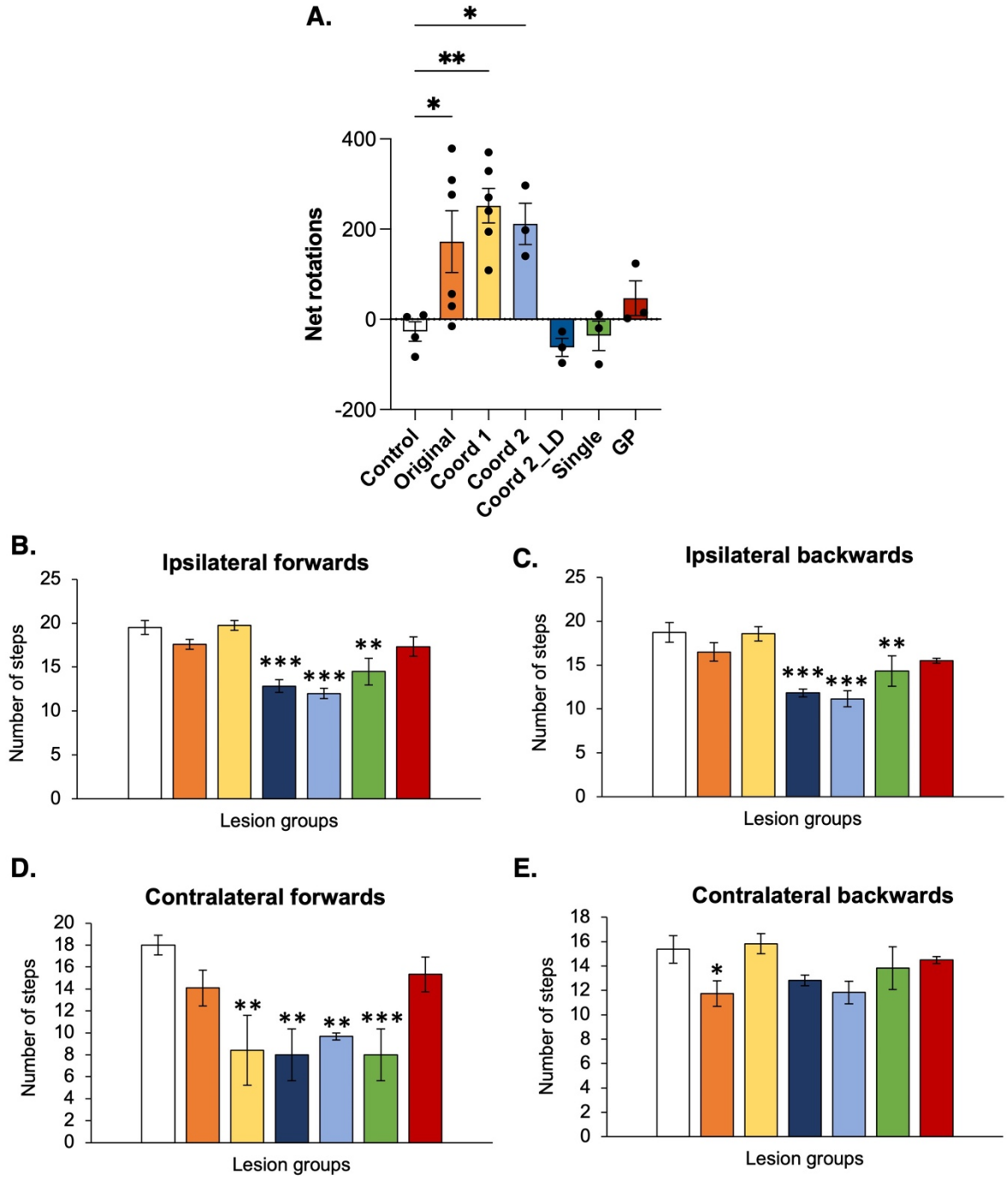

Figure 44 – Behavioural tasks performed 4 weeks post lesion. (A) Net rotations from APO rotations task. (B) Number of steps in the ipsilateral forward, (C) ipsilateral backwards, (D) contralateral forward and (E) contralateral backwards paw on the adjusting stepping test. Each bar represents the mean of each group and error bars represent SEM. (* indicates significant difference from sham group) (* $p<0.05$, ** $p<0.01$, *** $p<0.001$).

5.4. Discussion

5.4.1. IEG expression revealed changes in neural network activity in the QA model

The initial question addressed was whether IEG expression would reveal changes in afferent and efferent regions, which could be used as a potential biomarker of circuit reconstruction post-transplantation, to determine whether cell transplants would alleviate these changes in neural network activity induced by striatal loss. Results from **Experiment 4** revealed a significant reduction of Egr-1 expression in cortical regions, M1 and Cg1/Cg2. No differences were found in any of the assessed areas in c-Fos expression. This difference between both IEG could be due to the relation between EGR1 and DARPP32, as BDNF require EGR1 expression for induction of DARPP32 (Keilani et al., 2012), so striatal loss of MSNs after QA infusion might have an impact on Egr-1 expression.

Apart from the striatal atrophy, there is evidence of cortical projections loss in HD patients at early stages of the disease (de la Monte et al., 1988; McColgan et al., 2017) with an increased cortical excitability and impaired GABA-mediated cortical inhibition (Agarwal et al., 2019; Nardone et al., 2007; Philpott et al., 2016; Schippling et al., 2009). It had been also showed that the striatal QA lesions had an effect in cortical electrophysiological activity (Schwarz et al., 1992). All these evidence of cortical disruption with the downregulation of Egr-1 expression in cortical regions showed in **Experiment 4** is proving more evidence of the relevant effect of striatal degeneration in other brain regions, as the cortex. In Alzheimer's disease (AD), higher expression of EGR1-mRNA in early AD patients in prefrontal cortex (PFC) was found, and that expression is decreased in later AD stages (Hu et al., 2019). In PD, Egr-1 expression is downregulated in the 6-OHDA model after 4-5 months post lesion compared to control; even when animals are treated with methamphetamine to induce Egr-1 expression (Ishida et al., 2000). In this study, 6-OHDA lesion animals were subsequently transplanted with fetal rat VM and levels of Egr-1 expression were restored to control levels in the striatum in the grafted group.

All these evidence from the literature from HD patients and different neurodegenerative diseases, as well as the results obtained from **Experiment 4**, lead us to the conclusion that neural circuits disruption affects certain mechanism in later stages of neurodegenerative diseases in which IEG expression is affected, with the result being their downregulation. For future studies, IEGs could be a possible biomarker to assess neural circuit disruption.

5.4.2. Loss of GP neurons in the QA model

The first experiment of this chapter revealed a significant cell loss in the number of positive NeuN cells per area (mm^2) in the GP in the lesion group, compared to non-lesioned animals, not observed in cortical areas. This was an unexpected result that led me to investigate further the possible mechanism behind this neuronal cell loss. Although the striatal QA lesion model has been characterized along the years (Dobrossy et al., 2005; Dunnett et al., 1999; Fricker et al., 1997; Kalonia et al., 2011; Lelos et al., 2011, 2012) and used frequently in CRT preclinical studies (Lelos et al., 2016; Sanberg et al., 1997), there is a lack of knowledge about the effect of the neurotoxin in other areas of the basal ganglia, in particular the globus pallidus.

QA is an endogenous NMDA agonist (Stone et al., 1981), that when infused in the striatum, produces an excessive NDMA receptor stimulation, with an increase of glutamate that leads to an influx of sodium, calcium and water that produce cell death (Rothman et al., 1995). MSNs, especially the ones expressing substance P (SP) are sensitive to this toxin, whether MSNs expressing somatostatin and neuropeptide Y are being preserved (Beal et al., 1986). To date, it was not known if GP neurons could be affected by this toxin but **Experiment 5** showed there was already around 35% of cell loss in the GP 4 days post QA infusion that is increased over the time. Different imaging and *post-mortem* studies in HD patients reported atrophy and cell loss in the GP, specially at later stages of HD (Albin et al., 1989; Deng et al., 2004; Lange et al., 1976; Reiner et al., 1988; Singh-Bains et al., 2016; Vonsattel et al., 1985). But this early loss made us question if there was a direct effect of the toxin due to a possible leaking after infusion; if there was an indirect effect of the infusion through an unknown mechanism; or if it could be a combination of both. When in **Experiment 7** two new sets of coordinates were established, trying to avoid direct contact with the GP, cell loss in the GP was around 50%. When QA was directly infused into the GP, around a 30% cell loss was observed and when there was only one infusion site (away from the GP) or two infusion sites but half of the toxin volume, there were almost no cell loss in the GP. These results showed that there was a direct effect of the toxin in the GP, with that 30% cell loss when is directly infused, but there was also some other indirect mechanism that is still unknown to produce that other 20% loss to make a 50% total loss when lesioning the striatum with two infusion sites (as in Coord 1 and Coord 2).

Direct infusion on the GP had shown that there is a specific GP population that is sensitive to QA toxin. When looking at the GP in more detail, depending on its biochemical composition and innervation, neurons projecting to the external GP (GPe), express the dopamine receptor subtype 2 (D2R) and enkephalin (ENK); whether MSNs

projecting to the internal GP (GPi) and SN express dopamine receptor subtype 1 (D1R), substance P (SP) and dynorphin (Gerfen et al., 1990).The subtype of MSN expressing ENK are the main population of striatal MSNs projecting to the GPe and are the most affected in early stages of the disease (Deng 2004 and Singh-Bains 2016). As mentioned in the previous paragraph, SP expressing MSN are more vulnerable to QA, therefore, although ENK population is the most affected in HD patients, in this model SP expressing GP cells could be ones susceptible to QA exposure. It would be interesting for future experiments to study in more detail if there is a specific cell population in the GP that is more sensitive to the toxin, as staining GP lesions brains for SP and ENK to confirm this hypothesis.

The FG infusion in the GP revealed the coordinates chosen were appropriate and highlighted projected neurons from the dorso-lateral areas of the striatum to the GP. This dorso-lateral striatal area was affected in all striatal lesioned groups, however Coord 2_LD and Single groups showed almost no cell loss in the GP.

All this evidence is suggesting the observed cell loss in the GP may not be due to a possible diffusion of the toxin when infused in the striatum, but possibly there might be other indirect mechanism related to QA toxicity mechanism. The excessive excitotoxicity in the striatum could be somehow affecting GP cells, as after neuronal trauma, the imbalance of GABA neurotransmitter produced a neuronal depolarization that increased intracellular Ca^{2+} (van den Pol, Obrietan, & Chen, 1996) , leading to cell death. There could be also inflammatory events due to the toxin as microglia and macrophages activation (Guillemin, Smith, et al., 2003) or astrogliosis (Guillemin, Croitoru-Lamoury, et al., 2003; Ting, Brew, & Guillemin, 2009) that could impact survival of GP neurons.

5.4.3. Optimization of QA model

An optimised lesion model, with appropriate coordinates that balance a sufficient striatal atrophy, that produce certain behavioural deficits while maintaining GP integrity is critical for CRT. The current established QA lesion model is based on two striatal infusions, a more rostral set of coordinates and a second infusion more caudal to cover the whole striatal area. This second set of coordinates is the one closer to the GP.

Experiment 7 tested four new set of coordinates and a direct infusion in the GP. All new coordinates were based in the ones from Original group, that are published (Lelos et al., 2016) and used in the lab (**Experiment 5** used this set of coordinates). Original group showed cell loss in the GP and therefore, to avoid direct contact with the GP, Coord 1 coordinates were moved rostrally and significant cell loss was still observed in the GP. After Coord 1, Coord 2 group coordinates were moved even more rostrally

than Coord 1 and even though cell loss in the GP was observed, it was not significant compared to the intact hemisphere or to a non-lesioned group. As Coord_2 was still producing GP loss, Coord 2_LD used the same coordinates but half of the volume to try to avoid GP cell loss. In this group almost no cell loss was observed in the GP, which was a similar result to Single group. In this last group a single infusion (site 1 from Original group) was performed and no cell loss in the GP was observed. DARPP32 staining revealed extensive denervation of the striatum and the GP in Original and Coord1 groups, with less extensive denervation in each of Coord2, Coord2_LD and Single groups, and a minimum denervation in the striatum no denervation at all in the GP in the GP lesion. These data confirmed that bigger or more severe lesions, as Original and Coord 1, produced higher GP cell loss and DARPP32 denervation in the striatum and GP, whether smaller lesions as Coord 2_LD and Single groups produced almost no cell loss in the GP and less DARPP32 denervation. A similar result was published in the 6OHDA model, using a severe, an intermediate and a mild lesion and the more severe the lesion, the more TH denervation and the lower the number of contralateral steps in the adjusting stepping test (Grealish et al., 2010).

When behavioural testing was assessed, the groups with GP cell loss, Coord 1 and Coord 2, showed APO rotations deficits, whether the other two groups, Coord 2_LD and Single, did not. No deficits were found when directly lesion the GP. After a lesion in the striatum, striatal cells became supersensitivity to monoamines as dopamine (DA) and the treatment with APO, which is a dopamine receptor agonist, produced an hyperstimulation in superactivated DA receptors in the denervated striatum (Ungerstedt, 1971). Therefore, lesioned rats showed higher number of net rotations due to their turn to the contralateral side of the lesion. Based on this, animals with no deficits in this task might not have enough striatal denervation, or no denervation at all. Although no quantification of striatal cell loss was performed, it seems that Coord 2_LD and Single groups did not show enough striatal loss to show APO deficits and the GP group received the lesion in the GP but not in the striatum. In the adjusting stepping test, however, all groups showed a deficit in the contralateral forward paw, except for the GP lesion group. Again, the GP group is the only one with no striatal lesion, therefore this could explain the absence of deficits. In this task, animals with a striatal lesion showed a deficit in the contralateral side either in step length or number of steps (Olsson et al., 1995), however, Coord 2, Coor 2_LD and Single groups showed also significant less contralateral forward steps. Every group performed the adjusting stepping test at different times, as not all groups received the lesion on the same day. Coord 1 and GP lesions were performed at the same time, but not the rest of the groups. Hand testing is very dependable of the

researcher, although all groups were performed by the same researcher, some of the differences in the ipsilateral side compared to non-lesion animals could be due to this.

There is evidence in the literature that different lesion coordinates produce different behavioral output. As an example, lateral striatal lesions have greater impairments in the APO rotation task and skilled paw reaching (Fricker et al., 1996) and also in the cognitive 5-choice attencional task, compare with medial striatal lesions (Rogers 2001). It is known that the striatum is a big structure composed of three main channels: the sensorimotor, the associative and the limbic (Alexander, DeLong, & Strick, 1986; Haber, 2003; Parent & Hazrati, 1995) and on the last few years, there have been more studies trying to anatomically characterize more in detail this striatal area (N. N. Foster et al., 2021). In this chapter, it has been shown that different set of coordinates result in different motor behavioral outcomes. Answering the question of which set of coordinates would be the most appropriate for CRT, Coord 2 group would be chosen one. These group of animals showed striatal loss with consequent motor deficits in the APO rotations and adjusting stepping test task. Although it showed cell loss in the GP, was the only group which balance the appropriate required features of the model, maintaining as much as possible the degree of integrity of the GP. This set of coordinates had been used in Chapter 3 lesion animals with successful host-to-graft connectivity and GP innervation from the grafted cells.

Changing of stereotactic coordinates not only has an impact on efficacy of the lesion (Torres et al., 2011), but also, as demonstrated in this chapter, has an impact on the cell survival of adjacent brain regions, as the GP, and in the behavioural output. To conclude, is important to review lesion-based models, as well as to choose the most suitable lesion depending on our research question.

Chapter 6: General discussion

6.1. Key findings

Experiment 1 ▪ Host-to-graft connectivity observed from 5 weeks post-graft and maintained over time. ▪ Graft-to-host innervation to efferent areas of the basal ganglia.
Experiment 2 ▪ Grafts were significantly large and ventrally located but DARPP32 and CTIP2 positive. ▪ Only one rat showed traced projections on the edge of the graft.
Experiment 3 ▪ Host-to-graft connectivity was showed in WT and F344tgHD rats in young and aged animals
Experiment 4 ▪ Downregulation of EGR-1 expression in cortical areas.
Experiment 5 ▪ Significant cell loss in the GP at 4 days post striatal QA lesion that increased over time.
Experiment 6 ▪ Dorso-lateral areas of the striatum project to the GP.
Experiment 7 ▪ Two infusion sites in the striatum for QA lesion produced cells loss in the GP and behavioural deficits in APO rotations and adjusting stepping test. When moving the second infusion site away from the GP (more rostrally) the cell loss in the GP decreased. ▪ A single infusion site in the striatum or two sites with half of the volume in the striatum did not produce GP cells loss or deficits in the APO rotations task, but deficits in the adjusting stepping test. ▪ A lesion in the GP produced around 30% cell loss in the GP and no behavioural deficits in APO rotations or adjusting stepping test

6.2. General discussion

This thesis principally investigated whether hPSCs differentiated to an MSN phenotype were capable of forming synaptic connections with the host brain. This was explored in several ways – using histological characterization, such as STEM121; using the modified rabies virus as a neuronal tracer, and using IEG, although graft connectivity could not be assessed by IEG as the experimental aim was diverted to explore the unexpected finding that striatal QA lesions appeared to result in loss of GP cells – a key downstream nucleus of the striatum. Graft connectivity is relevant for CRT studies as new transplanted cells are expected to integrate into the host parenchyma and make new synaptic contacts to reconstruct the damaged neural circuits in order to recover the functionality of the affected area. MSNs progenitors were transplanted into two different HD rodent models, the QA lesion model and the F344tgHD genetic rat model. Reporting synaptic connectivity from grafted cells in these models is important because each model represents different disease characteristics. In the QA lesion model, excitotoxicity and striatal atrophy are represented and in the F344tgHD model animals express the mutant htt protein that characterizes the pathology of the disease.

The F344tgHD model was chosen not only for its similarities to the human disease, such as rats carry only 51 CAGs repeats, but also because graft survival is more successful when transplanting into rats rather than into mice. When comparing mouse versus rat models, there are several important differences to take in mind. Firstly, graft survival is model and species dependent as for example, there is evidence of poorer survival of grafts in the mouse brain compared to the rat (Roberton et al., 2013). Mouse models also present short-life span, compared to the rats, therefore long-term experiments might be limited, but this could be a benefit for accumulate data faster. Nevertheless, there are many more genetic mouse models than rat ones and deficits are more noticeable and appear earlier, which could be beneficial for testing different motor and cognitive tasks to assess graft functional recovery.

In **Chapter 3** evidence of host-to-graft connectivity was seen in hESC-MSN grafts placed into the QA lesioned striatum from 5 weeks post transplantation, using the monosynaptic tracing based on the modified rabies virus. This host-to-graft connectivity was maintained until at least 17 weeks which was the last timepoint assessed. Using the ΔG-rabies, 5 weeks was the earliest time reported for host-to-graft connectivity outside the host striatum after transplanting hPSC-derived MSNs, but not functional assessment has been performed in this chapter. Other studies using hPSC reported connectivity from the host striatum after four and eight weeks post grafting (Besusso et

al., 2020) and connectivity from afferent striatal areas after 6 months post-transplant (Schellino et al., 2023), and were combined with functional assessment of motor deficits. In Besusso et al. (2020), transplanted rats performed significantly better in the vibrissae-evoked hand placing after 1 month post grafting and in the adjusting step test after 1 and 2 months, but no improvements were found in the rotarod task. In Schellino et al. (2023), grafted animals performed significantly better in the rotarod after 6 months post transplantation. It is unknown if transplants of hPSC-derived MSNs will result in similar levels of connectivity when placed into the human brain. As outlined above, connectivity has been seen as early as 4 or 5 weeks, but it is possible that establishing synaptic connections in downstream brain regions could take longer due to the greater physical distances.

Human cytoplasm staining, STEM121 showed that grafted cells innervate the host striatum and extended connections to efferent striatal regions. Other published studies using hPSC have also reported graft innervation from IHC of NCAM staining (Besusso et al., 2020; Schellino et al., 2023). However, from IHC results we cannot determine if these connections were functional, therefore in this chapter graft-to-host connectivity was also assessed, infusing ΔG-rabies into the GP and SN. Unfortunately, connectivity could not be demonstrated, grafts were significantly large and ventrally located (these reasons that had been discussed in section 3.5), but the evidence from ΔG-rabies connectivity and STEM121 results are encouraging and deserve further study. There are also other tools to assess functionality of grafted cells connections such as electrophysiology or using Designer Receptors Exclusively Activated by Designer Drugs (DREADD) in combination with behavioral testing. DREADD are chemogenetic tools that can be selectively activated by certain drugs, translating into switching on and off grafted cells activity and in combination with behavioral testing is a powerful tool to assess functional recovery. DREADDs have been already used in transplantation studies in PD models (Aldrin-Kirk et al., 2016; Y. Chen et al., 2016).

When the brain regions projecting to the grafts were assessed in detail, it could be seen that grafted cells received connections from afferent striatal areas, such as prefrontal cortex, thalamic areas and SN, and extended projections to efferent regions as the GP and SN. These afferent and efferent regions and are known to be part of the basal ganglia circuitry (Lanciego et al., 2012). However, there were also other afferent and efferent areas that are not classically recognised as being part of normal striatum circuitry. Traced cells were found in the anteromedial thalamic nucleus, which is not known to extend projections to the striatum, but to the cortex, and grafted cells extended

projections to prefrontal cortical areas. One explanation for these particular off-target projections is that they originate from non-striatal-like cells in the graft (as discussed in section 3.5). In brief, both MSNs and cortical cells arise from the WGE, so these off-target cells could be originated during the differentiation protocol. During differentiation, cells were directed firstly to a telencephalic fate and then ventralized to a subpallial-LGE phenotype. Certain cells may not undergo the ventralisation, maybe because they did not receive the appropriate cellular/molecular signals, and subsequently take on a cortical phenotype. This is consistent with results from xenograft studies transplanting hWGE that had previously reported fiber outgrowth to cortical areas (Hurelbrink et al., 2005; Wictorin, Clarke, Bolam, Brundin, et al., 1990). Authors had hypothesized this could be due to the heterogenous nature of the WGE tissue, containing not only a striatal, but also cortical population, resulting in those extensive cortical projections.

In **Chapter 4**, host-to-graft connectivity was observed in the F344tgHD rat brain as well as in their WT littermates. This data demonstrated that grafted cells could integrate and innervate a transgenic HD brain as well as receive synaptic contacts from afferent striatal regions. This suggests that grafted cells can survive in the hostile inflammatory environment known to exist in the HD brain. However, the host HD brain environment was not identical to the wild-type environment, as grafts in the F344tgHD rat striatum were significantly smaller than those transplanted into the WT brain. This has also been briefly mentioned, but not quantified in transplanted R6/2 animals (Adil et al., 2018). One potential mechanism leading to smaller grafts in the HD brain is the presence of a heightened ongoing inflammatory response in the HD brain following graft placement, so this was explored further. No significant differences in OX42/Iba1 IHC expression intensity were found between F344tgHD and WT. However, differences were seen between the young F344tgHD and older F344tgHD rats; there was a more intense expression of activated microglia marker (OX42) and a hyper-ramified microglia phenotype in the young F344tgHD rats. The increased microglia ramifications have been previously reported in young R6/2 (3-10 weeks old), but not in aged mice (Savage et al., 2020), as microglial ramification is naturally decreased with age (Davies et al., 2017). It has been hypothesized that hyper-ramification could be a response to stress or an an excitotoxic environment (Hinwood et al., 2012). The higher OX42 intensity expression and the increased microglial ramification could have an impact on young F344tgHD rats graft size. The possible explanation for the smaller graft size of aged F344tgHD rats when compared to WT could be related to the presence of mHTT aggregates in the host striatum and surrounding the graft edges. Aggregates produce a gain of toxic function and imbalance of protein homeostasis (proteostasis), that is accentuated with age,

producing cellular dysfunction and cell death (Hipp, Park, & Hartl, 2014). Therefore, aggregates could affect graft size in aged F344tgHD rats. Fewer transplanting studies in genetic models have been performed compared to neurotoxic models, therefore further investigation with different genetic models is required to have a better understanding of the impact of HD brain environment.

In **Chapter 4** the effect of the host age on transplant was also questioned, as the best time window for transplantation is an important challenge when moving into clinical translation. It is still unknown if it would be better to transplant at an earlier disease stage or if later stages patients could be also benefit from this therapy. Clinical trials had reported that patients in advanced stages of HD are prone to develop subdural hematomas (Freeman et al., 2011) and have vascularization defects (Cisbani et al., 2013), which could impact graft survival. From this thesis data we can conclude that cells can integrate and extend projections at both ages, but further study is required.

Although many of the experiments ended up with relatively small numbers for various reasons, they have provided proof of concept that hESC-derived MSNs can integrate and make synaptic connections in two separate models of HD. Neurotoxic models are a common model for CRT studies but results from Chapter 4 had support the importance of also include genetic models to investigate the effect of the host environment in grafted cells.

However, although proof of concept of synaptic connectivity of grafted cells have been shown also in this thesis, it is still unknow if connectivity is the only mechanism or are there other mechanism in place. As have been described in section 1.4.2. in the introduction, the mechanism behind functional recovery have not been definitively stablished. Short term improvements might be due to a neuroprotection/support of the new transplanted cells to the damaged host cells, whether long-term improvements are likely to be due to reconstruction of the basal ganglia circuit, as transplanted cells reconnect with afferent and afferent regions to create new synaptic contacts that improved symptoms and recover the functionality of the area. However, there has been lately evidence of the possibility that functional recovery would involve both mechanism of circuit reconstruction and trophic support. Reidling et al. (2018) and Park et al. (2021, 2022) (Park et al., 2022; Park et al., 2021) transplanted hPSC-derived neuronal progenitor cells and observed improvements in motor tasks in R6/2 and Q140 in Reidling et al., and in YAC128 in Park et al. In these studies, 85% (Reidling et al., 2018) and 66% (Park et al., 2021) of transplanted cells were identified as astrocytes. In an alternative approach, Benraiss et al. (2016), transplanted human glial progenitor cells (hGPCs) isolated from human fetal brain into neonatal R6/2 mice (Benraiss et al., 2016).

Transplanted R6/2 mice survived longer (mean increase of 12 days), showed delayed onset of motor deterioration compared to untreated R6/2 controls and performance was better in certain behavioural tasks. Authors noted that there was substantial replacement of host mouse astroglia with normal htt-expressing human counterparts, and the graft-derived cells integrated into the host brain as astrocytes or GPCs and not neurons. This year, a new publication from Holley et al. (2023), grafted the same neuronal progenitor cells as Reidling et al. (2018), into 2.5 months zQ175 for 8 months. In this study grafted cells reported around 58% of NeuN positive and 7% were DARPP32 positive, although no quantification or bar chart was shown, grafted zQ175 mice showed improvements in different motor tasks from 5 months post transplantation. Authors hypothesized that transplanting a progenitor population will give rise not only neurons, but also glial cells and this cell product will recover the functionality as well as giving neuroprotection to host cells (Holley et al., 2023). Taken together, these studies might suggest that functional recovery may occur through multiple mechanisms (i.e. not just circuitry repair, but also through trophic or other effects) and that glial cells could have a beneficial impact on functional recovery. This data also raised the possibility of transplanting a cell product which combine neuronal with glial progenitors.

In **Chapter 5**, the original aim was to use IEGs as another tool to assess circuit reconstruction. Expression of EGR-1 and c-Fos was investigated in QA lesioned and non-lesioned rats in afferent and efferent striatal regions. A downregulation of EGR-1 expression was found in cortical areas in lesion animals, and quantification of total cell number was performed to confirm downregulation was due to an unknown mechanism rather than a cell loss. No differences in total number of cells were found in the cortex, but an unexpected significant cell loss was found in the GP. This finding is critical for CRT, because when transplanting cells into the damage striatum, the aim is to reconstruct the circuit to recover the functionality but if there is more than one area significantly damage, results could be affected by this. This GP cell loss was found at 21 weeks post lesion animals, so the first proposed hypothesis was a long-term degeneration after striatal atrophy. The excitotoxic lesion produced loss of MSNs, therefore, loss of projections to the GP and degeneration of the area. This first hypothesis was revoked when significantly cell loss was reported after 4 days post lesion, which is a very short period of time. Therefore, the second hypothesis was a possible diffusion of the toxin to the the GP when infused into the striatum. A direct infusion of QA was performed in the GP and striatal stereotactic coordinates were changed, more rostrally, to avoid a possible direct contact with the GP. Direct infusion of the toxin in the GP produced approximately a 30% cell loss and change of coordinates produced around

50% cell loss. These results strongly suggested that toxin diffusion was not the mechanism, as percentage of cell loss is higher when performing striatal lesions than when infusing the toxin directly into the GP. When striatal coordinates were infused with half of the volume or just one infusion site rather than two, there was almost no effect on the cell loss in the GP, despite the fact that striatal lesions were smaller. Thus, toxin diffusion as an explanation was revoked by these experiments so there must be another mechanism. Another possible explanation could be based on the acute excitotoxicity that is produce after the toxin infusion. When QA is infused, overstimulation of NMDA receptors produces a massive release of glutamate and an increase of Ca^{2+} into the cell. As MSNs project directly to the GP, one possibility is that this hyperexcitability of MSNs significantly affects GP cells with which they synapse leading to the observed cell loss.

The QA lesion model has been used for many decades in CRT but no review of the model has been performed in the last years. The unexpected finding of GP cell loss highlights the importance of evaluating animal models. The stereotactic placement of the injection, and the number of infusion sites as well as the volume infused was critical for the model output. Changing the surgical coordinates had a significant impact on other efferent areas of the striatum or in the functional deficits of the model. Although reviewing *in vivo* models could be very time consuming, it would be important for the field as, in this case, the cell loss in the GP could have a significant impact in CRT results.

To conclude, this work has reported proof-of-concept of the potential of hPSC for CRT, being able to integrate into two different rodent HD models and receiving new synaptic contacts from afferent striatal areas. There are still challenges to face, such as to determine the best time window for transplantation or how the mutant HD brain affect graft size and survival. More studies are needed in order to translate pre-clinical work into clinical trials.

References

Adil, M. M., Gaj, T., Rao, A. T., Kulkarni, R. U., Fuentes, C. M., Ramadoss, G. N., . . . Schaffer, D. V. (2018). hPSC-Derived Striatal Cells Generated Using a Scalable 3D Hydrogel Promote Recovery in a Huntington Disease Mouse Model. *Stem Cell Reports, 10*(5), 1481-1491. doi:10.1016/j.stemcr.2018.03.007

Agarwal, S., Koch, G., Hillis, A. E., Huynh, W., Ward, N. S., Vucic, S., & Kiernan, M. C. (2019). Interrogating cortical function with transcranial magnetic stimulation: insights from neurodegenerative disease and stroke. *J Neurol Neurosurg Psychiatry, 90*(1), 47-57. doi:10.1136/jnnp-2017-317371

Albin, R. L., Makowiec, R. L., Hollingsworth, Z. R., Dure, L. S. t., Penney, J. B., & Young, A. B. (1992). Excitatory amino acid binding sites in the basal ganglia of the rat: a quantitative autoradiographic study. *Neuroscience, 46*(1), 35-48. doi:10.1016/0306-4522(92)90006-n

Albin, R. L., Reiner, A., Anderson, K. D., Penney, J. B., & Young, A. B. (1990). Striatal and nigral neuron subpopulations in rigid Huntington's disease: implications for the functional anatomy of chorea and rigidity-akinesia. *Ann Neurol, 27*(4), 357-365. doi:10.1002/ana.410270403

Albin, R. L., Young, A. B., & Penney, J. B. (1989). The functional anatomy of basal ganglia disorders. *Trends Neurosci, 12*(10), 366-375. doi:10.1016/0166-2236(89)90074-x

Aldrin-Kirk, P., Heuer, A., Wang, G., Mattsson, B., Lundblad, M., Parmar, M., & Bjorklund, T. (2016). DREADD Modulation of Transplanted DA Neurons Reveals a Novel Parkinsonian Dyskinesia Mechanism Mediated by the Serotonin 5-HT6 Receptor. *Neuron, 90*(5), 955-968. doi:10.1016/j.neuron.2016.04.017

Alexander, G. E., DeLong, M. R., & Strick, P. L. (1986). Parallel organization of functionally segregated circuits linking basal ganglia and cortex. *Annu Rev Neurosci, 9*, 357-381. doi:10.1146/annurev.ne.09.030186.002041

Allen, S. J., Watson, J. J., Shoemark, D. K., Barua, N. U., & Patel, N. K. (2013). GDNF, NGF and BDNF as therapeutic options for neurodegeneration. *Pharmacol Ther, 138*(2), 155-175. doi:10.1016/j.pharmthera.2013.01.004

Alvarez-Medina, R., Cayuso, J., Okubo, T., Takada, S., & Marti, E. (2008). Wnt canonical pathway restricts graded Shh/Gli patterning activity through the regulation of Gli3 expression. *Development, 135*(2), 237-247. doi:10.1242/dev.012054

Anderson, K. D., & Reiner, A. (1991). Immunohistochemical localization of DARPP-32 in striatal projection neurons and striatal interneurons: implications for the localization of D1-like dopamine receptors on different types of striatal neurons. *Brain Res, 568*(1-2), 235-243. doi:10.1016/0006-8993(91)91403-n

Anderson, S. A., Marin, O., Horn, C., Jennings, K., & Rubenstein, J. L. (2001). Distinct cortical migrations from the medial and lateral ganglionic eminences. *Development, 128*(3), 353-363. doi:10.1242/dev.128.3.353

Andrew, S. E., Goldberg, Y. P., Kremer, B., Telenius, H., Theilmann, J., Adam, S., . . . et al. (1993). The relationship between trinucleotide (CAG) repeat length and

clinical features of Huntington's disease. *Nat Genet, 4*(4), 398-403. doi:10.1038/ng0893-398

Arber, C., Precious, S. V., Cambray, S., Risner-Janiczek, J. R., Kelly, C., Noakes, Z., . . . Li, M. (2015). Activin A directs striatal projection neuron differentiation of human pluripotent stem cells. *Development, 142*(7), 1375-1386. doi:10.1242/dev.117093

Arlotta, P., Molyneaux, B. J., Chen, J., Inoue, J., Kominami, R., & Macklis, J. D. (2005). Neuronal subtype-specific genes that control corticospinal motor neuron development in vivo. *Neuron, 45*(2), 207-221. doi:10.1016/j.neuron.2004.12.036

Arlotta, P., Molyneaux, B. J., Jabaudon, D., Yoshida, Y., & Macklis, J. D. (2008). Ctip2 controls the differentiation of medium spiny neurons and the establishment of the cellular architecture of the striatum. *J Neurosci, 28*(3), 622-632. doi:10.1523/JNEUROSCI.2986-07.2008

Armstrong, R. J., Watts, C., Svendsen, C. N., Dunnett, S. B., & Rosser, A. E. (2000). Survival, neuronal differentiation, and fiber outgrowth of propagated human neural precursor grafts in an animal model of Huntington's disease. *Cell Transplant, 9*(1), 55-64. doi:10.1177/096368970000900108

Aubry, L., Bugi, A., Lefort, N., Rousseau, F., Peschanski, M., & Perrier, A. L. (2008). Striatal progenitors derived from human ES cells mature into DARPP32 neurons in vitro and in quinolinic acid-lesioned rats. *Proc Natl Acad Sci U S A, 105*(43), 16707-16712. doi:10.1073/pnas.0808488105

Aylward, E. H., Sparks, B. F., Field, K. M., Yallapragada, V., Shpritz, B. D., Rosenblatt, A., . . . Ross, C. A. (2004). Onset and rate of striatal atrophy in preclinical Huntington disease. *Neurology, 63*(1), 66-72. doi:10.1212/01.wnl.0000132965.14653.d1

Bachoud-Levi, A., Bourdet, C., Brugieres, P., Nguyen, J. P., Grandmougin, T., Haddad, B., . . . Peschanski, M. (2000). Safety and tolerability assessment of intrastriatal neural allografts in five patients with Huntington's disease. *Exp Neurol, 161*(1), 194-202. doi:10.1006/exnr.1999.7239

Bachoud-Levi, A. C., & Perrier, A. L. (2014). Regenerative medicine in Huntington's disease: current status on fetal grafts and prospects for the use of pluripotent stem cell. *Rev Neurol (Paris), 170*(12), 749-762. doi:10.1016/j.neurol.2014.10.007

Bachoud-Levi, A. C., Remy, P., Nguyen, J. P., Brugieres, P., Lefaucheur, J. P., Bourdet, C., . . . Peschanski, M. (2000). Motor and cognitive improvements in patients with Huntington's disease after neural transplantation. *Lancet, 356*(9246), 1975-1979. doi:10.1016/s0140-6736(00)03310-9

Backman, M., Machon, O., Mygland, L., van den Bout, C. J., Zhong, W., Taketo, M. M., & Krauss, S. (2005). Effects of canonical Wnt signaling on dorso-ventral specification of the mouse telencephalon. *Dev Biol, 279*(1), 155-168. doi:10.1016/j.ydbio.2004.12.010

Bakels, H. S., Roos, R. A. C., van Roon-Mom, W. M. C., & de Bot, S. T. (2022). Juvenile-Onset Huntington Disease Pathophysiology and Neurodevelopment: A Review. *Mov Disord, 37*(1), 16-24. doi:10.1002/mds.28823

Balleine, B. W., & O'Doherty, J. P. (2010). Human and rodent homologies in action control: corticostriatal determinants of goal-directed and habitual action. *Neuropsychopharmacology, 35*(1), 48-69. doi:10.1038/npp.2009.131

Barnard, R. J., Elleder, D., & Young, J. A. (2006). Avian sarcoma and leukosis virus-receptor interactions: from classical genetics to novel insights into virus-cell membrane fusion. *Virology, 344*(1), 25-29. doi:10.1016/j.virol.2005.09.021

Bates, G. P., Dorsey, R., Gusella, J. F., Hayden, M. R., Kay, C., Leavitt, B. R., . . . Tabrizi, S. J. (2015). Huntington disease. *Nat Rev Dis Primers, 1*, 15005. doi:10.1038/nrdp.2015.5

Bates, P., Young, J. A., & Varmus, H. E. (1993). A receptor for subgroup A Rous sarcoma virus is related to the low density lipoprotein receptor. *Cell, 74*(6), 1043-1051. doi:10.1016/0092-8674(93)90726-7

Beal, M. F., Ferrante, R. J., Swartz, K. J., & Kowall, N. W. (1991). Chronic quinolinic acid lesions in rats closely resemble Huntington's disease. *J Neurosci, 11*(6), 1649-1659. doi:10.1523/JNEUROSCI.11-06-01649.1991

Beal, M. F., Kowall, N. W., Ellison, D. W., Mazurek, M. F., Swartz, K. J., & Martin, J. B. (1986). Replication of the neurochemical characteristics of Huntington's disease by quinolinic acid. *Nature, 321*(6066), 168-171. doi:10.1038/321168a0

Beal, M. F., Kowall, N. W., Swartz, K. J., Ferrante, R. J., & Martin, J. B. (1989). Differential sparing of somatostatin-neuropeptide Y and cholinergic neurons following striatal excitotoxin lesions. *Synapse, 3*(1), 38-47. doi:10.1002/syn.890030106

Belkadi, A. M., Geny, C., Naimi, S., Jeny, R., Peschanski, M., & Riche, D. (1997). Maturation of fetal human neural xenografts in the adult rat brain. *Exp Neurol, 144*(2), 369-380. doi:10.1006/exnr.1997.6414

Benraiss, A., Wang, S., Herrlinger, S., Li, X., Chandler-Militello, D., Mauceri, J., . . . Goldman, S. A. (2016). Human glia can both induce and rescue aspects of disease phenotype in Huntington disease. *Nat Commun, 7*, 11758. doi:10.1038/ncomms11758

Bertaina-Anglade, V., Tramu, G., & Destrade, C. (2000). Differential learning-stage dependent patterns of c-Fos protein expression in brain regions during the acquisition and memory consolidation of an operant task in mice. *Eur J Neurosci, 12*(10), 3803-3812. doi:10.1046/j.1460-9568.2000.00258.x

Besusso, D., Schellino, R., Boido, M., Belloli, S., Parolisi, R., Conforti, P., . . . Cattaneo, E. (2020). Stem Cell-Derived Human Striatal Progenitors Innervate Striatal Targets and Alleviate Sensorimotor Deficit in a Rat Model of Huntington Disease. *Stem Cell Reports, 14*(5), 876-891. doi:10.1016/j.stemcr.2020.03.018

Bhat, R. V., Cole, A. J., & Baraban, J. M. (1992). Role of monoamine systems in activation of zif268 by cocaine. *J Psychiatry Neurosci, 17*(3), 94-102. Retrieved from https://www.ncbi.nlm.nih.gov/pubmed/1356432

Bisler, S., Schleicher, A., Gass, P., Stehle, J. H., Zilles, K., & Staiger, J. F. (2002). Expression of c-Fos, ICER, Krox-24 and JunB in the whisker-to-barrel pathway of rats: time course of induction upon whisker stimulation by tactile exploration of an enriched environment. *J Chem Neuroanat, 23*(3), 187-198. doi:10.1016/s0891-0618(01)00155-7

Bocchi, V. D., Conforti, P., Vezzoli, E., Besusso, D., Cappadona, C., Lischetti, T., . . . Cattaneo, E. (2021). The coding and long noncoding single-cell atlas of the developing human fetal striatum. *Science, 372*(6542). doi:10.1126/science.abf5759

Bode, F. J., Stephan, M., Suhling, H., Pabst, R., Straub, R. H., Raber, K. A., . . . von Horsten, S. (2008). Sex differences in a transgenic rat model of Huntington's disease: decreased 17beta-estradiol levels correlate with reduced numbers of

DARPP32+ neurons in males. *Hum Mol Genet, 17*(17), 2595-2609. doi:10.1093/hmg/ddn159

Boitor-Borza, D., Turcu, F., Farcasanu, S., & Crivii, C. (2021). Early development of human ganglionic eminences assessed in vitro by using 7.04 Tesla micro-MRI - a pilot study. *Med Pharm Rep, 94*(1), 35-42. doi:10.15386/mpr-1715

Borycki, A., Brown, A. M., & Emerson, C. P., Jr. (2000). Shh and Wnt signaling pathways converge to control Gli gene activation in avian somites. *Development, 127*(10), 2075-2087. doi:10.1242/dev.127.10.2075

Brasted, P. J., Watts, C., Robbins, T. W., & Dunnett, S. B. (1999). Associative plasticity in striatal transplants. *Proc Natl Acad Sci U S A, 96*(18), 10524-10529. doi:10.1073/pnas.96.18.10524

Brazel, C. Y., Romanko, M. J., Rothstein, R. P., & Levison, S. W. (2003). Roles of the mammalian subventricular zone in brain development. *Prog Neurobiol, 69*(1), 49-69. doi:10.1016/s0301-0082(03)00002-9

Brennan, P. A., Schellinck, H. M., & Keverne, E. B. (1999). Patterns of expression of the immediate-early gene egr-1 in the accessory olfactory bulb of female mice exposed to pheromonal constituents of male urine. *Neuroscience, 90*(4), 1463-1470. doi:10.1016/s0306-4522(98)00556-9

Brimblecombe, K. R., & Cragg, S. J. (2017). The Striosome and Matrix Compartments of the Striatum: A Path through the Labyrinth from Neurochemistry toward Function. *ACS Chem Neurosci, 8*(2), 235-242. doi:10.1021/acschemneuro.6b00333

Buhusi, C. V., & Meck, W. H. (2005). What makes us tick? Functional and neural mechanisms of interval timing. *Nat Rev Neurosci, 6*(10), 755-765. doi:10.1038/nrn1764

Bulfone, A., Wang, F., Hevner, R., Anderson, S., Cutforth, T., Chen, S., . . . Rubenstein, J. L. (1998). An olfactory sensory map develops in the absence of normal projection neurons or GABAergic interneurons. *Neuron, 21*(6), 1273-1282. doi:10.1016/s0896-6273(00)80647-9

Calais, J. B., Ojopi, E. B., Morya, E., Sameshima, K., & Ribeiro, S. (2015). Experience-dependent upregulation of multiple plasticity factors in the hippocampus during early REM sleep. *Neurobiol Learn Mem, 122*, 19-27. doi:10.1016/j.nlm.2015.01.002

Campbell, K., Kalen, P., Wictorin, K., Lundberg, C., Mandel, R. J., & Bjorklund, A. (1993). Characterization of GABA release from intrastriatal striatal transplants: dependence on host-derived afferents. *Neuroscience, 53*(2), 403-415. doi:10.1016/0306-4522(93)90204-s

Canales, J. J. (2005). Stimulant-induced adaptations in neostriatal matrix and striosome systems: transiting from instrumental responding to habitual behavior in drug addiction. *Neurobiol Learn Mem, 83*(2), 93-103. doi:10.1016/j.nlm.2004.10.006

Cao, C., Temel, Y., Blokland, A., Ozen, H., Steinbusch, H. W., Vlamings, R., . . . Visser-Vandewalle, V. (2006). Progressive deterioration of reaction time performance and choreiform symptoms in a new Huntington's disease transgenic ratmodel. *Behav Brain Res, 170*(2), 257-261. doi:10.1016/j.bbr.2006.02.028

Capetian, P., Knoth, R., Maciaczyk, J., Pantazis, G., Ditter, M., Bokla, L., . . . Nikkhah, G. (2009). Histological findings on fetal striatal grafts in a Huntington's disease

patient early after transplantation. *Neuroscience, 160*(3), 661-675. doi:10.1016/j.neuroscience.2009.02.035

Card, J. P., Enquist, L. W., & Moore, R. Y. (1999). Neuroinvasiveness of pseudorabies virus injected intracerebrally is dependent on viral concentration and terminal field density. *J Comp Neurol, 407*(3), 438-452. doi:10.1002/(sici)1096-9861(19990510)407:3<438::aid-cne11>3.0.co;2-2

Cardoso, T., Adler, A. F., Mattsson, B., Hoban, D. B., Nolbrant, S., Wahlestedt, J. N., . . . Parmar, M. (2018). Target-specific forebrain projections and appropriate synaptic inputs of hESC-derived dopamine neurons grafted to the midbrain of parkinsonian rats. *J Comp Neurol, 526*(13), 2133-2146. doi:10.1002/cne.24500

Carlsson, T., Winkler, C., Lundblad, M., Cenci, M. A., Bjorklund, A., & Kirik, D. (2006). Graft placement and uneven pattern of reinnervation in the striatum is important for development of graft-induced dyskinesia. *Neurobiol Dis, 21*(3), 657-668. doi:10.1016/j.nbd.2005.09.008

Carmo, C., Naia, L., Lopes, C., & Rego, A. C. (2018). Mitochondrial Dysfunction in Huntington's Disease. *Adv Exp Med Biol, 1049*, 59-83. doi:10.1007/978-3-319-71779-1_3

Caron, N. S., Wright, G. E. B., & Hayden, M. R. (1993). Huntington Disease. In M. P. Adam, J. Feldman, G. M. Mirzaa, R. A. Pagon, S. E. Wallace, L. J. H. Bean, K. W. Gripp, & A. Amemiya (Eds.), *GeneReviews((R))*. Seattle (WA).

Castane, A., Theobald, D. E., & Robbins, T. W. (2010). Selective lesions of the dorsomedial striatum impair serial spatial reversal learning in rats. *Behav Brain Res, 210*(1), 74-83. doi:10.1016/j.bbr.2010.02.017

Cebrian, C., Parent, A., & Prensa, L. (2005). Patterns of axonal branching of neurons of the substantia nigra pars reticulata and pars lateralis in the rat. *J Comp Neurol, 492*(3), 349-369. doi:10.1002/cne.20741

Chambers, S. M., Fasano, C. A., Papapetrou, E. P., Tomishima, M., Sadelain, M., & Studer, L. (2009). Highly efficient neural conversion of human ES and iPS cells by dual inhibition of SMAD signaling. *Nat Biotechnol, 27*(3), 275-280. doi:10.1038/nbt.1529

Chatzi, C., Brade, T., & Duester, G. (2011). Retinoic acid functions as a key GABAergic differentiation signal in the basal ganglia. *PLoS Biol, 9*(4), e1000609. doi:10.1371/journal.pbio.1000609

Chemali, J. J., Kenny, J. D., Olutola, O., Taylor, N. E., Kimchi, E. Y., Purdon, P. L., . . . Solt, K. (2015). Ageing delays emergence from general anaesthesia in rats by increasing anaesthetic sensitivity in the brain. *Br J Anaesth, 115 Suppl 1*(Suppl 1), i58-i65. doi:10.1093/bja/aev112

Chen, S., & Aston-Jones, G. (1995). Evidence that cholera toxin B subunit (CTb) can be avidly taken up and transported by fibers of passage. *Brain Res, 674*(1), 107-111. doi:10.1016/0006-8993(95)00020-q

Chen, Y., Xiong, M., Dong, Y., Haberman, A., Cao, J., Liu, H., . . . Zhang, S. C. (2016). Chemical Control of Grafted Human PSC-Derived Neurons in a Mouse Model of Parkinson's Disease. *Cell Stem Cell, 18*(6), 817-826. doi:10.1016/j.stem.2016.03.014

Choi, E. Y., Ding, S. L., & Haber, S. N. (2017). Combinatorial Inputs to the Ventral Striatum from the Temporal Cortex, Frontal Cortex, and Amygdala: Implications for Segmenting the Striatum. *eNeuro, 4*(6). doi:10.1523/ENEURO.0392-17.2017

Cicchetti, F., Saporta, S., Hauser, R. A., Parent, M., Saint-Pierre, M., Sanberg, P. R., . . . Freeman, T. B. (2009). Neural transplants in patients with Huntington's disease undergo disease-like neuronal degeneration. *Proc Natl Acad Sci U S A, 106*(30), 12483-12488. doi:10.1073/pnas.0904239106

Cisbani, G., Freeman, T. B., Soulet, D., Saint-Pierre, M., Gagnon, D., Parent, M., . . . Cicchetti, F. (2013). Striatal allografts in patients with Huntington's disease: impact of diminished astrocytes and vascularization on graft viability. *Brain, 136*(Pt 2), 433-443. doi:10.1093/brain/aws359

Clarke, D. J., & Dunnett, S. B. (1993). Synaptic relationships between cortical and dopaminergic inputs and intrinsic GABAergic systems within intrastriatal striatal grafts. *J Chem Neuroanat, 6*(3), 147-158. doi:10.1016/0891-0618(93)90024-x

Clarke, D. J., Dunnett, S. B., Isacson, O., Sirinathsinghji, D. J., & Bjorklund, A. (1988). Striatal grafts in rats with unilateral neostriatal lesions--I. Ultrastructural evidence of afferent synaptic inputs from the host nigrostriatal pathway. *Neuroscience, 24*(3), 791-801. doi:10.1016/0306-4522(88)90067-x

Clemensson, E. K., Clemensson, L. E., Riess, O., & Nguyen, H. P. (2017). The BACHD Rat Model of Huntington Disease Shows Signs of Fronto-Striatal Dysfunction in Two Operant Conditioning Tests of Short-Term Memory. *PLoS One, 12*(1), e0169051. doi:10.1371/journal.pone.0169051

Coffey, P. J., Lund, R. D., & Rawlins, J. N. (1989). Retinal transplant-mediated learning in a conditioned suppression task in rats. *Proc Natl Acad Sci U S A, 86*(18), 7248-7249. doi:10.1073/pnas.86.18.7248

Colodner, K. J., Montana, R. A., Anthony, D. C., Folkerth, R. D., De Girolami, U., & Feany, M. B. (2005). Proliferative potential of human astrocytes. *J Neuropathol Exp Neurol, 64*(2), 163-169. doi:10.1093/jnen/64.2.163

Colpo, G. D., Furr Stimming, E., & Teixeira, A. L. (2019). Stem cells in animal models of Huntington disease: A systematic review. *Mol Cell Neurosci, 95*, 43-50. doi:10.1016/j.mcn.2019.01.006

Comella-Bolla, A., Orlandi, J. G., Miguez, A., Straccia, M., Garcia-Bravo, M., Bombau, G., . . . Canals, J. M. (2020). Human Pluripotent Stem Cell-Derived Neurons Are Functionally Mature In Vitro and Integrate into the Mouse Striatum Following Transplantation. *Mol Neurobiol, 57*(6), 2766-2798. doi:10.1007/s12035-020-01907-4

Connor, B. (2018). Concise Review: The Use of Stem Cells for Understanding and Treating Huntington's Disease. *Stem Cells, 36*(2), 146-160. doi:10.1002/stem.2747

Conte, W. L., Kamishina, H., & Reep, R. L. (2009a). The efficacy of the fluorescent conjugates of cholera toxin subunit B for multiple retrograde tract tracing in the central nervous system. *Brain Struct Funct, 213*(4-5), 367-373. doi:10.1007/s00429-009-0212-x

Conte, W. L., Kamishina, H., & Reep, R. L. (2009b). Multiple neuroanatomical tract-tracing using fluorescent Alexa Fluor conjugates of cholera toxin subunit B in rats. *Nat Protoc, 4*(8), 1157-1166. doi:10.1038/nprot.2009.93

Cover, K. K., Lieberman, A. G., Heckman, M. M., & Mathur, B. N. (2023). The rostral intralaminar nuclear complex of the thalamus supports striatally mediated action reinforcement. *Elife, 12*. doi:10.7554/eLife.83627

Coyle, J. T., & Schwarcz, R. (1976). Lesion of striatal neurones with kainic acid provides a model for Huntington's chorea. *Nature, 263*(5574), 244-246. doi:10.1038/263244a0

Crittenden, J. R., & Graybiel, A. M. (2011). Basal Ganglia disorders associated with imbalances in the striatal striosome and matrix compartments. *Front Neuroanat, 5*, 59. doi:10.3389/fnana.2011.00059

Crossman, A. R. (1987). Primate models of dyskinesia: the experimental approach to the study of basal ganglia-related involuntary movement disorders. *Neuroscience, 21*(1), 1-40. doi:10.1016/0306-4522(87)90322-8

Crossman, A. R., Mitchell, I. J., Sambrook, M. A., & Jackson, A. (1988). Chorea and myoclonus in the monkey induced by gamma-aminobutyric acid antagonism in the lentiform complex. The site of drug action and a hypothesis for the neural mechanisms of chorea. *Brain, 111 (Pt 5)*, 1211-1233. doi:10.1093/brain/111.5.1211

Dado, R. J., Burstein, R., Cliffer, K. D., & Giesler, G. J., Jr. (1990). Evidence that Fluoro-Gold can be transported avidly through fibers of passage. *Brain Res, 533*(2), 329-333. doi:10.1016/0006-8993(90)91358-n

Darnell, D., & Gilbert, S. F. (2017). Neuroembryology. *Wiley Interdiscip Rev Dev Biol, 6*(1). doi:10.1002/wdev.215

Davies, D. S., Ma, J., Jegathees, T., & Goldsbury, C. (2017). Microglia show altered morphology and reduced arborization in human brain during aging and Alzheimer's disease. *Brain Pathol, 27*(6), 795-808. doi:10.1111/bpa.12456

Day-Brown, J. D., Wei, H., Chomsung, R. D., Petry, H. M., & Bickford, M. E. (2010). Pulvinar projections to the striatum and amygdala in the tree shrew. *Front Neuroanat, 4*, 143. doi:10.3389/fnana.2010.00143

de la Monte, S. M., Vonsattel, J. P., & Richardson, E. P., Jr. (1988). Morphometric demonstration of atrophic changes in the cerebral cortex, white matter, and neostriatum in Huntington's disease. *J Neuropathol Exp Neurol, 47*(5), 516-525. doi:10.1097/00005072-198809000-00003

Deacon, T. W., Pakzaban, P., & Isacson, O. (1994). The lateral ganglionic eminence is the origin of cells committed to striatal phenotypes: neural transplantation and developmental evidence. *Brain Res, 668*(1-2), 211-219. doi:10.1016/0006-8993(94)90526-6

Deckel, A. W., Moran, T. H., Coyle, J. T., Sanberg, P. R., & Robinson, R. G. (1986). Anatomical predictors of behavioral recovery following fetal striatal transplants. *Brain Res, 365*(2), 249-258. doi:10.1016/0006-8993(86)91636-7

Delli Carri, A., Onorati, M., Castiglioni, V., Faedo, A., Camnasio, S., Toselli, M., . . . Cattaneo, E. (2013). Human pluripotent stem cell differentiation into authentic striatal projection neurons. *Stem Cell Rev Rep, 9*(4), 461-474. doi:10.1007/s12015-013-9441-8

Delli Carri, A., Onorati, M., Lelos, M. J., Castiglioni, V., Faedo, A., Menon, R., . . . Cattaneo, E. (2013). Developmentally coordinated extrinsic signals drive human pluripotent stem cell differentiation toward authentic DARPP-32+ medium-sized spiny neurons. *Development, 140*(2), 301-312. doi:10.1242/dev.084608

DeLong, M. R. (1971). Activity of pallidal neurons during movement. *J Neurophysiol, 34*(3), 414-427. doi:10.1152/jn.1971.34.3.414

DeLong, M. R. (1990). Primate models of movement disorders of basal ganglia origin. *Trends Neurosci, 13*(7), 281-285. doi:10.1016/0166-2236(90)90110-v

Deng, Y. P., Albin, R. L., Penney, J. B., Young, A. B., Anderson, K. D., & Reiner, A. (2004). Differential loss of striatal projection systems in Huntington's disease: a

quantitative immunohistochemical study. *J Chem Neuroanat, 27*(3), 143-164. doi:10.1016/j.jchemneu.2004.02.005

Deschenes, M., Bourassa, J., Doan, V. D., & Parent, A. (1996). A single-cell study of the axonal projections arising from the posterior intralaminar thalamic nuclei in the rat. *Eur J Neurosci, 8*(2), 329-343. doi:10.1111/j.1460-9568.1996.tb01217.x

Dey, N. D., Bombard, M. C., Roland, B. P., Davidson, S., Lu, M., Rossignol, J., . . . Dunbar, G. L. (2010). Genetically engineered mesenchymal stem cells reduce behavioral deficits in the YAC 128 mouse model of Huntington's disease. *Behav Brain Res, 214*(2), 193-200. doi:10.1016/j.bbr.2010.05.023

DiFiglia, M., Schiff, L., & Deckel, A. W. (1988). Neuronal organization of fetal striatal grafts in kainate- and sham-lesioned rat caudate nucleus: light- and electron-microscopic observations. *J Neurosci, 8*(4), 1112-1130. doi:10.1523/JNEUROSCI.08-04-01112.1988

Dobrossy, M. D., & Dunnett, S. B. (2001). The influence of environment and experience on neural grafts. *Nat Rev Neurosci, 2*(12), 871-879. doi:10.1038/35104055

Dobrossy, M. D., & Dunnett, S. B. (2003). Motor training effects on recovery of function after striatal lesions and striatal grafts. *Exp Neurol, 184*(1), 274-284. doi:10.1016/s0014-4886(03)00028-1

Dobrossy, M. D., & Dunnett, S. B. (2004). Environmental enrichment affects striatal graft morphology and functional recovery. *Eur J Neurosci, 19*(1), 159-168. doi:10.1111/j.1460-9568.2004.03105.x

Dobrossy, M. D., & Dunnett, S. B. (2005). Training specificity, graft development and graft-mediated functional recovery in a rodent model of Huntington's disease. *Neuroscience, 132*(3), 543-552. doi:10.1016/j.neuroscience.2005.01.016

Doerr, J., Schwarz, M. K., Wiedermann, D., Leinhaas, A., Jakobs, A., Schloen, F., . . . Brustle, O. (2017). Whole-brain 3D mapping of human neural transplant innervation. *Nat Commun, 8*, 14162. doi:10.1038/ncomms14162

Doig, N. M., Moss, J., & Bolam, J. P. (2010). Cortical and thalamic innervation of direct and indirect pathway medium-sized spiny neurons in mouse striatum. *J Neurosci, 30*(44), 14610-14618. doi:10.1523/JNEUROSCI.1623-10.2010

Dong, X. X., Wang, Y., & Qin, Z. H. (2009). Molecular mechanisms of excitotoxicity and their relevance to pathogenesis of neurodegenerative diseases. *Acta Pharmacol Sin, 30*(4), 379-387. doi:10.1038/aps.2009.24

Doyon, J., Bellec, P., Amsel, R., Penhune, V., Monchi, O., Carrier, J., . . . Benali, H. (2009). Contributions of the basal ganglia and functionally related brain structures to motor learning. *Behav Brain Res, 199*(1), 61-75. doi:10.1016/j.bbr.2008.11.012

Duan, D., Fu, Y., Paxinos, G., & Watson, C. (2013). Spatiotemporal expression patterns of Pax6 in the brain of embryonic, newborn, and adult mice. *Brain Struct Funct, 218*(2), 353-372. doi:10.1007/s00429-012-0397-2

Dubinsky, R. M. (2005). No going home for hospitalized Huntington's disease patients. *Mov Disord, 20*(10), 1316-1322. doi:10.1002/mds.20589

Dunnett, S. B., Kendall, A. L., Watts, C., & Torres, E. M. (1997). Neuronal cell transplantation for Parkinson's and Huntington's diseases. *Br Med Bull, 53*(4), 757-776. doi:10.1093/oxfordjournals.bmb.a011646

Dunnett, S. B., Nathwani, F., & Brasted, P. J. (1999). Medial prefrontal and neostriatal lesions disrupt performance in an operant delayed alternation task in rats. *Behav Brain Res, 106*(1-2), 13-28. doi:10.1016/s0166-4328(99)00076-5

Dunnett, S. B., & White, A. (2006). Striatal grafts alleviate bilateral striatal lesion deficits in operant delayed alternation in the rat. *Exp Neurol, 199*(2), 479-489. doi:10.1016/j.expneurol.2006.01.013

Duyao, M., Ambrose, C., Myers, R., Novelletto, A., Persichetti, F., Frontali, M., . . . et al. (1993). Trinucleotide repeat length instability and age of onset in Huntington's disease. *Nat Genet, 4*(4), 387-392. doi:10.1038/ng0893-387

Eagle, D. M., Humby, T., Dunnett, S. B., & Robbins, T. W. (1999). Effects of regional striatal lesions on motor, motivational, and executive aspects of progressive-ratio performance in rats. *Behav Neurosci, 113*(4), 718-731. doi:10.1037//0735-7044.113.4.718

Eid, L., Parent, A., & Parent, M. (2016). Asynaptic feature and heterogeneous distribution of the cholinergic innervation of the globus pallidus in primates. *Brain Struct Funct, 221*(2), 1139-1155. doi:10.1007/s00429-014-0960-0

Evans, A. E., Kelly, C. M., Precious, S. V., & Rosser, A. E. (2012). Molecular regulation of striatal development: a review. *Anat Res Int, 2012*, 106529. doi:10.1155/2012/106529

Fan, M. M., & Raymond, L. A. (2007). N-methyl-D-aspartate (NMDA) receptor function and excitotoxicity in Huntington's disease. *Prog Neurobiol, 81*(5-6), 272-293. doi:10.1016/j.pneurobio.2006.11.003

Fantie, B. D. (2015). Brain Damage: Neuropsychological Rehabilitation. In *International Encyclopedia of the Social & Behavioral Sciences* (pp. 813-820).

Federspiel, M. J., Bates, P., Young, J. A., Varmus, H. E., & Hughes, S. H. (1994). A system for tissue-specific gene targeting: transgenic mice susceptible to subgroup A avian leukosis virus-based retroviral vectors. *Proc Natl Acad Sci U S A, 91*(23), 11241-11245. doi:10.1073/pnas.91.23.11241

Feijen, A., Goumans, M. J., & van den Eijnden-van Raaij, A. J. (1994). Expression of activin subunits, activin receptors and follistatin in postimplantation mouse embryos suggests specific developmental functions for different activins. *Development, 120*(12), 3621-3637. doi:10.1242/dev.120.12.3621

FENNER F, B. P., GIBBS EPJ, MURPHY FA, STUDDERT MJ, WHITE DO. (1987). Structure and Composition of Viruses. *Veterinary Virology*.

Ferland, R. J., Cherry, T. J., Preware, P. O., Morrisey, E. E., & Walsh, C. A. (2003). Characterization of Foxp2 and Foxp1 mRNA and protein in the developing and mature brain. *J Comp Neurol, 460*(2), 266-279. doi:10.1002/cne.10654

Ferrante, R. J., Kowall, N. W., & Richardson, E. P., Jr. (1991). Proliferative and degenerative changes in striatal spiny neurons in Huntington's disease: a combined study using the section-Golgi method and calbindin D28k immunocytochemistry. *J Neurosci, 11*(12), 3877-3887. doi:10.1523/JNEUROSCI.11-12-03877.1991

Figueredo-Cardenas, G., Chen, Q., & Reiner, A. (1997). Age-dependent differences in survival of striatal somatostatin-NPY-NADPH-diaphorase-containing interneurons versus striatal projection neurons after intrastriatal injection of quinolinic acid in rats. *Exp Neurol, 146*(2), 444-457. doi:10.1006/exnr.1997.6549

Folstein, S., Abbott, M. H., Chase, G. A., Jensen, B. A., & Folstein, M. F. (1983). The association of affective disorder with Huntington's disease in a case series and in families. *Psychol Med, 13*(3), 537-542. doi:10.1017/s0033291700047966

Foroud, T., Gray, J., Ivashina, J., & Conneally, P. M. (1999). Differences in duration of Huntington's disease based on age at onset. *J Neurol Neurosurg Psychiatry, 66*(1), 52-56. doi:10.1136/jnnp.66.1.52

Foster, A. C., Collins, J. F., & Schwarcz, R. (1983). On the excitotoxic properties of quinolinic acid, 2,3-piperidine dicarboxylic acids and structurally related compounds. *Neuropharmacology, 22*(12A), 1331-1342. doi:10.1016/0028-3908(83)90221-6

Foster, N. N., Barry, J., Korobkova, L., Garcia, L., Gao, L., Becerra, M., . . . Dong, H. W. (2021). The mouse cortico-basal ganglia-thalamic network. *Nature, 598*(7879), 188-194. doi:10.1038/s41586-021-03993-3

Fowler, J. L., Ang, L. T., & Loh, K. M. (2020). A critical look: Challenges in differentiating human pluripotent stem cells into desired cell types and organoids. *Wiley Interdiscip Rev Dev Biol, 9*(3), e368. doi:10.1002/wdev.368

Freeman, T. B., Cicchetti, F., Bachoud-Levi, A. C., & Dunnett, S. B. (2011). Technical factors that influence neural transplant safety in Huntington's disease. *Exp Neurol, 227*(1), 1-9. doi:10.1016/j.expneurol.2010.08.031

Freeman, T. B., Cicchetti, F., Hauser, R. A., Deacon, T. W., Li, X. J., Hersch, S. M., . . . Isacson, O. (2000). Transplanted fetal striatum in Huntington's disease: phenotypic development and lack of pathology. *Proc Natl Acad Sci U S A, 97*(25), 13877-13882. doi:10.1073/pnas.97.25.13877

Fricker, R. A., Annett, L. E., Torres, E. M., & Dunnett, S. B. (1996). The placement of a striatal ibotenic acid lesion affects skilled forelimb use and the direction of drug-induced rotation. *Brain Res Bull, 41*(6), 409-416. doi:10.1016/s0361-9230(96)00083-4

Fricker, R. A., Torres, E. M., Hume, S. P., Myers, R., Opacka-Juffrey, J., Ashworth, S., . . . Dunnett, S. B. (1997). The effects of donor stage on the survival and function of embryonic striatal grafts in the adult rat brain. II. Correlation between positron emission tomography and reaching behaviour. *Neuroscience, 79*(3), 711-721. doi:10.1016/s0306-4522(96)00657-4

Fudge, J. L., Kunishio, K., Walsh, P., Richard, C., & Haber, S. N. (2002). Amygdaloid projections to ventromedial striatal subterritories in the primate. *Neuroscience, 110*(2), 257-275. doi:10.1016/s0306-4522(01)00546-2

Fujiyama, F., Sohn, J., Nakano, T., Furuta, T., Nakamura, K. C., Matsuda, W., & Kaneko, T. (2011). Exclusive and common targets of neostriatofugal projections of rat striosome neurons: a single neuron-tracing study using a viral vector. *Eur J Neurosci, 33*(4), 668-677. doi:10.1111/j.1460-9568.2010.07564.x

Garcia Jareno, P., Bartley, O. J. M., Precious, S. V., Rosser, A. E., & Lelos, M. J. (2022). Challenges in progressing cell therapies to the clinic for Huntington's disease: A review of the progress made with pluripotent stem cell derived medium spiny neurons. *Int Rev Neurobiol, 166*, 1-48. doi:10.1016/bs.irn.2022.09.003

Gerfen, C. R. (1984). The neostriatal mosaic: compartmentalization of corticostriatal input and striatonigral output systems. *Nature, 311*(5985), 461-464. doi:10.1038/311461a0

Gerfen, C. R., Engber, T. M., Mahan, L. C., Susel, Z., Chase, T. N., Monsma, F. J., Jr., & Sibley, D. R. (1990). D1 and D2 dopamine receptor-regulated gene

expression of striatonigral and striatopallidal neurons. *Science, 250*(4986), 1429-1432. doi:10.1126/science.2147780

Ghasemian-Shirvan, E., Farnad, L., Mosayebi-Samani, M., Verstraelen, S., Meesen, R. L. J., Kuo, M. F., & Nitsche, M. A. (2020). Age-related differences of motor cortex plasticity in adults: A transcranial direct current stimulation study. *Brain Stimul, 13*(6), 1588-1599. doi:10.1016/j.brs.2020.09.004

Grasbon-Frodl, E. M., Nakao, N., Lindvall, O., & Brundin, P. (1996). Phenotypic development of the human embryonic striatal primordium: a study of cultured and grafted neurons from the lateral and medial ganglionic eminences. *Neuroscience, 73*(1), 171-183. doi:10.1016/0306-4522(96)00008-5

Grasbon-Frodl, E. M., Nakao, N., Lindvall, O., & Brundin, P. (1997). Developmental features of human striatal tissue transplanted in a rat model of Huntington's disease. *Neurobiol Dis, 3*(4), 299-311. doi:10.1006/nbdi.1996.0124

Graveland, G. A., Williams, R. S., & DiFiglia, M. (1985). Evidence for degenerative and regenerative changes in neostriatal spiny neurons in Huntington's disease. *Science, 227*(4688), 770-773. doi:10.1126/science.3155875

Gray, M., Shirasaki, D. I., Cepeda, C., Andre, V. M., Wilburn, B., Lu, X. H., . . . Yang, X. W. (2008). Full-length human mutant huntingtin with a stable polyglutamine repeat can elicit progressive and selective neuropathogenesis in BACHD mice. *J Neurosci, 28*(24), 6182-6195. doi:10.1523/JNEUROSCI.0857-08.2008

Grealish, S., Heuer, A., Cardoso, T., Kirkeby, A., Jonsson, M., Johansson, J., . . . Parmar, M. (2015). Monosynaptic Tracing using Modified Rabies Virus Reveals Early and Extensive Circuit Integration of Human Embryonic Stem Cell-Derived Neurons. *Stem Cell Reports, 4*(6), 975-983. doi:10.1016/j.stemcr.2015.04.011

Grealish, S., Mattsson, B., Draxler, P., & Bjorklund, A. (2010). Characterisation of behavioural and neurodegenerative changes induced by intranigral 6-hydroxydopamine lesions in a mouse model of Parkinson's disease. *Eur J Neurosci, 31*(12), 2266-2278. doi:10.1111/j.1460-9568.2010.07265.x

Green, T. R. F., Murphy, S. M., & Rowe, R. K. (2022). Comparisons of quantitative approaches for assessing microglial morphology reveal inconsistencies, ecological fallacy, and a need for standardization. *Sci Rep, 12*(1), 18196. doi:10.1038/s41598-022-23091-2

Grimm, R., & Tischmeyer, W. (1997). Complex patterns of immediate early gene induction in rat brain following brightness discrimination training and pseudotraining. *Behav Brain Res, 84*(1-2), 109-116. doi:10.1016/s0166-4328(97)83330-x

Guillemin, G. J., Croitoru-Lamoury, J., Dormont, D., Armati, P. J., & Brew, B. J. (2003). Quinolinic acid upregulates chemokine production and chemokine receptor expression in astrocytes. *Glia, 41*(4), 371-381. doi:10.1002/glia.10175

Guillemin, G. J., Smith, D. G., Smythe, G. A., Armati, P. J., & Brew, B. J. (2003). Expression of the kynurenine pathway enzymes in human microglia and macrophages. *Adv Exp Med Biol, 527*, 105-112. doi:10.1007/978-1-4615-0135-0_12

Gunhaga, L., Marklund, M., Sjodal, M., Hsieh, J. C., Jessell, T. M., & Edlund, T. (2003). Specification of dorsal telencephalic character by sequential Wnt and FGF signaling. *Nat Neurosci, 6*(7), 701-707. doi:10.1038/nn1068

Gutin, G., Fernandes, M., Palazzolo, L., Paek, H., Yu, K., Ornitz, D. M., . . . Hebert, J. M. (2006). FGF signalling generates ventral telencephalic cells independently of SHH. *Development, 133*(15), 2937-2946. doi:10.1242/dev.02465

Haber, S. N. (2003). The primate basal ganglia: parallel and integrative networks. *J Chem Neuroanat, 26*(4), 317-330. doi:10.1016/j.jchemneu.2003.10.003

Haber, S. N. (2016). Corticostriatal circuitry. *Dialogues Clin Neurosci, 18*(1), 7-21. doi:10.31887/DCNS.2016.18.1/shaber

Hanashima, C., Fernandes, M., Hebert, J. M., & Fishell, G. (2007). The role of Foxg1 and dorsal midline signaling in the generation of Cajal-Retzius subtypes. *J Neurosci, 27*(41), 11103-11111. doi:10.1523/JNEUROSCI.1066-07.2007

Hart, G., Leung, B. K., & Balleine, B. W. (2014). Dorsal and ventral streams: the distinct role of striatal subregions in the acquisition and performance of goal-directed actions. *Neurobiol Learn Mem, 108*, 104-118. doi:10.1016/j.nlm.2013.11.003

He, J., Kleyman, M., Chen, J., Alikaya, A., Rothenhoefer, K. M., Ozturk, B. E., . . . Stauffer, W. R. (2021). Transcriptional and anatomical diversity of medium spiny neurons in the primate striatum. *Curr Biol, 31*(24), 5473-5486 e5476. doi:10.1016/j.cub.2021.10.015

Heng, M. Y., Detloff, P. J., & Albin, R. L. (2008). Rodent genetic models of Huntington disease. *Neurobiol Dis, 32*(1), 1-9. doi:10.1016/j.nbd.2008.06.005

Hikosaka, O., Nakamura, K., Sakai, K., & Nakahara, H. (2002). Central mechanisms of motor skill learning. *Curr Opin Neurobiol, 12*(2), 217-222. doi:10.1016/s0959-4388(02)00307-0

Hills, R., Mossman, J. A., Bratt-Leal, A. M., Tran, H., Williams, R. M., Stouffer, D. G., . . . Lelos, M. J. (2023). Neurite Outgrowth and Gene Expression Profile Correlate with Efficacy of Human Induced Pluripotent Stem Cell-Derived Dopamine Neuron Grafts. *Stem Cells Dev, 32*(13-14), 387-397. doi:10.1089/scd.2023.0043

Hinwood, M., Morandini, J., Day, T. A., & Walker, F. R. (2012). Evidence that microglia mediate the neurobiological effects of chronic psychological stress on the medial prefrontal cortex. *Cereb Cortex, 22*(6), 1442-1454. doi:10.1093/cercor/bhr229

Hipp, M. S., Park, S. H., & Hartl, F. U. (2014). Proteostasis impairment in protein-misfolding and -aggregation diseases. *Trends Cell Biol, 24*(9), 506-514. doi:10.1016/j.tcb.2014.05.003

Holley, S. M., Reidling, J. C., Cepeda, C., Wu, J., Lim, R. G., Lau, A., . . . Thompson, L. M. (2023). Transplanted human neural stem cells rescue phenotypes in zQ175 Huntington's disease mice and innervate the striatum. *Mol Ther, 31*(12), 3545-3563. doi:10.1016/j.ymthe.2023.10.003

Hu, Y. T., Chen, X. L., Huang, S. H., Zhu, Q. B., Yu, S. Y., Shen, Y., . . . Bao, A. M. (2019). Early growth response-1 regulates acetylcholinesterase and its relation with the course of Alzheimer's disease. *Brain Pathol, 29*(4), 502-512. doi:10.1111/bpa.12688

Hunnicutt, B. J., Jongbloets, B. C., Birdsong, W. T., Gertz, K. J., Zhong, H., & Mao, T. (2016). A comprehensive excitatory input map of the striatum reveals novel functional organization. *Elife, 5*. doi:10.7554/eLife.19103

Hunt, C. P. J., Moriarty, N., van Deursen, C. B. J., Gantner, C. W., Thompson, L. H., & Parish, C. L. (2023). Understanding and modeling regional specification of the human ganglionic eminence. *Stem Cell Reports, 18*(3), 654-671. doi:10.1016/j.stemcr.2023.01.010

Hurelbrink, C. B., Armstrong, R. J., Barker, R. A., Dunnett, S. B., & Rosser, A. E. (2000). Hibernated human fetal striatal tissue: successful transplantation in a rat model of Huntington's disease. *Cell Transplant, 9*(6), 743-749. doi:10.1177/096368970000900601

Hurelbrink, C. B., Armstrong, R. J., Dunnett, S. B., Rosser, A. E., & Barker, R. A. (2002). Neural cells from primary human striatal xenografts migrate extensively in the adult rat CNS. *Eur J Neurosci, 15*(7), 1255-1266. doi:10.1046/j.1460-9568.2002.01959.x

Hurelbrink, C. B., & Barker, R. A. (2005). Migration of cells from primary transplants of allo- and xenografted foetal striatal tissue in the adult rat brain. *Eur J Neurosci, 21*(6), 1503-1510. doi:10.1111/j.1460-9568.2005.03963.x

Hurelbrink, C. B., Tyers, P., Armstrong, R. J., Dunnett, S. B., Barker, R. A., & Rosser, A. E. (2003). Long-term hibernation of human fetal striatal tissue does not adversely affect its differentiation in vitro or graft survival: implications for clinical trials in Huntington's disease. *Cell Transplant, 12*(7), 687-695. doi:10.3727/000000003108747307

Isacson, O., Dunnett, S. B., & Bjorklund, A. (1986). Graft-induced behavioral recovery in an animal model of Huntington disease. *Proc Natl Acad Sci U S A, 83*(8), 2728-2732. doi:10.1073/pnas.83.8.2728

Ishida, Y., Hashiguchi, H., Ishizuka, Y., Todaka, K., Kuwahara, I., Mitsuyama, Y., & Nishimori, T. (2000). Basal expression of c-Fos and Zif268 in the rat basal ganglia: immunohistochemical characterization of striatal Zif268-positive neurons. *Eur J Neurosci, 12*(2), 771-775. doi:10.1046/j.1460-9568.2000.00968.x

Ishikawa, Y., Yamamoto, N., Yoshimoto, M., & Ito, H. (2012). The primary brain vesicles revisited: are the three primary vesicles (forebrain/midbrain/hindbrain) universal in vertebrates? *Brain Behav Evol, 79*(2), 75-83. doi:10.1159/000334842

Ito, N., Takayama, M., Yamada, K., Sugiyama, M., & Minamoto, N. (2001). Rescue of rabies virus from cloned cDNA and identification of the pathogenicity-related gene: glycoprotein gene is associated with virulence for adult mice. *J Virol, 75*(19), 9121-9128. doi:10.1128/JVI.75.19.9121-9128.2001

Jeon, I., Choi, C., Lee, N., Im, W., Kim, M., Oh, S. H., . . . Song, J. (2014). In Vivo Roles of a Patient-Derived Induced Pluripotent Stem Cell Line (HD72-iPSC) in the YAC128 Model of Huntington's Disease. *Int J Stem Cells, 7*(1), 43-47. doi:10.15283/ijsc.2014.7.1.43

Jeon, I., Lee, N., Li, J. Y., Park, I. H., Park, K. S., Moon, J., . . . Song, J. (2012). Neuronal properties, in vivo effects, and pathology of a Huntington's disease patient-derived induced pluripotent stem cells. *Stem Cells, 30*(9), 2054-2062. doi:10.1002/stem.1135

Jimenez-Castellanos, J., & Graybiel, A. M. (1989). Compartmental origins of striatal efferent projections in the cat. *Neuroscience, 32*(2), 297-321. doi:10.1016/0306-4522(89)90080-8

Jimenez-Sanchez, M., Licitra, F., Underwood, B. R., & Rubinsztein, D. C. (2017). Huntington's Disease: Mechanisms of Pathogenesis and Therapeutic Strategies. *Cold Spring Harb Perspect Med, 7*(7). doi:10.1101/cshperspect.a024240

Johnson, R. S., Spiegelman, B. M., & Papaioannou, V. (1992). Pleiotropic effects of a null mutation in the c-fos proto-oncogene. *Cell, 71*(4), 577-586. doi:10.1016/0092-8674(92)90592-z

Kalonia, H., Kumar, P., & Kumar, A. (2011). Licofelone attenuates quinolinic acid induced Huntington like symptoms: possible behavioral, biochemical and cellular alterations. *Prog Neuropsychopharmacol Biol Psychiatry, 35*(2), 607-615. doi:10.1016/j.pnpbp.2011.01.003

Kantor, O., Temel, Y., Holzmann, C., Raber, K., Nguyen, H. P., Cao, C., . . . Schmitz, C. (2006). Selective striatal neuron loss and alterations in behavior correlate with impaired striatal function in Huntington's disease transgenic rats. *Neurobiol Dis, 22*(3), 538-547. doi:10.1016/j.nbd.2005.12.014

Katoh, H., Yokota, K., & Fehlings, M. G. (2019). Regeneration of Spinal Cord Connectivity Through Stem Cell Transplantation and Biomaterial Scaffolds. *Front Cell Neurosci, 13*, 248. doi:10.3389/fncel.2019.00248

Kay, C., Collins, J. A., Miedzybrodzka, Z., Madore, S. J., Gordon, E. S., Gerry, N., . . . Hayden, M. R. (2016). Huntington disease reduced penetrance alleles occur at high frequency in the general population. *Neurology, 87*(3), 282-288. doi:10.1212/WNL.0000000000002858

Keene, C. D., Sonnen, J. A., Swanson, P. D., Kopyov, O., Leverenz, J. B., Bird, T. D., & Montine, T. J. (2007). Neural transplantation in Huntington disease: long-term grafts in two patients. *Neurology, 68*(24), 2093-2098. doi:10.1212/01.wnl.0000264504.14301.f5

Keilani, S., Chandwani, S., Dolios, G., Bogush, A., Beck, H., Hatzopoulos, A. K., . . . Ehrlich, M. E. (2012). Egr-1 induces DARPP-32 expression in striatal medium spiny neurons via a conserved intragenic element. *J Neurosci, 32*(20), 6808-6818. doi:10.1523/JNEUROSCI.5448-11.2012

Kelly, C. M., Precious, S. V., Penketh, R., Amso, N., Dunnett, S. B., & Rosser, A. E. (2007). Striatal graft projections are influenced by donor cell type and not the immunogenic background. *Brain, 130*(Pt 5), 1317-1329. doi:10.1093/brain/awm053

Kincaid, A. E., & Wilson, C. J. (1996). Corticostriatal innervation of the patch and matrix in the rat neostriatum. *J Comp Neurol, 374*(4), 578-592. doi:10.1002/(SICI)1096-9861(19961028)374:4<578::AID-CNE7>3.0.CO;2-Z

Kirkeby, A., Nelander, J., Hoban, D. B., Rogelius, N., Bjartmarz, H., Novo Nordisk Cell Therapy, R., . . . Parmar, M. (2023). Preclinical quality, safety, and efficacy of a human embryonic stem cell-derived product for the treatment of Parkinson's disease, STEM-PD. *Cell Stem Cell, 30*(10), 1299-1314 e1299. doi:10.1016/j.stem.2023.08.014

Klein, A., Lane, E. L., & Dunnett, S. B. (2013). Brain repair in a unilateral rat model of Huntington's disease: new insights into impairment and restoration of forelimb movement patterns. *Cell Transplant, 22*(10), 1735-1751. doi:10.3727/096368912X657918

Kovacs, K. J. (2008). Measurement of immediate-early gene activation- c-fos and beyond. *J Neuroendocrinol, 20*(6), 665-672. doi:10.1111/j.1365-2826.2008.01734.x

Kravitz, A. V., & Kreitzer, A. C. (2012). Striatal mechanisms underlying movement, reinforcement, and punishment. *Physiology (Bethesda), 27*(3), 167-177. doi:10.1152/physiol.00004.2012

Labbadia, J., & Morimoto, R. I. (2013). Huntington's disease: underlying molecular mechanisms and emerging concepts. *Trends Biochem Sci, 38*(8), 378-385. doi:10.1016/j.tibs.2013.05.003

Lafay, F., Coulon, P., Astic, L., Saucier, D., Riche, D., Holley, A., & Flamand, A. (1991). Spread of the CVS strain of rabies virus and of the avirulent mutant AvO1 along the olfactory pathways of the mouse after intranasal inoculation. *Virology, 183*(1), 320-330. doi:10.1016/0042-6822(91)90145-2

Lanciego, J. L., Luquin, N., & Obeso, J. A. (2012). Functional neuroanatomy of the basal ganglia. *Cold Spring Harb Perspect Med, 2*(12), a009621. doi:10.1101/cshperspect.a009621

Langbehn, D. R., Brinkman, R. R., Falush, D., Paulsen, J. S., Hayden, M. R., & International Huntington's Disease Collaborative, G. (2004). A new model for prediction of the age of onset and penetrance for Huntington's disease based on CAG length. *Clin Genet, 65*(4), 267-277. doi:10.1111/j.1399-0004.2004.00241.x

Lange, H., Thorner, G., Hopf, A., & Schroder, K. F. (1976). Morphometric studies of the neuropathological changes in choreatic diseases. *J Neurol Sci, 28*(4), 401-425. doi:10.1016/0022-510x(76)90114-3

Lavdas, A. A., Grigoriou, M., Pachnis, V., & Parnavelas, J. G. (1999). The medial ganglionic eminence gives rise to a population of early neurons in the developing cerebral cortex. *J Neurosci, 19*(18), 7881-7888. doi:10.1523/JNEUROSCI.19-18-07881.1999

Lavoie, B., & Parent, A. (1994). Pedunculopontine nucleus in the squirrel monkey: projections to the basal ganglia as revealed by anterograde tract-tracing methods. *J Comp Neurol, 344*(2), 210-231. doi:10.1002/cne.903440204

Lelos, M. J., Harrison, D. J., & Dunnett, S. B. (2011). Impaired sensitivity to Pavlovian stimulus-outcome learning after excitotoxic lesion of the ventrolateral neostriatum. *Behav Brain Res, 225*(2), 522-528. doi:10.1016/j.bbr.2011.08.017

Lelos, M. J., Harrison, D. J., & Dunnett, S. B. (2012). Intrastriatal excitotoxic lesion or dopamine depletion of the neostriatum differentially impairs response execution in extrapersonal space. *Eur J Neurosci, 36*(10), 3420-3428. doi:10.1111/j.1460-9568.2012.08256.x

Lelos, M. J., Roberton, V. H., Vinh, N. N., Harrison, C., Eriksen, P., Torres, E. M., . . . Dunnett, S. B. (2016). Direct Comparison of Rat- and Human-Derived Ganglionic Eminence Tissue Grafts on Motor Function. *Cell Transplant, 25*(4), 665-675. doi:10.3727/096368915X690297

Leptin, M. (2005). Gastrulation movements: the logic and the nuts and bolts. *Dev Cell, 8*(3), 305-320. doi:10.1016/j.devcel.2005.02.007

Li, X. J., Zhang, X., Johnson, M. A., Wang, Z. B., Lavaute, T., & Zhang, S. C. (2009). Coordination of sonic hedgehog and Wnt signaling determines ventral and dorsal telencephalic neuron types from human embryonic stem cells. *Development, 136*(23), 4055-4063. doi:10.1242/dev.036624

Lin, C. H., Tallaksen-Greene, S., Chien, W. M., Cearley, J. A., Jackson, W. S., Crouse, A. B., . . . Detloff, P. J. (2001). Neurological abnormalities in a knock-in mouse model of Huntington's disease. *Hum Mol Genet, 10*(2), 137-144. doi:10.1093/hmg/10.2.137

Lindgren, H. S., Wickens, R., Tait, D. S., Brown, V. J., & Dunnett, S. B. (2013). Lesions of the dorsomedial striatum impair formation of attentional set in rats. *Neuropharmacology, 71*, 148-153. doi:10.1016/j.neuropharm.2013.03.034

Lindvall, O., & Bjorklund, A. (2004). Cell replacement therapy: helping the brain to repair itself. *NeuroRx, 1*(4), 379-381. doi:10.1602/neurorx.1.4.379

Ma, L., Hu, B., Liu, Y., Vermilyea, S. C., Liu, H., Gao, L., . . . Zhang, S. C. (2012). Human embryonic stem cell-derived GABA neurons correct locomotion deficits in quinolinic acid-lesioned mice. *Cell Stem Cell, 10*(4), 455-464. doi:10.1016/j.stem.2012.01.021

Machida, M., Lonart, G., & Sanford, L. D. (2018). Effects of stressor controllability on transcriptional levels of c-fos, Arc, and brain-derived neurotrophic factor in mouse amygdala and medial prefrontal cortex. *Neuroreport, 29*(2), 112-117. doi:10.1097/WNR.0000000000000919

Maira, M., Long, J. E., Lee, A. Y., Rubenstein, J. L., & Stifani, S. (2010). Role for TGF-beta superfamily signaling in telencephalic GABAergic neuron development. *J Neurodev Disord, 2*(1), 48-60. doi:10.1007/s11689-009-9035-6

Mallet, N., Micklem, B. R., Henny, P., Brown, M. T., Williams, C., Bolam, J. P., . . . Magill, P. J. (2012). Dichotomous organization of the external globus pallidus. *Neuron, 74*(6), 1075-1086. doi:10.1016/j.neuron.2012.04.027

Manfre, G., Clemensson, E. K. H., Kyriakou, E. I., Clemensson, L. E., van der Harst, J. E., Homberg, J. R., & Nguyen, H. P. (2017). The BACHD Rat Model of Huntington Disease Shows Specific Deficits in a Test Battery of Motor Function. *Front Behav Neurosci, 11*, 218. doi:10.3389/fnbeh.2017.00218

Manfre, G., Novati, A., Faccini, I., Rossetti, A. C., Bosch, K., Molteni, R., . . . Homberg, J. R. (2018). BACHD rats expressing full-length mutant huntingtin exhibit differences in social behavior compared to wild-type littermates. *PLoS One, 13*(2), e0192289. doi:10.1371/journal.pone.0192289

Mangiarini, L., Sathasivam, K., Seller, M., Cozens, B., Harper, A., Hetherington, C., . . . Bates, G. P. (1996). Exon 1 of the HD gene with an expanded CAG repeat is sufficient to cause a progressive neurological phenotype in transgenic mice. *Cell, 87*(3), 493-506. doi:10.1016/s0092-8674(00)81369-0

Manuel, M., Martynoga, B., Yu, T., West, J. D., Mason, J. O., & Price, D. J. (2010). The transcription factor Foxg1 regulates the competence of telencephalic cells to adopt subpallial fates in mice. *Development, 137*(3), 487-497. doi:10.1242/dev.039800

Manuel, M., Tan, K. B., Kozic, Z., Molinek, M., Marcos, T. S., Razak, M. F. A., . . . Price, D. J. (2022). Pax6 limits the competence of developing cerebral cortical cells to respond to inductive intercellular signals. *PLoS Biol, 20*(9), e3001563. doi:10.1371/journal.pbio.3001563

Martel, A. C., & Galvan, A. (2022). Connectivity of the corticostriatal and thalamostriatal systems in normal and parkinsonian states: An update. *Neurobiol Dis, 174*, 105878. doi:10.1016/j.nbd.2022.105878

Martin-Ibanez, R., Crespo, E., Esgleas, M., Urban, N., Wang, B., Waclaw, R., . . . Canals, J. M. (2012). Helios transcription factor expression depends on Gsx2 and Dlx1&2 function in developing striatal matrix neurons. *Stem Cells Dev, 21*(12), 2239-2251. doi:10.1089/scd.2011.0607

Martynoga, B., Morrison, H., Price, D. J., & Mason, J. O. (2005). Foxg1 is required for specification of ventral telencephalon and region-specific regulation of dorsal telencephalic precursor proliferation and apoptosis. *Dev Biol, 283*(1), 113-127. doi:10.1016/j.ydbio.2005.04.005

Mayer, E., Brown, V. J., Dunnett, S. B., & Robbins, T. W. (1992). Striatal graft-associated recovery of a lesion-induced performance deficit in the rat requires

learning to use the transplant. *Eur J Neurosci, 4*(2), 119-126. doi:10.1111/j.1460-9568.1992.tb00858.x

Mazzocchi-Jones, D., Dobrossy, M., & Dunnett, S. B. (2009). Embryonic striatal grafts restore bi-directional synaptic plasticity in a rodent model of Huntington's disease. *Eur J Neurosci, 30*(11), 2134-2142. doi:10.1111/j.1460-9568.2009.07006.x

McColgan, P., Seunarine, K. K., Gregory, S., Razi, A., Papoutsi, M., Long, J. D., . . . Track-On, H. D. I. (2017). Topological length of white matter connections predicts their rate of atrophy in premanifest Huntington's disease. *JCI Insight, 2*(8). doi:10.1172/jci.insight.92641

McElvain, L. E., Chen, Y., Moore, J. D., Brigidi, G. S., Bloodgood, B. L., Lim, B. K., . . . Kleinfeld, D. (2021). Specific populations of basal ganglia output neurons target distinct brain stem areas while collateralizing throughout the diencephalon. *Neuron, 109*(10), 1721-1738 e1724. doi:10.1016/j.neuron.2021.03.017

McFarland, N. R., & Haber, S. N. (2000). Convergent inputs from thalamic motor nuclei and frontal cortical areas to the dorsal striatum in the primate. *J Neurosci, 20*(10), 3798-3813. doi:10.1523/JNEUROSCI.20-10-03798.2000

Meenakshi, P., Kumar, S., & Balaji, J. (2021). In vivo imaging of immediate early gene expression dynamics segregates neuronal ensemble of memories of dual events. *Mol Brain, 14*(1), 102. doi:10.1186/s13041-021-00798-3

Menalled, L. B., & Chesselet, M. F. (2002). Mouse models of Huntington's disease. *Trends Pharmacol Sci, 23*(1), 32-39. doi:10.1016/s0165-6147(00)01884-8

Mi, D., Li, Z., Lim, L., Li, M., Moissidis, M., Yang, Y., . . . Marin, O. (2018). Early emergence of cortical interneuron diversity in the mouse embryo. *Science, 360*(6384), 81-85. doi:10.1126/science.aar6821

Milardi, D., Gaeta, M., Marino, S., Arrigo, A., Vaccarino, G., Mormina, E., . . . Quartarone, A. (2015). Basal ganglia network by constrained spherical deconvolution: a possible cortico-pallidal pathway? *Mov Disord, 30*(3), 342-349. doi:10.1002/mds.25995

Miura, I., Overton, E. T. N., Nakai, N., Kawamata, T., Sato, M., & Takumi, T. (2020). Imaging the Neural Circuit Basis of Social Behavior: Insights from Mouse and Human Studies. *Neurol Med Chir (Tokyo), 60*(9), 429-438. doi:10.2176/nmc.ra.2020-0088

Miyoshi, G., Hjerling-Leffler, J., Karayannis, T., Sousa, V. H., Butt, S. J., Battiste, J., . . . Fishell, G. (2010). Genetic fate mapping reveals that the caudal ganglionic eminence produces a large and diverse population of superficial cortical interneurons. *J Neurosci, 30*(5), 1582-1594. doi:10.1523/JNEUROSCI.4515-09.2010

Moore, R. Y., & Bloom, F. E. (1978). Central catecholamine neuron systems: anatomy and physiology of the dopamine systems. *Annu Rev Neurosci, 1*, 129-169. doi:10.1146/annurev.ne.01.030178.001021

Moratalla, R., Robertson, H. A., & Graybiel, A. M. (1992). Dynamic regulation of NGFI-A (zif268, egr1) gene expression in the striatum. *J Neurosci, 12*(7), 2609-2622. doi:10.1523/JNEUROSCI.12-07-02609.1992

Naimi, S., Jeny, R., Hantraye, P., Peschanski, M., & Riche, D. (1996). Ontogeny of human striatal DARPP-32 neurons in fetuses and following xenografting to the adult rat brain. *Exp Neurol, 137*(1), 15-25. doi:10.1006/exnr.1996.0002

Nakao, N., Grasbon-Frodl, E. M., Widner, H., & Brundin, P. (1996). DARPP-32-rich zones in grafts of lateral ganglionic eminence govern the extent of functional recovery in skilled paw reaching in an animal model of Huntington's disease. *Neuroscience, 74*(4), 959-970. doi:10.1016/0306-4522(96)00238-2

Narang, N., Hunt, M. E., Pundt, L. L., Alburges, M. E., & Wamsley, J. K. (1993). Unilateral ibotenic acid lesion of the caudate putamen results in D2 receptor alterations on the contralateral side. *Exp Neurol, 121*(1), 40-47. doi:10.1006/exnr.1993.1069

Nardone, R., Lochner, P., Marth, R., Ausserer, H., Bratti, A., & Tezzon, F. (2007). Abnormal intracortical facilitation in early-stage Huntington's disease. *Clin Neurophysiol, 118*(5), 1149-1154. doi:10.1016/j.clinph.2007.01.009

Nasir, J., Floresco, S. B., O'Kusky, J. R., Diewert, V. M., Richman, J. M., Zeisler, J., . . . Hayden, M. R. (1995). Targeted disruption of the Huntington's disease gene results in embryonic lethality and behavioral and morphological changes in heterozygotes. *Cell, 81*(5), 811-823. doi:10.1016/0092-8674(95)90542-1

Nelson, A. J. D. (2021). The anterior thalamic nuclei and cognition: A role beyond space? *Neurosci Biobehav Rev, 126*, 1-11. doi:10.1016/j.neubiorev.2021.02.047

Nery, S., Fishell, G., & Corbin, J. G. (2002). The caudal ganglionic eminence is a source of distinct cortical and subcortical cell populations. *Nat Neurosci, 5*(12), 1279-1287. doi:10.1038/nn971

Nguyen, H. P., Kobbe, P., Rahne, H., Worpel, T., Jager, B., Stephan, M., . . . von Horsten, S. (2006). Behavioral abnormalities precede neuropathological markers in rats transgenic for Huntington's disease. *Hum Mol Genet, 15*(21), 3177-3194. doi:10.1093/hmg/ddl394

Nikolaev, E., Kaczmarek, L., Zhu, S. W., Winblad, B., & Mohammed, A. H. (2002). Environmental manipulation differentially alters c-Fos expression in amygdaloid nuclei following aversive conditioning. *Brain Res, 957*(1), 91-98. doi:10.1016/s0006-8993(02)03606-5

Nikolaev, E., Kaminska, B., Tischmeyer, W., Matthies, H., & Kaczmarek, L. (1992). Induction of expression of genes encoding transcription factors in the rat brain elicited by behavioral training. *Brain Res Bull, 28*(3), 479-484. doi:10.1016/0361-9230(92)90050-8

Norgren, R. B., Jr., & Lehman, M. N. (1998). Herpes simplex virus as a transneuronal tracer. *Neurosci Biobehav Rev, 22*(6), 695-708. doi:10.1016/s0149-7634(98)00008-6

Novak, M. J., & Tabrizi, S. J. (2010). Huntington's disease. *BMJ, 340*, c3109. doi:10.1136/bmj.c3109

Obara, M., Szeliga, M., & Albrecht, J. (2008). Regulation of pH in the mammalian central nervous system under normal and pathological conditions: facts and hypotheses. *Neurochem Int, 52*(6), 905-919. doi:10.1016/j.neuint.2007.10.015

Okuno, H. (2011). Regulation and function of immediate-early genes in the brain: beyond neuronal activity markers. *Neurosci Res, 69*(3), 175-186. doi:10.1016/j.neures.2010.12.007

Okuno, H., & Miyashita, Y. (1996). Expression of the transcription factor Zif268 in the temporal cortex of monkeys during visual paired associate learning. *Eur J Neurosci, 8*(10), 2118-2128. doi:10.1111/j.1460-9568.1996.tb00733.x

Olsson, M., Bjorklund, A., & Campbell, K. (1998). Early specification of striatal projection neurons and interneuronal subtypes in the lateral and medial ganglionic eminence. *Neuroscience, 84*(3), 867-876. doi:10.1016/s0306-4522(97)00532-0

Olsson, M., Nikkhah, G., Bentlage, C., & Bjorklund, A. (1995). Forelimb akinesia in the rat Parkinson model: differential effects of dopamine agonists and nigral transplants as assessed by a new stepping test. *J Neurosci, 15*(5 Pt 2), 3863-3875. doi:10.1523/JNEUROSCI.15-05-03863.1995

Onorati, M., Castiglioni, V., Biasci, D., Cesana, E., Menon, R., Vuono, R., . . . Cattaneo, E. (2014). Molecular and functional definition of the developing human striatum. *Nat Neurosci, 17*(12), 1804-1815. doi:10.1038/nn.3860

Ouimet, C. C., & Greengard, P. (1990). Distribution of DARPP-32 in the basal ganglia: an electron microscopic study. *J Neurocytol, 19*(1), 39-52. doi:10.1007/BF01188438

Ouimet, C. C., Langley-Gullion, K. C., & Greengard, P. (1998). Quantitative immunocytochemistry of DARPP-32-expressing neurons in the rat caudatoputamen. *Brain Res, 808*(1), 8-12. doi:10.1016/s0006-8993(98)00724-0

Ouimet, C. C., Miller, P. E., Hemmings, H. C., Jr., Walaas, S. I., & Greengard, P. (1984). DARPP-32, a dopamine- and adenosine 3':5'-monophosphate-regulated phosphoprotein enriched in dopamine-innervated brain regions. III. Immunocytochemical localization. *J Neurosci, 4*(1), 111-124. doi:10.1523/JNEUROSCI.04-01-00111.1984

Palma-Tortosa, S., Tornero, D., Gronning Hansen, M., Monni, E., Hajy, M., Kartsivadze, S., . . . Kokaia, Z. (2020). Activity in grafted human iPS cell-derived cortical neurons integrated in stroke-injured rat brain regulates motor behavior. *Proc Natl Acad Sci U S A, 117*(16), 9094-9100. doi:10.1073/pnas.2000690117

Pankratz, M. T., Li, X. J., Lavaute, T. M., Lyons, E. A., Chen, X., & Zhang, S. C. (2007). Directed neural differentiation of human embryonic stem cells via an obligated primitive anterior stage. *Stem Cells, 25*(6), 1511-1520. doi:10.1634/stemcells.2006-0707

Parent, A., & Hazrati, L. N. (1995). Functional anatomy of the basal ganglia. I. The cortico-basal ganglia-thalamo-cortical loop. *Brain Res Brain Res Rev, 20*(1), 91-127. doi:10.1016/0165-0173(94)00007-c

Park, H. J., Han, A., Kim, J. Y., Choi, J., Bae, H. S., Cho, G. B., . . . Song, J. (2022). SUPT4H1-edited stem cell therapy rescues neuronal dysfunction in a mouse model for Huntington's disease. *NPJ Regen Med, 7*(1), 8. doi:10.1038/s41536-021-00198-0

Park, H. J., Jeon, J., Choi, J., Kim, J. Y., Kim, H. S., Huh, J. Y., . . . Song, J. (2021). Human iPSC-derived neural precursor cells differentiate into multiple cell types to delay disease progression following transplantation into YAC128 Huntington's disease mouse model. *Cell Prolif, 54*(8), e13082. doi:10.1111/cpr.13082

Paulsen, J. S. (2011). Cognitive impairment in Huntington disease: diagnosis and treatment. *Curr Neurol Neurosci Rep, 11*(5), 474-483. doi:10.1007/s11910-011-0215-x

Paulsen, J. S., Nehl, C., Hoth, K. F., Kanz, J. E., Benjamin, M., Conybeare, R., . . . Turner, B. (2005). Depression and stages of Huntington's disease. *J Neuropsychiatry Clin Neurosci, 17*(4), 496-502. doi:10.1176/jnp.17.4.496

Paylor, R., Johnson, R. S., Papaioannou, V., Spiegelman, B. M., & Wehner, J. M. (1994). Behavioral assessment of c-fos mutant mice. *Brain Res, 651*(1-2), 275-282. doi:10.1016/0006-8993(94)90707-2

Payne, S. (2023). Family Rhabdoviridae. In *Viruses* (pp. 215-222).

Perez-Diaz, F., Diaz, E., Sanchez, N., Vargas, J. P., Pearce, J. M., & Lopez, J. C. (2017). Different involvement of medial prefrontal cortex and dorso-lateral striatum in automatic and controlled processing of a future conditioned stimulus. *PLoS One, 12*(12), e0189630. doi:10.1371/journal.pone.0189630

Philpott, A. L., Cummins, T. D. R., Bailey, N. W., Churchyard, A., Fitzgerald, P. B., & Georgiou-Karistianis, N. (2016). Cortical inhibitory deficits in premanifest and early Huntington's disease. *Behav Brain Res, 296*, 311-317. doi:10.1016/j.bbr.2015.09.030

Plank, A. C., Canneva, F., Raber, K. A., Urbach, Y. K., Dobner, J., Puchades, M., . . . von Horsten, S. (2018). Early Alterations in Operant Performance and Prominent Huntingtin Aggregation in a Congenic F344 Rat Line of the Classical CAG(n51trunc) Model of Huntington Disease. *Front Neurosci, 12*, 11. doi:10.3389/fnins.2018.00011

Pollock, K., Dahlenburg, H., Nelson, H., Fink, K. D., Cary, W., Hendrix, K., . . . Nolta, J. A. (2016). Human Mesenchymal Stem Cells Genetically Engineered to Overexpress Brain-derived Neurotrophic Factor Improve Outcomes in Huntington's Disease Mouse Models. *Mol Ther, 24*(5), 965-977. doi:10.1038/mt.2016.12

Pouladi, M. A., Morton, A. J., & Hayden, M. R. (2013). Choosing an animal model for the study of Huntington's disease. *Nat Rev Neurosci, 14*(10), 708-721. doi:10.1038/nrn3570

Poyhonen, S., Er, S., Domanskyi, A., & Airavaara, M. (2019). Effects of Neurotrophic Factors in Glial Cells in the Central Nervous System: Expression and Properties in Neurodegeneration and Injury. *Front Physiol, 10*, 486. doi:10.3389/fphys.2019.00486

Prager, E. M., & Plotkin, J. L. (2019). Compartmental function and modulation of the striatum. *J Neurosci Res, 97*(12), 1503-1514. doi:10.1002/jnr.24522

Precious, S. V., Kelly, C. M., Reddington, A. E., Vinh, N. N., Stickland, R. C., Pekarik, V., . . . Rosser, A. E. (2016). FoxP1 marks medium spiny neurons from precursors to maturity and is required for their differentiation. *Exp Neurol, 282*, 9-18. doi:10.1016/j.expneurol.2016.05.002

Pritzel, M., Isacson, O., Brundin, P., Wiklund, L., & Bjorklund, A. (1986). Afferent and efferent connections of striatal grafts implanted into the ibotenic acid lesioned neostriatum in adult rats. *Exp Brain Res, 65*(1), 112-126. doi:10.1007/BF00243834

Pundt, L. L., Kondoh, T., Conrad, J. A., & Low, W. C. (1996a). Transplantation of human fetal striatum into a rodent model of Huntington's disease ameliorates locomotor deficits. *Neurosci Res, 24*(4), 415-420. doi:10.1016/0168-0102(95)01009-2

Pundt, L. L., Kondoh, T., Conrad, J. A., & Low, W. C. (1996b). Transplantation of human striatal tissue into a rodent model of Huntington's disease: phenotypic expression of transplanted neurons and host-to-graft innervation. *Brain Res Bull, 39*(1), 23-32. doi:10.1016/0361-9230(95)02029-2

Rallu, M., Machold, R., Gaiano, N., Corbin, J. G., McMahon, A. P., & Fishell, G. (2002). Dorsoventral patterning is established in the telencephalon of mutants lacking

both Gli3 and Hedgehog signaling. *Development, 129*(21), 4963-4974. doi:10.1242/dev.129.21.4963

Ramaswamy, S., McBride, J. L., & Kordower, J. H. (2007). Animal models of Huntington's disease. *ILAR J, 48*(4), 356-373. doi:10.1093/ilar.48.4.356

Reidling, J. C., Relano-Gines, A., Holley, S. M., Ochaba, J., Moore, C., Fury, B., . . . Thompson, L. M. (2018). Human Neural Stem Cell Transplantation Rescues Functional Deficits in R6/2 and Q140 Huntington's Disease Mice. *Stem Cell Reports, 10*(1), 58-72. doi:10.1016/j.stemcr.2017.11.005

Reiner, A., Albin, R. L., Anderson, K. D., D'Amato, C. J., Penney, J. B., & Young, A. B. (1988). Differential loss of striatal projection neurons in Huntington disease. *Proc Natl Acad Sci U S A, 85*(15), 5733-5737. doi:10.1073/pnas.85.15.5733

Reiner, A., Dragatsis, I., & Dietrich, P. (2011). Genetics and neuropathology of Huntington's disease. *Int Rev Neurobiol, 98*, 325-372. doi:10.1016/B978-0-12-381328-2.00014-6

Reuter, I., Tai, Y. F., Pavese, N., Chaudhuri, K. R., Mason, S., Polkey, C. E., . . . Piccini, P. (2008). Long-term clinical and positron emission tomography outcome of fetal striatal transplantation in Huntington's disease. *J Neurol Neurosurg Psychiatry, 79*(8), 948-951. doi:10.1136/jnnp.2007.142380

Roberton, V. H., Evans, A. E., Harrison, D. J., Precious, S. V., Dunnett, S. B., Kelly, C. M., & Rosser, A. E. (2013). Is the adult mouse striatum a hostile host for neural transplant survival? *Neuroreport, 24*(18), 1010-1015. doi:10.1097/WNR.0000000000000066

Rosenstock, T. R., Carvalho, A. C., Jurkiewicz, A., Frussa-Filho, R., & Smaili, S. S. (2004). Mitochondrial calcium, oxidative stress and apoptosis in a neurodegenerative disease model induced by 3-nitropropionic acid. *J Neurochem, 88*(5), 1220-1228. doi:10.1046/j.1471-4159.2003.02250.x

Ross, C. A., & Tabrizi, S. J. (2011). Huntington's disease: from molecular pathogenesis to clinical treatment. *Lancet Neurol, 10*(1), 83-98. doi:10.1016/S1474-4422(10)70245-3

Rosser, A. E., Barker, R. A., Harrower, T., Watts, C., Farrington, M., Ho, A. K., . . . Nest, U. K. (2002). Unilateral transplantation of human primary fetal tissue in four patients with Huntington's disease: NEST-UK safety report ISRCTN no 36485475. *J Neurol Neurosurg Psychiatry, 73*(6), 678-685. doi:10.1136/jnnp.73.6.678

Rothman, S. M., & Olney, J. W. (1995). Excitotoxicity and the NMDA receptor--still lethal after eight years. *Trends Neurosci, 18*(2), 57-58. doi:10.1016/0166-2236(95)93869-y

Rubenstein, J. L., Shimamura, K., Martinez, S., & Puelles, L. (1998). Regionalization of the prosencephalic neural plate. *Annu Rev Neurosci, 21*, 445-477. doi:10.1146/annurev.neuro.21.1.445

Ruocco, H. H., Lopes-Cendes, I., Li, L. M., Santos-Silva, M., & Cendes, F. (2006). Striatal and extrastriatal atrophy in Huntington's disease and its relationship with length of the CAG repeat. *Braz J Med Biol Res, 39*(8), 1129-1136. doi:10.1590/s0100-879x2006000800016

Sagar, S. M., Sharp, F. R., & Curran, T. (1988). Expression of c-fos protein in brain: metabolic mapping at the cellular level. *Science, 240*(4857), 1328-1331. doi:10.1126/science.3131879

Saleeba, C., Dempsey, B., Le, S., Goodchild, A., & McMullan, S. (2019). A Student's Guide to Neural Circuit Tracing. *Front Neurosci, 13*, 897. doi:10.3389/fnins.2019.00897

Sanberg, P. R., Borlongan, C. V., Koutouzis, T. K., Norgren, R. B., Jr., Cahill, D. W., & Freeman, T. B. (1997). Human fetal striatal transplantation in an excitotoxic lesioned model of Huntington's disease. *Ann N Y Acad Sci, 831*, 452-460. doi:10.1111/j.1749-6632.1997.tb52217.x

Sapp, E., Ge, P., Aizawa, H., Bird, E., Penney, J., Young, A. B., . . . DiFiglia, M. (1995). Evidence for a preferential loss of enkephalin immunoreactivity in the external globus pallidus in low grade Huntington's disease using high resolution image analysis. *Neuroscience, 64*(2), 397-404. doi:10.1016/0306-4522(94)00427-7

Sapp, E., Kegel, K. B., Aronin, N., Hashikawa, T., Uchiyama, Y., Tohyama, K., . . . DiFiglia, M. (2001). Early and progressive accumulation of reactive microglia in the Huntington disease brain. *J Neuropathol Exp Neurol, 60*(2), 161-172. doi:10.1093/jnen/60.2.161

Sato, F., Lavallee, P., Levesque, M., & Parent, A. (2000). Single-axon tracing study of neurons of the external segment of the globus pallidus in primate. *J Comp Neurol, 417*(1), 17-31. Retrieved from https://www.ncbi.nlm.nih.gov/pubmed/10660885

Sattler, R., & Rothstein, J. D. (2006). Regulation and dysregulation of glutamate transporters. *Handb Exp Pharmacol*(175), 277-303. doi:10.1007/3-540-29784-7_14

Saudou, F., & Humbert, S. (2016). The Biology of Huntingtin. *Neuron, 89*(5), 910-926. doi:10.1016/j.neuron.2016.02.003

Saunders, A., Oldenburg, I. A., Berezovskii, V. K., Johnson, C. A., Kingery, N. D., Elliott, H. L., . . . Sabatini, B. L. (2015). A direct GABAergic output from the basal ganglia to frontal cortex. *Nature, 521*(7550), 85-89. doi:10.1038/nature14179

Savage, J. C., St-Pierre, M. K., Carrier, M., El Hajj, H., Novak, S. W., Sanchez, M. G., . . . Tremblay, M. E. (2020). Microglial physiological properties and interactions with synapses are altered at presymptomatic stages in a mouse model of Huntington's disease pathology. *J Neuroinflammation, 17*(1), 98. doi:10.1186/s12974-020-01782-9

Scattoni, M. L., Valanzano, A., Popoli, P., Pezzola, A., Reggio, R., & Calamandrei, G. (2004). Progressive behavioural changes in the spatial open-field in the quinolinic acid rat model of Huntington's disease. *Behav Brain Res, 152*(2), 375-383. doi:10.1016/j.bbr.2003.10.021

Schellino, R., Besusso, D., Parolisi, R., Gomez-Gonzalez, G. B., Dallere, S., Scaramuzza, L., . . . Buffo, A. (2023). hESC-derived striatal progenitors grafted into a Huntington's disease rat model support long-term functional motor recovery by differentiating, self-organizing and connecting into the lesioned striatum. *Stem Cell Res Ther, 14*(1), 189. doi:10.1186/s13287-023-03422-4

Schippling, S., Schneider, S. A., Bhatia, K. P., Munchau, A., Rothwell, J. C., Tabrizi, S. J., & Orth, M. (2009). Abnormal motor cortex excitability in preclinical and very early Huntington's disease. *Biol Psychiatry, 65*(11), 959-965. doi:10.1016/j.biopsych.2008.12.026

Schmued, L. C., & Fallon, J. H. (1986). Fluoro-Gold: a new fluorescent retrograde axonal tracer with numerous unique properties. *Brain Res, 377*(1), 147-154. doi:10.1016/0006-8993(86)91199-6

Schroder, K. F., Hopf, A., Lange, H., & Thorner, G. (1975). [Morphometrical-statistical structure analysis of human striatum, pallidum and subthalamic nucleus]. *J Hirnforsch, 16*(4), 333-350. Retrieved from https://www.ncbi.nlm.nih.gov/pubmed/1214057

Schuurmans, C., & Guillemot, F. (2002). Molecular mechanisms underlying cell fate specification in the developing telencephalon. *Curr Opin Neurobiol, 12*(1), 26-34. doi:10.1016/s0959-4388(02)00286-6

Schwarcz, R., & Coyle, J. T. (1977). Striatal lesions with kainic acid: neurochemical characteristics. *Brain Res, 127*(2), 235-249. doi:10.1016/0006-8993(77)90538-8

Schwarcz, R., Foster, A. C., French, E. D., Whetsell, W. O., Jr., & Kohler, C. (1984). Excitotoxic models for neurodegenerative disorders. *Life Sci, 35*(1), 19-32. doi:10.1016/0024-3205(84)90148-6

Schwarz, M., Block, F., Topper, R., Sontag, K. H., & Noth, J. (1992). Abnormalities of somatosensory evoked potentials in the quinolinic acid model of Huntington's disease: evidence that basal ganglia modulate sensory cortical input. *Ann Neurol, 32*(3), 358-364. doi:10.1002/ana.410320309

Seifert, G., Schilling, K., & Steinhauser, C. (2006). Astrocyte dysfunction in neurological disorders: a molecular perspective. *Nat Rev Neurosci, 7*(3), 194-206. doi:10.1038/nrn1870

Shear, D. A., Dong, J., Haik-Creguer, K. L., Bazzett, T. J., Albin, R. L., & Dunbar, G. L. (1998). Chronic administration of quinolinic acid in the rat striatum causes spatial learning deficits in a radial arm water maze task. *Exp Neurol, 150*(2), 305-311. doi:10.1006/exnr.1998.6767

Sheng, M., & Greenberg, M. E. (1990). The regulation and function of c-fos and other immediate early genes in the nervous system. *Neuron, 4*(4), 477-485. doi:10.1016/0896-6273(90)90106-p

Singh-Bains, M. K., Tippett, L. J., Hogg, V. M., Synek, B. J., Roxburgh, R. H., Waldvogel, H. J., & Faull, R. L. (2016). Globus pallidus degeneration and clinicopathological features of Huntington disease. *Ann Neurol, 80*(2), 185-201. doi:10.1002/ana.24694

Slow, E. J., van Raamsdonk, J., Rogers, D., Coleman, S. H., Graham, R. K., Deng, Y., . . . Hayden, M. R. (2003). Selective striatal neuronal loss in a YAC128 mouse model of Huntington disease. *Hum Mol Genet, 12*(13), 1555-1567. doi:10.1093/hmg/ddg169

Smith, J. B., Smith, Y., Venance, L., & Watson, G. D. R. (2022). Editorial: Thalamic Interactions With the Basal Ganglia: Thalamostriatal System and Beyond. *Front Syst Neurosci, 16*, 883094. doi:10.3389/fnsys.2022.883094

Solberg, O. K., Filkukova, P., Frich, J. C., & Feragen, K. J. B. (2018). Age at Death and Causes of Death in Patients with Huntington Disease in Norway in 1986-2015. *J Huntingtons Dis, 7*(1), 77-86. doi:10.3233/JHD-170270

Standaert, D. G., Friberg, I. K., Landwehrmeyer, G. B., Young, A. B., & Penney, J. B., Jr. (1999). Expression of NMDA glutamate receptor subunit mRNAs in neurochemically identified projection and interneurons in the striatum of the rat. *Brain Res Mol Brain Res, 64*(1), 11-23. doi:10.1016/s0169-328x(98)00293-9

Stiles, J., & Jernigan, T. L. (2010). The basics of brain development. *Neuropsychol Rev, 20*(4), 327-348. doi:10.1007/s11065-010-9148-4

Stone, T. W., & Perkins, M. N. (1981). Quinolinic acid: a potent endogenous excitant at amino acid receptors in CNS. *Eur J Pharmacol, 72*(4), 411-412. doi:10.1016/0014-2999(81)90587-2

Strom, C., Rasmussen, L. S., & Sieber, F. E. (2014). Should general anaesthesia be avoided in the elderly? *Anaesthesia, 69 Suppl 1*(Suppl 1), 35-44. doi:10.1111/anae.12493

Surmeier, D. J., Eberwine, J., Wilson, C. J., Cao, Y., Stefani, A., & Kitai, S. T. (1992). Dopamine receptor subtypes colocalize in rat striatonigral neurons. *Proc Natl Acad Sci U S A, 89*(21), 10178-10182. doi:10.1073/pnas.89.21.10178

Szucsik, J. C., Witte, D. P., Li, H., Pixley, S. K., Small, K. M., & Potter, S. S. (1997). Altered forebrain and hindbrain development in mice mutant for the Gsh-2 homeobox gene. *Dev Biol, 191*(2), 230-242. doi:10.1006/dbio.1997.8733

Tabrizi, S. J., Scahill, R. I., Owen, G., Durr, A., Leavitt, B. R., Roos, R. A., . . . Investigators, T.-H. (2013). Predictors of phenotypic progression and disease onset in premanifest and early-stage Huntington's disease in the TRACK-HD study: analysis of 36-month observational data. *Lancet Neurol, 12*(7), 637-649. doi:10.1016/S1474-4422(13)70088-7

Tabrizi, S. J., Schobel, S., Gantman, E. C., Mansbach, A., Borowsky, B., Konstantinova, P., . . . Huntington's Disease Regulatory Science, C. (2022). A biological classification of Huntington's disease: the Integrated Staging System. *Lancet Neurol, 21*(7), 632-644. doi:10.1016/S1474-4422(22)00120-X

Tai, Y. F., Pavese, N., Gerhard, A., Tabrizi, S. J., Barker, R. A., Brooks, D. J., & Piccini, P. (2007). Microglial activation in presymptomatic Huntington's disease gene carriers. *Brain, 130*(Pt 7), 1759-1766. doi:10.1093/brain/awm044

Tao, W., & Lai, E. (1992). Telencephalon-restricted expression of BF-1, a new member of the HNF-3/fork head gene family, in the developing rat brain. *Neuron, 8*(5), 957-966. doi:10.1016/0896-6273(92)90210-5

Temel, Y., Cao, C., Vlamings, R., Blokland, A., Ozen, H., Steinbusch, H. W., . . . Visser-Vandewalle, V. (2006). Motor and cognitive improvement by deep brain stimulation in a transgenic rat model of Huntington's disease. *Neurosci Lett, 406*(1-2), 138-141. doi:10.1016/j.neulet.2006.07.036

Thomas A. Terleph, L. A. T. (2006). The Use of Immediate Early Genes as Mapping Tools for Neuronal Activation: Concepts and Methods. In.

Tiklova, K., Nolbrant, S., Fiorenzano, A., Bjorklund, A. K., Sharma, Y., Heuer, A., . . . Parmar, M. (2020). Single cell transcriptomics identifies stem cell-derived graft composition in a model of Parkinson's disease. *Nat Commun, 11*(1), 2434. doi:10.1038/s41467-020-16225-5

Ting, K. K., Brew, B. J., & Guillemin, G. J. (2009). Effect of quinolinic acid on human astrocytes morphology and functions: implications in Alzheimer's disease. *J Neuroinflammation, 6*, 36. doi:10.1186/1742-2094-6-36

Toresson, H., & Campbell, K. (2001). A role for Gsh1 in the developing striatum and olfactory bulb of Gsh2 mutant mice. *Development, 128*(23), 4769-4780. doi:10.1242/dev.128.23.4769

Toresson, H., Potter, S. S., & Campbell, K. (2000). Genetic control of dorsal-ventral identity in the telencephalon: opposing roles for Pax6 and Gsh2. *Development, 127*(20), 4361-4371. doi:10.1242/dev.127.20.4361

Tornero, D., Tsupykov, O., Granmo, M., Rodriguez, C., Gronning-Hansen, M., Thelin, J., . . . Kokaia, Z. (2017). Synaptic inputs from stroke-injured brain to grafted

human stem cell-derived neurons activated by sensory stimuli. *Brain, 140*(3), 692-706. doi:10.1093/brain/aww347

Torres, E. M., Lane, E. L., Heuer, A., Smith, G. A., Murphy, E., & Dunnett, S. B. (2011). Increased efficacy of the 6-hydroxydopamine lesion of the median forebrain bundle in small rats, by modification of the stereotaxic coordinates. *J Neurosci Methods, 200*(1), 29-35. doi:10.1016/j.jneumeth.2011.06.012

Tsumori, T., Yokota, S., Ono, K., & Yasui, Y. (2002). Synaptic organization of GABAergic projections from the substantia nigra pars reticulata and the reticular thalamic nucleus to the parafascicular thalamic nucleus in the rat. *Brain Res, 957*(2), 231-241. doi:10.1016/s0006-8993(02)03554-0

Ugolini, G. (1992). Transneuronal transfer of herpes simplex virus type 1 (HSV 1) from mixed limb nerves to the CNS. I. Sequence of transfer from sensory, motor, and sympathetic nerve fibres to the spinal cord. *J Comp Neurol, 326*(4), 527-548. doi:10.1002/cne.903260404

Ungerstedt, U. (1971). Postsynaptic supersensitivity after 6-hydroxy-dopamine induced degeneration of the nigro-striatal dopamine system. *Acta Physiol Scand Suppl, 367*, 69-93. doi:10.1111/j.1365-201x.1971.tb11000.x

Unified Huntington's Disease Rating Scale: reliability and consistency. Huntington Study Group. (1996). *Mov Disord, 11*(2), 136-142. doi:10.1002/mds.870110204

Urbach, Y. K., Raber, K. A., Canneva, F., Plank, A. C., Andreasson, T., Ponten, H., . . . von Horsten, S. (2014). Automated phenotyping and advanced data mining exemplified in rats transgenic for Huntington's disease. *J Neurosci Methods, 234*, 38-53. doi:10.1016/j.jneumeth.2014.06.017

Valjent, E., Pages, C., Rogard, M., Besson, M. J., Maldonado, R., & Caboche, J. (2001). Delta 9-tetrahydrocannabinol-induced MAPK/ERK and Elk-1 activation in vivo depends on dopaminergic transmission. *Eur J Neurosci, 14*(2), 342-352. doi:10.1046/j.0953-816x.2001.01652.x

van den Pol, A. N., Obrietan, K., & Chen, G. (1996). Excitatory actions of GABA after neuronal trauma. *J Neurosci, 16*(13), 4283-4292. doi:10.1523/JNEUROSCI.16-13-04283.1996

van Gorp, S., Leerink, M., Kakinohana, O., Platoshyn, O., Santucci, C., Galik, J., . . . Marsala, M. (2013). Amelioration of motor/sensory dysfunction and spasticity in a rat model of acute lumbar spinal cord injury by human neural stem cell transplantation. *Stem Cell Res Ther, 4*(3), 57. doi:10.1186/scrt209

Vann, S. D., Brown, M. W., Erichsen, J. T., & Aggleton, J. P. (2000). Fos imaging reveals differential patterns of hippocampal and parahippocampal subfield activation in rats in response to different spatial memory tests. *J Neurosci, 20*(7), 2711-2718. doi:10.1523/JNEUROSCI.20-07-02711.2000

Vastagh, C., Gardoni, F., Bagetta, V., Stanic, J., Zianni, E., Giampa, C., . . . Di Luca, M. (2012). N-methyl-D-aspartate (NMDA) receptor composition modulates dendritic spine morphology in striatal medium spiny neurons. *J Biol Chem, 287*(22), 18103-18114. doi:10.1074/jbc.M112.347427

Vertes, R. P., & Hoover, W. B. (2008). Projections of the paraventricular and paratenial nuclei of the dorsal midline thalamus in the rat. *J Comp Neurol, 508*(2), 212-237. doi:10.1002/cne.21679

Vertes, R. P., Linley, S. B., & Rojas, A. K. P. (2022). Structural and functional organization of the midline and intralaminar nuclei of the thalamus. *Front Behav Neurosci, 16*, 964644. doi:10.3389/fnbeh.2022.964644

Vlamings, R., Zeef, D. H., Janssen, M. L., Oosterloo, M., Schaper, F., Jahanshahi, A., & Temel, Y. (2012). Lessons learned from the transgenic Huntington's disease rats. *Neural Plast, 2012*, 682712. doi:10.1155/2012/682712

von Horsten, S., Schmitt, I., Nguyen, H. P., Holzmann, C., Schmidt, T., Walther, T., . . . Riess, O. (2003). Transgenic rat model of Huntington's disease. *Hum Mol Genet, 12*(6), 617-624. doi:10.1093/hmg/ddg075

Vonsattel, J. P., Myers, R. H., Stevens, T. J., Ferrante, R. J., Bird, E. D., & Richardson, E. P., Jr. (1985). Neuropathological classification of Huntington's disease. *J Neuropathol Exp Neurol, 44*(6), 559-577. doi:10.1097/00005072-198511000-00003

Walker, F. O. (2007). Huntington's disease. *Lancet, 369*(9557), 218-228. doi:10.1016/S0140-6736(07)60111-1

Wallace, M. L., Saunders, A., Huang, K. W., Philson, A. C., Goldman, M., Macosko, E. Z., . . . Sabatini, B. L. (2017). Genetically Distinct Parallel Pathways in the Entopeduncular Nucleus for Limbic and Sensorimotor Output of the Basal Ganglia. *Neuron, 94*(1), 138-152 e135. doi:10.1016/j.neuron.2017.03.017

Watt, F. M., & Hogan, B. L. (2000). Out of Eden: stem cells and their niches. *Science, 287*(5457), 1427-1430. doi:10.1126/science.287.5457.1427

Watts, C., Brasted, P. J., & Dunnett, S. B. (2000). Embryonic donor age and dissection influences striatal graft development and functional integration in a rodent model of Huntington's disease. *Exp Neurol, 163*(1), 85-97. doi:10.1006/exnr.1999.7341

Wheeler, V. C., Gutekunst, C. A., Vrbanac, V., Lebel, L. A., Schilling, G., Hersch, S., . . . MacDonald, M. E. (2002). Early phenotypes that presage late-onset neurodegenerative disease allow testing of modifiers in Hdh CAG knock-in mice. *Hum Mol Genet, 11*(6), 633-640. doi:10.1093/hmg/11.6.633

Wheeler, V. C., White, J. K., Gutekunst, C. A., Vrbanac, V., Weaver, M., Li, X. J., . . . MacDonald, M. E. (2000). Long glutamine tracts cause nuclear localization of a novel form of huntingtin in medium spiny striatal neurons in HdhQ92 and HdhQ111 knock-in mice. *Hum Mol Genet, 9*(4), 503-513. doi:10.1093/hmg/9.4.503

White, R. E., & Barry, D. S. (2015). The emerging roles of transplanted radial glial cells in regenerating the central nervous system. *Neural Regen Res, 10*(10), 1548-1551. doi:10.4103/1673-5374.165317

Wictorin, K., & Bjorklund, A. (1989). Connectivity of striatal grafts implanted into the ibotenic acid-lesioned striatum--II. Cortical afferents. *Neuroscience, 30*(2), 297-311. doi:10.1016/0306-4522(89)90255-8

Wictorin, K., Clarke, D. J., Bolam, J. P., & Bjorklund, A. (1990). Fetal striatal neurons grafted into the ibotenate lesioned adult striatum: efferent projections and synaptic contacts in the host globus pallidus. *Neuroscience, 37*(2), 301-315. doi:10.1016/0306-4522(90)90401-o

Wictorin, K., Clarke, D. J., Bolam, J. P., Brundin, P., Gustavii, B., Lindvall, O., & Bjorklund, A. (1990). Extensive efferent projections of intra-striatally transplanted striatal neurons as revealed by a species-specific neurofilament marker and anterograde axonal tracing. *Prog Brain Res, 82*, 391-399. doi:10.1016/s0079-6123(08)62627-8

Wictorin, K., Lagenaur, C. F., Lund, R. D., & Bjorklund, A. (1991). Efferent Projections to the Host Brain from Intrastriatal Striatal Mouse-to-rat Grafts: Time Course

and Tissue-type Specificity as Revealed by a Mouse Specific Neuronal Marker. *Eur J Neurosci, 3*(1), 86-101. doi:10.1111/j.1460-9568.1991.tb00814.x

Wictorin, K., Ouimet, C. C., & Bjorklund, A. (1989). Intrinsic Organization and Connectivity of Intrastriatal Striatal Transplants in Rats as Revealed by DARPP-32 Immunohistochemistry: Specificity of Connections with the Lesioned Host Brain. *Eur J Neurosci, 1*(6), 690-701. doi:10.1111/j.1460-9568.1989.tb00375.x

Wijeyekoon, R., & Barker, R. A. (2011). The Current Status of Neural Grafting in the Treatment of Huntington's Disease. A Review. *Front Integr Neurosci, 5*, 78. doi:10.3389/fnint.2011.00078

Wu, M., Zhang, D., Bi, C., Mi, T., Zhu, W., Xia, L., . . . Wu, Y. (2018). A Chemical Recipe for Generation of Clinical-Grade Striatal Neurons from hESCs. *Stem Cell Reports, 11*(3), 635-650. doi:10.1016/j.stemcr.2018.08.005

Xu, X., Holmes, T. C., Luo, M. H., Beier, K. T., Horwitz, G. D., Zhao, F., . . . Sandri-Goldin, R. M. (2020). Viral Vectors for Neural Circuit Mapping and Recent Advances in Trans-synaptic Anterograde Tracers. *Neuron, 107*(6), 1029-1047. doi:10.1016/j.neuron.2020.07.010

Xu, Z. C., Wilson, C. J., & Emson, P. C. (1991). Restoration of thalamostriatal projections in rat neostriatal grafts: an electron microscopic analysis. *J Comp Neurol, 303*(1), 22-34. doi:10.1002/cne.903030104

Xuan, S., Baptista, C. A., Balas, G., Tao, W., Soares, V. C., & Lai, E. (1995). Winged helix transcription factor BF-1 is essential for the development of the cerebral hemispheres. *Neuron, 14*(6), 1141-1152. doi:10.1016/0896-6273(95)90262-7

Yasukawa, T., Kita, T., Xue, Y., & Kita, H. (2004). Rat intralaminar thalamic nuclei projections to the globus pallidus: a biotinylated dextran amine anterograde tracing study. *J Comp Neurol, 471*(2), 153-167. doi:10.1002/cne.20029

Yin, H. H., & Knowlton, B. J. (2006). The role of the basal ganglia in habit formation. *Nat Rev Neurosci, 7*(6), 464-476. doi:10.1038/nrn1919

Young, J. A., Bates, P., & Varmus, H. E. (1993). Isolation of a chicken gene that confers susceptibility to infection by subgroup A avian leukosis and sarcoma viruses. *J Virol, 67*(4), 1811-1816. doi:10.1128/JVI.67.4.1811-1816.1993

Yu-Taeger, L., Petrasch-Parwez, E., Osmand, A. P., Redensek, A., Metzger, S., Clemens, L. E., . . . Nguyen, H. P. (2012). A novel BACHD transgenic rat exhibits characteristic neuropathological features of Huntington disease. *J Neurosci, 32*(44), 15426-15438. doi:10.1523/JNEUROSCI.1148-12.2012

Zangenehpour, S., & Chaudhuri, A. (2002). Differential induction and decay curves of c-fos and zif268 revealed through dual activity maps. *Brain Res Mol Brain Res, 109*(1-2), 221-225. doi:10.1016/s0169-328x(02)00556-9

Zeef, D. H., van Goethem, N. P., Vlamings, R., Schaper, F., Jahanshahi, A., Hescham, S., . . . Temel, Y. (2012). Memory deficits in the transgenic rat model of Huntington's disease. *Behav Brain Res, 227*(1), 194-198. doi:10.1016/j.bbr.2011.11.009

Appendix

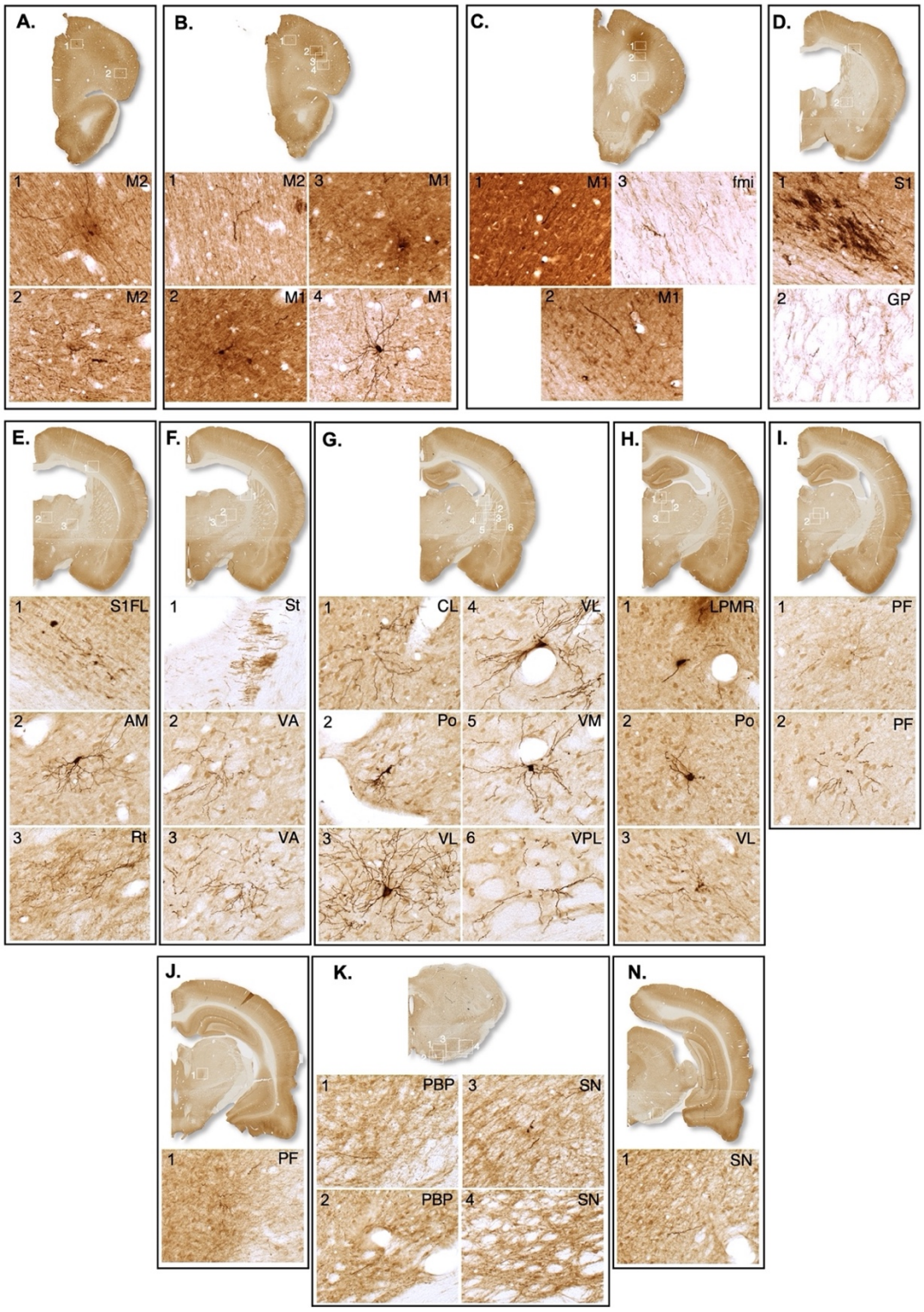

Appendix Figure 1 – Traced cells and projections found in different brain regions after 5 weeks post transplantation. Coronal sections from mCherry IHC are

represented. A white square in coronal sections represents the area of a higher magnification images of each of the numbered areas.

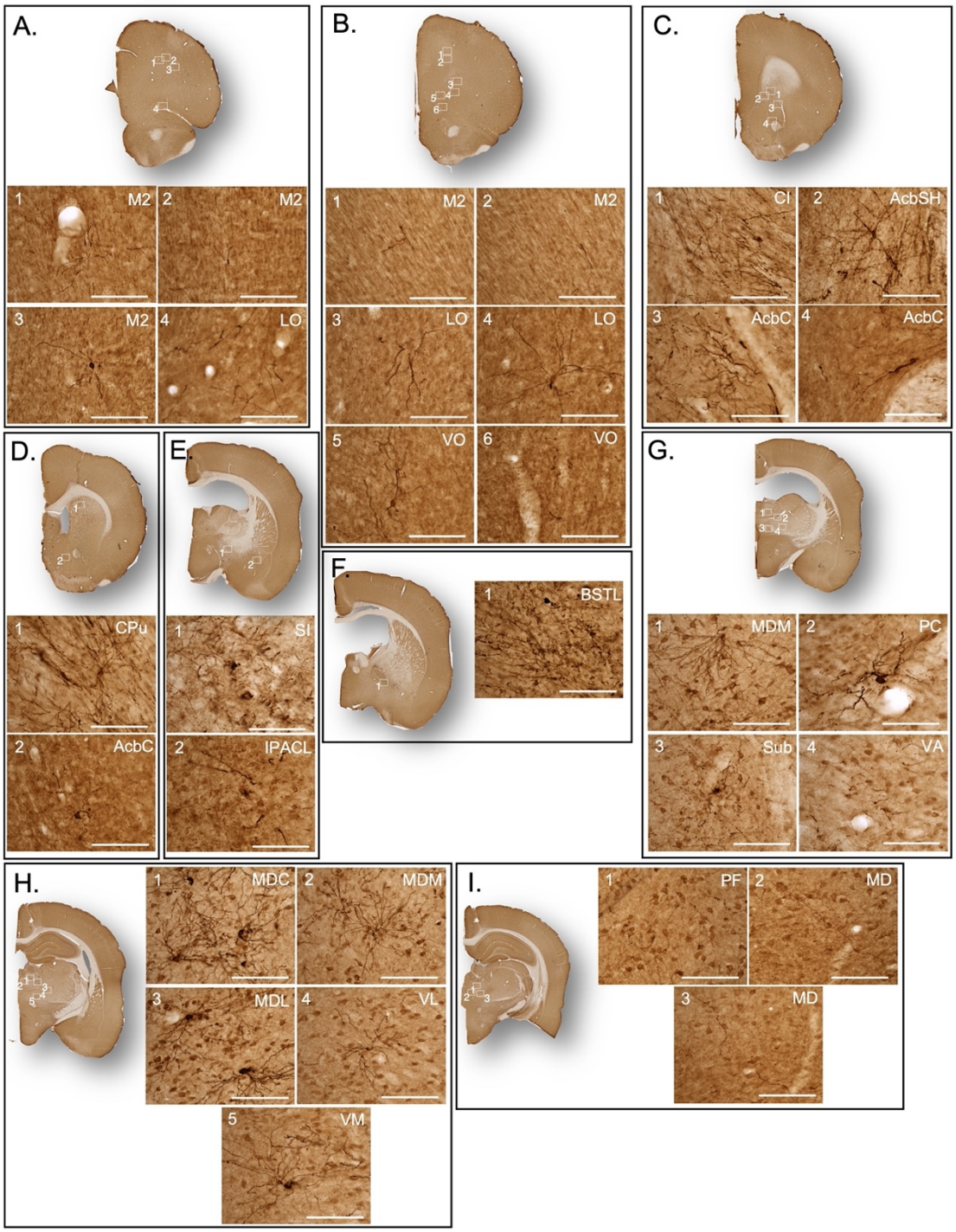

Appendix Figure 2 - Traced cells and projections found in different brain regions after 9 weeks post transplantation. Coronal sections from mCherry IHC are represented. A white square in coronal sections represents the area of a higher magnification images of each of the numbered areas.

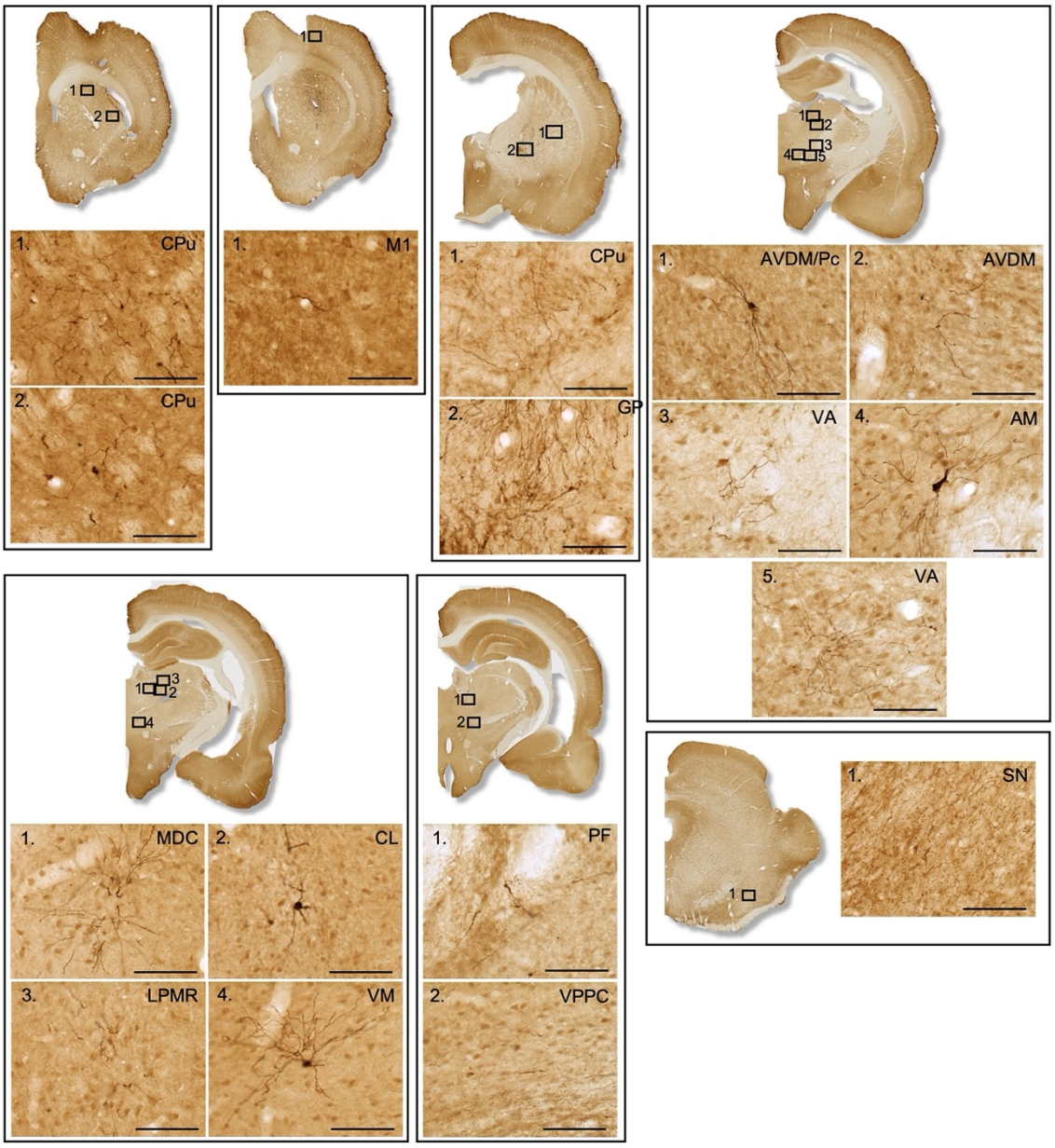

Appendix Figure 3 – Traced cells and projections found in different brain regions after 12 weeks post transplantation. Coronal sections from mCherry IHC are represented. A black square in coronal sections represents the area of a higher magnification images of each of the numbered areas.

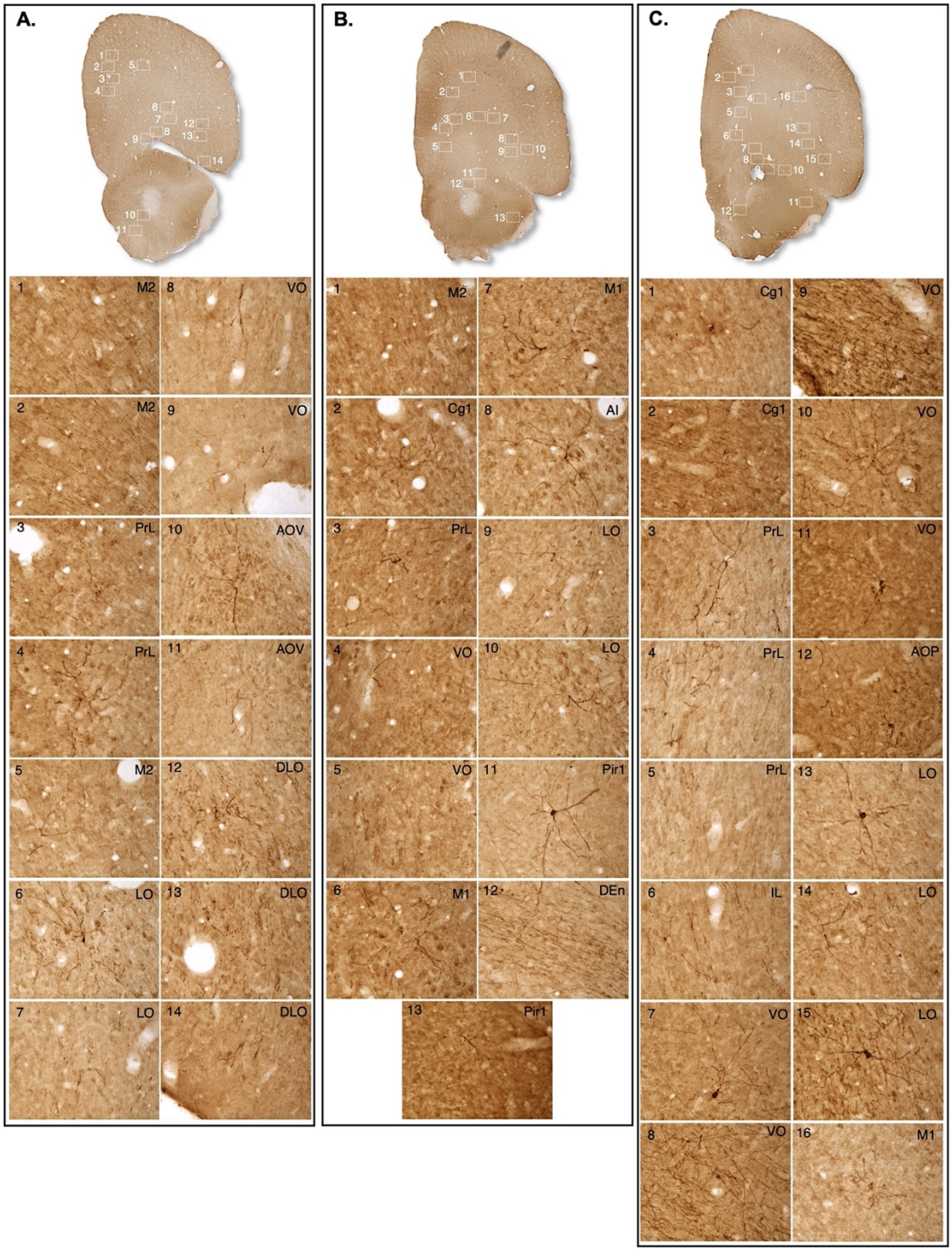

Appendix Figure 4 – Traced cells and projections found in different brain regions after 17 weeks post transplantation. Coronal sections from mCherry IHC are represented. A white square in coronal sections represents the area of a higher magnification images of each of the numbered areas.

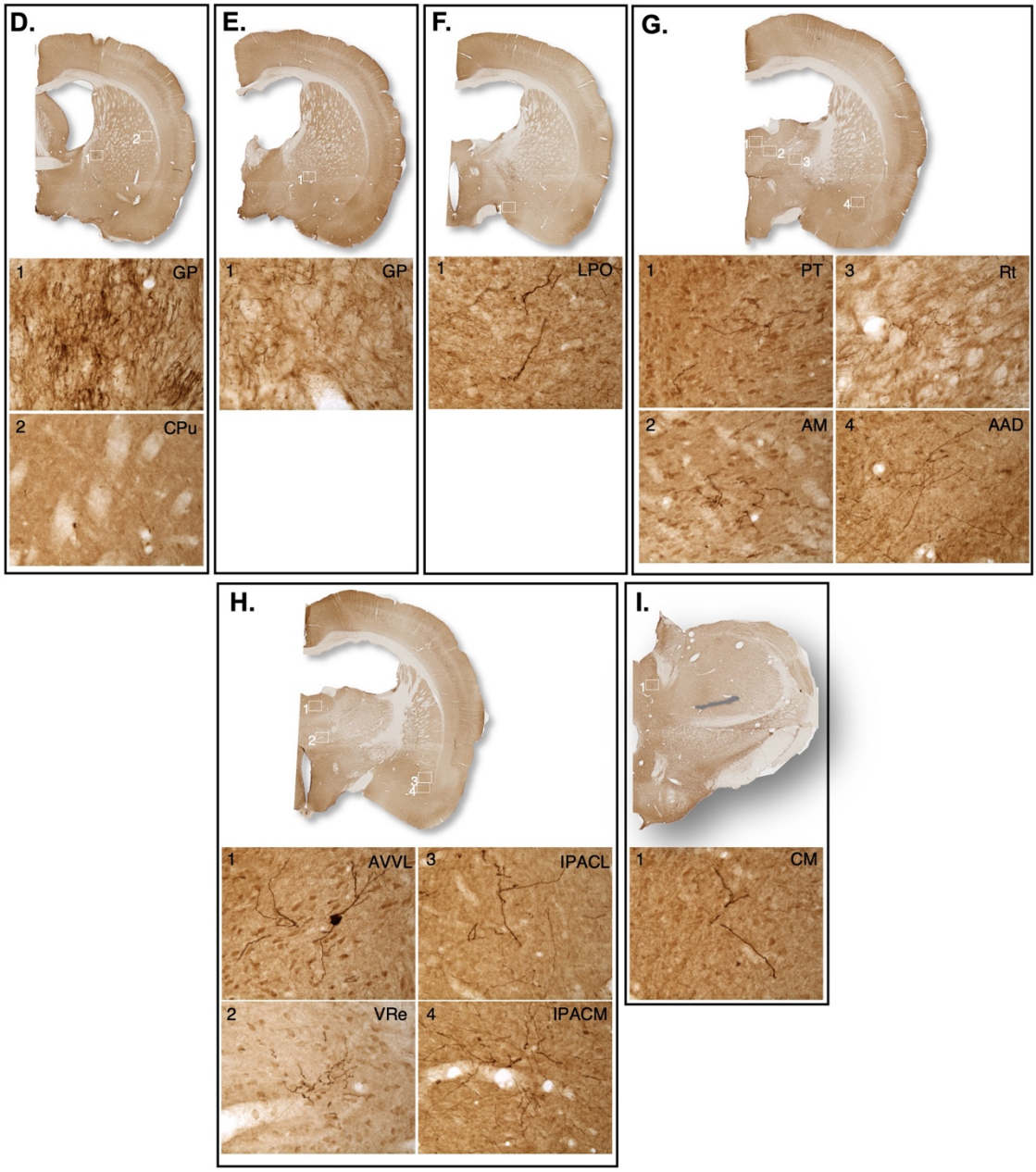

Appendix Figure 5 – Traced cells and projections found in different brain regions after 9 weeks post transplantation. Coronal sections from mCherry IHC are represented. A white square in coronal sections represents the area of a higher magnification images of each of the numbered areas.

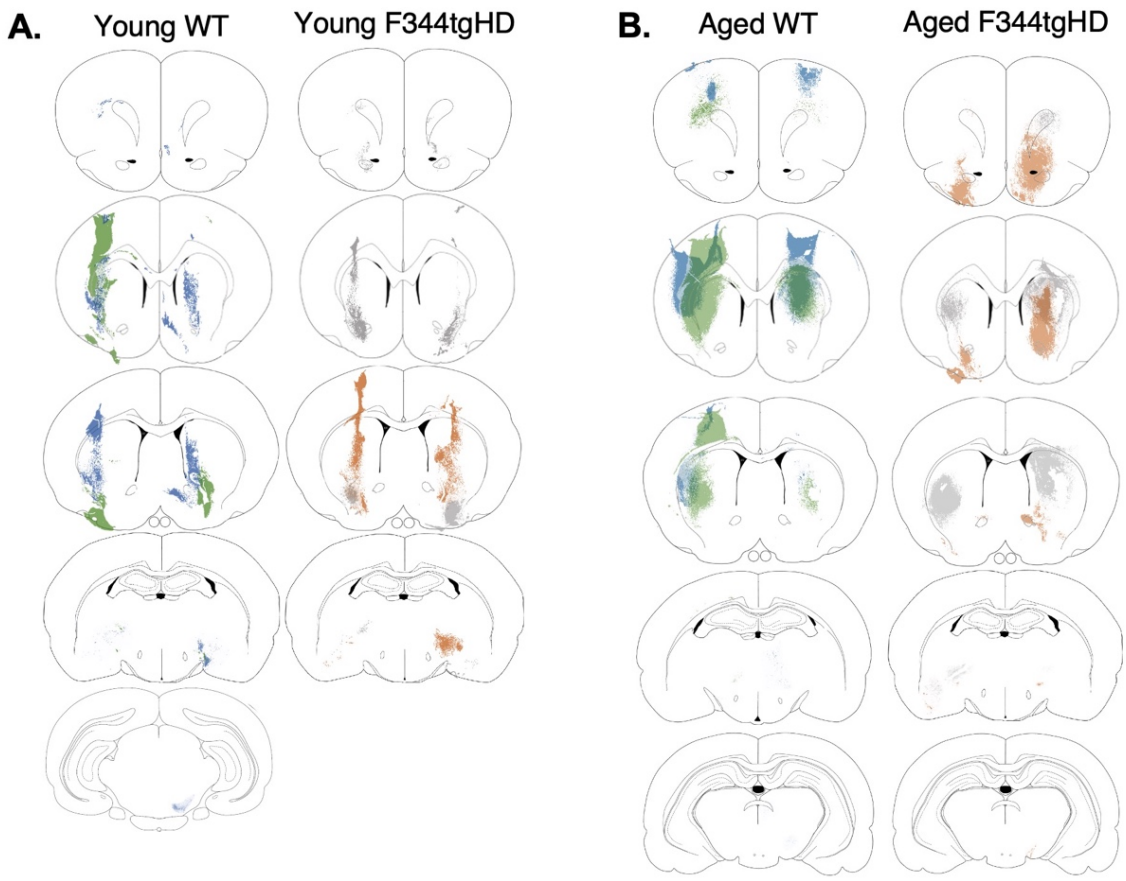

Appendix Figure 6 – Grafted cells integrate into the host brain andextend projections to relevant areas of the thalamo-cortical circuit Representations of two different rat STEM121 staining across the whole brain in WT animals (green and blue) and in F344tgHD animals (orange and grey) in young (A) and aged (B) rats.

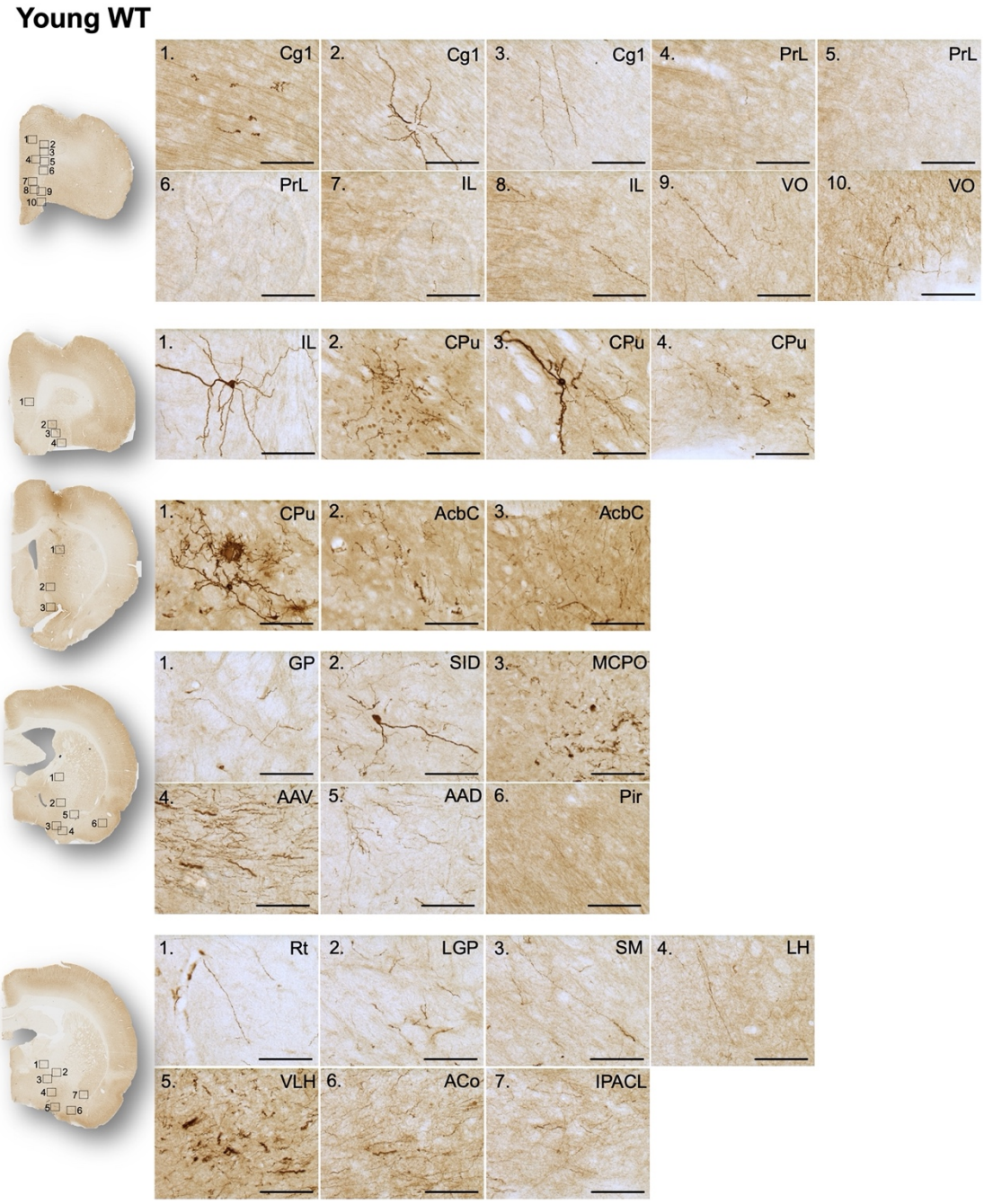

Appendix Figure 7 – Traced cells and projections found in different brain regions after 10 weeks post transplantation in young WT rats. Coronal sections from mCherry IHC are represented. A black square in coronal sections represents the area of a higher magnification images of each of the numbered areas.

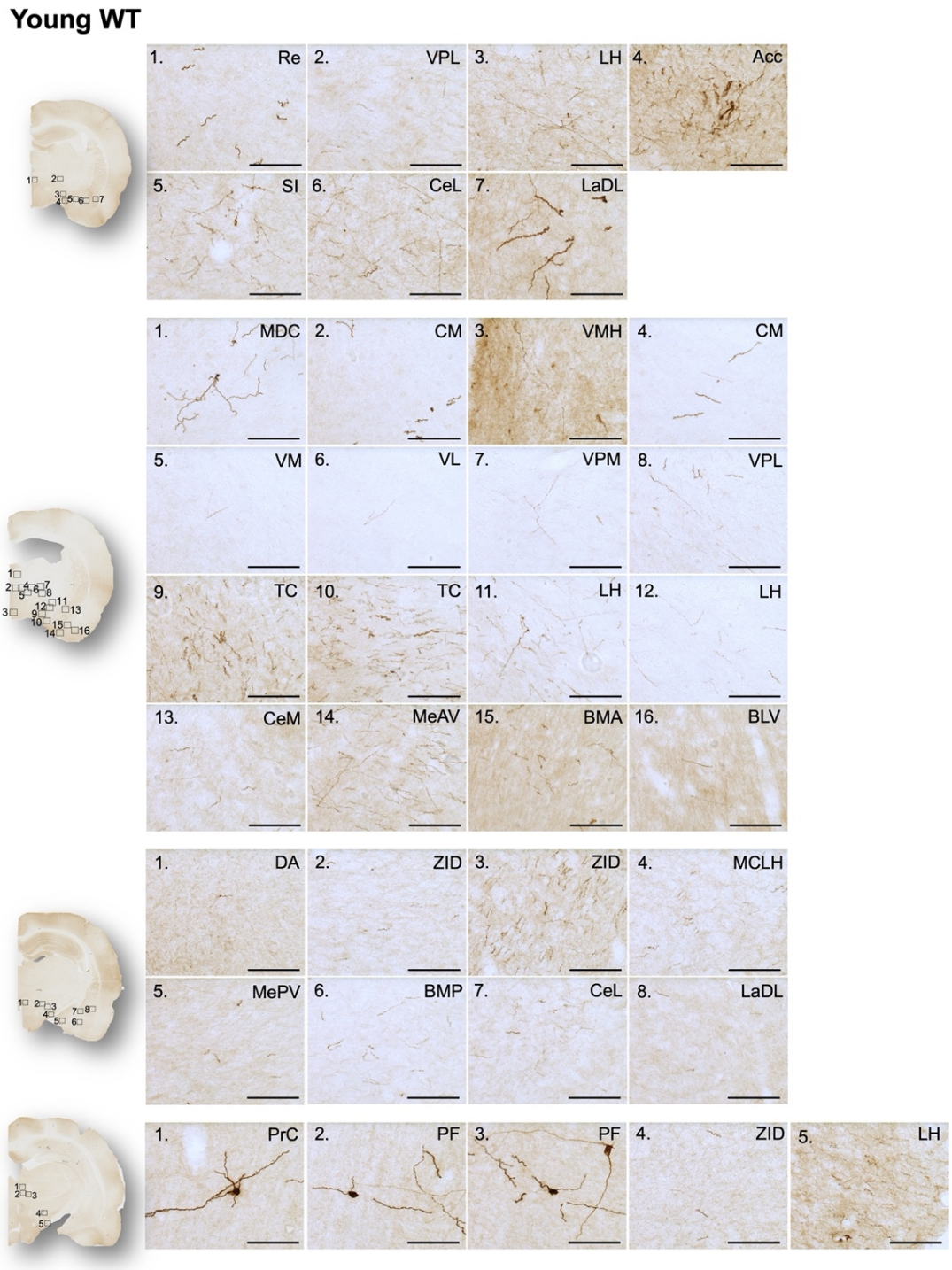

Appendix Figure 8 – Traced cells and projections found in different brain regions after 10 weeks post transplantation in young WT rats. Coronal sections from mCherry IHC are represented. A black square in coronal sections represents the area of a higher magnification images of each of the numbered areas.

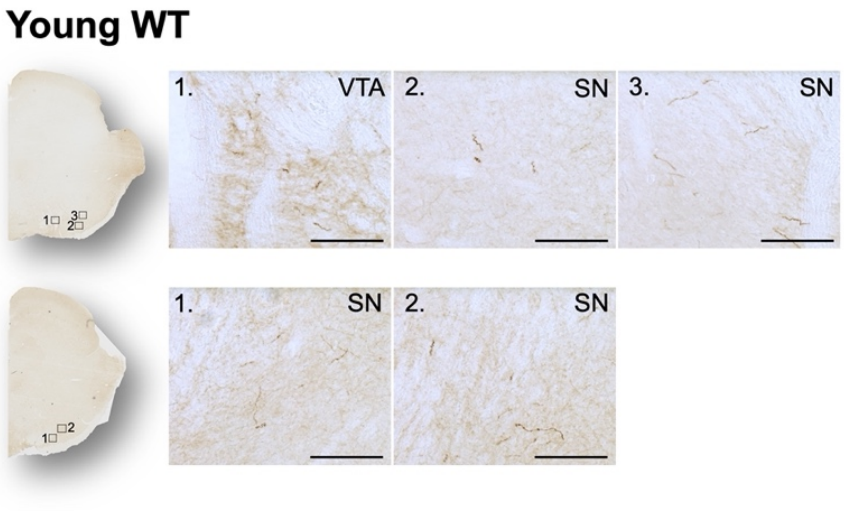

Appendix Figure 9 – Traced cells and projections found in different brain regions after 10 weeks post transplantation in young WT rats. Coronal sections from mCherry IHC are represented. A black square in coronal sections represents the area of a higher magnification images of each of the numbered areas.

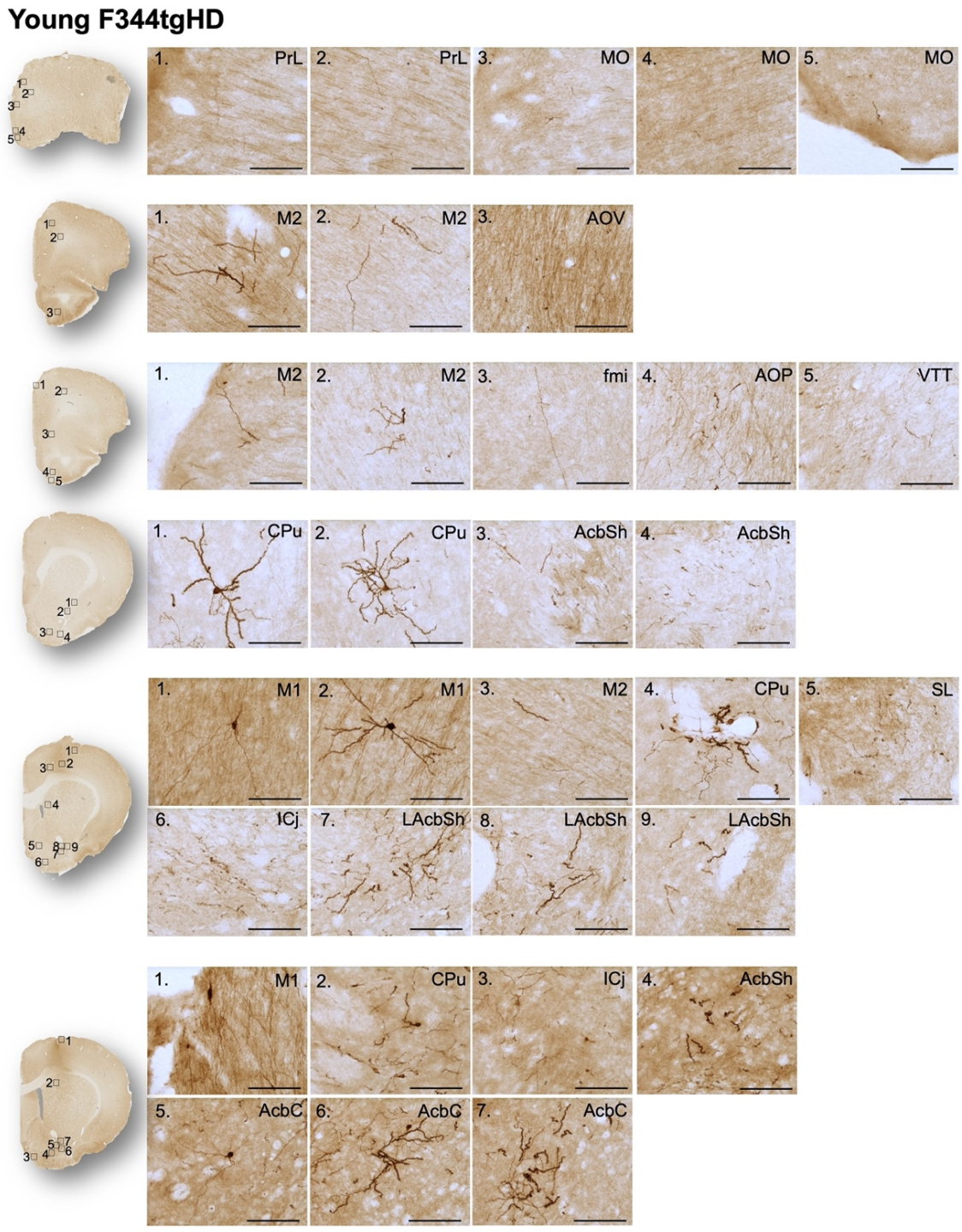

Appendix Figure 10 – Traced cells and projections found in different brain regions after 10 weeks post transplantation in young F344tgHD rats. Coronal sections from mCherry IHC are represented. A black square in coronal sections represents the area of a higher magnification images of each of the numbered areas.

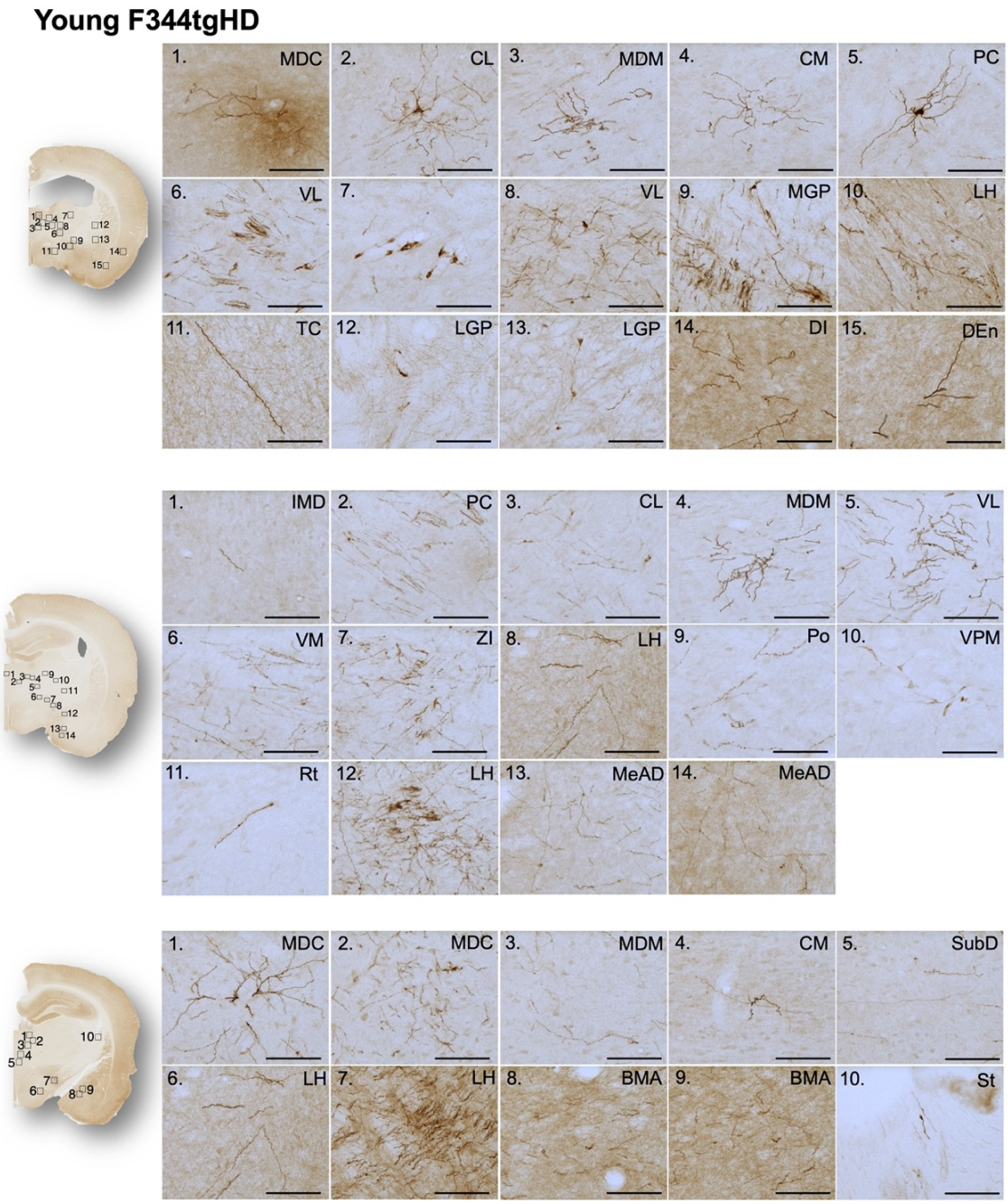

Appendix Figure 11 – Traced cells and projections found in different brain regions after 10 weeks post transplantation in young F344tgHD rats. Coronal sections from mCherry IHC are represented. A black square in coronal sections represents the area of a higher magnification images of each of the numbered areas.

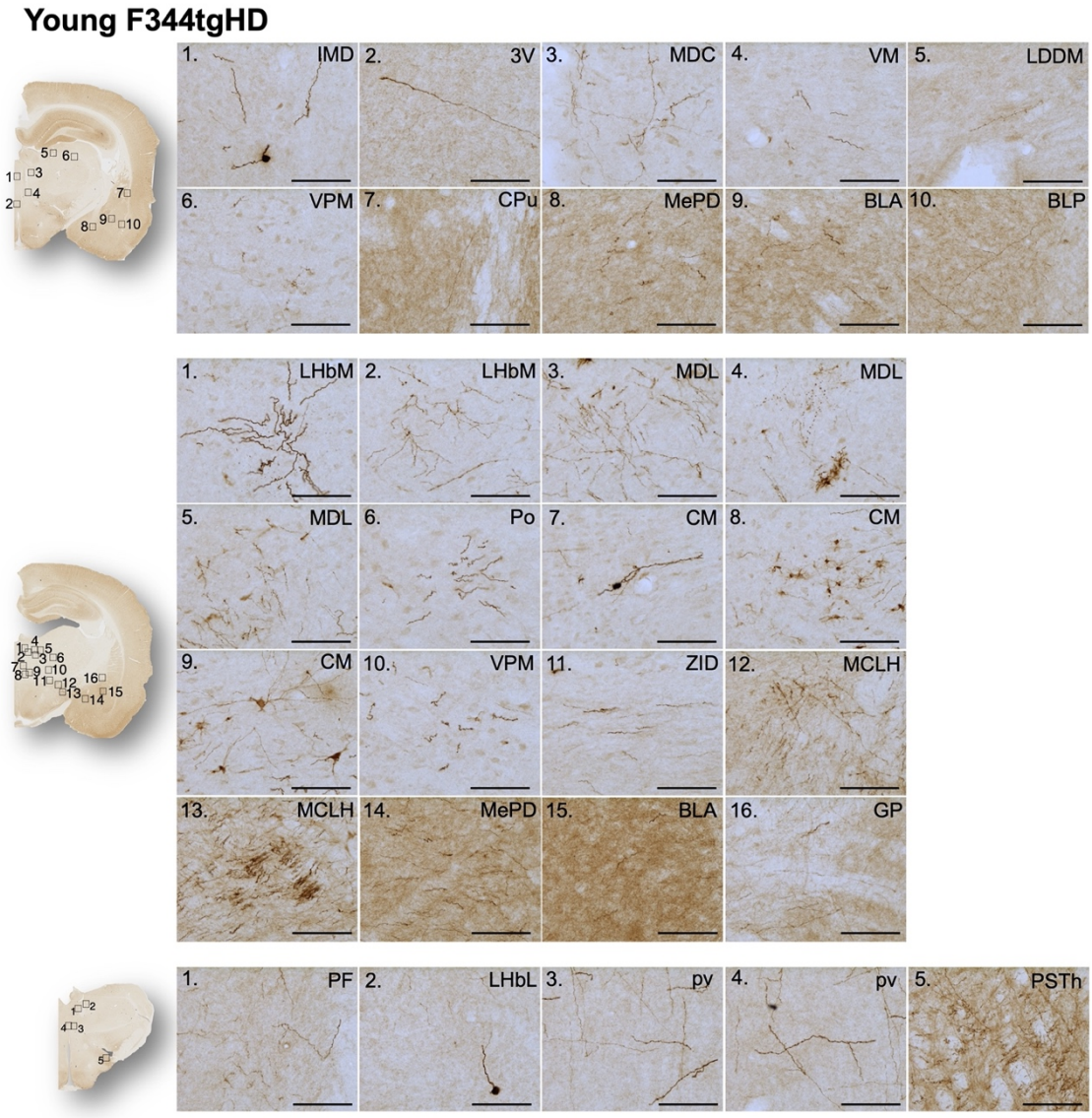

Appendix Figure 12 - Traced cells and projections found in different brain regions after 10 weeks post transplantation in young F344tgHD rats. Coronal sections from mCherry IHC are represented. A black square in coronal sections represents the area of a higher magnification images of each of the numbered areas.

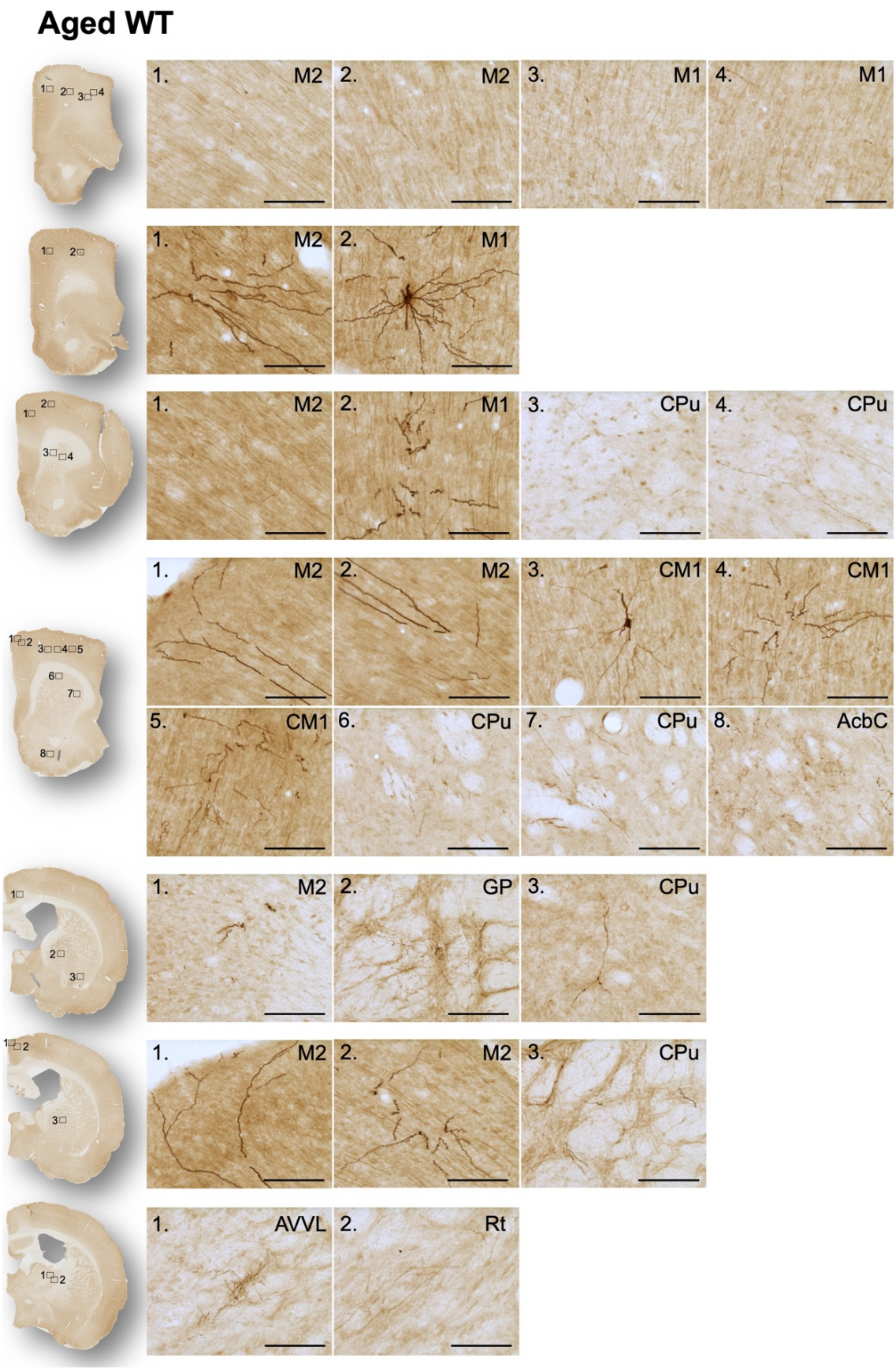

Appendix Figure 13 – Traced cells and projections found in different brain regions after 10 weeks post transplantation in aged WT rats. Coronal sections from mCherry

IHC are represented. A black square in coronal sections represents the area of a higher magnification images of each of the numbered areas.

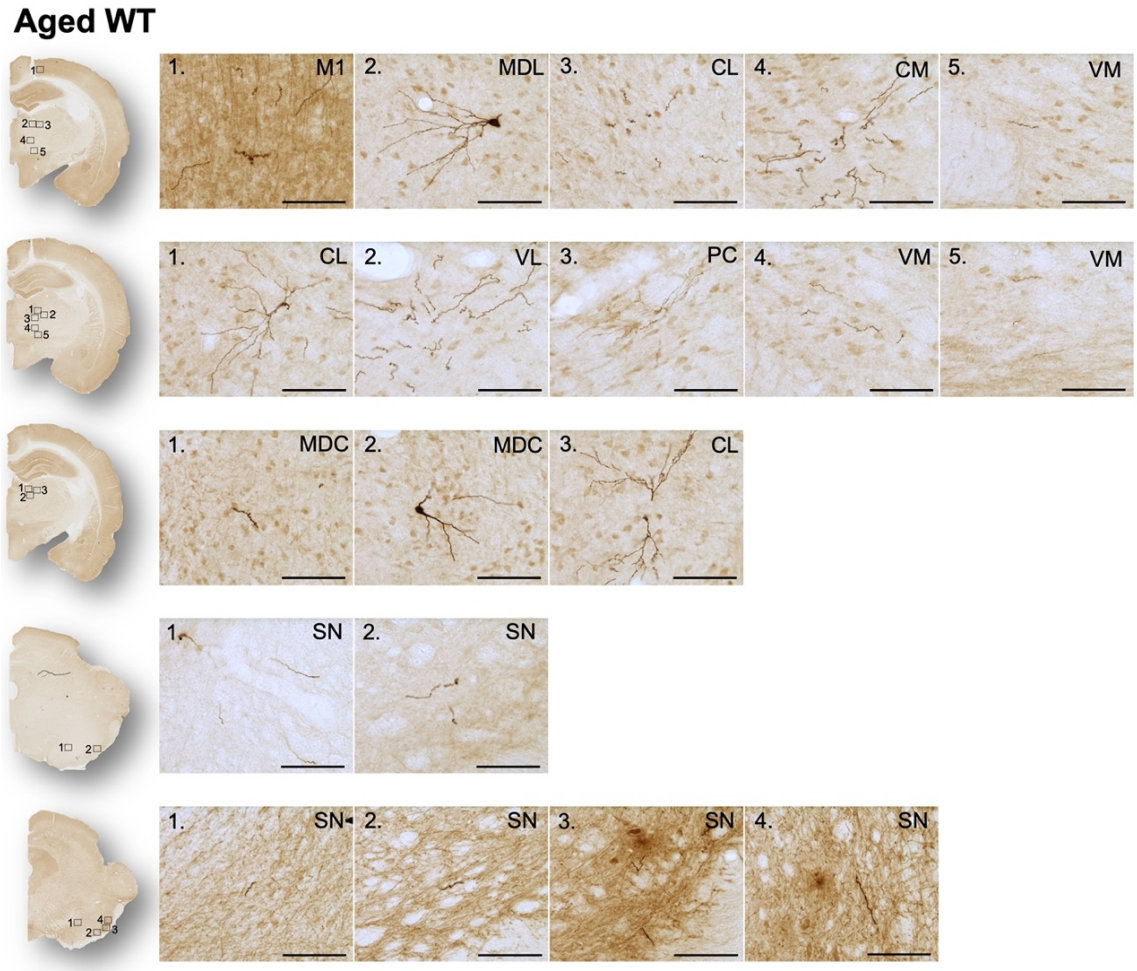

Appendix Figure 14 – Traced cells and projections found in different brain regions after 10 weeks post transplantation in aged WT rats. Coronal sections from mCherry IHC are represented. A black square in coronal sections represents the area of a higher magnification images of each of the numbered areas.

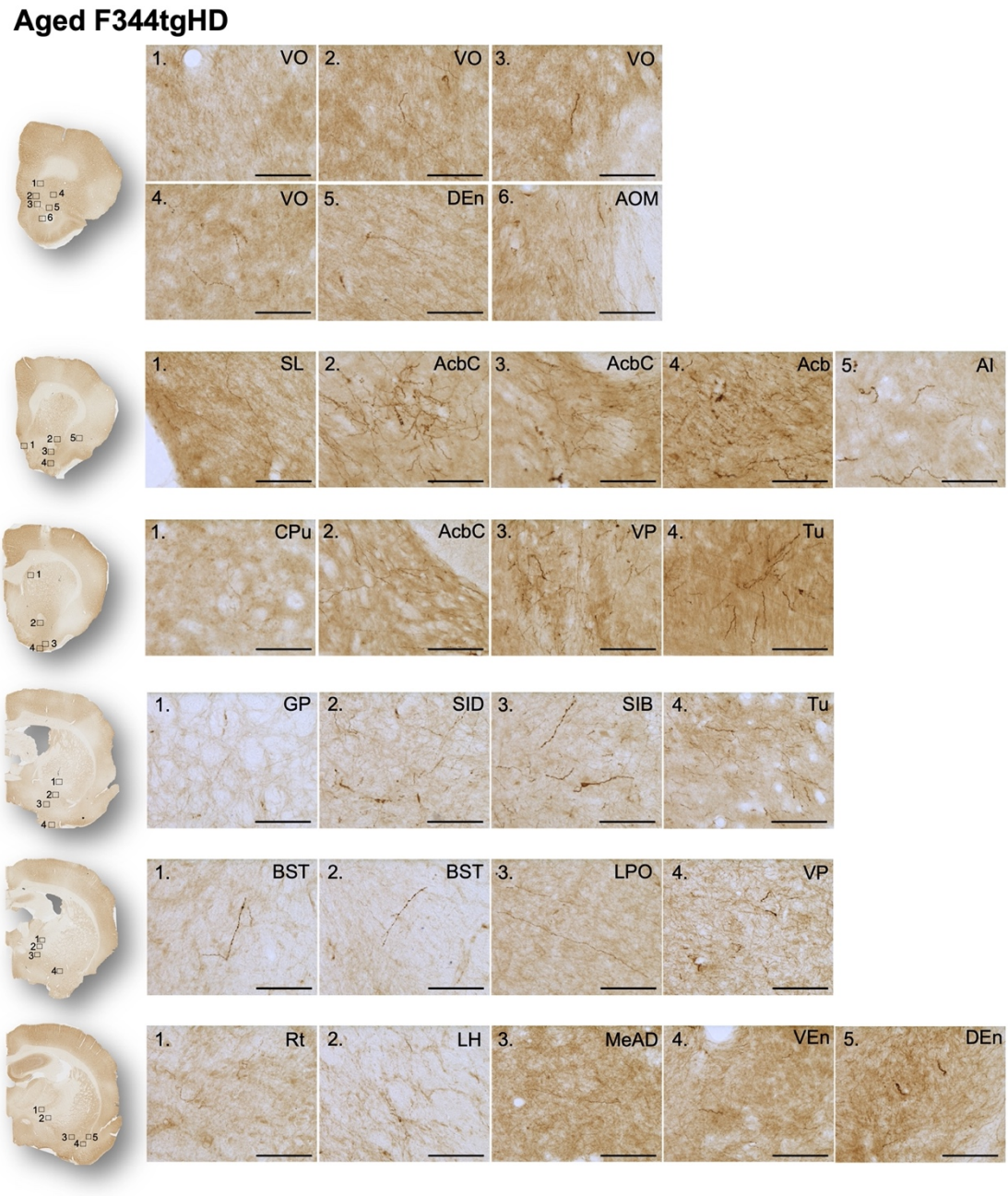

Appendix Figure 15 – Traced cells and projections found in different brain regions after 10 weeks post transplantation in aged F344tgHD rats. Coronal sections from mCherry IHC are represented. A black square in coronal sections represents the area of a higher magnification images of each of the numbered areas.

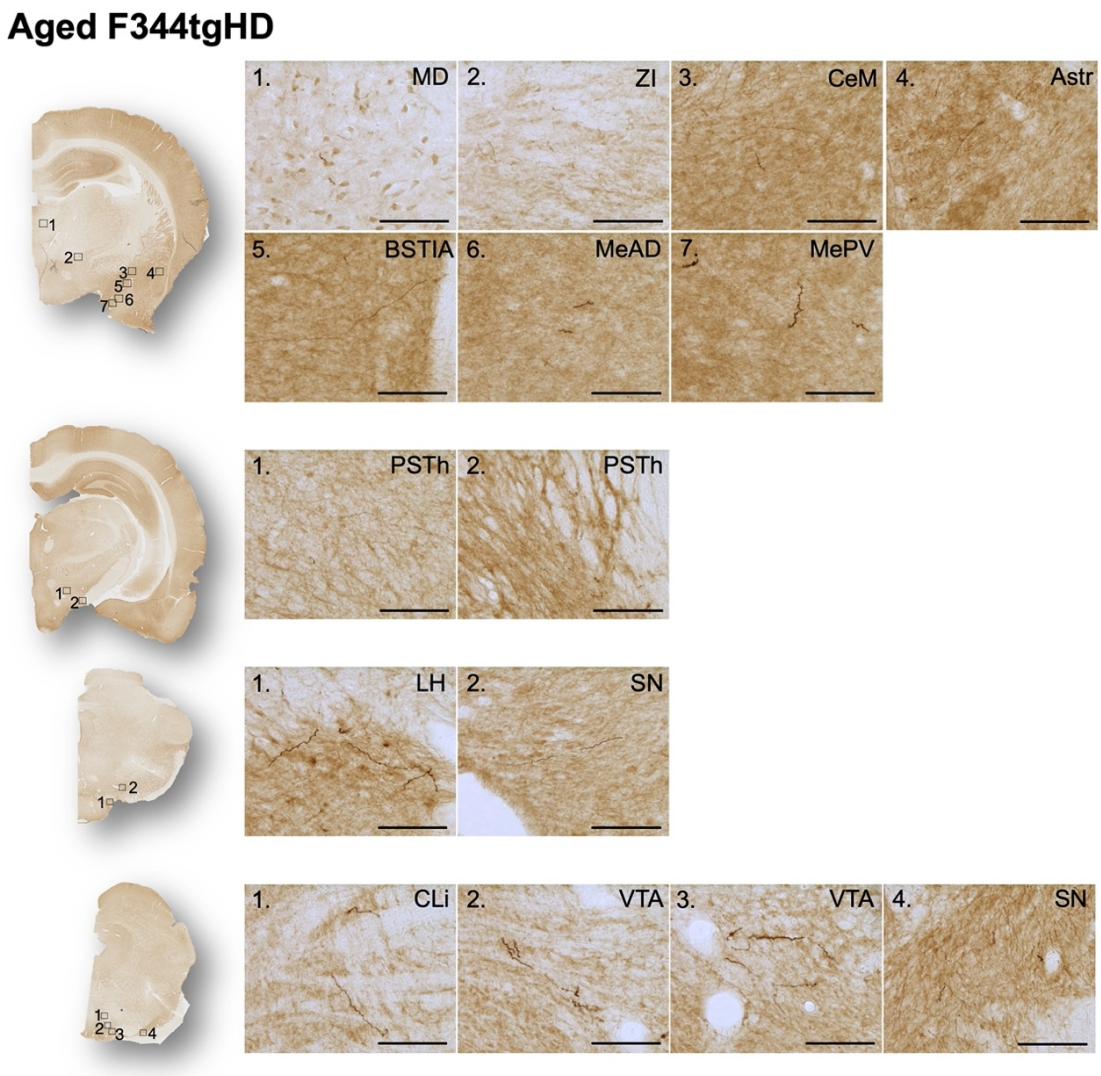

Appendix Figure 16 – Traced cells and projections found in different brain regions after 10 weeks post transplantation in aged F344tgHD rats. Coronal sections from mCherry IHC are represented. A black square in coronal sections represents the area of a higher magnification images of each of the numbered areas.